Computer simulation studies of vector spin glasses

Dissertation

zur Erlangung des Grades
„Doktor der Naturwissenschaften"

am Fachbereich Physik

der Johannes Gutenberg-Universität Mainz

vorgelegt von

Frank Beyer

geboren in Rostock

Mainz im Juli 2012

1. Berichterstatter: *(removed)*

2. Berichterstatter: *(removed)*

Tag der mündlichen Prüfung: 21.11.2012

D77

Parts of this thesis have already been published in:

- F. Beyer, M. Weigel
  Spin stiffness of vector spin glasses
  Computer Physics Communications **182**(9) pp. 1883–1887 (2011).

- F. Beyer, M. Weigel, M.A. Moore
  One-dimensional infinite component vector spin glass with long-range interactions
  Physical Review B, **86**(1), p. 014431 (2012); arXiv:1205.3975v1 (2012)

Zusammenfassung

Die vorliegende Doktorarbeit befasst sich mit klassischen Vektor-Spingläsern – eine Art von ungeordneten Magneten – auf verschiedenen Gittertypen. Da sie bedeutsam für eine experimentelle Realisierung sind, ist ein theoretisches Verständnis von Spinglas-Modellen mit wenigen Spinkomponenten und niedriger Gitterdimension von großer Bedeutung. Da sich dies jedoch als sehr schwierig erweist, sind neue, aussichtsreiche Ansätze nötig. Diese Arbeit betrachtet daher den Limes unendlich vieler Spindimensionen. Darin entstehen mehrere Vereinfachungen im Vergleich zu Modellen niedriger Spindimension, so dass für dieses bedeutsame Problem Eigenschaften sowohl bei Temperatur Null als auch bei endlichen Temperaturen überwiegend mit numerischen Methoden ermittelt werden.

Sowohl hyperkubische Gitter als auch ein vielseitiges 1d-Modell werden betrachtet. Letzteres erlaubt es, unterschiedliche Universalitätsklassen durch bloßes Abstimmen eines einzigen Parameters zu untersuchen. "Finite-size scaling"-Formen, kritische Exponenten, Quotienten kritischer Exponenten und andere kritische Größen werden nahegelegt und mit numerischen Ergebnissen verglichen. Eine detaillierte Beschreibung der Herleitungen aller numerisch ausgewerteter Gleichungen wird ebenso angegeben. Bei Temperatur Null wird eine gründliche Untersuchung der Grundzustände und Defektenergien gemacht. Eine Reihe interessanter Größen wird analysiert und insbesondere die untere kritische Dimension bestimmt. Bei endlicher Temperatur sind der Ordnungsparameter und die Spinglas-Suszeptibilität über die numerisch berechnete Korrelationsmatrix zugänglich.

Das Spinglas-Modell im Limes unendlich vieler Spinkomponenten kann man als Ausgangspunkt zur Untersuchung der natürlicheren Modelle mit niedriger Spindimension betrachten. Wünschenswert wäre natürlich ein Modell, das die Vorteile des ersten mit den Eigenschaften des zweiten verbände. Daher wird ein Modell mit Anisotropie vorgeschlagen und getestet, mit welchem versucht wird, dieses Ziel zu erreichen. Es wird auf reizvolle Wege hingewiesen, das Modell zu nutzen und eine tiefergehende Beschäftigung anzuregen.

Zuletzt werden sogenannte "real-space" Renormierungsgruppenrechnungen sowohl analytisch als auch numerisch für endlich-dimensionale Vektor-Spingläser mit endlicher Anzahl von Spinkomponenten durchgeführt. Dies wird mit einer zuvor bestimmten neuen Migdal-Kadanoff Rekursionsrelation geschehen. Neben anderen Größen wird die untere kritische Dimension bestimmt.

Abstract

The present thesis deals with classical vector spin glasses – some kind of disordered magnets – on various types of lattices. Since they are significant for experimental realizations, it is of importance to have a theoretical insight into spin-glass models with a low finite number of spin components on low dimensional lattices. As this turns out to be very hard to come by, novel and promising approaches are in need. To this end the limit of infinitely many spin components is considered in this thesis. There are several simplifications as compared to the models of low spin-dimension, so that for this important problem both zero and finite temperature properties are investigated mostly with numerical techniques.

Attention is paid to hypercubic lattices as well as to a versatile 1d model which allows to analyze different universality classes by tuning only one parameter. "Finite-size scaling" forms, critical exponents, critical exponent ratios and other critical values are suggested and compared to numerical findings. A detailed description of the derivation of all equations evaluated numerically is given as well. At zero temperature a careful study of ground states and defect energies is carried out. A number of interesting quantities will be analyzed there and the lower critical dimension is determined. At finite temperature the order parameter and the spin-glass susceptibility are accessible through the correlation matrix being calculated numerically.

The spin-glass model in its infinite-component limit can be considered as a starting point for investigations of the more natural low (spin-)dimensional models. Therefore, a numerical approach to combine the benefits of the former with the properties of the latter is suggested and tested by introducing a model with anisotropy. It will be pointed to appealing ways to exploit it and extent the analysis.

Lastly, also real-space renormalization-group calculations are carried out both numerically and analytically for finite dimensional vector spin glasses with a finite number of spin dimensions after calculating a new Migdal-Kadanoff recursion relation. Amongst other quantities the lower critical dimension is determined.

Acknowledgments

(removed)

Contents

Contents

Contents

x

List of Figures

List of Tables

List of Tables

Chapter 1.

Introduction

Categorized into the large container of disordered systems, spin glasses are a type of random magnets in which magnetic moments are coupled by both ferromagnetic and antiferromagnetic interactions. They do not play any role in every-day life and also reasonable applications were not known at the beginning of experimental, theoretical and numerical investigations. So spin glasses are materials being dealt with usually for their own sake. Nevertheless, they constitute a model which is easily formulated (although its treatment is not that easy) and gives a formidable basis for studying glass phases.

Glass phases [BK05] in turn appear quite often in physics and related areas. They are one of the paradigmatic examples of complex systems. In contrast to spin glasses structural glasses are one of the most prominent examples exhibiting a glassy phase if temperature drops below a certain critical temperature. In principle, atoms can move like in a fluid, but strong interactions and large energy barriers prevent this. The glass structure is then frozen in time and the arrangement of molecules is geometrically random on large length scales. The glass phase is therefore a random or amorphous solid state and is very hard to study. In general, however, it does not matter whether we are dealing with structural or spin glasses – compared to crystalline solids it is the absence of any kind of symmetry which makes it hard (and slow) to study the glassy phase.

The canonical type of experimentally realized spin glasses consists of non-magnetic hosts doped randomly with magnetic impurities. E.g. copper or gold might be the host with dopants such as manganese or iron creating spin-glass materials like AuFe or CuMn. Magnetic moments of the dopant atoms interact with each other through an indirect exchange with the conduction electrons. Derived from electronic structure calculations the exchange is the RKKY-interaction which oscillates in strength and sign according to

$$ J_{ij} \sim \frac{\cos 2k_F r_{ij}}{r_{ij}^3} \; , \tag{1.1} $$

with two interacting particles at site i and j at distance r_{ij} and k_F being the Fermi wavevector. Since these atoms are randomly distributed in their host, but frozen in time, the magnitude and sign of the interaction between two of them depend on the distance between them. The interactions are constant in time and are thus called quenched variables. This is due to the slow relaxation of spin (or atom) positions towards equilibrium. Spin fluctuations are much faster. First published experiments with these dilute magnetic alloys were performed by Canella and Mydosh in 1972 [CM72]. A sign of a thermodynamic transition

was found with a sharp cusp in the susceptibility. An introduction to the experimental investigation of spin-glass materials can be found in Ref. [Myd93].

In the simplest theoretical models of spin glasses, on the other hand, the concept of geometrical randomness (metal atom dopants in a non-magnetic host) is substituted by magnetic moments on a regular lattice but with a randomness in the interactions. The abundance of obstacles, pitfalls and insights of the model of spin glasses is astonishing. A broad view is given in Refs. [BY86b, MPV87]. However, compared to studying the glass phase in (real) structural glasses with exponentially growing relaxation times, spin glasses offer at least a simpler model with a slightly more convenient mathematical approach. It should be kept in mind, though, that structural and spin glasses are essentially different.

Apart from the discussion of experimentally realized spin glasses or the theoretical treatment of the model also applications of spin glasses are existing. E.g. connections to error-correcting codes, image restoration and associative memory [Nis01] are made. Also stock market issues [Mas02] or biological systems [Ste92] are mapped to the spin-glass problem.

Going into more mathematical detail, we want to find out properties of the function $\mathcal{H}$, called Hamiltonian, describing a system of classical spins which interact mutually. The system is modeled by

$$\mathcal{H} = -\frac{1}{2} \sum_{\substack{i,j=1 \\ i \neq j}}^{N} J_{ij} \, \mathbf{S}_i \cdot \mathbf{S}_j \, , \tag{1.2}$$

where the J_{ij} are quenched variables specifying the strength and type of the interaction between spin $\mathbf{S}_i$ and $\mathbf{S}_j$. They are also called coupling variables, or simply couplings. Both the range and strength of interaction differ for various flavors of the model. The spins $\mathbf{S}_i$ are classical vector spins embedded in $\mathbb{R}^m$ with $m \in \mathbb{N} \cup \infty$.

Throughout the whole work we will use some notions and concepts of general equilibrium statistical mechanics. Some of them might appear quite abstract at first sight. This is why the next section is devoted to introducing them and employing the easily understood ferromagnet as a guinea pig at which the concepts can be used and checked immediately. Core concepts discussed will be the partition function, the free energy, the critical temperature, the phase transition, the order parameter, the correlation length, the scaling hypothesis, critical exponents, finite-size scaling and the lower and upper critical dimension. This can also be taken from any textbook, e.g. Refs. [Yeo93, Set06].

After being prepared with the concepts to be used, we will delve into the topic of spin glasses. Fundamental ingredients and three different models will be introduced – the Edwards-Anderson, the Sherrington-Kirkpatrick and the 1d power-law model. The order parameter will be given and the two most prominent working hypotheses, called pictures, will be discussed – the replica symmetry breaking (RSB) and the droplet picture. Next, vector spin glasses will be introduced as they seem more appropriate for experimental realizations of spin-glass materials than Ising models with only one spin dimension.

All in all, it will become clear that spin glasses are very hard to deal with both analytically and numerically. To find a possible way out of this dilemma it will be argued that the study of vector spin glasses in the limit of infinitely many spin components might be highly beneficial. It is the core of the current thesis to work out properties of this limit in order to have a well-understood starting point for novel attempts to tackle low-dimensional spin-glass models.

Following the recapitulation of different aspects of equilibrium statistical mechanics and spin-glass models the last section of the current chapter (Sec. 1.5) describes the program according to which the thesis is structured.

1.1. Basic notions exemplified on the ferromagnet

The easiest possible flavor of the quoted Hamiltonian can be used to mathematically describe a ferromagnet. Considering a three dimensional ($d = 3$) world and thinking of the small piece of metal keeping the shopping list at the right place in the middle of the refrigerator door, everybody is familiar with a magnet. At room temperature it can be placed onto the fridge door without falling off, or in other words, it is in its ferromagnetic phase. Microscopically, a ferromagnet can be thought of as a system with spins placed on a hypercubic lattice which are coupled through short-ranged (more precisely finite-ranged) interactions. In order to gain a sound model for a ferromagnet it is completely sufficient to let the spins interact only with their nearest neighbors (amounting to $z = 2d$ neighbor spins per site, where z is also called 'coordination number') and for these couplings $J_{ij} = J$. The choice of the sign in the Hamiltonian function (1.2) is conventional. The ferromagnet is then characterized by $J > 0$ [1]. If $J < 0$ the system is anti-ferromagnetic. The spins can be chosen to reside in an only one-dimensional (spin-)space giving them the opportunity to point up or down. In this case they are called Ising spins. Note, that the spin-space is not coupled to the lattice-space. The (one-dimensional) Ising spins could be organized in any fashion. E.g. they might be placed on a lattice of arbitrary dimension d.

The knowledge of the Hamiltonian function (1.2) itself is not sufficient yet to unveil the information about the physical system. The field of statistical mechanics nominates the partition function as the guardian of all equilibrium properties of the system. In general it reads

$$Z = \mathrm{Tr}\, e^{-\beta\mathcal{H}} \,, \tag{1.3}$$

where $\beta = 1/(k_B T)$, with temperature T and the Boltzmann constant k_B. Unfortunately, this function is most often too difficult to evaluate.

For our current situation with the ferromagnet made up of Ising spins, however, the trace operation reduces to a 'simple' sum over all possible states, reading

$$Z(\beta) = \sum_{\{S_i=\pm 1\}} e^{-\beta\mathcal{H}(\{S_i\})} \,. \tag{1.4}$$

---

[1]A ferromagnet is actually already realized if only $J_{ij} > 0$ is required.
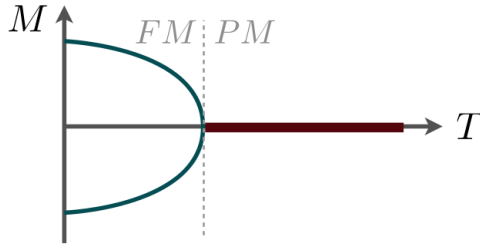
Figure 1.1.: Magnetization M of a ferromagnet in vanishing external field in $3d$. There are two phases – the ferromagnetic one below T_c, where the order parameter $M \neq 0$ and the paramagnetic one above T_c, where $M = 0$. A tiny external magnetic field would pick out the branch with $M > 0$ (e.g. all spins up) or $M < 0$ (all spins down), respectively.

But note that in a system of N spins there are 2^N different configurations in total! The partition function is related to the (physically more relevant) free energy via

$$F = -\frac{1}{\beta} \ln Z \tag{1.5}$$

of the system. Nature tries to minimize it and one finds that the spins tend to align, if the temperature T is low enough. There exists a *critical temperature* T_c (or more general *critical point*) above which the ferromagnetic phase breaks down and the metal becomes paramagnetic – it falls off the fridge door. Then spins point into random directions. In other words, T_c marks the point of the transition between two different phases, namely the paramagnetic and the ferromagnetic one. The *phase transition* itself is usually characterized by an *order parameter* which (in the simplest case) changes from zero in the disordered phase to a finite value in the ordered phase. The order parameter, being some property of the system of interest, is, e.g., the magnetization M for the ferromagnet, cf. Fig. 1.1. Above T_c it is zero, i.e. non- or para-magnetic, and non-zero below, i.e. ferromagnetic. The order parameter, however, is not unique. Every quantity which changes behavior fundamentally at the critical point would do. E.g. the square of the magnetization M^2 would be equally good. Furthermore, depending on the system, the order parameter may be a scalar, a vector, any complex quantity, or whatever quantity discriminating unfailingly between two phases.

Many thermodynamic quantities can be extracted out of the free energy (1.5) by differentiation with respect to appropriate parameters. Let us imagine our ferromagnet would be exposed to an external field h. The internal energy U is the first and the specific heat C_h the second derivative with respect to temperature. They read

$$U = -T^2 \frac{\partial \frac{1}{T} F}{\partial T} , \quad C_h = \left(\frac{\partial U}{\partial T} \right)_h , \tag{1.6}$$

where the index indicates that the external magnetic field h is kept constant. Likewise the

magnetization is one of the first derivatives of the free energy and the isothermal suscepti-
bility the according second one, reading

$$M = -\left(\frac{\partial F}{\partial h}\right)_T , \quad \chi_T = \left(\frac{\partial M}{\partial h}\right)_T , \tag{1.7}$$

where the index indicates a constant temperature T. The second derivatives are in a more
general sense quantities describing fluctuations. If they do not bear an additional special
name, like the specific heat, they are called susceptibilities.

All the thermodynamic variables are macroscopic quantities. On the other hand, we started
the introduction with Eq. (1.2) using exclusively microscopic quantities. To really under-
stand what is going on in a phase transition and to quantify it we need to look at the
microscopic level.

Correlation functions measure the correlations of certain characteristics in a physical sys-
tem. For the ferromagnet this might be the spin-spin correlation function

$$\Gamma(\mathbf{r}_i, \mathbf{r}_j) = \langle \, (\mathbf{S}_i - \langle \mathbf{S}_i \rangle)(\mathbf{S}_j - \langle \mathbf{S}_j \rangle) \, \rangle , \tag{1.8}$$

where $\mathbf{r}_i$ is the position of spin $\mathbf{S}_i$ and $\langle \cdot \rangle$ denotes the thermal average. Above as well as
below T_c the correlations will decay to zero with the distance of two spins (note, that we
talk about the correlations between fluctuations of the spins away from their mean values
and not between mean values themselves). Many systems are translationally invariant and
the correlation function depends only on the distance $r = |\mathbf{r}_i - \mathbf{r}_j|$ between two spins at site
i and j. Then, for almost all temperatures T the decay for large r is exponential like

$$\Gamma(r) \sim r^{-\tau} e^{-r/\xi} , \tag{1.9}$$

where r is the distance between the spins, τ some number and ξ the correlation length.
It estimates the size of the largest fluctuations. Right at the critical point T_c, however,
correlations diverge, because long-range order develops. Therefore, the correlation function
decays with distance r as

$$\Gamma(r) \sim \frac{1}{r^{d-2+\eta}} , \tag{1.10}$$

where η is a so called critical exponent, to be introduced below.

The phase transition is classified *first order* if at least one of the first derivatives of the
free energy is discontinuous at the transition temperature T_c. On the other hand if they are
not, it is classified *continuous*. Phase transitions are then characterized by singularities in
the second (or higher) derivatives of F. For well-behaved Hamiltonian functions, singulari-
ties do only appear in infinitely large systems. That is why a phase transition can actually
only occur in the *thermodynamic limit*, which is the limit of an infinitely large system.

The phase transition from the paramagnetic to the ferromagnetic phase of a ferromagnet is
continuous. None of the first derivatives of F show any discontinuity. But the second ones
do diverge as also the correlation length diverges at the critical temperature.

According to the *scaling hypothesis*, for continuous phase transitions the singularities in
any thermodynamic quantity can be described by simple power-laws in the vicinity of the

critical temperature T_c. This hypothesis comes from experimental observation and was later shown to follow from the presence of a diverging correlation length within the framework of the renormalization group. The exponents of the power-laws are consequently called *critical exponents*. They describe the leading behavior of the thermodynamic quantities. As it turns out, if certain requirements are met, these power-laws show some universal behavior and therefore identify apparently quite distant physical systems as being rather equivalent in terms of their behavior around the critical point. For the Ising ferromagnet important quantities show power-law critical behavior with the following critical exponents

$$M \quad \sim \quad t^{\beta} , \quad t < 0 \tag{1.11a}$$

$$\chi_T \quad \sim \quad |t|^{-\gamma} \tag{1.11b}$$

$$\xi \quad \sim \quad |t|^{-\nu} \tag{1.11c}$$

$$C_h \quad \sim \quad |t|^{-\alpha} , \tag{1.11d}$$

where we use the reduced temperature $t = (T - T_c)/T_c$, which is a convenient measure of the deviation from the critical point. Note, that Eqs. (1.11) describe the asymptotic behavior as $t \to 0$. Furthermore, the upper relations do not distinguish between the behavior of the thermodynamic variable coming from above T_c and from below (apart from the order parameter M, which is zero for $T > T_c$). For instance the correlation length could scale as $\xi \sim t^{-\nu}$ from below and $\xi \sim t^{-\nu'}$ from above T_c. Renormalization group, however, proved the critical exponents to be actually identical ($\nu = \nu'$ for the correlation length). However, the amplitudes are not. Another remarkable fact about the critical exponents themselves is their dependence on each other. Actually, there are only two independent exponents, while the others can be determined by certain *scaling laws*. They are based on the scaling hypothesis arising from renormalization group (RG). Following its flow under the RG transformation in coupling constant space one can investigate the properties near fixed points which determine the critical behavior. In order to elucidate critical exponents one can check how the correlation length transforms to find, e.g., the Josephson scaling law (hyperscaling)

$$d\nu = 2 - \alpha , \tag{1.12}$$

or the Rushbrooke scaling law

$$\alpha + 2\beta + \gamma = 2 . \tag{1.13}$$

These scaling laws can be taken from textbooks and a nice introduction and discussion is given in Ref. [Gol92].

Readdressing the issue of the thermodynamic limit, in computer simulations, of course, only finite system sizes can be studied. Infinitely large systems are out of reach. Although power-law behavior in the thermodynamic limit can be made plausible for a thermodynamic variable by increasing the finite system size successively and watching a singularity develop, it is not possible to directly estimate the critical temperature or the associated critical exponent. The correlation length ξ diverges, cf. Eq. (1.11c), and since lattices with $L \gg \xi \to \infty$ are required we are in need of another approach. The method of choice to determine the exponents is the *finite-size scaling* analysis.

All length scales appearing in a numerical treatment are cut off at the finite system size L, so that ξ is limited by it. This is why right at the critical point L is of the same order as ξ. In other words, L scales like ξ in Eq. (1.11c). We can make use of this observation and extend the concept of the scaling hypothesis by including the lattice size L as a parameter. Using

$$|t| \sim \xi^{-1/\nu} \sim L^{-1/\nu} \, , \tag{1.14}$$

the magnetization for the ferromagnet would thus be

$$M \sim t^\beta \sim L^{-\beta/\nu} \tag{1.15}$$

in the vicinity of the critical point. The same can be done for all the other thermodynamic quantities.

We already indicated some universal behavior. After introducing the power laws with the according critical exponents we should now explain what is meant with the notion of *universality*. Generally speaking, it refers to a certain universal behavior between different models of the critical exponents defined in the power laws (1.11). They depend only on three fundamental parameters: the dimensionality of space d, the symmetry of the order parameter and whether the forces are short ranged or not. It does not matter what the precise microscopic details are. This is in contrast to quantities like T_c which do depend on microscopic details. Therefore, universality enables one to elucidate properties of difficult physical systems by using simple models such as the Ising ferromagnet if they are in the same universality class. Universality classes are usually named after the simplest model belonging to that class. E.g. the long wavelength effective Hamiltonian in Landau theory of phase transitions and the Ising model reside in the Ising universality class. All models in that class are characterized by only one set of critical exponents.

In all the discussion above we did not go into much detail in terms of the dependence of the existence of a finite temperature phase-transition on the dimensionality of the system. We rather had roughly in mind our beloved three-dimensional world. Indeed, the critical temperature T_c depends on the dimensionality and it is time to classify possible behaviors at this stage.
In $d = 1$, i.e., for a chain of ferromagnetically coupled spins with interactions only between nearest neighbors, there is no phase transition at finite temperature. Only at zero temperature long-range order establishes, in other words $T_c = 0$. The tiniest increase in temperature will destroy this order immediately. Already in $d = 2$ there is a finite temperature phase transition, i.e. $T_c > 0$, as shown by the celebrated Onsager solution [Ons44]. Increasing the dimensionality, T_c will always be greater than zero. The dimension, however, from which on the phase transition will be at finite temperature is called *lower critical dimension* and is often denoted by d_l. Right at $d = d_l$, T_c might either be zero or finite. For the ferromagnet $d_l = 1$, with $T_c = 0$.
There is another important dimensionality – the one from which on critical exponents do not change anymore, although the dimension is increased and the system is short-ranged. This is the *upper critical dimension* d_u. Right at d_u the exponents take on their mean-field
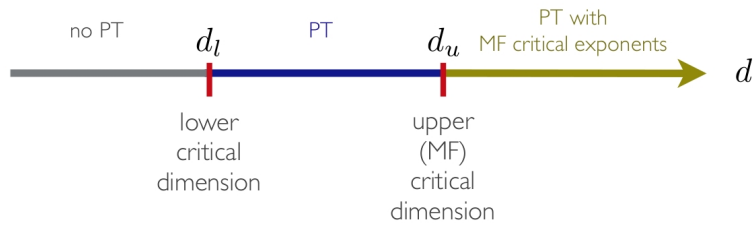
Figure 1.2.: The concepts of the lower and upper critical dimension d_l and d_u. Below d_l there exists no finite temperature phase transition (PT). Between d_l and d_u there is one and above d_u critical exponents assume their mean-field (MF) values and do not change upon increasing the dimensionality d of the system.

values and for the ferromagnet $d_u = 4$. Mean-field theory is an approximation method simplifying a physical system by neglecting fluctuations to solve it exactly. In a sense one can regard it as the lattice dimension limit $d \to \infty$ since a geometric structure does not exist anymore.

Fig. 1.2 depicts a sketch of the critical dimensions.

A number of important concepts of equilibrium statistical mechanics have been introduced now. We looked at the ferromagnet for explaining them. The next section will lead us to the spin-glass model, reveal some of its properties and use several definitions from above.

1.2. Spin glasses

We will leave the simple ferromagnet behind now. Starting out from Eq. (1.2) we set $J_{ij} = J > 0$. A mere relaxation of this condition again to randomly chosen $J_{ij} \lesseqgtr 0$ makes us face the spin-glass problem. And all of a sudden, physics changes dramatically. Two additional and fundamental ingredients arise at this point: *disorder* and *frustration*. The low-temperature region and especially finding ground states, which is a combinatorial optimization problem, becomes hard. A ground state of a system is a configuration the energy of which cannot be lowered by any operation on a finite subset of the system. Speaking in the language of complexity theory, the spin-glass problem is among the hardest mathematical problems and classified $\mathcal{NP} - hard$ [Bar82, HR01], which stands for 'nondeterministic-polynomial-time-hard'. It is most unlikely that there exists an algorithm with a runtime increasing polynomially with the size of the problem (or of the system). For the Ising spin glass see e.g. Ref. [Bar82].

Placing the magnetic moments (classical spins) onto a regular lattice and endowing them with fixed ('quenched') random interactions J_{ij} between each other there is disorder

incorporated in the system. And so, an average over many different disorder realizations (characterized by distinct sets of variables $\{J_{ij}\}$) has to be performed. Calculating any observable of the system means to not only thermally average but to also make a disorder average. The reason as to why to first make the thermal average while keeping the interaction variables fixed, is due to the general understanding of the glassy phase (of an amorphous system): The positions of spins are fixed (and so are the interactions) in the time scale of rapid thermal motion. The additional average over the disorder is redundant for some systems, which are comprised by those possessing the property of *self-averaging*. A heuristic argument [BK05] for short-range interactions states that the average over the disorder is implicitly accomplished in a sufficiently *large* system, or more precisely, this holds only in the infinite volume limit. Split up into sub-systems which have one realization of disorder each, the whole system is henceforth considered to be self-averaging. Nevertheless, for numerical simulations the heuristic argument does not hold in general. The infinite volume limit as a pre-condition, is unreachable for this case. Instead, we need to do the disorder average over many samples. Apart from that there are also quantities which are not self-averaging because the thermodynamic limit is not that straightforward for disordered systems in which pure states are depending on the disorder realization. The order parameter $q(x)$ of the SK model, for instance, is not self-averaging and its distribution $P(q)$ depends on the disorder realization even in the thermodynamic limit [KR05].

Frustration, as the second important ingredient of spin glasses prevents the system to satisfy the bonds altogether, i.e. to find a global configuration in which every single pair of spins is in its very own minimal energy state. In Ref. [Bey08] there is an example vivifying the notion of frustration with an example of social life, which we will repeat here.

In a group of three people, hereinafter referred to as A, B and C, all but A and C do like each other (A and C may actually hate each other). For reasons of simplicity, their lives are assumed to be a bit boring, meaning that their evenings can only proceed as follows: a person can either go to a pub, or to the reader's club. Thus, they can adopt the state of going-to-pub or going-to-club. It is obvious that two people who like each other also like to spend their evenings together and tend to be sad if they do not show up in the same location. The other way around, two people who dislike each other prefer not to spend their evenings together and tend to be sad if they do show up in the same location.
After running through all possibilities of the three persons to organize their evening (there are $2^3 = 8$ of them[2]), the sorrowful discovery is that there is not a single evening all three persons' desires can be satisfied altogether such that they are completely happy. Every day at least one of them will feel sad.

---

[2]e.g. A and B visit the pub and C the reader's club accordingly - then

- A is completely happy/satisfied (friend B comes along and the disliked C does something else)

- B is sad about C who is not spending the evening with him (this friend does not come along).

Translated into the more formal language of disordered systems the following sketches show the "frustration". Before, the analogy between the upper example and a spin system should be made clear:

$$\begin{aligned}
\text{amicable/hostile connection} \quad &\longleftrightarrow \quad \text{ferromagnetic/anti-ferromagnetic bond} \\
\text{going to pub/reader's club} \quad &\longleftrightarrow \quad \text{spin pointing up/down .}
\end{aligned}$$

It is a spin system consisting of three spins (analogous to the three persons A, B and C). A single line represents a ferromagnetic interaction ($J = 1$, 'amicable connection') and a double line an anti-ferromagnetic one ($J = -1$, 'hostile connection'), accordingly. Based on this convention, solid black lines illustrate a satisfied bond, whereas dashed red lines indicate a broken bond.

| $E = -1$ | $E = -1$ | $E = 3$ | $E = -1$ | $E = -1$ | $E = 3$ | $E = -1$ | $E = -1$ |
| ($E_I = -3$) | ($E_I = 1$) | ($E_I = 1$) | ($E_I = 1$) | ($E_I = 1$) | ($E_I = 1$) | ($E_I = 1$) | ($E_I = -3$) |
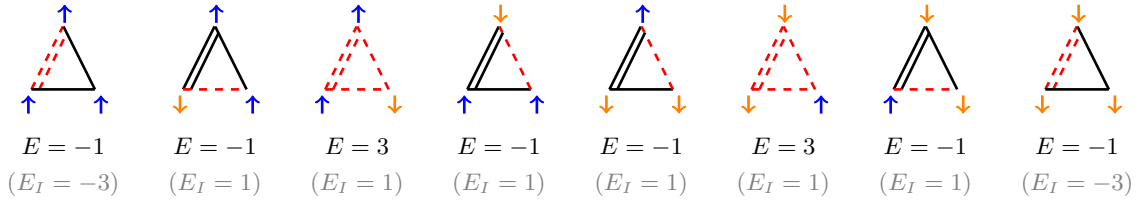
Indeed, as in the example with three persons, not a single configuration can satisfy all three bonds. The plaquette, as it has been chosen here, is a frustrated one and is actually nothing else than the formal description of the situation with person A, B and C. Generally, a plaquette is frustrated, if there exists an odd number of anti-ferromagnetic bonds. Then it is impossible to find a configuration satisfying all couplings.

The two labels below each configuration contain the energy, evaluated by

$$E = -\sum_{i<j} J_{ij} S_i S_j \ .$$

The upper one gives the energy evaluated for the shown plaquette, the lower for an ferromagnetic Ising plaquette ($J_{ij} = J \equiv 1$). Frustrated plaquettes cannot reach an energy being as low as for non-frustrated plaquettes, as the small example indicates.

Due to disorder and frustration the spin-glass phase is strange – in the "ordered" phase no long-range order does develop. Spins freeze in random relative orientations and thereby mask their intrinsic nature. However, missing long-range order is also one of the key features of structural glasses.

1.2.1. Edwards-Anderson model

Choosing a simple description but incorporating all essential ingredients for a spin-glass Edwards and Anderson introduced [EA75] their short-range model with spins on a hypercubic lattice and nearest-neighbor interaction in 1975. In this case a spin on a d-dimensional lattice has only $z = 2d$ nearest neighbors. Thus, almost all interaction variables J_{ij} are zero. Nevertheless, all necessary ingredients accounting for a spin-glass system (disorder and frustration) are incorporated and questions concerning a real microscopic realization
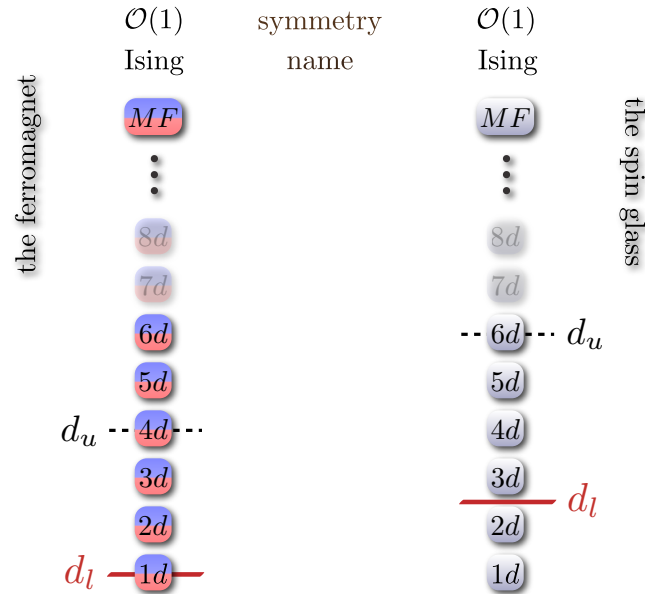
Figure 1.3.: The Ising model with O(1), i.e. up/down, symmetry for the ferromagnet (left) and the spin-glass model (right). The lower critical dimension d_l is lifted from 1 to 2.5 when comparing the two models. The upper critical dimension d_u changes from 4 to 6.

including a "natural type" of interactions or anisotropies are wiped away. Comparing a spin-glass model to a ferromagnet with positive interaction variables one finds randomness in sign (and strength) of the interactions such that the physics behind it changes dramatically. Often interactions are chosen according to a Gaussian distribution with zero mean and standard deviation unity. Also a bimodal distribution is used frequently, e.g. with $J_{ij} \in \{-1, 1\}$.

The additional features a spin-glass model exhibits beyond the ones of the ferromagnet also have impact on the characteristics of the critical dimension. It seems settled now that the lower critical dimension d_l of the Edwards-Anderson Ising spin-glass model amounts to[3] 2.5 [Boe05b]. The upper critical dimension is lifted from $d_u = 4$ for the ferromagnet to $d_u = 6$, cf. Fig. 1.3. Critical properties can be found summarized in [KR05].

1.2.2. Sherrington-Kirkpatrick model and mean-field theory

Mean-field theory is a simplification of microscopic mechanisms. First, the concept of distance does not exist, and second fluctuations of microscopic variables around their mean value are simply neglected. If one wished to simplify the approach even more, i.e., one goes beyond the mean-field approximation, there is only the possibility of neglecting even all interactions. In order to keep certain physical quantities extensive the exchange couplings need to be scaled by some function of the inverse of the system size. All this makes calculations feasible. Exactly this strategy was chosen by Sherrington and Kirkpatrick [SK75] to tackle disordered systems, like Edwards and Anderson also in 1975.

---

[3]Physical systems in non-integer dimensions can be modeled by using hierarchical lattices.

Recalling the number of nearest neighbors, $z = 2d$, in the Edwards-Anderson model and taking the lattice dimension to infinity the notion of distance gets lost. In a sense, this limit is the Sherrington-Kirkpatrick model.

1.2.3. One-dimensional power-law model

The short-range Edwards-Anderson model of spin glasses in low lattice dimensions is most often treated on hypercubic lattices with nearest-neighbor interactions and coordination number $z = 2d$. For a linear lattice size of L the whole system consists then of $N = L^d$ spins. In terms of a numerical treatment we encounter a severe drawback of hypercubic lattices: As the dimension d is increased, the system size N increases exponentially for equal L. This means that for large d only very small sizes L can be considered, where finite-size effects are dramatic. This makes life hard as a phase transition is strictly only existent for $N \to \infty$.

The limit $d \to \infty$, however, can be regarded as a model with infinite-ranged interactions. If we imagine that the structure of space has vanished in this limit we can think of it resembling the Sherrington-Kirkpatrick model. For it an analytical treatment is possible. For the short-range Edwards-Anderson model one runs into problems with quite small ranges of lattice sizes the higher the lattice dimension d is.

However, since low-dimensional systems – describing natural spin glasses – exhibit interesting physics we want to circumvent problems with hypercubic lattices and take a look at a canny alternative. It was recognized already in 1969 [Dys69, Dys71] that a ferromagnet can be modeled by a one-dimensional spin chain with long-range interactions in order to obtain non-trivial critical behavior analogous to higher dimensional models. Modeling the interactions with a decay as $1/r^\sigma$ it depends on the choice of the power-law exponent σ as to whether it is possible to let the model exhibit a phase transition at finite temperature or not (r is the distance between two spins).

Motivated by the lack of a satisfactory theory for 3 space-dimensions, the same idea was used in 1982 [KAS83] to investigate Ising spin glasses. In that course a high-temperature series expansion of the free energy and the Fisch-Harris non-local order parameter signaled a finite temperature phase transition for $\sigma < 1$. Furthermore, critical behavior has been found Gaussian and mean-field theory valid for $1/2 < \sigma < 2/3$ and the model is expected to behave SK-like (in the fully connected version) for $\sigma < 1/2$. The latter is supported by the fact that starting from $\sigma = 1/2$ downwards, the thermodynamic limit does not exist anymore, i.e. thermodynamic quantities are not extensive anymore, unless a scaling with a function of the inverse of the system size is applied. The limit $\sigma \to 0$ corresponds to the Sherrington-Kirkpatrick model. A visual impression of the model geometry is given in Fig. 2.1.

In contrast to hypercubic lattices, the $1d$ spin chain with power-law interactions enables to simulate a relatively large range of system sizes, being valuable for a finite-size scaling analysis. This comes about due to scaling corrections being dependent on the *linear* lattice size. And since the power-law exponent σ is some kind of effective lattice dimension in disguise, another advantage of the model is the formidable ease of tuning the model from

short-range behavior without a finite temperature phase transition (below the lower critical dimension) across non-mean-field behavior (between lower and upper critical dimension) with finite-T phase transition up to the infinite-range SK behavior (above the upper critical dimension). In other words, it is attempted to get insights into the nature of short-range spin glasses (in various low lattice dimensions) with the help of a versatile long-range model, without running into trouble with fast growing system sizes when the lattice dimension increases.

1.2.4. The order parameter

Spin glasses have been keeping theoretical physicists busy for decades. And it is not resolved yet what the nature of the spin-glass phase really is. Up to now there is no answer to the question of which symmetry is broken by the spin-glass transition in low lattice dimensions. The ferromagnetic transition is much simpler: At high temperatures and zero external field it is in its paramagnetic phase, characterized by a vanishing global magnetization

$$M = \frac{1}{N} \sum_{i=1}^{N} \langle S_i \rangle = 0 , \tag{1.16}$$

if thermally averaged (denoted by $\langle \cdot \rangle$). Below the critical temperature T_c, the magnetization M is different from zero – even $\langle S_i \rangle = \langle S_j \rangle \neq 0$ for all i and j. If an infinitesimal external field is applied, one of the two states the system can be in is chosen (with either positive or negative magnetization, but still some thermal fluctuations). All spins point either down or up for $T = 0$, i.e. there is only one way to order (and its symmetry counterpart). In conclusion, coming from high temperatures at the critical temperature T_c the Z_2 symmetry is spontaneously broken and the order parameter M changes from zero to a finite value. Instead of T_c we will usually refer to T_{SG} as the critical temperature in a spin glass model.

In the high-temperature phase also for the spin glass Eq. (1.16) is valid. Things change below the transition temperature T_{SG}. In the thermodynamic limit a spin glass with a symmetric coupling distribution will still satisfy Eq. (1.16) but on the other hand develop spontaneously a non-zero *local* magnetization, such that $\langle S_i \rangle \neq 0$ being different for each i. Furthermore, there are infinitely many states the system can be in – $\langle S_i \rangle$ varies for each of them and spins always polarize into random directions which cannot be determined analytically. It would be more accurate then to introduce another index labeling the state. These states (also called phases) are not related by any symmetry. It is therefore hopeless to use the trick of applying an external field, as for the ferromagnet, to polarize spins into a desired state (or phase). There are many ways the system can order.
Eq. (1.16) cannot be an appropriate order parameter – it does not change from zero to non-zero at the critical temperature. A simple one for the spin glass which does meet the requirements of an order parameter is

$$q = \frac{1}{N} \sum_i \langle S_i \rangle^2 . \tag{1.17}$$

A detailed discussion of the order parameter of spin glasses can be found in Ref. [BY86b].

1.2.5. Rivaling spin-glass pictures

In this section we will briefly discuss different working hypotheses, often called "pictures", according to which low-dimensional spin glasses are usually tried to be described. Most important are the 'replica symmetry breaking' (RSB) [Par79, Par80] and the 'droplet' picture [McM84b, FH86, BM87a]. But also the 'trivial non-trivial' (TNT) [KM00, PY00] and the 'sponge' picture [HM00] were introduced. None of these are proved to give the accurate description for spin glass models below their upper critical dimension and it is a long standing debate about which of them is most promising. Tests concerning their correctness have predominantly been done numerically – but on the other hand the theories behind the pictures are only asymptotically correct. Thus, it might also be that none of them is valid and a completely new approach is needed.

Being analytically tractable, but far from easily understandable, the mean-field model of the Ising spin glass has been solved by Parisi [Par79, Par80]. Only in the year 2003 it was rigorously proved by Talagrand [Tal03] that Parisi's solution is actually correct. However, the solution implies that there is a vast abundance of metastable states the system can be in. Thus, the spin glass is of a completely different nature than the ferromagnet. Even worse, it is not known how these states are related to each other at all. Only the structure of phase space is known to be organized hierarchically and thus building an ultrametric space [MPS$^+$84]. At least nomenclature gives us a name at hand, so that we knowingly speak about the abstract 'replica symmetry' being broken at the spin-glass transition. Consequently, this solution is called replica-symmetry-breaking (RSB) solution. Besides, due to the lack of any symmetry in the spin-glass phase the introduction of the concept of replica symmetry can be regarded as some kind of auxiliary symmetry. It is introduced to simplify the calculation of the free energy, cf. Eq. (1.5). The disordered system requires a configurational average $[\ln Z(\{J_{ij}\})]_{\text{av}}$ which is very complicated to evaluate. The so called *replica trick* facilitates the calculation by using the identity

$$[\ln Z(\{J_{ij}\})]_{\text{av}} = \lim_{n \to 0} \frac{[Z(\{J_{ij}\})^n]_{\text{av}} - 1}{n} . \qquad (1.18)$$

A subtle point here is, that one always thinks of n being a natural number standing for some replicas. At the end of the calculation, however, the limit $n \to 0$ needs to be taken. The replica symmetry is only broken for $n < 1$! To cut a long story short, this turns out not to be a problem, at least in the mean-field region.

Inspired by the replica method an order parameter used in numerical treatment is defined by

$$q = \frac{1}{N} \sum_i \mathbf{S}_i^{(1)} \mathbf{S}_i^{(2)} , \qquad (1.19)$$

where two identical copies $\{\mathbf{S}_i^{(1)}\}$ and $\{\mathbf{S}_i^{(2)}\}$ of just one system with coinciding interaction variables are considered. q is commonly called the overlap order parameter and measures the similarity between two spin configurations. Applied to a ferromagnet the overlap distribution looks like $P(q) = 0.5\,[\delta(q - q_0) + \delta(q + q_0)]$ in the thermodynamic limit. At $T = 0$ we have $q_0 = 1$ due to the normalization in Eq. (1.19) – this expresses that the system
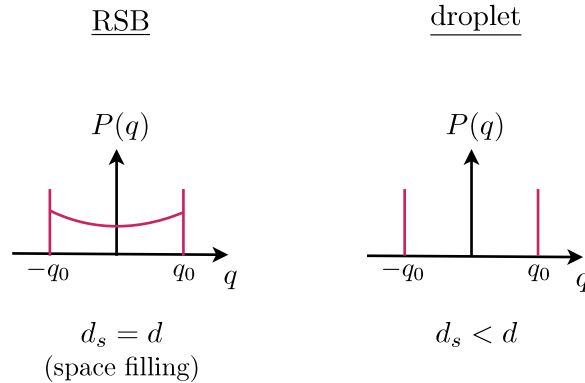
Figure 1.4.: The two most prominent spin-glass pictures describing properties of systems in low lattice dimensions. The order parameter distribution function $P(q)$ is a continuous function on $-q_0 < q < q_0$ with two δ-peaks at $q = q_0 = \pm 1$ in the RSB picture (left panel), as it actually is the case in the mean-field (SK) model. Furthermore, the domain-wall is supposed to be space-filling. The droplet picture (right panel), on the other hand, expects the order-parameter probability distribution function to mimic the one of a simple ferromagnet for dimensions lower than the upper critical dimension. Droplet excitations have a fractal dimension d_s lower than the space dimension d.

can only be in two distinct states (all spins up or all spins down for the Ising model), cf. Fig. 1.4. At $T > T_{SG}$ $q_0 = 0$ – the system takes on all configurations. Increasing T from zero to T_{SG} we will see a declining value of q_0. For all temperatures the system is in a replica symmetric phase.

The RSB picture of the mean-field spin-glass phase predicts a 'full replica symmetry breaking' (full-RSB). It can be imagined best with having a look at 'one-step replica symmetry breaking' (1-RSB) first, where there are many free energy valleys which are equidistant in phase space. Usually the valleys are not correlated and $P(q)$ looks like the one of the ferromagnet with an additional peak at $q = 0$. 1-RSB is exact for the random-energy model [Der80, MPV87] and believed to take place in structural glasses.

Breaking the symmetry more than once and eventually infinitely often results in the full-RSB picture. Then low lying valleys are correlated and $P(q)$ is described by a continuous function on $-q_0 < q < q_0$ and the two peaks known from the ferromagnet at $q = \pm q_0$, cf. Fig. 1.4.

Further predictions of the RSB picture concern the behavior of the system under perturbation, or inducing defects as large as the system itself. Let us briefly look at this topic. If a defect of such kind does not cost any energy (in the thermodynamic limit) the spin-glass phase is believed to exist only at zero temperature. Already the slightest perturbation destroys the spin-glass order. Vice versa, if a defect can only be introduced at the expense of an infinitely large amount of energy the spin-glass phase is stable also at finite temperature. The border-line case is a finite cost for inducing a defect. In a numerical treatment the thermodynamic limit is not available. Finite-size scaling assumptions, however, predict the

scaling of the energy of a defect according to [BM84]

$$E_{\text{def}} \sim L^\theta \ , \tag{1.20}$$

where θ is known as the domain-wall stiffness exponent and L is the linear system size. E_{def} is usually called *defect energy* and characterizes the ground-state energy difference between a system before and after having introduced a defect. Coming back to the just introduced classification a negative value of θ indicates a defect of zero cost in the thermodynamic limit, so that $T_{\text{SG}} = 0$. A positive one indicates $T_{\text{SG}} > 0$ and $\theta = 0$ is the border-line case with $T_{\text{SG}} \geq 0$, respectively.

Whatever value θ might have – in the Ising model (with spin-space dimension $m = 1$, i.e. an up/down symmetry) a defect introduces a domain-wall into the system. This is a line encircling the area of excitation when comparing the system before and after introducing a defect. Domain walls are assumed to have a fractal dimension $d - 1 \leq d_s \leq d$. The RSB picture predicts a space-filling domain-wall, i.e. its fractal dimension d_s coincides with the space dimension d of the system. As a look ahead, the concept of the defect energy is also used in terms of spin-glass models with larger dimensions of spin space $m > 1$. However, it is not obvious there how to understand a "domain-wall" which is smeared out in these cases. Also the value of d_s is not obviously limited by the above inequality.

Using the RSB solution to try to elucidate the nature of the spin-glass phase in the more relevant lower lattice dimensions, i.e. especially lower than the upper critical dimension, is done by the replica-field theory. The concept of RSB would carry over then [MP00, MP01]. However, it is vibrantly debated whether the RSB picture is correct for low dimensional spin glasses, since technical difficulties (divergencies) arise as the upper critical dimension is reached. Thus, starting out from the mean-field model, the RSB picture did not succeed up to now to give an unambiguous description of low-dimensional spin glasses. A long standing rival of the RSB scenario is the phenomenological droplet picture [McM84b, FH86, BM87a]. It arises from an ansatz for the scaling of low-lying large-scale-droplet excitations [FH86], rendering the spin glass to nothing more than a ferromagnet in disguise, also with merely two states. Replica symmetry would be regained in that case. Furthermore, a low-dimensional spin glass should not exhibit a phase transition in a field in analogy to the ferromagnet. Due to that the debate between supporters of each of the two pictures has often concentrated on deciding about the existence of an de Almeida-Thouless (AT) line [AJKT78], see e.g. Ref. [KLY09]. This line represents the transition line from a replica symmetric[4] to a spin-glass phase with broken replica symmetry in the presence of a magnetic field, cf. Fig. 1.5. This scenario takes place for the SK spin-glass model with finite spin-space dimension. Accepting the RSB solution in the mean-field region, any attempt to write down a replica symmetric solution in the spin-glass phase must fail. Unfortunately, a similar attempt below the upper critical dimension does fail, too. However, there is a suggestion [Moo05] that this failure can be lifted. Nevertheless, the calculation would be tough and is already being attacked in Ref. [Tem06].

---

[4]Sometimes this phase is called 'paramagnetic'. This is, however, a bit imprecise since the magnetic field h creates a certain polarization. In any case it is a replica symmetric phase.
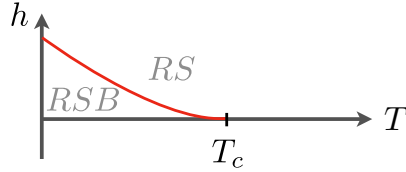
Figure 1.5.: The de Almeida-Thouless (AT) line (solid red) represents the transition line from a replica symmetric (RS) to a spin-glass phase with broken replica symmetry (RSB) in the presence of an external magnetic field h. Its existence is intimately connected to the question of whether the RSB or droplet picture is more suitable, or even correct, for low dimensional spin-glass models.

Droplets are localized clusters of spins which are assigned a characteristic radius r with energies scaling as $r^{\theta_{\mathrm{drop}}}$ with a characteristic exponent θ_{drop}. In this framework the scaling is predicted to equal the scaling of the domain-wall defect energy, i.e. $\theta_{\mathrm{drop}} = \theta$, cf. [HM00]. θ as well as d_s are not explicitly calculated within this theory. But at least it is predicted that $d_s < d$, i.e. it is not space-filling as in the RSB picture. Furthermore, according to the droplet picture the probability distribution function $P(q)$ of the order parameter should resemble the one of the ferromagnet, cf. Fig. 1.4. The RSB picture on the other hand predicts the dissimilarity between the characteristic exponents of the droplet scaling and the defect energy scaling, i.e. $\theta \neq \theta_{\mathrm{drop}}$[HM00].

The core information about the RSB and droplet picture is summarized in Fig. 1.4. A nice overview of various spin-glass pictures is given in [NS03]. Many references in there provide fast access to an in-depth study.

Summarizing the knowledge of spin glasses in finite space dimensions with short-range interactions, many things have been tried, nothing is known for sure. Most regarded are the RSB and the droplet picture. Perturbative expansions of the former have been tried to provide insight into the physics of spin glasses below their upper critical dimension d_u. In other words, the properties of finite dimensional models are tackled started out from $d = \infty$. This approach seems problematic.

Up to now we were only considering the dimensionality of the space in which the lattice is embedded. The spins themselves were embedded in a one-dimensional space, i.e. they are endowed with an $\mathrm{O}(m = 1)$ symmetry. In the next section, though, we will see that it can make sense to also alter the spin-space dimension m. Thus, from this point on, it is very important not to confuse the spatial dimension d and the rotational spin-space dimension m. The spins are then endowed with a general $\mathrm{O}(m)$ symmetry. We will first discuss finite spin-space dimensions in the next section and discuss the limit $m \to \infty$ in section 1.4.

1.3. Vector spin glasses

The simplicity of the Ising model made it be used a significant number of times in numerical simulations. It is, however, endowed with a strong anisotropy (only directions up and

down) and does therefore not really cover all spin-glass materials. It appears more natural to employ a vector model, since magnetic interactions tend to be nearly isotropic. At least the magnetic anisotropy is much weaker than the (RKKY) exchange interaction. E.g. the Heisenberg model with $m = 3$ spin-space dimensions seems more appropriate in that light [Kaw10], where spins are embedded in a space with continuous symmetry.

Whichever finite $m > 1$ is used – the most important step is done by getting rid of the strong-anisotropy limit which lets the lower critical dimension d_l increase. Unfortunately, both analytical work as well as numerical simulations are still very hard in low lattice dimensions. One of the attempts to calculate the lower critical dimension for $m > 1$ (but finite) is in Ref. [BM79]. Infrared divergences occurred using perturbation theory yielding a break-down of the expansion for the order parameter in dimensions $d \leq 4$. The conclusion was that $d_l = 4$ for m-vector spins with $1 < m < \infty$. Using the replica method also here the problem of the analytic continuation of $n \to 0$, cf. (1.18), is debated by the authors themselves. In their paper they also suggest $d_l = 4$ to be the lower critical dimension of the Ising spin glass ($m = 1$). At those times this prediction was in accord with other analytical [FH77] and numerical [BM77] work. By now, the lower critical dimension for vector spin glasses with $1 < m < \infty$ is accepted to be approximately 3 [KR05]. Recalling the meaning of this dimension we expect a finite temperature phase transition to occur for dimensions higher or equal to 3. For a closer look at the XY model ($m = 2$) we refer to, e.g., [PY08] and to [VK09, CCAMM+06, FMMPG+09] for the Heisenberg model ($m = 3$). However, it is not ultimately known whether the lower critical dimension depends on the number of spin components for general m.

The above mentioned vector spin-glass models are very hard to tackle. A whole lot of elaborate tools and instruments have been developed over years [HN96, THT04, WG06, Wei07, BNJ08]. They are needed especially to overcome problems with the extreme rugged free energy landscape.

Instead of playing tricks at a certain fixed spin-space dimension m one can use the observation of an intriguing successive simplification of phase space which takes place if the dimensionality of spin space is increased. Accordingly, the Ising model turns out to be hindered most by a pronounced metastability in the system. Metastability reduces every time m gets larger. A sketch is shown in Fig. 1.6. This is the reason for numerical simulations to allow for bigger system sizes the larger m is, cf. e.g. Ref. [HPV08] for the Ising spin glass (with $L \leq 28$ in $3d$) and Ref. [VK09] for the Heisenberg model (with $L \leq 32$ in $3d$). The simplification of phase space leads us to the limit of infinitely many spin-space dimensions discussed in the next section.

1.4. Vector spin glasses in the infinite spin-component limit

As illustrated in Fig. 1.6, increasing the spin-space dimension m simplifies the (free) energy landscape. In the limit $m \to \infty$ the phase space exhibits no metastability anymore at all [BM81, MCM+86]. The ground-state is unique and easy to determine. This is the first virtue of the model. More precisely, for finite lattices at zero temperature spins condense into a
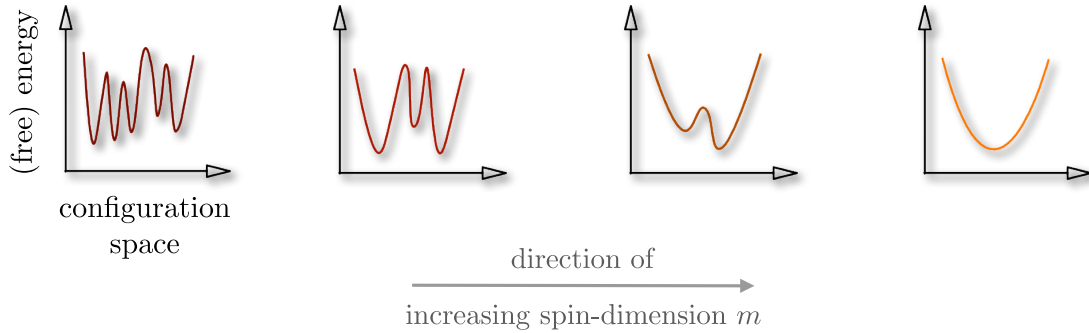
Figure 1.6.: The (free) energy landscape of a spin-glass system flattens out with increasing spin dimension m. For $m = 1$, the Ising model, it is most rugged. In the limit $m \to \infty$ all metastability has vanished and the ground state is unique.

finite dimensional subspace in spin space with $m_0 < m$ spin dimensions [Has00, Cha08]. As a consequence, for each system size (and disorder realization) there exists a finite critical number m^* of spin components above which the ground-state energy does not change upon further adding spin dimensions, such that the system effectively describes the limit $m \to \infty$. This fact is used in numerical calculations where finite systems of size N are considered with spins of dimension $m \geq m^*(N)$. Compared to the field theoretic calculations [GBM82, Via88], this corresponds to an interchange of the limits $N \to \infty$ and $m \to \infty$, so that the thermodynamic limit $N \to \infty$ is taken first in the perturbative calculations, whereas the infinite-component limit $m \to \infty$ is taken first in the numerical approach. This leads to some subtleties and the numerical approach might be considered the zeroth-order term in a $1/m$ expansion around the field-theoretic calculation [LY05].

There is a rigorous upper bound on the number of spin components beyond which no further change in the ground-state energy is observed [Cha08],

$$m_{\max}(N) = \left\lfloor \left(\sqrt{8N+1} - 1\right)/2 \right\rfloor \sim N^{\mu}, \ \mu = 1/2 \ , \qquad (1.21)$$

where $\lfloor x \rfloor$ stands for the largest integer smaller than or equal to x. For the SK model it was predicted that the average number of occupied spin dimensions m_0 scales in the ground state with system size with an exponent $\mu = 2/5$ [Has00]. E.g. in [AM04] this has been supported by Aspelmeier and Moore numerically. Lowering the connectivity, e.g. considering short-range nearest-neighbor models on hypercubic lattices, or tuning up the power-law exponent σ in the 1d power-law model, on the other hand, spins require only a somewhat smaller number of spin components, with $\mu \leq 2/5$ [LY05], with μ being a function of the lattice dimension d or the power-law exponent σ. This situation allows for the limit of an infinite number of spin components to be studied numerically for finite systems using only a finite number of spin components, for instance determining the lower critical dimension

from defect-energy calculations. Previously reported results [LY05, MCM$^+$86], however, did not reach up to the lattice dimensions above the apparent lower critical dimension $d_l \geq 6$ – to be discussed below – where an ordering effect would be expected at finite temperatures. According to the scaling behavior (1.21) the ratio $m_0/N \sim N^{-(1-\mu)}$ vanishes as $N \to \infty$, such that the nature of a ground state in the $m \to \infty$ model compared to the usual Bose-Einstein condensation with one unique ground state becomes indistinguishable. That is why the condensation of spins into an m_0-dimensional spin space is referred to as a *generalized* Bose-Einstein condensation.

Compared to models with finite m like Ising ($m = 1$), XY ($m = 2$) or Heisenberg ($m = 3$) models there is a second important virtue. The latter models show the existence of RSB in their mean-field version. The (undesirable) effect is that the order parameter splits up into an infinite number of values and mutates to a function defined over an interval of real numbers. Thus, the spin glass ordered state breaks spontaneously the replica symmetry. The $m \to \infty$ model does not. It is replica symmetric [AJKT78] irrespective of the lattice dimension or range of interactions, from the long-range SK to the short-range EA version. The order parameter remains a single number. After all, this fact makes an analytical treatment easier for mean-field calculations as well as for arbitrary lattice dimensions. There is hope that results gained may be extended in a $1/m$ expansion to the more natural spin-glass models having a finite number of spin dimensions m, cf. Ref. [AM04]. This would be an interesting alternative to the perturbative expansion of replica-field theory, mentioned in Sec. 1.2.5, where $d = \infty$ is the starting point. A picture which possibly makes the vast abundance of spin-glass models more comprehensible is given in Fig. 1.7. With it we will briefly fix some name conventions now. Whenever we refer to an 'Ising', 'XY', 'Heisenberg' or $m = \infty$ model we mean nothing else than a model with spin dimension $m = 1, 2, 3$ or ∞. Analogously, for the hypercubic lattice dimension we will refer to models with $1, 2, 3, \ldots$ dimensions and the SK model is always the fully connected model independent of the spin dimension[5].

Critical properties in the high temperature phase of the $m \to \infty$ model have been considered beginning in 1982. Using a field theory Hamiltonian the upper critical dimension has been determined to be $d_u = 8$ [GBM82]. The same value has been obtained for a perturbation expansion of the order parameter in the low-temperature phase [Via88]. The latter work contained also results indicating the equivalence of the upper and lower critical dimension, i.e. $d_u = d_l$. The fact that d_u is lifted compared to $m < \infty$ leads to a violation of hyperscaling even for dimensions smaller than d_u [GBM82]. The lower critical dimension is predicted to be $d_l = 6$ [GBM82].

Taking into account the two cornerstones of the $m \to \infty$ model, missing metastability and the replica symmetry, numerical treatment becomes a relatively easy task. At zero temperature we can do ground-state calculations with the help of straightforward methods. By means of treating the partition function by saddle-point methods, also finite temperature

---

[5]The SK model introduced in [SK75] was actually using Ising spins.
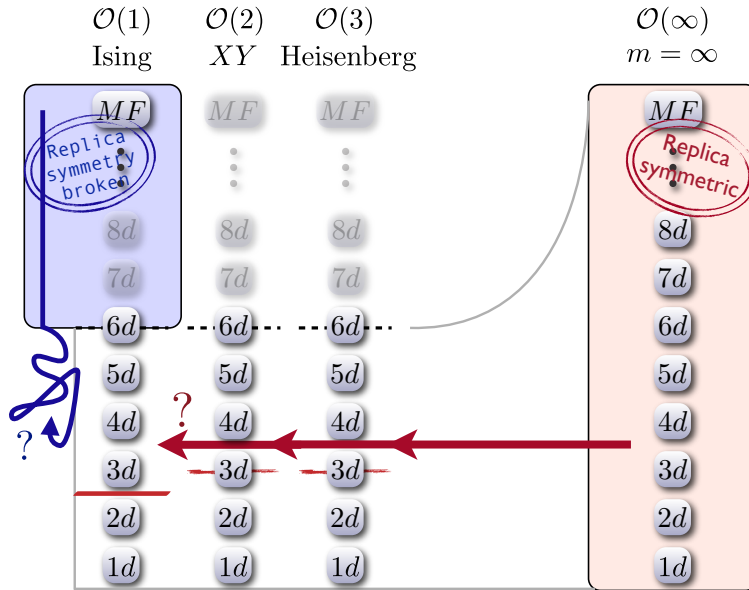
Figure 1.7.: An overview of different spin-glass models. From bottom to top the lattice dimension increases and the lower and upper critical dimensions are sketched in as red solid and black dashed lines, respectively. From left to right the spin-space dimension increases. d_l is believed to be 2.5 in the Ising model and roughly 3 at least for the XY and Heisenberg model. $d_u = 6$ for all models with $m < \infty$. A long standing question is whether low-dimensional spin glasses break the replica symmetry or not. Replica-field theory (the blue tangled up arrow) runs into problems for dimensions $d < d_u$. The hope is to infer sound physical results when starting out from the replica symmetric limit $m \to \infty$ on low-dimensional spin-glass models (large red arrow) by means of $1/m$-expansions or other approaches.

calculations can be done in a very convenient way [BM82]. Precise discussions will follow in the corresponding chapters, cf. Chap. 3 and 4.

1.5. The program of the thesis

As we saw in the last sections the spin-glass model in the infinite component-limit does have some remarkable simplifications compared to models with finite spin dimension m. Metastability does not exist and the model is replica symmetric irrespective of lattice dimension or interaction range. Apart from the interest in the model in itself, we might be able to use it as a starting point in order to elucidate properties of the more natural low dimensional spin-glass models with finite spin-space dimension. We can have in mind a picture like Fig. 1.7 in order to gather thoughts.

First, of course, we need to understand the nature and properties of the replica symmetric $m \to \infty$ model. This is the key issue of the present thesis. After introducing different

flavors of the spin-glass Hamiltonian suited to the Edwards-Anderson, the Sherrington Kirk-patrick and the 1d power-law model we will discuss the phase diagram and critical behavior expected for the $m \to \infty$ model in chapter 2. Similarities and differences to vector models with finite numbers of spin dimensions m will be highlighted. Particular emphasis will be put to finite-size scaling assumptions, especially above the upper critical dimension, as already published in [BWM12].

Ground-state calculations have been found useful long time ago. The ordering properties of the infinite-component spin-glass model will be analyzed in chapter 3 for all geometries introduced in chapter 2 before. Missing metastability allows for relatively large system sizes, enhancing the quality of our finite-size scaling analyzes. Various aspects at $T = 0$ are considered and with the help of defect-energy calculations we will be able to give estimates of the upper and lower critical exponents (σ_u and σ_l) of the 1d power-law model (Sec. 3.2) and the lower critical dimension d_l of the hypercubic model (Sec. 3.3), respectively. Concerning the hypercubic model many passages have been published as a journal article already in [BW11]. Most of the results of this thesis have been published in [BWM12] in terms of the 1d power-law model.

We will show in chapter 4 that in the course of a saddle-point analysis of the partition function of the spin glass in the infinite component-limit $m \to \infty$, a set of equations originate which can be solved iteratively to gain insight into numerous properties and quantities at finite temperature. We will give a full account of the saddle-point approximation and suggest a novel way to calculate the spin-glass susceptibility and the order parameter of the model. All numerical techniques will be described in detail. Various critical exponents and temperatures are calculated and compared to the predictions of chapter 2. Many passages concerning the results have been published in [BWM12].

Having made conclusive progress in the infinite component-limit $m \to \infty$, we suggest to use the knowledge about the model in order to gently move back to finite spin-space dimensions m in chapter 5. This will be exemplified with a Heisenberg model ($m = 3$) the spin-space of which is linked up to an auxiliary spin-space enlarging the effective spin-space to the limit $m \to \infty$. We adjust the Hamiltonian such that a single parameter κ controls the energy penalty for using the auxiliary dimensions, effectively introducing an anisotropy into the model. Amazingly, κ enables one to continuously tune the metastability in the model. This approach might facilitate future research of low-dimensional finite-m vector spin glasses. Various techniques will be described to use this model numerically. They will be tested on a Heisenberg model. Finally, we will propose a novel algorithm to elucidate the low-temperature properties of low-m spin glasses similar to a well-known one.

Sliding further down towards finite spin dimensions we revisit real-space renormalization-group calculations in chapter 6. With these it has not been possible to determine the (assumingly) correct lower critical dimension d_l of finite-m vector spin glasses. We adopt the approach for the ferromagnet and investigate the renormalization procedure for a spin glass.

With it we are able to determine the correct value of d_l and also other quantities. Calculations are done both analytically and numerically. Results are compared to each other and to former ones.

Each one of the chapters mentioned above will be ended by a section summarizing the results. A coarse summary of the content and an outlook concludes the thesis in chapter 7.

Chapter 2.

The models

As indicated in Chap. 1 we have a variety of different models to investigate. In the current chapter we want to go into more detail concerning the short-range Edwards-Anderson, the long-range Sherrington-Kirkpatrick and the long-range 1d power-law models. The first and second have been studied extensively to understand the spin-glass problem. The third one, on the other hand, attracted interest only recently again, since it is capable of simulating spin-glass systems in different universality classes with relative ease. Due to that it will be the focus of the discussion in the present chapter. Some of the models will be found to be equivalent to each other in certain limits. Attention is paid to the choice of couplings for all models considered and each time the notation of the Hamiltonian will be adjusted slightly. We will discuss finite-size scaling issues and compare properties of vector spin-glass models with $1 < m < \infty$ and $m \to \infty$. This chapter also states predictions for the scaling behavior and prepares us for doing the numerical work in the following chapters.

2.1. The general model

We study flavors of the well-known Edwards-Anderson Hamiltonian

$$\mathcal{H} = -\frac{1}{2} \sum_{\substack{i,j=1 \\ i \neq j}}^{N} J_{ij} \, \mathbf{S}_i \cdot \mathbf{S}_j \,, \tag{2.1}$$

where the $\mathbf{S}_i \in \mathbb{R}^m, i = 1, \ldots, N$, are vector spins with m components, normalized as $|\mathbf{S}_i| = \sqrt{m}$. To avoid confusion, the sum runs over all i and j for now. Below, we will refine the definition of the model and always adjust the notation of the Hamiltonian according to the range of interactions J_{ij} to be specified and the dilution.

2.2. The hypercubic model

For the hypercubic version of our classical spin-glass model, we choose the couplings to be short-ranged by restricting them to nearest-neighbor sites. Thus we adjust the notation of the Hamiltonian the first time and have

$$\mathcal{H} = -\sum_{\langle i,j \rangle} J_{ij} \, \mathbf{S}_i \cdot \mathbf{S}_j \,. \tag{2.2}$$

The exchange couplings $J_{ij} \in \mathcal{N}(0,1)$ are drawn independent of each other from a Gaussian probability distribution with zero mean and unit standard deviation. It was mentioned in the beginning that we cannot access large linear system sizes L, especially for high lattice dimensions d. one runs into severe problems concerning the accessibility of large linear lattice sizes L in high dimensions. Finite-size corrections, however, depend on the *linear* extension of the lattice. One should keep that in mind if one sets out to determine properties like the lower critical dimension d_l, which is expected to be between $d = 6$ [GBM82] and $d = 8$ [Via88] for the $m \to \infty$ model. Older attempts to numerically determine d_l [LY05, MCM$^+$86] did not reach up to the lattice dimensions above the apparent lower critical dimension, where an ordering effect would be expected at finite temperatures.

2.3. The 1d power-law model

Apart from the hypercubic lattices we will also consider a model with spins being organized in an effectively one-dimensional (1d) geometry. It is either chosen to be a chain with periodic boundary conditions or a ring as depicted in the left panel of Fig. 2.1 and the Hamiltonian is given by Eq. (2.1). In this fully connected version the exchange interactions are between all spin pairs, decaying as a power law with distance,

$$J_{ij} \sim \frac{\varphi_{ij}}{r_{ij}^{\sigma}} \; , \tag{2.3}$$

where $r_{ij} = |\mathbf{r}_i - \mathbf{r}_j|$ and φ_{ij} is a (usually) Gaussian random variable of zero mean. The exact form of the variables J_{ij} will be given below. A diluted version of the model will be introduced as well, where the interaction constants do not depend on distance. A relation to hypercubic lattices will only be known due to analogies of the (hypercubic) lower and upper critical dimension (d_l and d_u) with corresponding critical upper and lower power-law exponents σ_u and σ_l. Note the somehow awkward notation in the correspondences $d_l \leftrightarrow \sigma_u$ and $d_u \leftrightarrow \sigma_l$. They come about due to the fact that increasing d corresponds to lowering σ.

For the case of Ising spins ($m = 1$) [KAS83, BMY86, Leu99, KY03, KY05, LPRTRL08, KLY09] and, more recently, Heisenberg spins ($m = 3$) [VK10, SY11b, SY11a], this model has been extensively investigated. It is found that, as the range of interactions is tuned by varying σ, the model has a behavior which mimics that of the short-range spin glass as its dimension d is tuned. For large σ the spin-glass transition temperature $T_{\mathrm{SG}} = 0$. This corresponds to dimensions below the lower critical dimension d_l. A non-mean-field regime is adjacent at intermediate σ continuing on to a mean-field region for small σ, which corresponds to the dimensions above the upper critical dimension, d_u. For $\sigma \to 0$ the interaction constants J_{ij} are independent of r. Choosing a suitable proportionality constant depending on the number N of spins in the system for Eq. (2.3) lets us recover the Sherrington-Kirkpatrick model [SK75] if considering the fully connected model. The phase diagram of the model as a function of σ is shown in Fig. 2.2, and will be discussed in more detail below. A dictionary can be set up relating the behavior of the 1d power-law model at a given σ and a corresponding short-range model on hypercubic lattices of dimension d
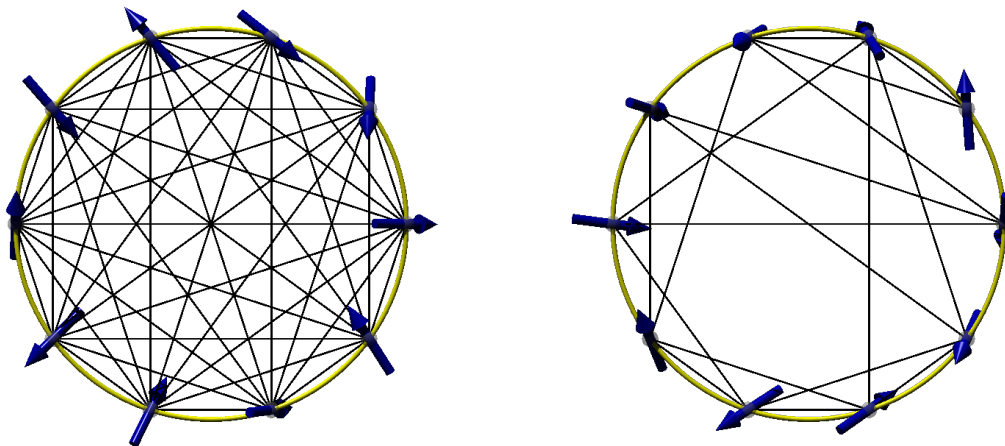
Figure 2.1.: (Color online). The 1d power-law spin-glass model on a ring geometry. The left panel shows the fully connected version where the magnitude of the interaction strength falls off with distance. The right panel shows the diluted model with the bond existence probability falling off with distance, whereas the bond strengths are distance independent.

[LPRTRL08, KLY09]. We shall see here that for the limit of an infinite number m of spin components, the phase diagram is modified as shown in the lower part of Fig. 2.2.

Choice of couplings

We studied the 1d power-law model in different variants and on different geometries as described in the next three subsections.

2.3.1. Fully connected version

The fully connected system implied by Eq. (2.1) is realized with interaction constants

$$J_{ij} = c(\sigma, L) \frac{\varphi_{ij}}{r_{ij}^\sigma} \, , \tag{2.4}$$

where $\varphi_{ij} \in \mathcal{N}(0,1)$ are random variables drawn from a Gaussian distribution with zero mean and standard deviation unity. It is the strength of interactions that falls off as $1/r^\sigma$ here. The mean-field transition temperature,

$$\left[T_{\mathrm{SG}}^{\mathrm{MF}}(c)\right]^2 = \frac{1}{L} \sum_{\substack{i,j=1 \\ i \neq j}}^{L} \left[J_{ij}^2\right]_{\mathrm{av}} = \frac{c(\sigma, L)^2}{L} \sum_{\substack{i,j=1 \\ i \neq j}}^{L} \frac{1}{r_{ij}^{2\sigma}} \, , \tag{2.5}$$

diverges for $\sigma \leq 1/2$, unless we prevent this by an appropriate L dependent choice of the normalization factor $c(\sigma, L)$, for instance by requiring that

$$T_{\mathrm{SG}}^{\mathrm{MF}}(c) \overset{!}{=} 1 \, , \tag{2.6}$$
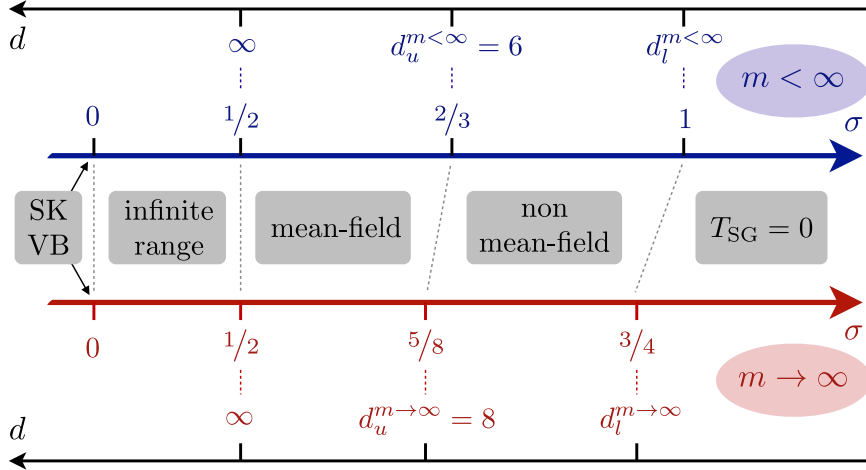
Figure 2.2.: (Color online). Correspondence between the 1d spin-glass model with power-law interactions characterized by an exponent σ and the short-range model on hypercubic lattices of dimension d. The upper part of the figure applies to finite spin dimensions m, whereas the lower part describes the limit $m = \infty$ discussed here. Increasing σ corresponds to decreasing the analogous lattice dimension d. We use the notation of correspondences $d_l \leftrightarrow \sigma_u$ and $d_u \leftrightarrow \sigma_l$.

which fixes $c(\sigma, L)$. While this is only strictly necessary for $\sigma \leq 1/2$, we apply the same normalization for all σ. Clearly, the limit $\sigma \to 0$ corresponds to the SK model. In fact, it can be shown that mean-field theory is exact (at any temperature) for all $\sigma \leq 1/2$ [Mor11]. For numerical simulations employing single-spin manipulations, this fully connected model is slow as the number of bonds equals $L(L-1)/2$, so that the cost of a lattice sweep of updates scales quadratically with the system size L.

2.3.2. Bond-diluted version

To improve on this costly update for the fully connected model and allow numerical studies to get closer to the large system limit, studies have been made of a diluted version of the 1d power-law spin glass [LPRTRL08]. Its Hamiltonian reads

$$\mathcal{H} = -\frac{1}{2\sqrt{z}} \sum_{\substack{i,j=1 \\ i \neq j}}^{L} \varepsilon_{ij} J_{ij} \mathbf{S}_i \cdot \mathbf{S}_j , \qquad (2.7)$$

where now $J_{ij} \in \mathcal{N}(0, 1)$, but the probability distribution of the dilution variables $\varepsilon_{ij} \in \{0, 1\}$ falls off with the distance r_{ij} as

$$\varepsilon_{ij} = \begin{cases} 1, & p < p_{ij} , \\ 0, & \text{otherwise} , \end{cases} \qquad (2.8)$$

$$p_{ij} \sim r_{ij}^{-2\sigma} , \qquad (2.9)$$

with $p \in \mathcal{U}[0,1]$ a uniform random number from the interval $[0,1]$. To ensure that the form of p_{ij} is a proper probability density function, we normalize [KLY09]

$$p_{ij} = 1 - \exp(-A/r_{ij}^{2\sigma}) , \qquad (2.10)$$

and determine A by fixing the *average* coordination number

$$z = \sum_{i=1}^{L-1} p_{iL} . \qquad (2.11)$$

Unless stated otherwise we used $z = 12$ for the numerical data discussed here. This corresponds to a hypercubic lattice dimension $d = 6$, which might be the lower critical dimension[1] d_l [GBM82].

The usual Newton method [FTVP07] in A can be employed in order to iterate the probabilities p_{iL} until their sum equals the desired coordination number to a certain precision. The factor $1/\sqrt{z}$ in Eq. (2.7) ensures that $T_{\mathrm{SG}}^{\mathrm{MF}} = 1$, consistent with the fully connected model. This diluted version of the model was previously studied for the Ising [KLY09], Heisenberg [SY11b, SY11a] and p-spin [LKMY10] spin-glass models. On theoretical grounds, it is expected that the fully connected and diluted models exhibit the same universal behavior [LPRTRL08]. We shall see below, however, that for large $\sigma > 1$, significant deviations from the fully connected model can be observed. Apart from universality considerations also certain other quantities (sample to sample fluctuations) differ for $\sigma < 1/2$, as will be shown below. Note that here the infinite-range limit $\sigma \to 0$ corresponds to the Viana-Bray model [VB85]. Numerically, the diluted system with $zL/2$ bonds reduces the sweep time from quadratic to linear in L.

In Tab. 2.1 we give a visual impression of the hypercubic and the 1d power-law model in its diluted version. For the latter we encounter a fixed average coordination number z. A low (hypercubic) dimension corresponds to high bond existence probabilities for spins being spatially close together, cf. Tab. 2.1, e.g. $d = 2$ and $\sigma = 1$. Otherwise, for high (hypercubic) lattice dimensions the bond existence probabilities for spins far apart becomes large, cf. Tab. 2.1, e.g. the mean-field case (MF) and $\sigma = 0.1$.

The spatial differences of the models are also reflected in the structure of the interaction matrices J_{ij}. Tab. 2.2 gives an impression of their occupancy, which, of course, depends on the storage organization used. Below we will see that there is a range of σ for which an effective lattice dimension d_{eff} can be specified.

2.3.3. Choice of geometry

Two different effectively one-dimensional geometries have been considered in the past in studying power-law spin glasses: a ring of spins [KY03] as depicted in Fig. 2.1 and the possibly more natural linear chain with periodic boundary conditions without any embedding space [BY86a]. In the ring model, the distances are measured according to the Euclidean metric in the plane,

$$r_{ij}^{\circ} = \frac{L}{\pi} \sin\left(\frac{\pi|i-j|}{L}\right) , \qquad (2.12)$$

---

[1]Note that we do *not* bias the outcome towards $d_l = 6$ by this choice.
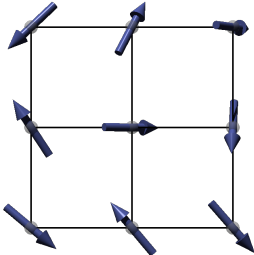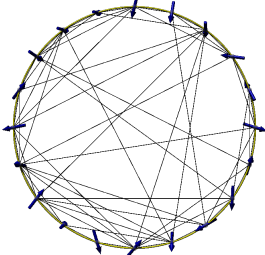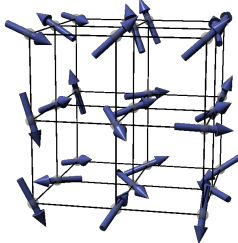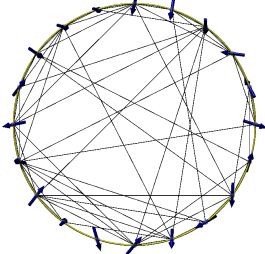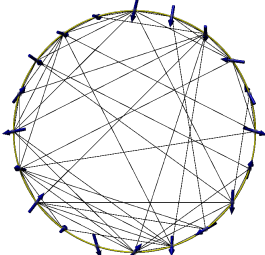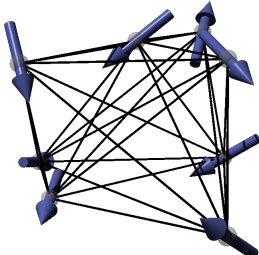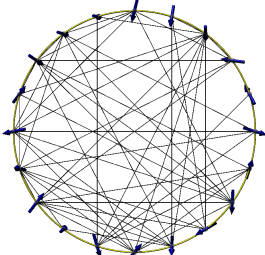
	hypercubic	**1d power-law (diluted)**	
2d			$\sigma = 1$
3d			$\sigma = 0.85$
–			$\sigma = 0.75$
MF			$\sigma = 0.1$

Table 2.1.: A visual impression of the hypercubic (left) and 1d power-law spin-glass model (right) in their geometrical appearance. Varying only the power-law parameter σ will tune the 1d power-law model through all possible behaviors from short-range (low-dimensional) models down to infinite-range (mean-field) models.

Despite the lower left panel showing a random geometrical structure the concept of distance is not existent in the mean-field case. All black lines between spins indicate interactions of arbitrary sign and strength not depending on any geometry. The according interaction-matrix occupancy is visualized in Tab. 2.2.

hypercubic	**1d power-law** (diluted, $d_{\text{eff}} = 3$)	**1d power-law** (diluted, $d_{\text{eff}} = 6$)
(a) $2d$ ($N = 121$)	(b) $\sigma = 1$ ($N = 128$)	(c) $\sigma = 1$ ($N = 128$)
(d) $3d$ ($N = 125$)	(e) $\sigma = 0.85$ ($N = 128$)	(f) $\sigma = 0.85$ ($N = 128$)
(g) $4d$ ($N = 81$)	(h) $\sigma = 0.65$ ($N = 128$)	(i) $\sigma = 0.65$ ($N = 128$)
(j) MF ($N = 128$)	(k) $\sigma = 0.1$ ($N = 128$)	(l) $\sigma = 0.1$ ($N = 128$)
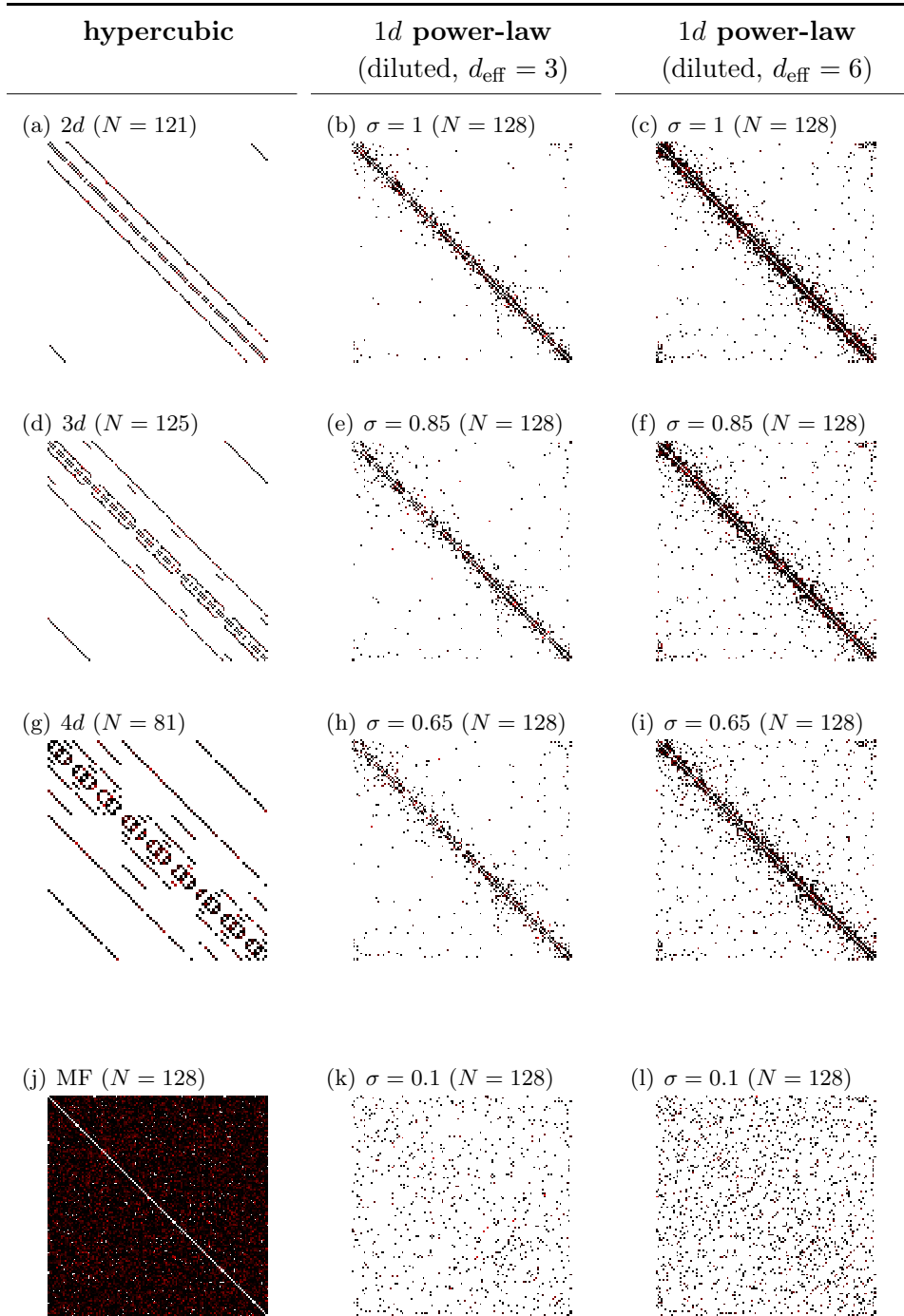
Table 2.2.: A visual impression of the interaction-matrix occupancy. All of the matrices are symmetric since $J_{ij} = J_{ji}$. The exact structure, however, depends on the ordering of neighbors and may thus differ from the shown one. In the left column the matrices for hypercubic lattices are displayed. The matrices for the diluted $1d$ power-law model are shown for effective dimension $d_{\text{eff}} = 3$ in the center column and for $d_{\text{eff}} = 6$ in the right one. Large values of σ (e.g. panels (b,c)) correspond to small effective lattice dimensions (a) and distances to interaction-neighbors are small. Small values of σ correspond to large lattice dimensions and interactions become system-wide. In the mean-field SK model (j) all spins interact with all others. The spin systems themselves are visualized in Tab. 2.1.

31
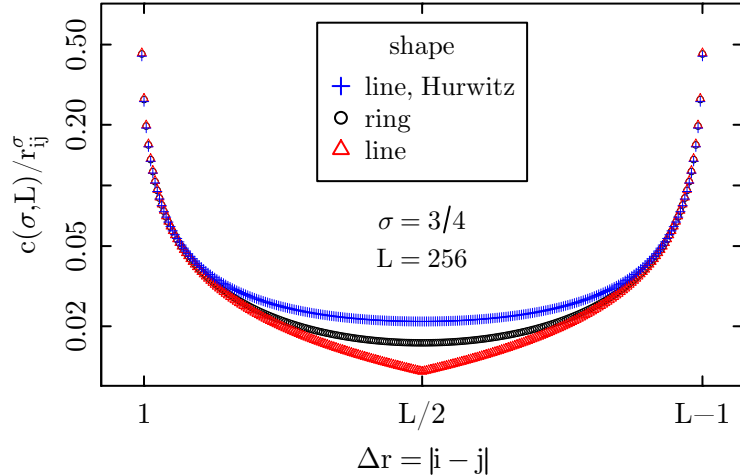
Figure 2.3.: (Color online). The non-random part $c(\sigma, L)/r^\sigma$ of the interaction constants in Eq. (2.4), i.e. for the fully connected model, for the line and ring geometries and the resummed (Hurwitz) version ($\sigma = 3/4$ and $L = 256$). Note the logarithmic scale of the ordinate.

and periodic boundaries are incorporated automatically. In the chain formulation, spins are located at integer positions i on a straight line with distances

$$r_{ij}^! = \min(|i - j|, L - |i - j|) , \qquad (2.13)$$

again assuming periodic boundary conditions. While one expects the specific form of the geometry to influence the finite-size behavior, in the limit of large distances on large chains or rings, both formulations become equivalent. Universal properties, of course, should not depend on these details. On the other hand, one might argue that finite-size corrections, which are notoriously important in the study of spin-glass systems, will differ between the two formulations and might thus lead to an effective advantage for one or the other form.

When studying long-range interactions one needs to be careful about defining a controlled approach to the thermodynamic limit. Using the periodic boundary conditions preferred to suppress boundary effects, each spin effectively interacts with an infinite set of periodic images. The resulting infinite sums are usually performed in reciprocal space (Ewald summation). For the fully connected one-dimensional chain, i.e. Eq. (2.13), they can be performed without cut-off. Summing over images for the couplings of Eq. (2.4) one

obtains the effective coupling

$$
\begin{aligned}
\tilde{J}_{ij} &= c(\sigma, L) \sqrt{\sum_{n=-\infty}^{\infty} \frac{1}{|r_{ij}^\shortmid + Ln|^{2\sigma}}} \; \varphi_{ij} \\
&= \frac{c(\sigma, L)}{|L|^\sigma} \sqrt{\sum_{n=-\infty}^{\infty} \frac{1}{|r_{ij}^\shortmid/L + n|^{2\sigma}}} \; \varphi_{ij} \\
&= \frac{c(\sigma, L)}{|L|^\sigma} \sqrt{\zeta\left(2\sigma, \frac{r_{ij}^\shortmid}{L}\right) + \zeta\left(2\sigma, 1 - \frac{r_{ij}^\shortmid}{L}\right)} \; \varphi_{ij} \;,
\end{aligned}
\tag{2.14}
$$

with the Hurwitz Zeta function [AS65]

$$
\zeta(s, q) := \sum_{k=0}^{\infty} \frac{1}{(k+q)^s} \;.
\tag{2.15}
$$

The corresponding mean-field critical temperature reads then

$$
\left[T_{\mathrm{SG}}^{\mathrm{MF}}(c)\right]^2 = \frac{1}{L} \sum_{i \neq j} \left[\tilde{J}_{ij}^2\right]_{\mathrm{av}} = c(\sigma, L)^2 \frac{1}{|L|^{2\sigma+1}} \times
$$

$$
\times \sum_{i \neq j} \left[\zeta\left(2\sigma, \frac{r_{ij}^\shortmid}{L}\right) + \zeta\left(2\sigma, 1 - \frac{r_{ij}^\shortmid}{L}\right)\right] \;,
\tag{2.16}
$$

which fixes $c(\sigma, L)$ for a certain normalization. We set $T_{\mathrm{SG}}^{\mathrm{MF}}(c) = 1$.

While for ferromagnetic systems summation over image "charges" is crucial, for a spin-glass system with average magnetization $\langle m \rangle = 0$ it should not change the asymptotic behavior [AF10]. Finite-size corrections, though, might be affected. To start with, Fig. 2.3 compares the non-random part of the interactions for the ring geometry as well as the bare and summed chain interactions. The differences away from $r = 0$ are small and, as we shall see below, the alterations of the FSS behavior are rather minor. Note that for the special case $\sigma = 1$ the constants $c(\sigma, L)$ for the ring and the summed line geometries coincide, which is easily understood from the identity [AS65]

$$
\zeta\left(2, r_{ij}^\shortmid/L\right) + \zeta\left(2, 1 - r_{ij}^\shortmid/L\right) = \frac{\pi^2}{\sin^2(\pi r_{ij}^\shortmid/L)} = \left(\frac{L}{r_{ij}^\circ}\right)^2 \;.
\tag{2.17}
$$

2.4. Phase diagram and critical behavior

To understand the expected critical behavior of the model in the $m = \infty$ limit, it is useful to review and generalize the results for the $m < \infty$ case. The most distinct feature of the $m = \infty$ limit on hypercubic lattices is the elevation of the upper critical dimension (UCD) to $d_u = 8$ and the accompanying violation of hyperscaling [GBM82].

2.4.1. Mean-field critical exponents

Recall that the mean-field exponents for a ferromagnet are, see above in Sec. 1.4,

$$\alpha = 0, \quad \beta = 1/2, \quad \gamma = 1, \quad \nu = 1/2, \quad \eta = 0 . \tag{2.18}$$

These satisfy hyperscaling (the Josephson scaling law)

$$d\nu = 2 - \alpha , \tag{2.19}$$

(only) at the standard UCD $d_u = 4$. For the ($m < \infty$) spin glass, the upper critical dimension is elevated to $d_u = 6$ [BY86b]. Assuming again that hyperscaling works at the UCD and that the fundamental exponents ν and η take their mean-field values, one infers

$$\alpha = 2 - d\nu = 2 - 6 \cdot \frac{1}{2} = -1 \tag{2.20}$$

and

$$\beta = \frac{(2 - \alpha) - \gamma}{2} = 1 , \tag{2.21}$$

so that the correct exponents of the SK model [BY86b] read

$$\alpha = -1, \quad \beta = 1, \quad \gamma = 1, \quad \nu = 1/2, \quad \eta = 0 . \tag{2.22}$$

Arguing in the same way for the $m = \infty$ limit with $d_u = 8$ [GBM82], one might conclude that $\alpha = -2$ and $\beta = 3/2$. This model, however, violates hyperscaling also in the non-mean-field regime, and the hyperscaling relation is replaced by the dimensionally reduced version

$$(d - 2)\nu = 2 - \alpha . \tag{2.23}$$

Therefore, mean-field exponents for the $m = \infty$ model are the same as those of the Ising spin glass i.e.

$$\alpha = -1, \quad \beta = 1, \quad \gamma = 1, \quad \nu = 1/2, \quad \eta = 0 . \tag{2.24}$$

2.4.2. Finite-size scaling above the upper critical dimension

To understand the behavior of the model in the mean-field regime, it is useful to recall the relevant form of scaling and finite-size scaling above the upper critical dimension (UCD). For a singular quantity A below the UCD the expected finite-size scaling form is [Pri90]

$$A \sim L^{\kappa/\nu} \mathcal{A}(L^{1/\nu} t), \quad d < d_u , \tag{2.25}$$

where $t = (T - T_c)/T_c$ is the reduced temperature and κ the critical exponent associated to A. This comes about due to finite-size corrections being dependent on the ratio $\xi_L/\xi_\infty \sim L t^\nu$ below the UCD. For a dimensionless quantity such as the correlation length normalized by the system size, we expect

$$\xi/L \sim \mathcal{X}(L^{1/\nu}t), \quad d < d_u . \tag{2.26}$$

At and above the UCD, FSS should hold with mean-field exponents with the role of the correlation length $\xi_L \sim L$ taken on by some effective length [Bin85, JY05] $\zeta_L \sim \ell \sim N^{1/d_u} = L^{d/d_u}$, such that

$$A \sim N^{\kappa/d_u\nu}\mathcal{A}(L^{d/d_u\nu}t), \quad d \geq d_u, \tag{2.27}$$

where ν and κ take on their mean-field values. Similarly, for the case of a dimensionless quantity, we arrive at

$$\xi/L^{d/d_u} \sim \mathcal{X}(L^{d/d_u\nu}t), \quad d \geq d_u. \tag{2.28}$$

We can therefore extend the hyperscaling law beyond its usual range of validity $d \leq d_u$ by replacing the correlation length exponent ν with a renormalized value

$$\nu' = \begin{cases} \nu, & d < d_u, \\ d_u\nu/d = d_u/2d, & d \geq d_u, \end{cases} \tag{2.29}$$

since then $d\nu' = 2 - \alpha$ in *all* dimensions. As a consequence, at $d = d_u$ we find

$$d\nu' = d_u/2 = 2 - \alpha, \tag{2.30}$$

leading to $\alpha = 0$ for $d_u = 4$ and $\alpha = -1$ for $d_u = 6$.

Comparing the critical scaling of the Landau-Ginzburg-Wilson (GLW) effective Hamiltonian for the one-dimensional long-range model and the short-range model in general dimensions d, one infers that close to the UCD one has [LPRTRL08]

$$d_{\text{eff}} = \frac{2}{2\sigma - 1} . \tag{2.31}$$

As we will see below, $\nu = 1/(2\sigma - 1) = d_{\text{eff}}/2$ in the mean-field region, such that $d/d_u = d_{\text{eff}}/d_u = \nu/3$ and $d/d_u\nu = 1/3$ and it follows from Eqs. (2.27) and (2.28) that

$$\chi_{\text{SG}} \sim N^{1/3}\mathcal{C}(tN^{1/3}), \tag{2.32a}$$

$$q_{\text{EA}} \sim N^{-1/3}\mathcal{Q}(tN^{1/3}), \tag{2.32b}$$

$$\frac{\xi}{L^{\nu/3}} \sim \mathcal{X}(tN^{1/3}). \tag{2.32c}$$

2.4.3. 1d long-range spin glass

The long-range Ising spin glass was discussed analytically in Refs. [KAS83, BMY86, FH88, Moo10]. In Ref. [EH85] it was proven rigorously that there is no phase transition for $\sigma > 1$. Studying the effective GLW Hamiltonian in replica space [KAS83], it was inferred that there is a finite-temperature phase transition for $1/2 \leq \sigma \leq 1$, which is of mean-field type for $1/2 \leq \sigma \leq 2/3$ and of non-mean-field type for $2/3 < \sigma \leq 1$. Therefore, the lower critical $\sigma_l = 2/3$ corresponds to the upper critical $d_u = 6$ for systems on hypercubic lattices and

similarly for the upper critical $\sigma_u = 1$ and the lower critical d_l. It is useful to set up a dictionary of correspondences between the 1d long-range model and the short-range models on hypercubic lattices, cf. Fig. 2.2. Arguments were given in Larson et al. [LKMY10] that the effective dimensionality for $2/3 \leq \sigma \leq 1$ was approximately given by [KLY09]

$$d_{\text{eff}} = \frac{2 - \eta(d_{\text{eff}})}{2\sigma - 1} \, , \tag{2.33}$$

where $\eta(d_{\text{eff}})$ is the exponent of the corresponding short-range model.

The upper critical $\sigma_u = 1$ can be inferred from the result [BMY86]

$$\theta_{\text{LR}} = 1 - \sigma \tag{2.34}$$

for the long-range defect energy exponent (see Sec. 1.2.5). Since $\theta_{\text{SR}} = -1$ for the short-range Ising spin glass in 1d, a finite-temperature transition ceases to exist at $\theta_{\text{LR}} = 0$, that is, at $\sigma_u = 1$.

In order to determine the correlation length ξ for long-range models with power-law interactions, one uses the fact that the propagator is modified from the well-known Ornstein-Zernicke form to (in reciprocal space) [Ste72, Suz73]

$$G(k) \sim \frac{1}{m^2 + k^{2\sigma-1}}. \tag{2.35}$$

For the spin glass, the analogous form is for the spin-glass correlator $\chi_{\text{SG}}(k)$. Consequently, the second-moment definition of the correlation length is modified to

$$\xi_{\text{SG}} = \frac{1}{2\sin(k_{\text{min}}/2)} \left[\frac{\chi_{\text{SG}}(0)}{\chi_{\text{SG}}(\mathbf{k}_{\text{min}})} - 1 \right]^{1/(2\sigma-1)} , \tag{2.36}$$

with $\mathbf{k}_{\text{min}} = (2\pi/L)\,\vec{e}_1 \in \mathbb{R}^d$, where $\vec{e}_1$ is a lattice basis vector.

At criticality (where $m = 1/\xi = 0$), it is found that the Gaussian propagator $\sim 1/k^{2\sigma-1}$ does not receive any corrections away from mean field [FMN72] and hence

$$2 - \eta = 2\sigma - 1, \quad \sigma \leq 1 \, . \tag{2.37}$$

The upper critical value $\sigma_u = 1$ also follows directly from observing that at the lower critical dimension (LCD), we expect the critical correlation function decay $G(r) \sim 1/r^{d-2+\eta}$ to be constant i.e. $d_l - 2 + \eta = 0$. Since we have $d = 1$ and $2 - \eta = 2\sigma - 1$, it follows that $\sigma_u = 1$.

In the mean-field regime of the Ising model, Kotliar, Anderson and Stein (KAS) find [KAS83]

$$\nu = 1/(2\sigma - 1), \quad 1/2 \leq \sigma \leq 2/3 \, . \tag{2.38}$$

This implies that

$$\gamma = (2 - \eta)\nu = 1, \quad 1/2 \leq \sigma \leq 2/3 \, .$$

Using modified hyperscaling, Eq. (2.30), for $\sigma < 2/3$, we expect

$$d\nu' = 1 \cdot \frac{1}{2\sigma - 1} \frac{6}{2/(2\sigma - 1)} = 3 \overset{!}{=} 2 - \alpha \, ,$$
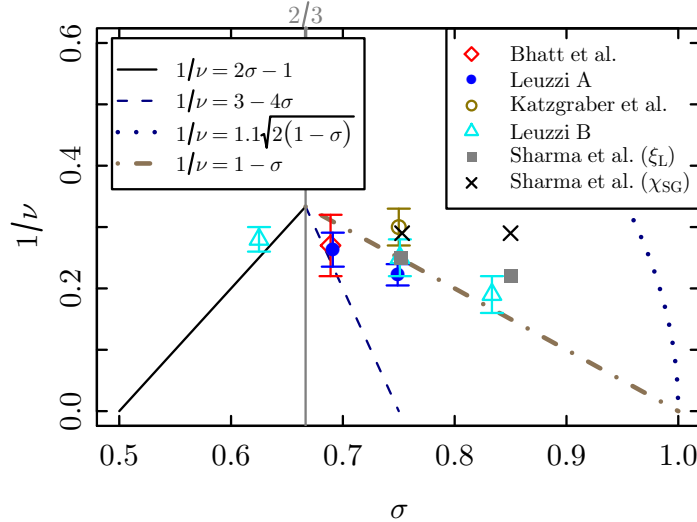
Figure 2.4.: (Color online). Previous estimates of $1/\nu$ for the 1d power-law Ising spin glass in comparison with various theoretical predictions discussed in Sec. 2.4.3, in particular the exact mean-field form (2.38) and the estimates (2.40), (2.41) and (2.42) in the non-mean-field regime. The numerical results are taken from Bhatt et al. [BY86a], Leuzzi A [Leu99], Katzgraber et al. [KY03], Leuzzi B [LPRTRL08] and Sharma et al. [SY11b]. Recall that for $m < \infty$ the mean-field regime is $1/2 < \sigma < 2/3$, see Fig. 2.2.

i.e., $\alpha = -1$ and $\nu' = 3$ for $1/2 \le \sigma \le 2/3$ and, consequently,

$$\beta = \frac{(2-\alpha)-\gamma}{2} = 1, \quad 1/2 \le \sigma \le 2/3 .$$

Note that with

$$2 - \eta = 2\sigma - 1 = (2 - \eta_{\mathrm{MF}})/d_{\mathrm{eff}} \tag{2.39}$$

and

$$\nu = \frac{1}{2\sigma - 1} = \nu_{\mathrm{MF}} d_{\mathrm{eff}} ,$$

with $d_{\mathrm{eff}} = 2/(2\sigma - 1)$, all exponents take their expected mean-field values.

In the non-mean-field regime, $2/3 < \sigma < 1$, KAS showed that an expansion around the lower critical value $\sigma_l = 2/3$ in the variable $\epsilon = \sigma - 2/3$ was possible and yielded to first order in ϵ

$$\frac{1}{\nu} = \frac{1}{3} - 4\epsilon = 3 - 4\sigma . \tag{2.40}$$

Expansions around the upper critical $\sigma_u = 1$ have also been proposed [KAS83] and resulted in the estimate

$$\frac{1}{\nu} = 1.1\sqrt{2\epsilon} = 1.1\sqrt{2(1-\sigma)} . \tag{2.41}$$

Comparing these to the previously found numerical results, both estimates appear to be rather poorly converged, cf. the data collected in Fig. 2.4 and Tab. 2.3 (see also the discussion in Ref. [SY11b]). A suggestion by Moore in Ref. [Moo10],

$$\nu = 1/(1-\sigma), \quad 2/3 \le \sigma \le 1 \tag{2.42}$$

σ	T_c	$1/\nu$	η	model	Ref.
0.625	2.191(5)	0.28(2)	1.751(8)	diluted	[LPRTRL08]
0.69	0.73, 0.78	0.27(5)		fully	[BY86a]
0.69	0.75	0.26(3)(*)	1.62(8)	fully	[Leu99]
0.75	0.63(8)	0.22(1)(*)	1.4(1)	fully	[Leu99]
0.75	1.758(4)	0.25(3)	1.502(8)	diluted	[LPRTRL08]
0.75	0.62(3)	0.30(3)	1.34(3)	fully	[KY03]
$0.8\overline{3}$	1.36(1)	0.19(3)	1.32(1)	diluted	[LPRTRL08]

Table 2.3.: A survey of results on the one-dimensional power law spin-glass model for Ising spins. The upper part of the table refers to simulations, whereas the lower part displays theoretical predictions given earlier. All considered values are from the non-mean-field region.

Values with the sign (*) were actually given as ν in the reference instead of $1/\nu$. We evaluated the according error-estimates by simple error-propagation.

seems to work significantly better, cf. the data collected in Fig. 2.4. This would imply

$$\gamma = (2 - \eta)\nu = \frac{2\sigma - 1}{1 - \sigma}, \quad 2/3 \leq \sigma \leq 1 .$$

Since hyperscaling should work in this regime, we also expect (assuming $1/\nu = 1 - \sigma$)

$$2 - \alpha = d\nu = \nu = 1/(1 - \sigma), \quad 2/3 \leq \sigma \leq 1 ,$$

and

$$\beta = \frac{(2 - \alpha) - \gamma}{2} = 1, \quad 2/3 \leq \sigma \leq 1 .$$

2.4.4. The 1d long-range $m = \infty$ spin glass

For the $m = \infty$ model we know that for it the UCD is elevated from the usual (spin-glass) $d_u = 6$ to $d_u = 8$ [GBM82] and this is accompanied by a failure of hyperscaling, even below the UCD. For hypercubic lattices at the UCD, FSS should work in N (see above), e.g.,

$$\chi_{\mathrm{SG}} \sim L^{\gamma/\nu} = L^{2-\eta} = N^{(2-\eta)/d} = N^{1/4}, \quad d \geq 8 . \tag{2.43}$$

For the 1d long-range model, we expect the long-range form of the exponent of the correlation function, Eq. (2.39), to carry over to the $m = \infty$ model. At the lower critical σ_l, where mean-field behavior first becomes modified, we should find

$$(2 - \eta)/d = 2 - \eta = 2\sigma_l - 1 \overset{!}{=} 1/4 \tag{2.44}$$

or $\sigma_l = 5/8$. Therefore, the mean-field regime is here defined as

$$1/2 \leq \sigma \leq 5/8 . \tag{2.45}$$

Of course, this range can be also obtained directly via the calculational methods in Green et al. [GBM82]. The effective correlation length exponent thus becomes $\nu' = 4$ and, due to dimensional reduction, we expect a modified hyperscaling relation to hold,

$$(d - \Theta)\nu' = 2 - \alpha \,, \tag{2.46}$$

with some violation-of-hyperscaling exponent Θ for the long-range case. Since we should have $\alpha = -1$, we infer $\Theta = 1/4$ for $1/2 \leq \sigma \leq 5/8$. The "bare" correlation length exponent should be unaltered,

$$\nu = \frac{1}{2\sigma - 1} = \nu_{\text{MF}} d_{\text{eff}} \,, \tag{2.47}$$

so that then $\gamma = 1$ and $\beta = 1$ as expected from mean-field theory.

The FSS forms of the critical quantities become modified by $d_u = 8$ according to the discussion outlined above in Sec. 2.4.2 to read

$$\chi_{\text{SG}} \quad \sim \quad N^{1/4}\mathcal{C}(tN^{1/4}), \tag{2.48a}$$
$$q_{\text{EA}} \quad \sim \quad N^{-1/4}\mathcal{Q}(tN^{1/4}), \tag{2.48b}$$
$$\frac{\xi}{L^{\nu/4}} \quad \sim \quad \mathcal{X}(tN^{1/4}). \tag{2.48c}$$

A consistent definition of the violation-of-hyperscaling exponent Θ is given by

$$\Theta = \begin{cases} 2\sigma - 1 = 2/d_{\text{eff}}, & 5/8 \leq \sigma, \\ 1/4, & 1/2 \leq \sigma < 5/8. \end{cases} \tag{2.49}$$

When $\sigma > 5/8$, this follows from the form of the propagators at T_c, which go as $1/k^{2\sigma - 1}$ and the results in Ref. [GBM82]. Θ is used in scaling relations which involve the dimensionality d when one replaces d by $d - \Theta$. Thus the scaling relation $\beta/\nu = (d - 2 + \eta)/2$, with the replacements $d \to d - \Theta$, $2 - \eta = 2\sigma - 1$, and $d = 1$ becomes

$$\beta/\nu = (3 - 4\sigma)/2 \,. \tag{2.50}$$

This is consistent with our numerical results shown in Fig. 4.12.

The exponent Θ appears also in the scaling relation

$$(d - \Theta)\nu = 2 - \alpha \,.$$

Thus if one can calculate ν, one can determine α.

It is possible to determine exactly the value of the upper critical σ_u from generalizing the argument that at the lower critical dimension $d - 2 + \eta = 0$. Replacing once again $d \to d - \Theta$ and $2 - \eta = 2\sigma - 1$, one has at a $\sigma = \sigma_u$, $1 - (2\sigma_u - 1) - (2\sigma_u - 1) = 3 - 4\sigma_u = 0$, so $\sigma_u = 3/4$.

As will be discussed below, the defect energy calculations for $m = \infty$ presented here, cf. Fig. 3.11, can be summarized as $\theta(\sigma = 3/4) = 0$, i.e., $\sigma_u = 3/4$, and $\theta(\sigma = 1/2) = 1/4$, which lead us to conjecture that

$$\theta_{LR} = 3/4 - \sigma \,. \tag{2.51}$$

In the following, we refer to θ_{LR} simply as θ. The form (2.51) works over a rather wide range of σ, even for $\sigma > 3/4$ in the fully connected model. When $\sigma > 3/4$, there is no finite temperature transition. We have been unable to give a formal derivation of this result, but suspect that this might be possible by generalizing the formalism of Aspelmeier et al. [AMY03] to spatially varying solutions. All we can do here is offer the following "argument" for it, which has been given by Moore [2].

From the scaling arguments in Ref. [BMY86] for long-range Ising spin glasses $2\theta = 2d - 2\sigma$. This would also follow from the formalism of Ref. [AMY03] which would result in an expression for the variance of the defect energy, (which scales as $L^{2\theta}$) proportional to a double sum over i and j of $[J_{ij}^2]_{\mathrm{av}}$ if a spatially non-uniform solution for the defect energies is considered. We have to consider how the failure of hyperscaling for the large-m limit might affect this relation.

θ is not a critical point exponent, but an exponent associated with the fixed point at zero temperature. For it, we suspect that the mean-field form of $\Theta = 1/4$ is relevant for both σ greater than and less than $5/8$, since zero-temperature exponents like θ can usually be obtained by a simple minimization of the defect energy, just as one determines mean-field behavior by minimizing the total energy of the system. Thus allowing for the failure of hyperscaling, the equation $2\theta = 2d - 2\sigma$ becomes $2\theta = 2(d - \Theta) - 2\sigma$. With $\Theta = 1/4$, Eq. (2.51) for θ is obtained on setting $d = 1$. We would expect this argument to still be valid in the fully connected model even for $\sigma > 3/4$ when there is no finite temperature transition. It would be good though to have a formal treatment of θ in order to check the validity of Eq. (2.51).

McMillan [McM84b, FH88] has argued that the relevant renormalization group equation for the flow of the temperature T near the lower critical dimension is

$$\frac{\mathrm{d}T}{\mathrm{d}\ln L} = -\theta T + cT^3 + \dots . \tag{2.52}$$

For θ small and positive, (i.e., for σ below, but close to $3/4$), one finds a fixed point at $T_{\mathrm{SG}} \propto \sqrt{\theta} \propto \sqrt{3 - 4\sigma}$. If we choose c so that $T_{\mathrm{SG}}(\sigma \leq 0.5) = 1$, then

$$T_{\mathrm{SG}} = \sqrt{3 - 4\sigma} , \tag{2.53}$$

which we find to fit the critical temperature quite well in the whole regime $1/2 \leq \sigma \leq 3/4$ (cf. Fig. 4.12). The eigenvalue at this fixed point is

$$\nu = \frac{1}{2\theta} = \frac{2}{3 - 4\sigma} . \tag{2.54}$$

This appears to be consistent with the data shown in Fig. 4.10 for the regime $5/8 \leq \sigma \leq 3/4$, but it cannot be regarded as anything but an interpolation formula, exact only at the end points $\sigma = 5/8$ and $\sigma = 3/4$. For $\sigma > 3/4$ $T_{\mathrm{SG}} = 0$. Then one expects $\nu = -1/\theta$ [BM87b].

From the scaling relation $\gamma = \nu(2 - \eta)$ with ν given by Eq. (2.54) one has the approximate result that

$$\gamma = \frac{4\sigma - 2}{3 - 4\sigma} ,$$

---

[2]This has been given by M.A. Moore in [BWM12]

in the regime $5/8 \leq \sigma \leq 3/4$. $\gamma = 1$ is thus expected at $\sigma = 5/8$ and $\gamma \to \infty$ as $\sigma \to 3/4$ from below.

By combining Eq. (2.50) with Eq. (2.54) one finds $\beta = 1$ throughout the interval $5/8 \leq \sigma \leq 3/4$. Thus the expectation is that β remains close to its mean-field value even in the non-mean-field region.

fully connected	quantity	diluted
–	bond-existence probability ε_{ij}	$\varepsilon_{ij} = \begin{cases} 0, & p > p_{ij}, \\ 1, & \text{otherwise,} \end{cases}$ $p_{ij} = 1 - \mathrm{e}^{-\frac{A}{r^{2\sigma}}},$ $z = \sum_{i=1}^{L-1} p_{iL}$ fixed, $p \in \mathcal{U}[0,1]$
$J_{ij} = c(\sigma, L)\frac{\varphi_{ij}}{r_{ij}^{\sigma}}$ $\varphi_{ij} \in \mathcal{N}(0,1)$ $c(\sigma, L) = \sqrt{1/\sum_{ij}\frac{1}{r_{ij}^{2\sigma}}}$	interaction-strength J_{ij}	$J_{ij} \in \mathcal{N}(0,1)$
$\frac{1}{2}L(L-1)$	number of bonds	$\frac{1}{2}Lz$

Table 2.4.: A comparison of the fully connected and diluted 1d power-law spin-glass model. We start out with the Hamiltonian Eq. (2.1) for the fully connected (with all bonds existing) and Eq. (2.7) for the diluted version. Taking into account the ring geometry, such that Eq. (2.12) is valid, the bond-existence probability, the interaction-strength and the number of bonds can be read off this table.

2.5. Summary

In this chapter we introduced various flavors of the general Hamiltonian (2.1) the notation of which was adjusted to different geometrical models. We started out with the hypercubic model and pointed to its shortcomings in high lattice dimensions since finite-size corrections are dependent on the *linear* lattice size. Increasing the lattice dimension d means to change the geometry (and by this also the coordination number z), while the interaction is always among nearest neighbors. We will use this model to determine its zero-temperature properties and determine the lower critical dimension using different types of boundary conditions in chapter 3. For the finite-temperature approach in chapter 4 limitations of this model will become obvious.

In order to circumvent problems arising for the hypercubic model we suggested to also consider a one-dimensional model for which the power-law interaction strength is tuned in order to effectively vary the corresponding (hypercubic) lattice dimension. One of the virtues of this model is the geometry being fixed and thus enabling one to investigate short-range as well as long-range behavior with comparable system sizes by merely varying a power-law exponent σ. Both a fully connected and a dilute version was introduced. We saw that the fundamental difference between these two is that instead of the *magnitude of the interaction strength* falling off like $1/r^{\sigma}$ in the former, the *probability of the existence*

of a bond falls off with distance in the latter. The interaction strength is then a Gaussian random number with standard deviation unity, independent of distance. To avoid confusion concerning the two 1d power-law versions we summarize their properties on the ring geometry in Tab. 2.4.

Attracted by the possibility of using rather large lattice sizes in the diluted version of the 1d model one might tend to use it predominantly. As we will see below, this advantage shall not outbalance the scaling corrections due to dilution or increase the quality of final results. We will use both the diluted and the fully connected version for the $T = 0$ calculations in chapter 3. We will stay with the fully connected model for the $T > 0$ calculations in chapter 4 since the nature of the employed equations suggests it, cf. Sec. 4.2.

Apart from sticking to the ring geometry of the 1d model, also alternatives using a line geometry with and without resummed (Hurwitz) couplings were mentioned. However, they will play a minor role in this thesis, since we do not see an overwhelming difference between all of the mentioned versions. Evidence will be given later that differences from the ring to the line geometry in finite-size scaling behavior are minor, cf. sections 3.2.3 and 4.7.2. Merely the visual aids turned the balance towards the ring geometry. Unless stated otherwise, all of the calculations presented below have been performed for it.

Furthermore, the phase diagram was introduced for the $m = \infty$ model and compared to the one with $m < \infty$. Differences in the critical behavior are related to the shift in the lower and upper critical dimensions. Correspondences of the lower critical dimension d_l with the upper critical σ_u and the upper critical dimension d_u with the lower critical σ_l have been motivated as well as the values $\sigma_u = 3/4$ and $\sigma_l = 5/8$. Since $d_u = 8$ it was pointed out that hyperscaling is violated in our model. However, finite-size scaling forms were suggested for dimensions above d_u. In terms of the 1d power-law model where even calculations in regions corresponding to $d > d_u$ can be done easily, there were additionally phenomenological scaling arguments determining critical behavior in various intervals of σ. They will be compared to numerical results below.

Chapter 3.

Zero-temperature calculations

A number of interesting quantities can be studied by considering ground states. These are the states found at zero temperature. The current chapter deals with this topic for vector spin glasses in the limit $m \to \infty$ of an infinite number of spin components.

We will explain the mechanisms which facilitate numerical calculations and describe the techniques used to implement them. Due to the relative ease of changing the universality class, i.e., changing the range of interactions, we discuss results for the 1d power-law model first. Later we will switch to the hypercubic model. For both of them we analyze the ground states in various aspects such as the scaling behavior, sample to sample fluctuations, energy distributions and the scaling behavior of the spin dimensions. Finally, we employ the defect-energy approach to determine the upper critical σ for the 1d power-law and the lower critical dimension for the hypercubic model.

3.1. Methods and techniques

Compared to the ground-state problem for generic spin glasses, which is found to be $\mathcal{NP}$-hard [Bar82], the $m = \infty$ case is much easier to determine. Starting out with the Ising model, so that $m = 1$, with increasing spin dimension the energy landscape simplifies gradually until, for $m \to \infty$, all metastability has vanished and the ground state becomes unique.

The possibility to realize the limit $m \to \infty$ in numerical calculations rests on the fact that for a finite system of N spins, the ground state occupies a finite dimensional sub-manifold in spin space [Has00, Cha08], the dimension of which is limited by the rigorous upper bound

$$m_{\max}(N) = \left\lfloor \left(\sqrt{8N + 1} - 1 \right) / 2 \right\rfloor \sim N^{\mu}, \; \mu = 1/2 \;, \tag{3.1}$$

where $\lfloor x \rfloor$ stands for the largest integer smaller than or equal to x. Hence, for each system size a *finite* number $m^*(N) \leq m_{\max}(N)$ of spin components is sufficient to describe the $m = \infty$ model. For commonly used spin-glass models, the scaling is in fact weaker than $m^*(N) \sim N^{1/2}$. For the SK model realized, e.g., in the limit $\sigma \to 0$ of our fully connected 1d spin glass, one finds $\mu = 2/5$ [Has00, AM04]. As the degree of connectivity is lowered, μ is reduced. In a trial run, we determined the required number of spin components $m^*(N)$ for each single realization of the bonds J_{ij} and calculated the disorder average $m_0 = [m^*(N)]_{\mathrm{av}}$. This average is found to have only very small fluctuations, such that using $m_{\mathrm{act}} \approx 1.1[m^*(N)]_{\mathrm{av}}$ was sufficient to ensure that $m = \infty$ ground states are found

for all realizations. The procedure of determining the number of necessary spin dimensions m^* will be described at the end of Sec. 3.2.1.

Due to the lack of metastability for $m \to \infty$, it is quite straightforward to determine true ground states numerically. Here, we employ a local spin-quench procedure, for which the spins are iteratively aligned with their respective local molecular fields $\mathbf{H}_i$, so that the new value $\mathbf{S}'_i$ of the spin at site i is given by

$$\mathbf{S}'_i \parallel \mathbf{H}_i = \sum_{j \in \mathcal{N}(i)} J_{ij} \mathbf{S}_j \,, \tag{3.2}$$

where the sum runs over the set $\mathcal{N}(i)$ of connected neighbors. It is easily seen that alignment of each spin with its molecular field is a necessary condition for the system to be in its ground state (the reasoning is given later in section 5.1.3). For the present case of a system without metastable states [Has00], it is also sufficient. The spin-quench updates are interspersed with sweeps of over-relaxation moves to speed up convergence, which have also been found to improve the decorrelation of systems with finite spin dimension m in Monte Carlo simulations [CCAMM$^+$06]. These moves, again being local, preserve the energy of the whole spin configuration since the updated spin is merely rotated around its local field and therefore moves at constant energy. The simplest way of implementing such a procedure, in particular for the case of arbitrary spin dimensions m, is to reflect the spin along $\mathbf{H}_i$, such that

$$\mathbf{S}'_i = -\mathbf{S}_i + 2\frac{\mathbf{S}_i \cdot \mathbf{H}_i}{|\mathbf{H}_i|^2}\mathbf{H}_i \,. \tag{3.3}$$

This maximal movement can also be argued to lead to a maximal decorrelation effect within the constant-energy manifold of single-spin movements. In Fig. 3.1 one can immediately convince oneself that with

$$\mathbf{x}_i = \mathbf{S}_i \cdot \frac{\mathbf{H}_i}{|\mathbf{H}_i|} \tag{3.4a}$$

$$\mathbf{S}'_i = 2|\mathbf{x}_i|\frac{\mathbf{H}_i}{|\mathbf{H}_i|} - \mathbf{S}_i \tag{3.4b}$$

$$\cos\vartheta = \frac{|\mathbf{x}_i|}{|\mathbf{S}_i|} \tag{3.4c}$$

$$\mathbf{S}_i\mathbf{H}_i = |\mathbf{S}_i||\mathbf{H}_i|\cos\vartheta \tag{3.4d}$$

Eq. (3.3) is correct.
Fortunately, the whole procedure of spin-quench and over-relaxation moves is simple and can be implemented very efficiently, since only a few elementary operations are required for each step. In particular not even random numbers are involved.
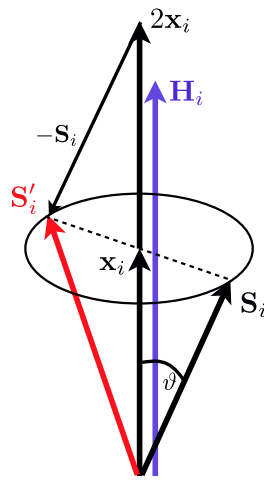
Figure 3.1.: (Color online). Overrelaxation moves speed up convergence. They improve decorrelation and preserve energy. This sketch helps in understanding Eqs. (3.3) and (3.4), the first of which suggests to reflect $\mathbf{S}_i$ along $\mathbf{H}_i$ (blue) for a maximal effect. The spin $\mathbf{S}'_i$ (red) is the resulting spin.

3.2. The 1d power-law model

For the case of the 1d power-law model it is tempting to employ the diluted version, i.e. Eq. (2.7). Rather large system sizes become accessible with it. Nevertheless, calculations have been done using both the diluted and the fully connected version. Unless stated otherwise, the ring arrangement of spins was used.

3.2.1. Ground-state properties

Finite-size corrections to the ground-state energy of spin glasses have been extensively discussed recently for the case of the short-range Edwards-Anderson system [BKM03, CHK04, BF11], spin glasses on the Bethe lattice and random graphs [Boe10], and the SK model [ABMM08]. The dominant contribution for short-range systems is due to the presence of domain-wall defects, leading to corrections proportional to $L^{d-\theta}$ [CHK04]. For the system studied here, however, these effects, although presumably present, are masked by corrections stemming from the power-law nature of the interactions. As indicated in Eq. (2.5), the relevant energy scale for the case of unrenormalized coupling strengths, i.e., $c(\sigma, L) = 1$, is set by the integral over the couplings,

$$\frac{1}{L} \sum_{\substack{i,j=1 \\ i \neq j}}^{L} \left[J_{ij}^2 \right]_{\mathrm{av}} = \frac{1}{L} \sum_{\substack{i,j=1 \\ i \neq j}}^{L} \frac{1}{r_{ij}^{2\sigma}} \sim \mathrm{const.} + cL^{1-2\sigma}, \quad L \gg 1 \ . \tag{3.5}$$

Hence, the ground-state energy per spin and spin-component, i.e. $e(L) = E/Lm$, is expected to scale as

$$e'(L) = -\sqrt{{e'_\infty}^2 + c'L^{1-2\sigma}} + \cdots \ , \tag{3.6}$$

where further finite-size corrections stemming from the presence of domain-wall excitations etc. have been neglected. We will see below that these are sub-leading and cannot be resolved by the numerics. The primed quantities in Eq. (3.6) are meant to indicate the unrenormalized case with $c(\sigma, L) = 1$. For large systems, we therefore expect different limiting behaviors depending on whether $\sigma \gtrless 1/2$, viz.

$$e'(L) \sim \begin{cases} e'_\infty \left(1 + \dfrac{c'}{2{e'_\infty}^2} L^{1-2\sigma} \right), & \sigma > 1/2, \ \ L \gg 1 \ , \\ \sqrt{c'} L^{1/2-\sigma}, & \sigma < 1/2, \ \ L \gg 1 \ , \end{cases} \tag{3.7}$$

with logarithmic scaling right at $\sigma = 1/2$. If we choose to make the energy scale convergent for $\sigma \leq 1/2$ by setting

$$c(\sigma, L)^2 = \sum_{i=1}^{L-1} \frac{1}{r_{ij}^{2\sigma}} \ , \tag{3.8}$$

we instead consider $e(L) = e'(L) \cdot c(\sigma, L)$ with limiting behavior

$$e(L) \sim \begin{cases} e_\infty + cL^{1-2\sigma}, & \sigma > 1/2, \ \ L \gg 1 \ , \\ \mathrm{const}, & \sigma < 1/2, \ \ L \gg 1 \ . \end{cases} \tag{3.9}$$

For the case of the diluted model, similar considerations lead to the same results, where now A of Eq. (2.10) takes on the role of $c(\sigma, L)^2$. In Fig. 3.2 the results of the scaling of
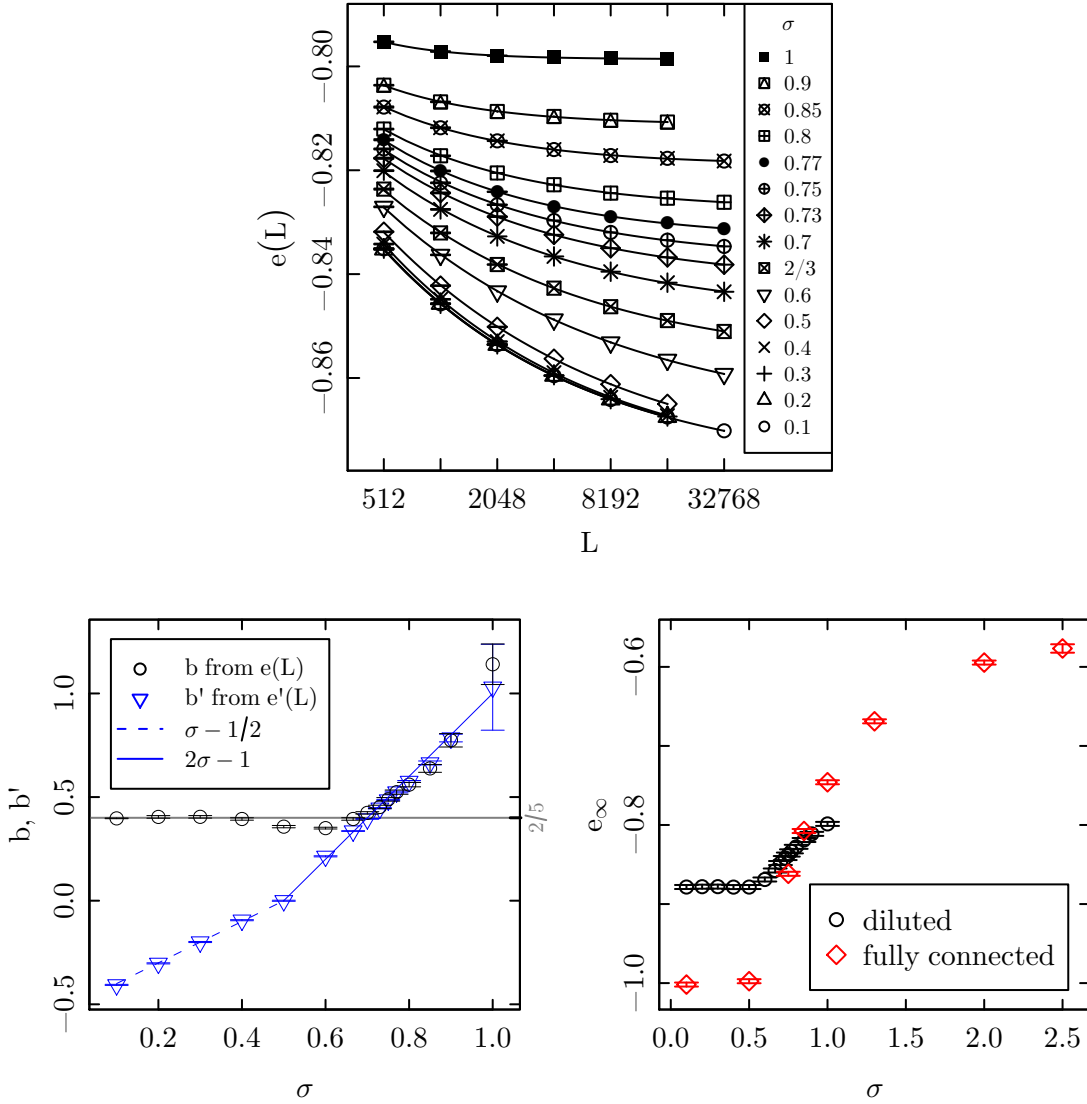
Figure 3.2.: (Color online). Average ground-state energies of the $1d$ power-law model in the $m \rightarrow \infty$ limit. Top panel: ground-state energies e as a function of system size L and interaction range σ. The lines show fits of the form (3.10) to the data. The corresponding correction exponents b are shown in the lower left panel. The solid blue line indicates the expectations for the unrenormalized energies $e'(L)$ which are $b = \sigma - 1/2$ for $\sigma < 1/2$ and $b = 2\sigma - 1$ for $\sigma \geq 1/2$. The lower right panel shows the resulting asymptotic ground-state energies e_∞, for the diluted and the fully connected model, respectively.

ground-state energies are presented. The correction exponents result from fits of the general form

$$
\begin{aligned}
e(L) &= e_\infty + cL^{-b} \ , \\
e'(L) &= e'_\infty + c'L^{-b'} \ ,
\end{aligned}
\tag{3.10}
$$

to the data. The number of disorder realizations used for the ground-state calculations are summarized in Tab. 3.1. As is seen from the middle panel of Fig. 3.2, the predictions

$$
b' = \left\{ \begin{array}{ll} 2\sigma - 1, & \sigma > 1/2 \ , \\ \sigma - 1/2, & \sigma < 1/2 \ , \end{array} \right.
\tag{3.11}
$$

for the $e'(L)$ and

$$
b = \ 2\sigma - 1, \ \ \sigma > 1/2 \ ,
\tag{3.12}
$$

in the renormalized case are borne out well in the data. For $\sigma < 1/2$, where we predict $b = 0$, sub-leading corrections become visible. The resulting correction exponent $b = 2/5$ is consistent with the expectations for the SK model, cf. Ref. [BA06] and the discussion in Sec. 4.7.1 below. For the renormalized energies $e(L)$, we see a dip of the correction exponent for $0.5 \leq \sigma \lesssim 0.6$, which is possibly due to additional finite-size effects resulting from the crossover between the forms for $\sigma \gtrless 1/2$. As shown in the bottom panel of Fig. 3.2, the asymptotic ground-state energy e_∞ smoothly increases for interaction ranges $\sigma > 1/2$. For $\sigma \leq 1/2$ it is independent of σ and takes the value -1 in the fully connected version of the model [BM81]. The independence of this non-universal quantity on σ in this regime is a clear sign of the exactness of mean-field theory for $\sigma \leq 1/2$ as proposed in Ref. [Mor11]. For models of lower connectivity, however, this energy is increased. Calculations on a Bethe lattice [BA06] are consistent with our results, for instance $e_\infty(\sigma = 0.1) = -0.8784(1)$, if the average coordination number is taken into account.

3.2.2. Sample to sample fluctuations

At $T = 0$ the free energy F reduces to the internal energy. We can use this fact to consider its sample to sample fluctuations in a finite size scaling analysis. Rather than investigating the *exact form* of the distribution function of the free energy we will first calculate its width $\sigma(E_{\mathrm{GS}}(N))$ as a key quantity. Only in the next section the exact form will be analyzed shortly. For the replica symmetric spherical model [KTJ76] it is known that it falls into the Tracy-Widom universality class [ABM04a] with a scaling of the sample to sample fluctuations as

$$
\Delta F \sim \sigma(E_{\mathrm{GS}}(N)) \sim N^{\Theta_f} \ ,
\tag{3.13}
$$

with $\Theta_f = 1/3$ [ABM04a]. Being also replica symmetric, one might suspect the $m \to \infty$ model also to fall into that class but in [Asp10] it was predicted that $\Theta_f = 1/5$ might be the correct sample to sample exponent in the SK limit using bond chaos calculations. Therefore, we expect to see $\Theta_f = 1/5$ only for $\sigma \leq 1/2$, whereas $\Theta_f = 1/2$ for $\sigma > 1/2$, which is the trivial value. Besides, for the SK ($m = 1$) Ising spin glass model it seems that consensus has been found for $\Theta_f = 1/6$ now [ABMM08].
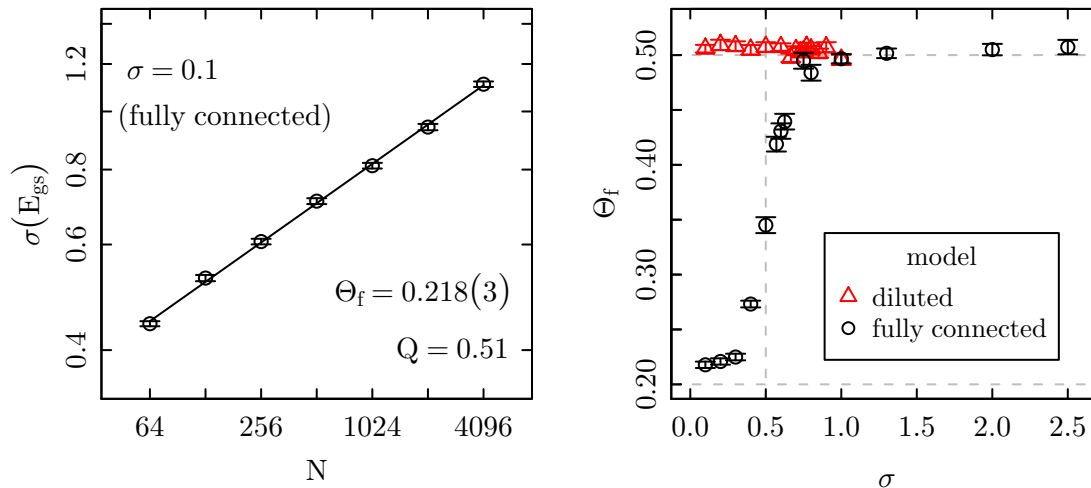
Figure 3.3.: (Color online). The scaling behavior of the sample to sample fluctuations char-
acterized by an exponent Θ_f. The left panel shows an example for the fully connected
model and indicates the correctness of the prediction $\Theta_f = 1/5$ in the SK limit ($\sigma \to 0$).
The fit range is controlled by the quality-of-fit parameter Q. In the right panel Θ_f is
plotted over a wide range of values of σ. Sample to sample fluctuations differ for the
diluted and the fully connected model. Whereas the characteristic exponent is fixed to
$1/2$ for the diluted model, it has a jump from $1/5$ to $1/2$ when changing from $\sigma < 1/2$ to
$\sigma > 1/2$. For our finite size systems this jump is smeared out and goes along with strong
finite-size effects.

Since we have direct access to the ground-state energies we can calculate the width of their
distribution function to arrive at the sample to sample fluctuations $\sigma(E_{gs}(N))$, see the left
panel of Fig. 3.3 for a showcase example for the fully connected model with a power-law
exponent $\sigma = 0.1$. We find that in the infinite-range region $0 < \sigma < 1/2$ the exponent Θ_f
goes to $1/5$ as was predicted. This confirms the $m \to \infty$ model to fall into a universality
class other than the spherical model as claimed in Ref. [Asp10].

The jump from $1/5$ for $\sigma < 0.5$ to $1/2$ for $\sigma \geq 0.5$ is governed by strong finite size effects
smearing it out, see Fig. 3.3.

The calculations in [Asp10] are valid for the SK model which can be reached for $\sigma \to 0$ in
the fully connected 1d power-law model. For the diluted version, where $\sigma \to 0$ corresponds
to the Viana-Bray model, the sample to sample exponent amounts to $\Theta_f = 1/2$ irrespective
of σ, cf. Fig. 3.3 (right). With this observation we find a first piece of evidence for the 1d
power-law model in its fully connected and the diluted versions not to being equivalent in
the universality sense. A similar result was reported in Ref. [PR10] for diluted Ising models.
These authors claim that Gaussian behavior of the sample to sample fluctuations have to
be expected whenever there is no local homogeneity of the interactions.
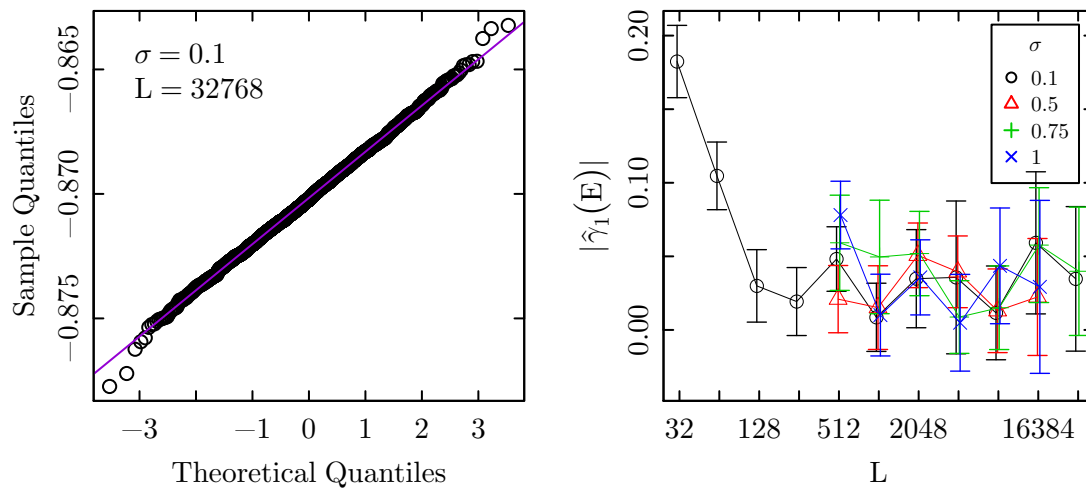
Figure 3.4.: (Color online). Evidence of the Gaussian nature of the ground-state energy
distributions for some of the values $0.1 \leq \sigma \leq 1$. The left panel shows a normal quantile-
quantile-plot in a showcase example for $\sigma = 0.1$ and the largest available lattice size
$N = L = 32\,768$. Sample quantiles do not deviate from the theoretical straight line
assuming a Gaussian distribution function. The right panel shows the scaling of the
(modulus of the) skewness according to Eq. (3.14) for $\sigma = 0.1$, 0.5, 0.75, and 1. It
vanishes for all σ verifying the Gaussian. Data stems from the diluted model but is
similar in the fully connected one.

3.2.3. Ground-state energy distribution

We also checked the distribution functions of the ground-state energies for the diluted as well as the fully connected model and each power-law exponent σ. While these show a non-trivial form for the (Ising) SK model [Boe05a], Gaussian distributions have been reported for short-range models [BKM03]. For the 1d Ising power-law chain, a crossover from Gaussian to non-trivial has been found on moving into the mean-field regime [KKL$^+$05]. The distribution of ground-state energies for the 1d $m = \infty$ model is analyzed in Fig. 3.4. For all values of the power-law exponent σ considered here ($0.1 \leq \sigma \leq 1$) the distributions seem to be compatible with a Gaussian. This is the case in both the diluted and the fully connected model indicated by a showcase example for $\sigma = 0.1$ and $N = 32\,678$ with a quantile-quantile plot as well as an analysis of the skewness of the distribution, estimated by

$$\hat{\gamma}_1(E) = \frac{1}{N_\mathrm{s}} \sum_{i=1}^{N_\mathrm{s}} \left(\frac{E_i - \hat{E}}{\hat{\sigma}_E} \right)^3 \tag{3.14}$$

in dependence of the system size for several values of σ spanning the mean-field as well as non-mean-field regimes. Here, N_s denotes the number of disorder realizations.

$$\hat{E} = \frac{1}{N_\mathrm{s}} \sum_{j=1}^{N_\mathrm{s}} E_j \tag{3.15}$$

is the usual estimator for the expectation value $\langle E \rangle$ and

$$\hat{\sigma}_E^2 = \frac{1}{N_\mathrm{s} - 1} \sum_{j=1}^{N_\mathrm{s}} (E_j - \hat{E})^2 \tag{3.16}$$

estimates the variance σ_E^2. In Ref. [KKL$^+$05] $\hat{\gamma}_1(E)$ was analyzed for the Ising spin glass. There they found a decay for increasing lattice size. We made test runs – with very small lattice sizes otherwise not required for our purposes – for $\sigma = 0.1$ and also found a similar behavior for the spin glass in the limit $m \to \infty$. This is shown in the right panel of Fig. 3.4. For the lattice sizes $L \geq 512$ (in the diluted model) $\hat{\gamma}_1(E)$ has vanished already. However, it is useful to note that lattice sizes used in Ref. [KKL$^+$05] were considerably smaller ($L \leq 192$) due to the fact that a Monte Carlo simulation was employed on the *fully connected* 1d power-law model.

3.2.4. Ground-state spin-components

For the $m = \infty$ model another zero-temperature property concerns the average number $m_0 = [m^*]_\mathrm{av}$ of spin components required to form the ground state. We determine m^* for each realization by ordering all spin vectors of the ground state configuration into an $m \times N$-matrix $M = \{\mathbf{S}_1, \ldots, \mathbf{S}_N\}$ and perform a singular value decomposition (SVD) in order to calculate the number of non-zero singular values, which is equal to the rank of the matrix. Since the rank of a matrix determines the number of linearly independent columns, i.e. spin vectors, it is the desired number m^*. In practice, we monitor the size of all singular values of M online as the quench into the ground state proceeds. As the
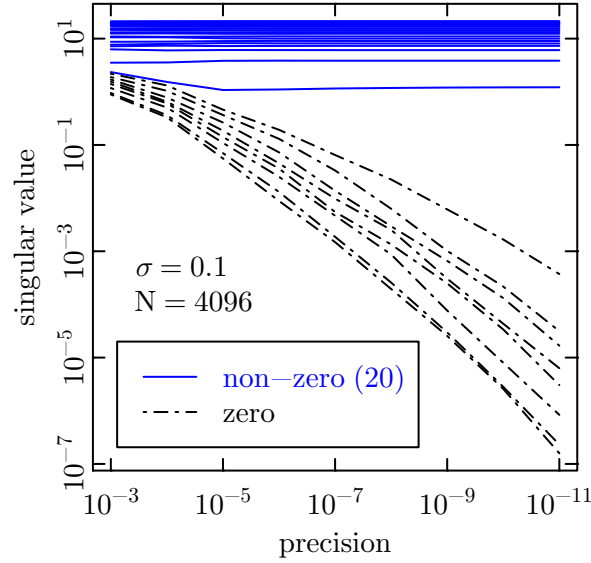
Figure 3.5.: (Color online). Scaling of the singular values of the spin matrix M for a sample with $L = 4096$, $\sigma = 0.1$ as the system is quenched into its ground state (here using the diluted model). The "precision" refers to the relative change of the configurational energy after a fixed number of sweeps.
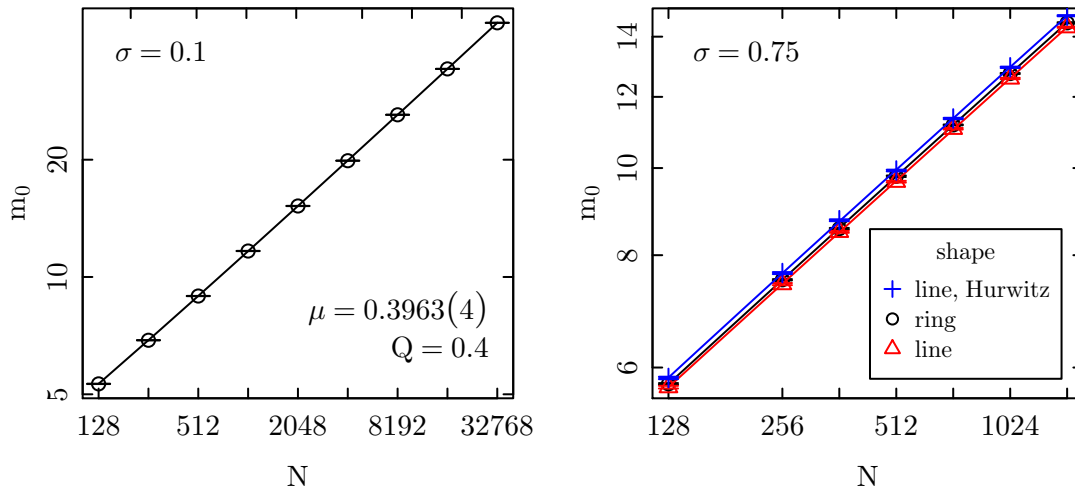
Figure 3.6.: Average number of spin dimensions m_0 a ground state occupies as a function of N. Left panel: The scaling behavior for $\sigma = 0.1$. This value is in the infinite-range region $\sigma \leq 1/2$ where we expect $m_0 = 2/5$ [Has00]. The line shows a fit of the form (3.17) to the data (obtained from the diluted model). Right panel: Comparison of the average number of spin dimensions m_0 a ground state occupies for the ring geometry and the line geometry with bare and resummed interactions (Hurwitz) for $\sigma = 0.75$. Deviations are minor.
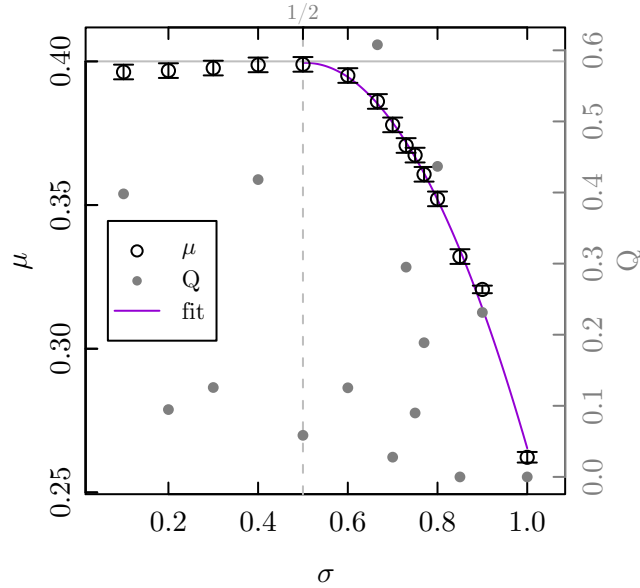
Figure 3.7.: (Color online). Variation of the exponent μ with the interaction range exponent σ. The points are results of fits of the form (3.17) to the data for the average number of occupied spin components in the ground state. Gray full points show the quality-of-fit parameter Q (right scale). The purple line corresponds to the functional form $\mu(\sigma) = 0.3995 - 0.55(\sigma - 0.504)^2$.

precision of the ground-state determination is increased those singular values that vanish in the exact ground state will scale to zero, whereas all the other singular values reach finite limiting values. This is illustrated for a sample of size $N = 4096$ and $\sigma = 0.1$ in Fig. 3.5.

For the average number of spin components in the ground state, we assume the scaling form

$$m_0 = [m^*]_{\mathrm{av}} = \mathrm{constant}\ N^\mu + c\ , \tag{3.17}$$

where the additive correction c can account for the fact that for small systems, m_0 will not scale to zero, but will be $m_0 = 1$ for tiny systems with $N = 1$ and $N = 2$. We present the results of this analysis for the infinite-range value $\sigma = 0.1$ (using the diluted model) in Fig. 3.6. Since mean-field theory is exact there, we expect to see the value $\mu = 2/5$ found for the SK model [Has00, AM04]. For $\sigma > 1/2$, μ continuously decreases below $\mu = 2/5$, cf. the summary of our data in Fig. 3.7. A fit to a parabola yields $\mu(\sigma) = 0.3995 - 0.55(\sigma - 0.504)^2$. Note that since $m_0 \sim N^\mu$ and due to the boundedness of $\mu \le 2/5 < 1$, it follows that $m_0/N \sim N^{\mu-1} \to 0$ in the thermodynamic limit. Hence, as $T \to 0$ the spins condense into a subspace of vanishing relative size, just as in the more familiar Bose-Einstein condensation [AM04].

To check for the influence of the different geometries introduced above in Sec. 2.3.3 on the scaling results, we performed some calculations for the bare and resummed line geometries. The effect of these changes on m_0 is illustrated for $\sigma = 3/4$, where we expect

the largest deviations, in the right panel of Fig. 3.6. Apart from a small overall shift in m_0, as expected we do not find any change in μ, but also no significant alterations of corrections to the leading finite-size scaling behavior.

3.2.5. Defect energies

The defect-energy approach [BC82] is widely used in studying systems with spin-glass phases. It is based on the assumption that the cost E_{def} of the insertion of a system-size defect into a state of the ordered phase scales as [BM84]

$$E_{\text{def}} \propto L^{\theta} \, , \tag{3.18}$$

where θ is known as the spin-stiffness exponent. Generalizing Peierls' argument for the stability of the ordered phase of a ferromagnet, one predicts $T_{\text{SG}} = 0$ whenever $\theta < 0$, whereas the ordered phase is stable at finite temperatures for $\theta > 0$. The limiting case $\theta = 0$ corresponds to the LCD of the system. Additionally, for the case $\theta < 0$ with a zero-temperature transition, θ is related to the correlation length exponent as $\nu = -1/\theta$ [BM84].

Numerically, defect energies are conventionally determined by comparing ground states of systems with a pair of different boundary conditions (BCs) chosen such that the respective ground states must differ by a relative domain-wall type excitation. Then the defect energy corresponds to the energy difference. The most commonly used set of such BCs are periodic and anti-periodic boundaries. The defect energy of a given realization is then

$$\Delta E = |E_{AP} - E_P| \, , \tag{3.19}$$

where the modulus is required since, for symmetric coupling distributions, the two boundary conditions are statistically equivalent. For the case of the long-range ring geometry considered here, a ground-state search is performed for the original coupling configuration, yielding E_P. In the second step, the boundary exchange couplings are flipped to the anti-periodic state by choosing *one arbitrary* nearest neighbor pair $\mathbf{S}_a$, $\mathbf{S}_{a+1}$, $a \in 1, \ldots, N$ (without having them necessarily interact in the diluted version of the model) and changing the sign of all interaction constants J_{ij} between spin $\mathbf{S}_i$ and $\mathbf{S}_j$ for all $i \neq j$ if the shorter path between those two spins falls on top of the path between $\mathbf{S}_a$ and $\mathbf{S}_{a+1}$ [KY03]. A second ground-state search for this altered configuration then yields E_{AP}. There has been some discussion in the past about whether this setup is suitable for the case of continuous spins, since both periodic and anti-periodic boundaries induce some defects, such that the energy difference $E_P - E_{AP}$ does not directly correspond to a defect energy [KA99, WG06, WG08]. Therefore, boundary conditions that allow directly to measure the energy of a single defect seem preferable. For the case of the $m = \infty$ spin glass on hypercubic lattices we will be able to extract different stiffness exponents from such "domain wall" BCs, cf. Sec. 3.3.5. For the 1d long-range system, however, it is not obvious how to implement such alternative prescriptions.

The resulting energy differences are averaged,

$$E_{\text{def}} = [\Delta E]_{\text{av}} = [|E_{AP} - E_P|]_{\text{av}} \, . \tag{3.20}$$
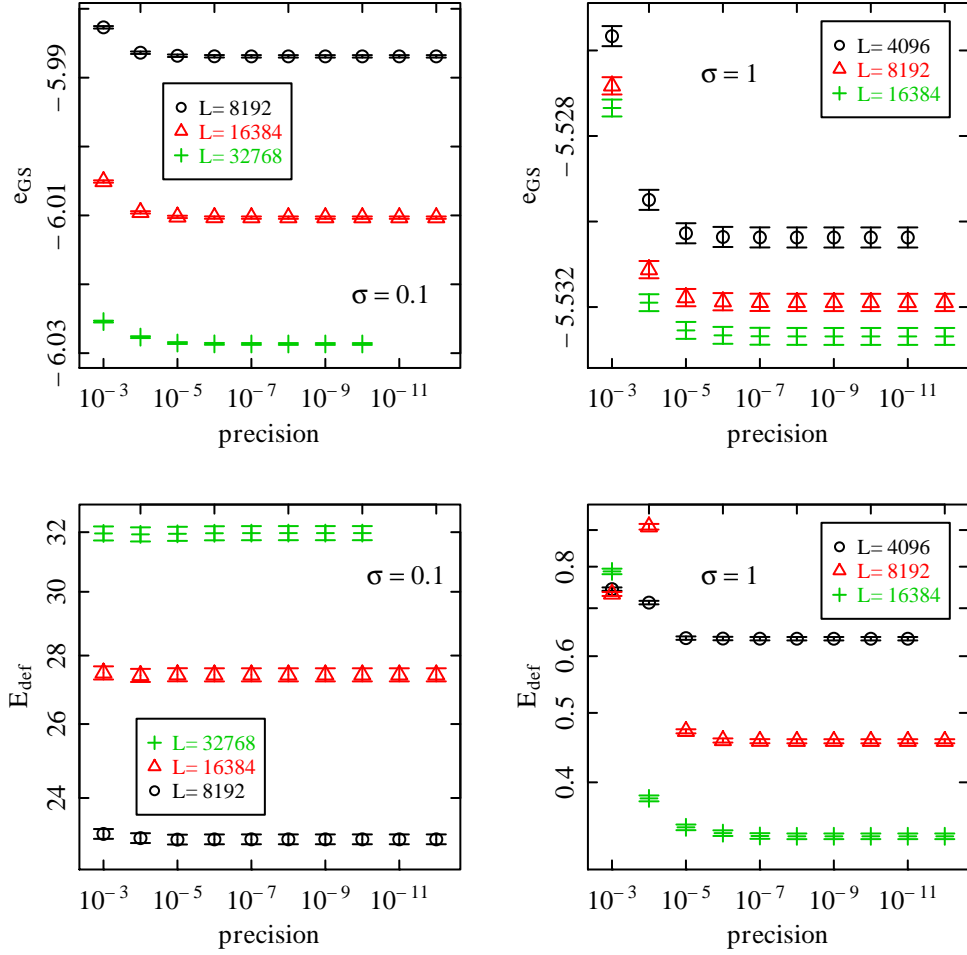
Figure 3.8.: The defect-energy approach relies on computing the ground-state energies e_{GS} (top figures). These energies are calculated up to a certain precision. This number refers to the average difference in energy per spin before and after one lattice sweep of local-field quenches. Also the defect energy E_{def} can be analyzed in its evolution with precision (lower figures). This quantity is slightly less sensitive to precision than the ground-state energy e_{GS} itself. This is probably due to E_{def} being an average over energy differences of almost identical disorder copies with a defect of the system size where effects of a certain realization cancel roughly.
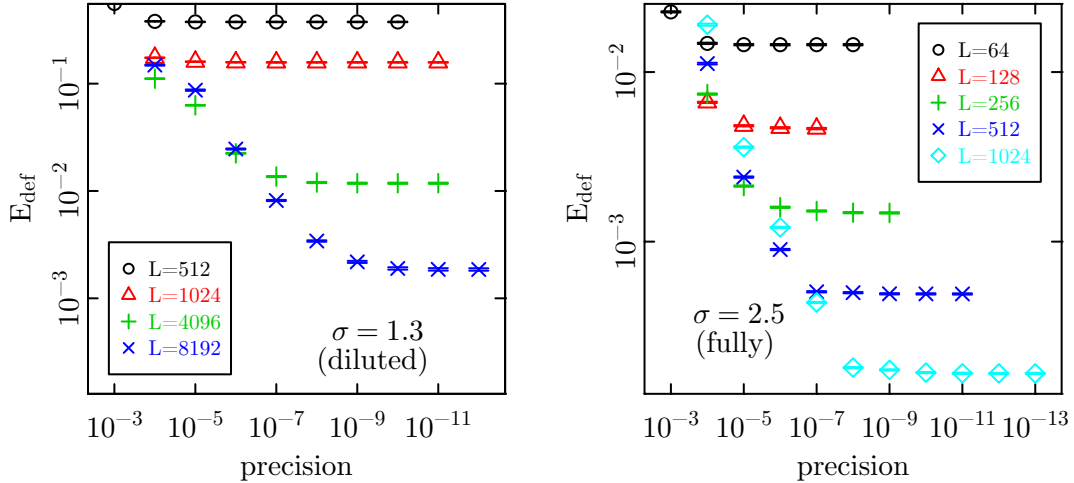
Figure 3.9.: (Color online). Convergence of the defect energy for the diluted (left) and fully connected (right) model as a function of precision of the ground-state energy calculation. For large σ this should be monitored accurately.

to yield an estimate E_{def} of the defect energy. Ground states were computed for both the diluted and the fully connected version of the 1d power-law model. For the former a set of values for the power-law exponent in the interval $0.1 \leq \sigma \leq 1$ was used and for most of the values of σ a range of system sizes $512 \leq L \leq 32\,768$ has been considered with around $2\,000$ disorder realizations for larger and up to $10\,000$ samples for smaller system sizes, see the parameters collected in Tab. 3.1. For the fully connected version the interval of power-law exponents can be easily broadened and we used $0.1 \leq \sigma \leq 2.5$. System sizes considered can be found in Tab. 3.2. Apart from largest values of σ we used around 4000 disorder realizations for each system size in the interval $128 \leq L \leq 4096$.

We ensured convergence by monitoring e_{GS} and E_{def} as the ground-state quench proceeds, cf. Fig. 3.8. This is of particular importance for large σ, where choosing a fixed precision fails to produce converged results for sufficiently large systems, cf. Fig. 3.9.

The averaged defect energies are shown for the available interaction ranges σ in Fig. 3.10. To extract the stiffness exponents, we performed fits of the functional form

$$E_{\text{def}} = aL^{\theta}(1 + b/L) \tag{3.21}$$

to the data. We found this form to describe the corrections rather well, cf. Sec. 3.3.5. While this form parametrizes the leading analytical correction for $\theta < 0$, a constant would be asymptotically dominant over b/L for $\theta > 0$. Fits including a constant but no $1/L$ correction, however, are not found to describe the data well for $\theta > 0$, such that we stick with the form (3.21) for all σ. Any non-analytic corrections, if present, appear to be subleading. These fits are shown in Fig. 3.10 and the corresponding fit parameters are collected in Tab. 3.1. Fit qualities are found to be high throughout, indicating the suitability of the form chosen in Eq. (3.21).

σ	samples/10^3	$aL^\theta(1+b/L)$				θ_∞
		$L_{\min}$	$L_{\max}$	θ	Q	
0.1	$2.4 - 10$	32	32768	0.245(02)	0.12	
0.2	$2.9 - 10$	512	16384	0.243(09)	0.39	
0.3	$3.1 - 9.1$	512	16384	0.255(08)	0.70	
0.4	$3.3 - 9.5$	1024	16384	0.260(12)	0.54	
0.5	$3.6 - 10$	512	16384	0.245(08)	0.31	
0.6	$3.1 - 9.5$	512	32768	0.177(06)	0.98	
2/3	$3.2 - 9.2$	512	32768	0.126(07)	0.13	
0.7	$3.2 - 10$	1024	32768	0.076(08)	0.96	
0.73	$3.2 - 9.1$	512	32768	0.046(07)	0.89	
0.75	$3.2 - 9.1$	512	32768	0.021(07)	0.56	0.03(5)
0.77	$3.2 - 9.3$	1024	32768	$-0.006(09)$	0.28	
0.8	$3.2 - 9.0$	512	32768	$-0.046(06)$	0.75	
0.85	$3.1 - 6.4$	512	32768	$-0.127(07)$	0.44	$-0.04(3)$
0.9	$2.8 - 10$	2048	16384	$-0.183(26)$	0.65	
1.0	$1.8 - 9.7$	512	16384	$-0.467(09)$	0.67	$-0.19(2)$

Table 3.1.: Estimates of the spin stiffness exponent θ in the *diluted* model resulting from fits of the functional form (3.21) to the data. Fit ranges were restricted to include lattice sizes $N_{\min} \leq N \leq N_{\max}$. Q denotes the quality-of-fit. The last column contains the extrapolated value of $\theta(z)$ in the limit of an infinitely large coordination number z. The values of θ_∞ found for the z-dependent test calculations coincide with the according values of θ of the fully connected model, cf. Tab. 3.2.

σ	samples$/10^3$	$N_{\min}$	$N_{\max}$	θ	Q
0.1	$3.9 - 4$	64	4096	0.238(19)	0.98
0.2	$3.9 - 4$	64	4096	0.238(19)	0.06
0.3	$3.9 - 4$	64	4096	0.275(20)	0.12
0.4	$3.9 - 4$	64	4096	0.247(21)	0.31
0.5	$3.9 - 4$	64	4096	0.262(24)	0.76
0.57	$3.9 - 4$	128	4096	0.180(41)	0.86
0.6	$3.8 - 4$	128	4096	0.200(46)	0.52
0.625	$3.9 - 4$	64	4096	0.168(36)	0.52
0.75	$3.8 - 4$	64	4096	0.052(95)	0.87
0.8	$3.8 - 4$	256	4096	0.014(15)	0.73
1.0	2	256	4096	$-0.209(21)$	0.28
1.3	$1.9 - 2$	256	4096	$-0.436(33)$	0.99
2.0	$1 - 2$	256	2048	$-1.132(37)$	0.96
2.5	$1 - 2$	128	1024	$-1.518(47)$	0.96

Table 3.2.: Estimates of the spin stiffness exponent θ in the *fully connected* model resulting from fits of the functional form (3.23) for $\sigma \leq 3/4$ and (3.21) for $\sigma > 3/4$. Fit ranges were restricted to include lattice sizes between $N_{\min}$ and $N_{\max}$. Q denotes the quality-of-fit.

Figure 3.11 summarizes our results for θ as a function of σ. The stiffness or defect energy exponent θ clearly becomes constant at a value compatible with the $\theta = 1/4$ in the infinite-range regime $\sigma \leq 1/2$. To determine the upper critical σ_u where $\theta(\sigma_u) = 0$, we performed a linear fit to the results. In the diluted version this fit was done in the range $0.5 \leq \sigma \leq 0.9$, resulting in an intercept of $\sigma_u = 0.760(32)$. In the fully connected version we extracted $\sigma_u = 0.80(4)$ for a fit in $0.5 \leq \sigma \leq 2.5$. In connection with the observation of a linear behavior in the regime $1/2 \leq \sigma \leq 3/4$, this leads to the conjectured form $\theta_{\mathrm{LR}} = 3/4 - \sigma$, cf. Eq. (2.51). This behavior is clearly different from the corresponding Ising spin-glass model with $\theta_{\mathrm{LR}} = 1 - \sigma$. Notice that the change to the value $1/4$ at $\sigma = 1/2$ is not due to a failure of Eq. (2.51) for $\sigma < 1/2$, but because for $\sigma < 1/2$ we have rescaled the bonds down by a factor of $L^{1/2-\sigma}$. If we had not done that θ would have continued to be fitted by Eq. (2.51).

For larger σ, however, we observe clear deviations of the data for the diluted model from $\theta = 3/4 - \sigma$. In fact, the data for E_{def} at $\sigma = 1.3$, not shown in Fig. 3.10, (but see the lower left panel of Fig. 3.12), show a strong downward curvature, more resembling an exponential decay. A closer look reveals that there is no universality between the diluted and fully connected model for $\sigma > 1$, where the properties of the diluted graphs change significantly. As has been shown in Refs. [Sch83, NS86], 1d graphs defined by Eq. (2.10) always percolate for $\sigma \leq 1/2$ and they percolate for sufficiently large A (namely, for any average coordination number $z > 1/2$) in the regime $1/2 < \sigma \leq 1$. In contrast, percolation is (asymptotically) absent for $\sigma > 1$. For the defect-energy calculations considered here, this means that such non-percolating samples contribute $\Delta E = 0$ to E_{def}, leading to much smaller averages than expected from the scaling Eq. (3.18). For the average coordination
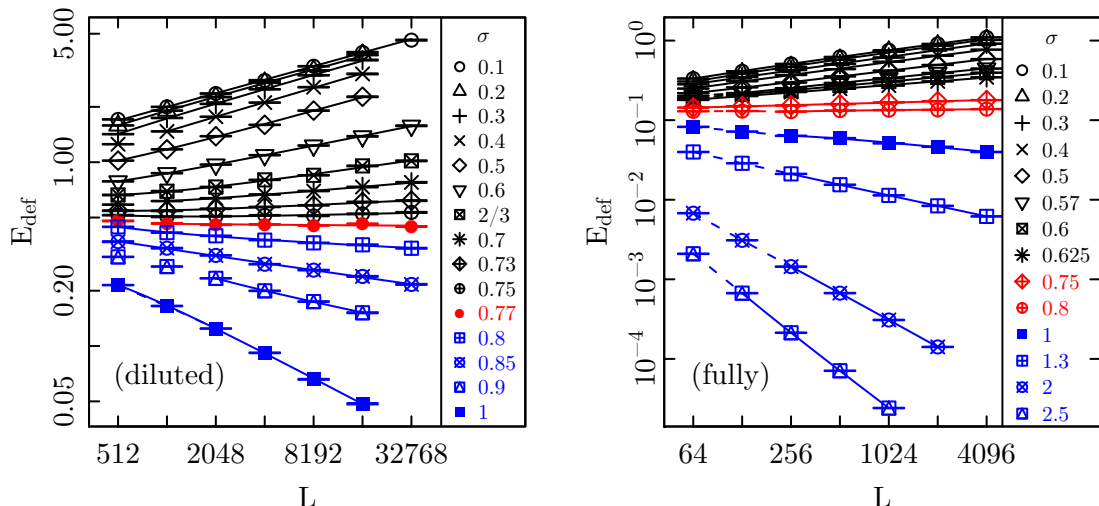
Figure 3.10.: (Color online). Defect energies for the 1d power-law $m = \infty$ spin glass as a function of lattice size L for a number of different interaction ranges σ. Left: the diluted version of the model with solid lines showing fits of the functional form (3.21) to the data. The corresponding fit parameters are summarized in Tab. 3.1. The spin-stiffness exponent θ changes sign in the vicinity of $\sigma = 0.77$, to be analyzed in Fig. 3.11. Right panel: the fully connected version of the model. The range of power-law exponents σ can be extended more easily than for the diluted case. θ changes sign in $0.72 \leq \sigma \leq 0.84$, cf. Fig. 3.11.

numbers considered here, such breakdown of percolation is only observed for very large systems, mostly beyond the reach of our numerical calculations. If we remove the links up to a finite range, however, for instance all nearest-neighbor links, the remaining graph does not percolate for $\sigma > 1$ already for moderate sizes such that the long-range nature is lost. An alternative way of understanding this phenomenon is to note that the diameters of the graphs considered here grow proportional to $(\log L)^{\delta}$ for $1/2 \leq \sigma < 1$, corresponding to an infinite-dimensional or small-world graph, whereas they grow proportional to L for $\sigma > 1$, corresponding to a truly one-dimensional graph [BB01]. This explains the strong downwards deviations of θ from the form $\theta = 3/4 - \sigma$ seen in Fig. 3.11 for $\sigma \geq 1$. Right at $\sigma = 1$, we expect non-universality with θ depending on the average coordination number z which, in turn, is a function of the parameter A in Eq. (2.10).

In order to confirm this claim we checked the dependence of the defect energy scaling on the coordination number z at four different values of σ. At $\sigma = 3/4$ we expect the z dependence of θ negligible since observed deviations from the data of the fully connected model are minor. Tests at $\sigma = 0.85$ and 1.0 should reveal a quite strong dependence. Both considerations turn out true regarding Fig. 3.12. For all quoted values of σ calculations were made for (average) coordination numbers $z = 6, 12, 24, 48$. Data was then extrapolated to $z \to \infty$ using

$$\theta = \theta_{\infty} + \text{const.} \, z^{a} \, . \tag{3.22}$$
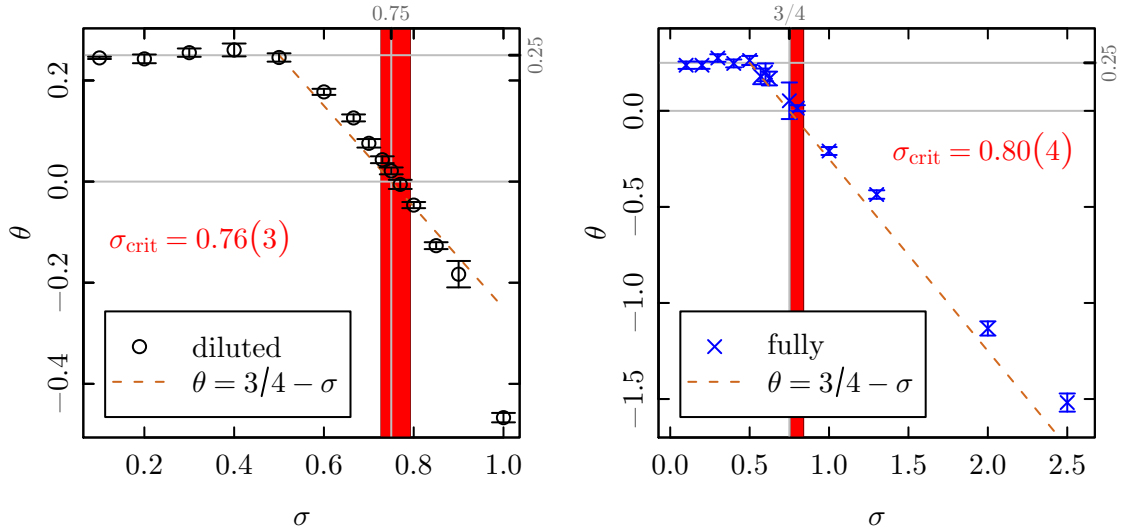
Figure 3.11.: (Color online). Left panel: the stiffness exponents θ in the interaction-range exponent interval $0 < \sigma \leq 1$. They are extracted using the diluted model, cf. Tab. 3.1 for corresponding fit parameters. θ changes sign for the critical value $\sigma_u = 0.76(3)$ marked by the red shaded area. Below $\sigma = 1/2$, the spin stiffness exponent levels off at the infinite-range value $\theta = 1/4$. The dashed line denotes the conjectured form $\theta = 3/4 - \sigma$, cf. Eq. (2.51). Right panel: The analogous plot for the fully connected model. See Tab. 3.2 for fit parameters. Here, a wider range of σ could be used. The conjecture (2.51) seems fulfilled roughly for all $\sigma \geq 1/2$ and θ changes sign for the critical value $\sigma_u = 0.80(4)$ again marked by a red area.

In doing so, we found values θ_∞ quoted in Tab. 3.1. These values should be in agreement with results gained for the fully connected model. The right panel of Fig. 3.11 shows the stiffness exponents found and Tab. 3.2 summarizes the fit parameters. As expected, θ's for the fully connected model and the extrapolated values θ_∞ are in perfect agreement. For $\sigma > 1$, however, the defect energy scaling stops to be power-law like and seems either to cross over to $\theta = -\infty$ or an exponential decay as expected for real short-range 1d systems [MCM$^+$86]. The z-dependence of θ for $3/4 < \sigma \leq 1$ is most probably due to cross-over effects. A similar z-dependent critical behavior at $\sigma = 1$ was also recently found for random walks on the fully connected model [Juh12]. These deviations are specific to the diluted model: defect-energy calculations for the fully connected model, summarized in the right panel of Fig. 3.11, are consistent with $\theta = 3/4 - \sigma$ also for $\sigma > 1$. The relevant parameters and results for this model are summarized in Tab. 3.2. In contrast to the diluted model, a constant was found to be a good description of the leading scaling corrections for $\theta > 0$, such that we used the form

$$E_{\text{def}} = aL^\theta + c \tag{3.23}$$

for $\sigma \leq 3/4$ and the form (3.21) for $\sigma > 3/4$. Only the fully connected model does represent the long-range universality class for $\sigma \geq 1$. Furthermore, we also find scaling corrections for $\sigma < 1$ to be less pronounced there than for the diluted system although considerably
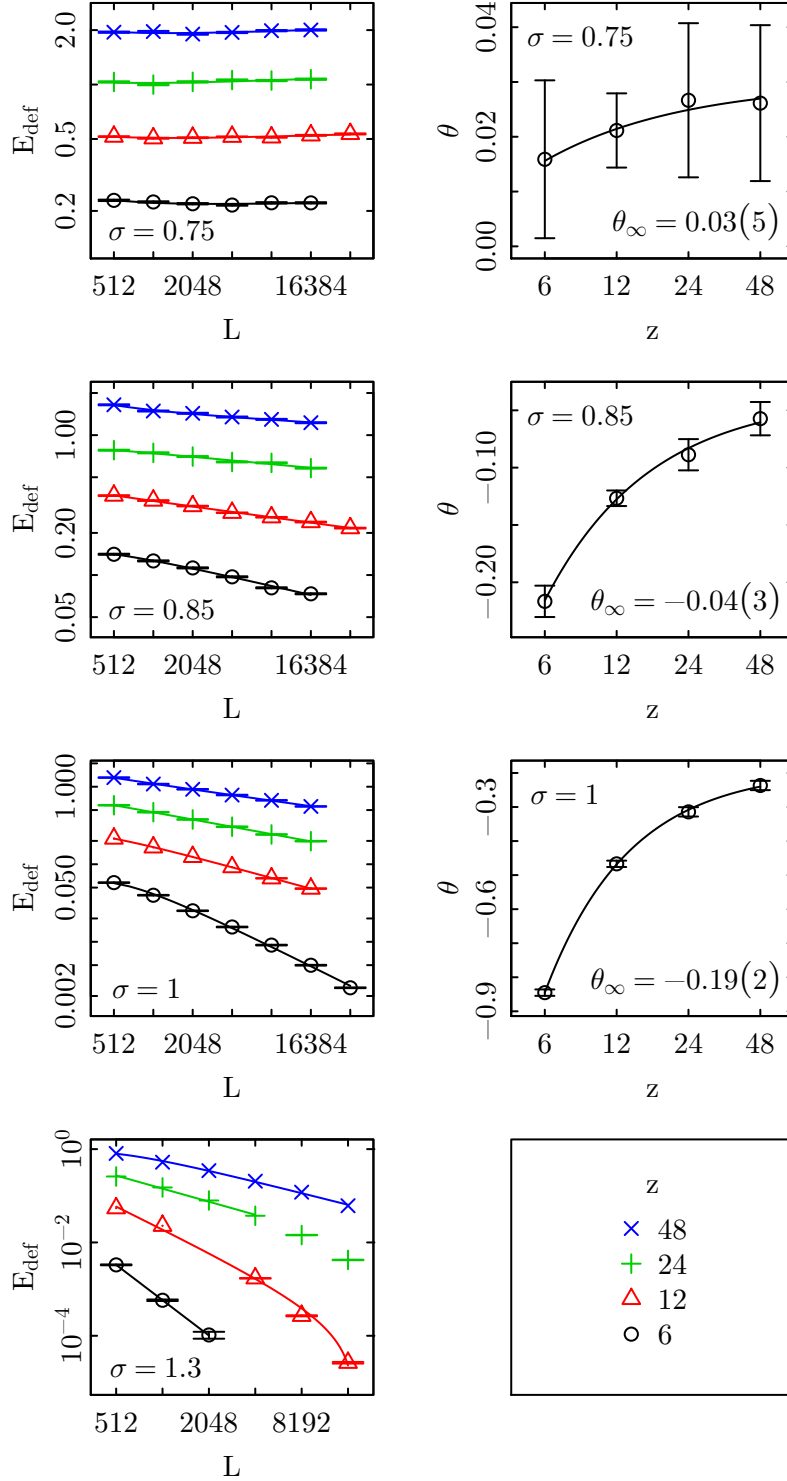
Figure 3.12.: (Color online). The defect energy scaling (left panels) in the diluted version of the model for $\sigma = 0.75, 0.85, 1, 1.3$ gets dependent on the coordination number z for $\sigma > 3/4$ as a cross-over effect. For $\sigma > 1$ the diluted and the fully connected model are not universal anymore. An extrapolation to $z \to \infty$ (right panels) yields values θ_∞ for the stiffness exponent which are in perfect agreement with values gained from cross-checks to the fully connected version of the model, cf. Tabs. 3.1 and 3.2.

larger system sizes have been used in the latter. Therefore, it appears questionable whether considering the diluted model offers a significant advantage in terms of the precision and accuracy of the final results.

Note that the results for θ as σ is increased are in contrast to those for the Ising case, where $\theta_{\text{SR}} = -1$, so that the (fully connected) long-range Ising system is governed by short-range behavior for $\theta_{\text{SR}} > \theta_{\text{LR}}$ viz. $\sigma > 2$ (whereas the diluted Ising system would be truly short ranged already for $\sigma > 1$). The $m = \infty$ model, instead, is truly long-range everywhere, and crossover to the $\theta_{\text{SR}} = -1$ of the nearest-neighbor 1d chain system is not seen. Instead, the limit $\sigma \to \infty$ of our fully connected model corresponds to the 1d ladder system with [MCM$^+$86] $\theta = -\infty$.

Although we found agreement of the diluted and the fully connected models in the interval $0 < \sigma \leq 1$, we note that the values of θ are systematically slightly above the theoretical prediction of Eq. (2.51) in the range $1/2 < \sigma \leq 1$ for both models. Additionally, this is also found to apply in the range $1 < \sigma \leq 2.5$ for the fully connected model.

Next we can have a look at the distribution of the defect energies $P(E_{\text{def}})$ at fixed system sizes L. Here for $m \to \infty$ we find that the distribution function P is merely a Gaussian throughout the whole range of σ, i.e. even in the limit of small σ, see Fig. 3.13. This is valid for both the diluted as well as for the fully connected version.

Returning back to the diluted model, one small remark is missing. The power-law decay of bond probabilities according to $p_{ij} \sim r_{\text{ij}}^{-2\sigma}$ is not modeled completely accurately by the version of Katzgraber et al. [KY03] we used in our analyzes. For very small distances r the bond probabilities are underestimated slightly, see Fig. 3.14.

An idea to model this decay of bond probabilities according to the theoretical p_{ij} more precisely would be to take up the approach of Leuzzi et al. [LPRTRL08] and change it slightly as we will explain now. Originally it was suggested to put exactly $zL/2$ bonds by repeating the following procedure the same number of times:

> Select two spins at random having a distance of r, which is chosen with probability $r^{-2\sigma}/\sum_{k=1}^{L/2} k^{-2\sigma}$. If there is a bond already, make a new attempt, otherwise put the bond.

According to this procedure there will be some attempts to set a bond which are rejected, of course. One can change this by allowing to put multiple bonds, meaning to add their strengths. The recipe would read as follows:

> Select two spins at random having a distance of r, which is chosen with probability $r^{-2\sigma}/\sum_{k=1}^{L/2} k^{-2\sigma}$. If there is a bond already, add the bond strength to the old one, otherwise put an initial bond.

A bond which has been put n times effectively has been drawn from a Gaussian distribution with zero mean and standard deviation $\sqrt{n}$. Note that the average coordination number is
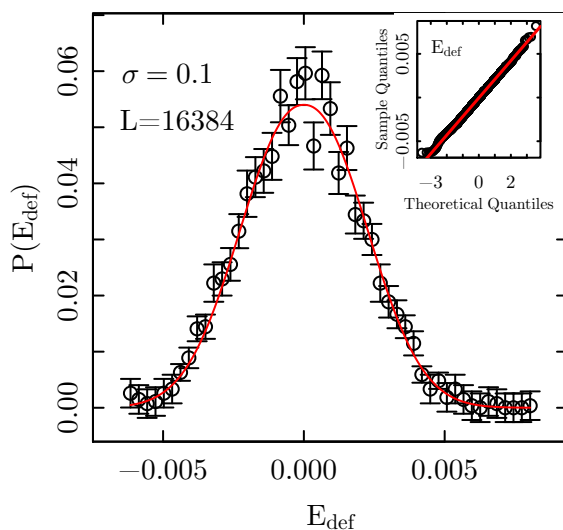
Figure 3.13.: (Color online). The defect energies are Gaussian for all values of σ. This showcase example verifies that observation for a value from the infinite-range region of σ. We observe this for both the diluted as well as the fully connected model. The shown plot is for the diluted model and the normalization $(1/2\sqrt{z})$, cf. Eq. (2.7), has been skipped. The inset shows a normal quantile-quantile plot of the defect energies approving their Gaussian nature.
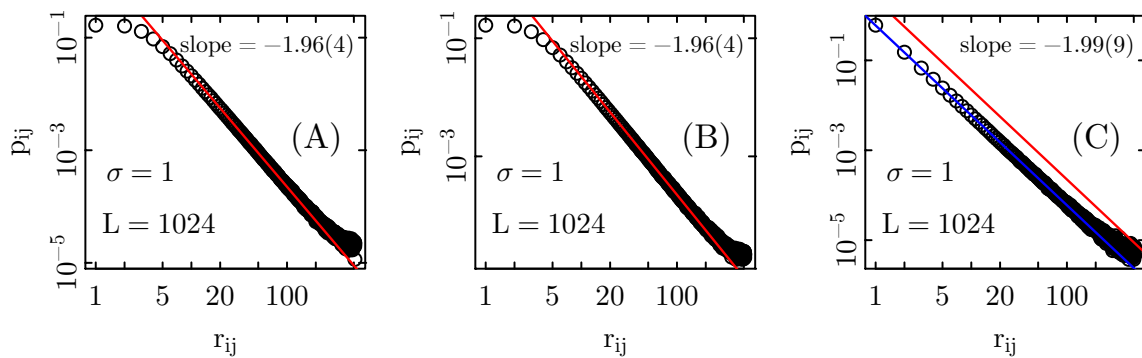
Figure 3.14.: (Color online). The bond probabilities p_{ij} which we require to fall off like a power-law as $r^{-2\sigma}$. Katzgraber et al. [KY03] (left, A) and Leuzzi et al. [LPRTRL08] (middle, B) suggested versions which fix the average and the exact coordination number z, accordingly. Both of them necessarily underestimate the theoretical decay (red line) at small distances r. The modified Leuzzi version allowing multiple bonds between one pair of spins (right, C) does not have this minor flaw, but suffers from an even stronger z-dependence at large σ. The red line is a reference and the same in all plots.

then smaller than z. In Fig. 3.14 one can see the effect of allowing to put multiple bonds. The bond probabilities are slightly off the theoretical power-law decay for very small distances r for the Katzgraber version and the Leuzzi version. The multiple bond version does not suffer from this minor flaw.

We made a test with the three bond probability versions and regarding θ we found perfect agreement of Leuzzi's and the multiple-bond with the Katzgraber version at $\sigma = 0.1$. For $\sigma = 1$, however, the z-dependent effects described above were more pronounced. This lead us to the conclusion that the slightly deviating bond probabilities at very small distances r do not play a crucial role.
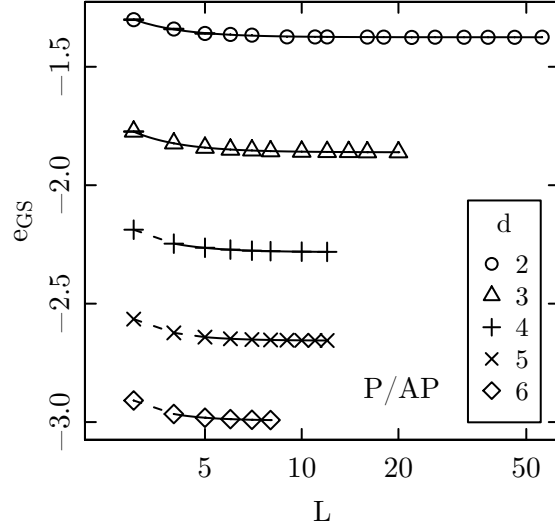
Figure 3.15.: (Color online). Average ground-state energies e_{GS} of the hypercubic model in the $m \to \infty$ limit depending on system size L and the lattice dimension d. Boundary conditions used were periodic.

3.3. The hypercubic model

All terms and definitions we will use in this section have already been introduced and employed in section 3.2. In order not to repeat all this we will refer to it frequently.
For the hypercubic model we will use the Hamiltonian Eq. (2.2).

3.3.1. Ground-state properties

Similar to the approach in Sec. 3.2.1 ground states were determined by a local quench procedure with interspersed overrelaxation moves. Again, convergence of the ground-state energies is assured by monitoring e_{GS} as a function of precision, cf. Fig. 3.19. For small dimensions d, corresponding to large values of σ in the 1d power-law model, one does not run into too big trouble with ground-state energies being strongly dependent on precision but sees the same trend for the defect energies, cf. Fig. 3.19, as for $\sigma > 1$ in Fig. 3.9.

In Fig. 3.15 we present the results of the scaling of ground-state energies. The correction exponents result from fits of the general form

$$e(L) = e_{\infty} + cL^{-b} \tag{3.24}$$

to the data. Details and results concerning the ground-state calculations are summarized in Tab. 3.3.

d	samples/10^3	e_∞	b	Q
2	$3-5$	$-1.37534(8)$	$-2.85(11)$	0.04
3	3	$-1.8611(1)$	$-2.89(6)$	0.14
4	3	$-2.2827(1)$	$-3.09(8)$	0.35
5	$9-18$	$-2.65635(3)$	$-3.39(3)$	0.64
6	$5-13$	$-2.99365(5)$	$-3.73(3)$	0.22

Table 3.3.: Estimates of the ground-state energy e_∞ in the thermodynamic limit for all lattice dimensions considered. Boundary conditions used were periodic. Fits were made according to Eq. (3.24). Q denotes the quality-of-fit and is good throughout.

d	Θ_f	$Q[\Theta_f]$	μ	$Q[\mu]$
2	$0.497(3)$	0.11	$0.263(20)$	0.39
3	$0.499(2)$	0.004	$0.307(11)$	0.13
4	$0.501(3)$	0.33	$0.352(05)$	0.26
5	$0.500(1)$	0.96	$0.372(03)$	0.62
6	$0.498(2)$	0.63	$0.380(02)$	0.66
7	$0.496(3)$	0.19	$-$	$-$

Table 3.4.: The sample to sample exponent Θ_f and the spin-component scaling exponent μ in various lattice dimensions d of the hypercubic model. Fits were monitored by the quality-of-fit parameter Q.

3.3.2. Sample to sample fluctuations

For the sample to sample fluctuations of the free energy we have

$$\Delta F \sim \sigma(E_{\mathrm{GS}}(N)) \sim N^{\Theta_f} \,, \tag{3.25}$$

cf. Sec. 3.2.2. We cannot go beyond $d = 7$ and expect $\Theta_f = 1/2$ for all lattice dimensions $d = 2, \ldots, 7$, as verified by the numerical calculations with the 1d power-law model and the range of power-law exponents $\sigma > 1/2$.

Confirming this expectation nicely, Tab. 3.4 compiles all values of Θ_f among other quantities to be discussed below.

3.3.3. Ground-state energy distribution

In Sec. 3.2.3 the distribution functions of the ground-state energies were found to be Gaussian in the 1d power-law model. Nothing else would be expected for the hypercubic model. The exact same analysis verifies this, cf. Fig. 3.16. For short-range Ising spin glasses the Gaussian nature was reported in Ref. [BKM03].
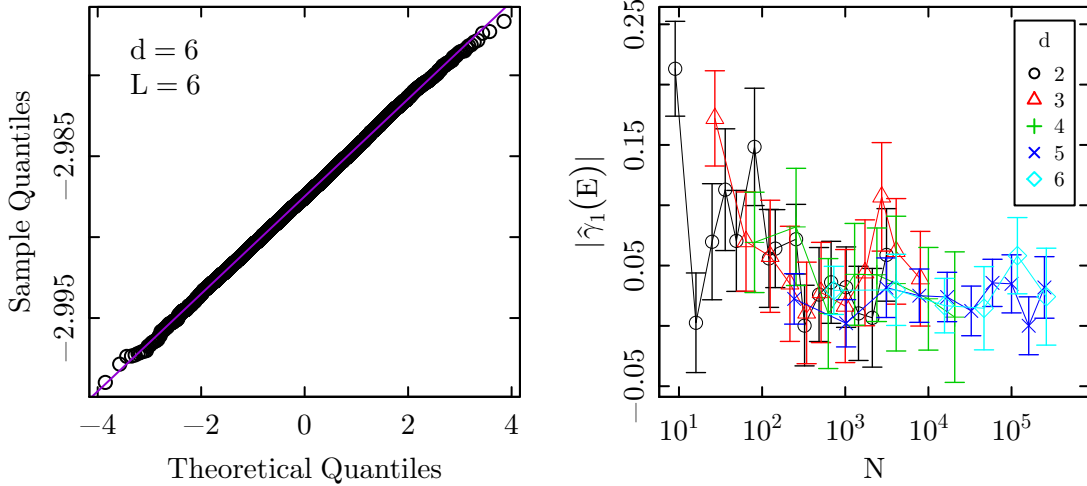
Figure 3.16.: (Color online). Evidence of the Gaussian nature of the ground-state energy distributions for dimensions $d = 2, \ldots, 6$. The left panel shows a normal quantile-quantile-plot in a showcase example for $d = 6$ and linear lattice size $L = 6$. Sample quantiles do not deviate from the theoretical straight line assuming a Gaussian distribution function. The right panel shows the scaling of the (modulus of the) skewness according to Eq. (3.14). It vanishes for all d verifying the Gaussian. This is in accordance with the observations for the 1d power-law model in Sec. 3.2.3.

3.3.4. Ground-state spin-components

The analysis of the average number $m_0 = [m^*]_{av}$ of spin components required to form the ground state is done according to Sec. 3.2.4. We expect m_0 to increase with dimension, until in the mean-field region ($d \geq d_u$) the scaling should not exceed but stick to $\mu = 2/5$. The present work covers only dimensions up to $d = 6$. However, the scaling exponent is already in the vicinity of 2/5 there, cf. Fig. 3.17. We assume again that

$$m_0 = \text{constant } N^\mu + c , \qquad (3.26)$$

and Tab. 3.4 contains the values of μ in dependence of lattice dimension d.

3.3.5. Defect energies

Also for the hypercubic model, of course, we assume that a defect inserted into the ordered state has a cost that scales according to Eq. (3.18). We used this in Sec. 3.2.5 for the 1d power-law model. The method to induce a defect of size L will become slightly more intuitive for the hypercubic model, as we will see. Due to the simple structure of a hypercube inducing a defect of linear size L, i.e. a domain wall, can be accomplished by manipulating the boundaries in *one* lattice dimension. To reduce additional surface effects, boundary conditions in all other lattice directions were chosen periodic. We decided to use three different setups aimed at reducing problems with domain walls trapped due to the periodicity
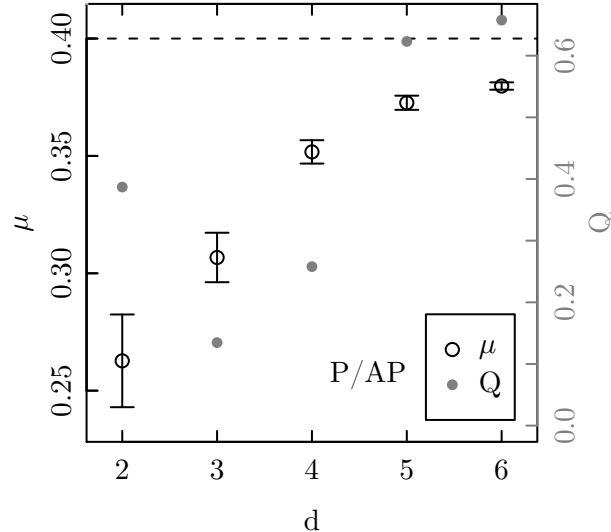
Figure 3.17.: (Color online). Variation of the exponent μ with lattice dimension d. The points are results of fits of the form (3.26) to the data for the average number of occupied spin components in the ground state. Gray full points show the quality-of-fit parameter Q (right scale).

and possibly discriminating between spin (rotational symmetry) and chiral [Vil77] (discrete symmetry) defects [WG06]. Firstly, we investigated the case of periodic and anti-periodic (P/AP) boundary conditions as the standard setup to probe continuous or "spin" excitations. For calculating the defect energy one compares the ground-state energy gained for periodic boundaries and the one resulting from the same system for which two opposing boundaries changed the sign of their connecting bonds, see the top panel of Fig. 3.18 for an illustration. Since for this case domain walls might be trapped in *both* configurations due to the imposed periodicity, the difference between the two ground-state energies does not directly correspond to the excitation energy of a single defect [KA99, WG08]. To alleviate this problem, we also investigated two other boundary conditions – open/domain-wall (O/DW) and open/spin-pair (O/SP) boundary conditions.

For O/DW boundary conditions the defect energy is determined by comparing the energies of a system with open boundaries in one direction and a second one with *fixed spins on two opposing boundaries*. The fixed spins are chosen to stay in the configuration found for open boundaries on one side and rotated around a common axis perpendicular to the hyperplane in spin space occupied by the boundary spins on the other side. This choice is possible since anyway the dimension of the spin space m is chosen larger ($m > m^*$) than the configuration would actually need to assume its ground state. Due to the open boundaries in the first case, the insertion of exactly one domain wall is guaranteed. The setup is depicted in the middle panel of Fig. 3.18.
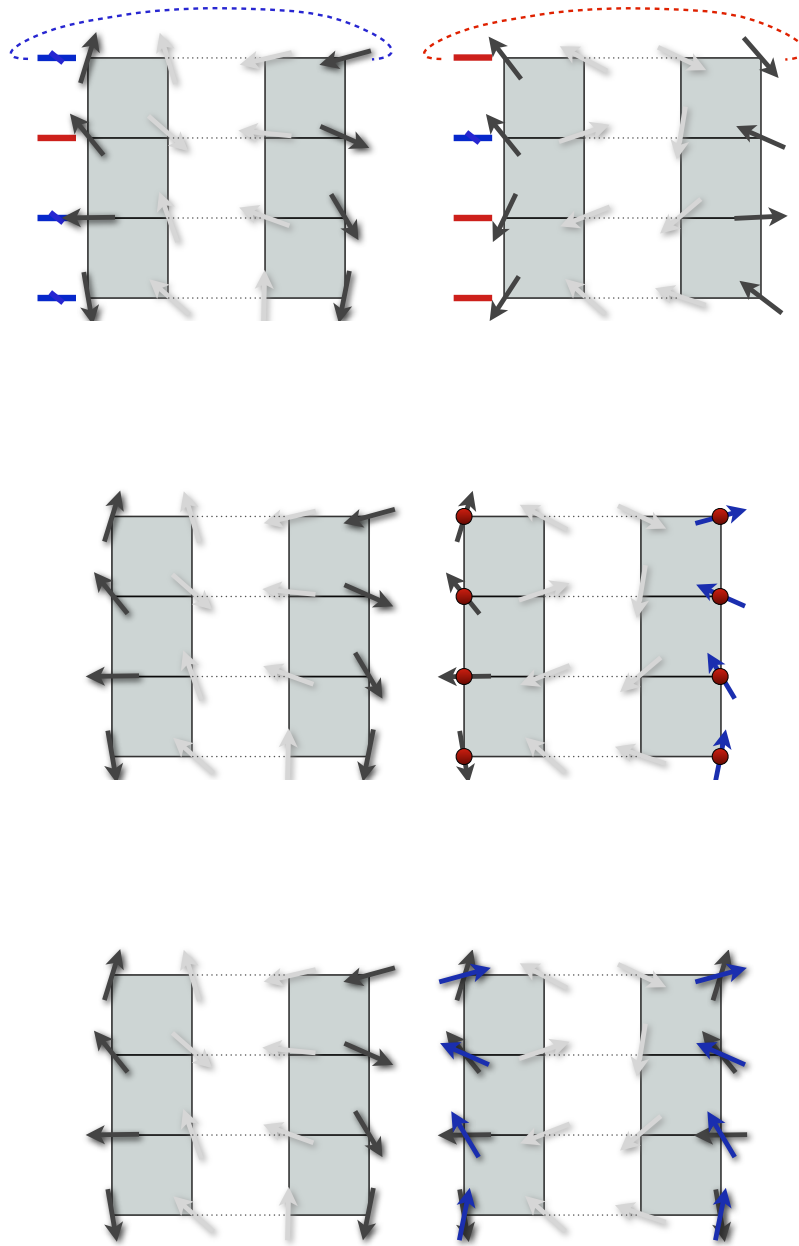
Figure 3.18.: (Color online). Different setups for the boundary conditions on hypercubic lattices. These sketches exemplify the respective main idea for each of the three different boundary conditions, as there is the periodic/anti-periodic (top), open/domain-wall (middle) and open/spin-pair (bottom) setup. Left figures refer to the first ground-state determination and right ones illustrate the same system with changed boundaries in one direction for which a ground state is determined as well. Comparison of these two energies results in the defect energy.

		aL^θ			$aL^\theta(1+b/L)$				$aL^\theta(1+b/L^2)$			
d	$N_s/10^3$	$L_{\min}$	θ	Q	$L_{\min}$	θ	b	Q	$L_{\min}$	θ	b	Q
2	$3-5$	5	$-1.558(4)$	0.76	4	$-1.56(1)$	$-0.09(14)$	0.76	4	$-1.562(7)$	$-0.26(36)$	0.77
3	3	7	$-1.03(2)$	0.99	3	$-1.02(3)$	$0.21(22)$	0.30	3	$-1.03(2)$	$0.31(30)$	0.30
4	3	6	$-0.57(2)$	0.23	3	$-0.52(6)$	$0.51(44)$	0.36	3	$-0.57(3)$	$0.49(43)$	0.31
5	$10-18$	7	$-0.14(1)$	0.97	4	$-0.07(5)$	$0.64(39)$	0.99	3	$-0.11(1)$	$1.17(22)$	0.99
6	$5-13$	5	$0.27(2)$	0.49	3	$0.7(19)$	$5.0(380)$	0.60	3	$0.33(5)$	$1.60(55)$	0.56
7	0.5	3	$0.56(7)$	0.98	–	–	–	–	–	–	–	–

Table 3.5.: Parameters for the defect energy scaling with the P/AP setup for fits with different functional forms. Fits where performed for lattice sizes $L \geq L_{\min}$.

For O/SP boundary conditions one starts out with open boundaries in one direction as in the last setup, as well. The according ground-state energy is then compared to the one determined after changing the boundaries as follows. Based on the ground state, all spins of one of the two sides with open boundaries are rotated about a common axis perpendicular to their according spin-space. Then, these spins are coupled to their corresponding ones on the other side of the system. Their relative orientations are kept *constant pairwise* in the successive ground-state search. This is illustrated in the bottom panel of Fig. 3.18. The new ground state will have a different energy.

If not derived analytically, corrections to scaling are often points of debate. As we will see below, we can come up with arguments justifying certain forms of the corrections to the defect-energy scaling. Reasonably good values of the quality-of-fit parameter Q confirm the arguments given but do not exclude the possibility of other correction terms to be the actual leading ones.

A well-known method minimizing the corrections to scaling is the aspect-ratio approach. The main idea for a hypercubic system of size $L \times \ldots \times L \times L = L^d$ is to elongate it by a factor of R in only one dimension to suppress the influence of the boundaries at which the boundary conditions are being changed. Then the system size is enlarged to $L \times \ldots \times L \times RL = RL^d$. In effect the choice of boundary conditions eventually becomes irrelevant in the limit $R \to \infty$. It is quite convenient that the system size increase does not scale with a power of the dimension. The aspect-ratio approach is discussed and thoroughly tested in Ref. [CBM02] for Ising spin glasses. Also employed rather successfully in Ref. [WG08] for an XY spin-glass model we will use this technique here, as well. To come to the point, as the placement (Sec. 3.3.8) of the section discussing the aspect-ratio approach suggests, we do not find a clear sign that this method is extremely useful for the $m \to \infty$ spin-glass model. For this reason and unless stated otherwise we resorted to the choice $R = 2$ for the determination of defect energies in the sections below. Only afterwards we will briefly come back to the topic of aspect ratios.
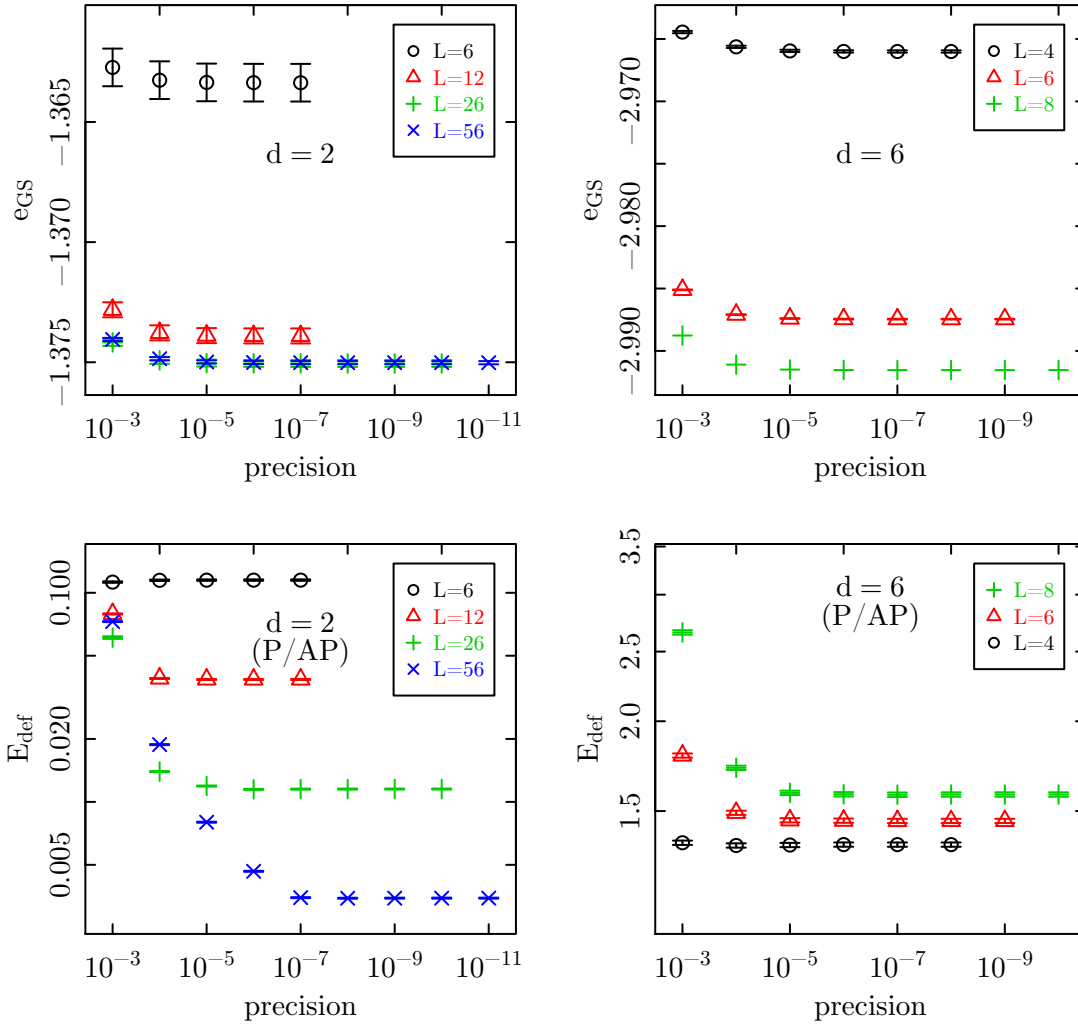
Figure 3.19.: The defect-energy approach relies on computing the ground-state energies e_{GS} (top figures). These energies are calculated up to a certain precision. This number refers to the average difference in energy-per-spin before and after one lattice sweep of local-field quenches. Also the defect energy E_{def} can be analyzed in its evolution with precision (lower figures). For hypercubic models this quantity is more sensitive to precision than the ground-state energy e_{GS} itself. The lower the lattice dimension the more pronounced the dependence on precision is. This is in accordance with the situation for large σ in the 1d power-law model, cf. Sec. 3.2.5.

3.3.6. Defect energies with P/AP boundary conditions

For P/AP boundary conditions ground states were computed for a range of system sizes using between 3000 and 18 000 disorder realizations per lattice size. More realizations have been used for the crucial cases with $|\theta|$ small. Due to the large computational effort, for $d = 7$ our data include only 500 disorder configurations and we resorted to an aspect ratio $R = 1$, shifting the amplitudes of the defect energies. The stiffness exponent is not affected. The number of disorder configurations N_s for each lattice dimension is indicated in Tab. 3.5. The resulting defect energies from P/AP boundary conditions for all lattice dimensions $d = 2, \ldots, 7$ are shown in Fig. 3.20. Furthermore, excluding $d = 7$ due to the differing aspect ratio, Fig. 3.21 shows the curves summarized in one plot. As is most clearly seen for the cases $d = 5$ and $d = 6$ with small $|\theta|$, corrections to the pure power-law behavior expected according to Eq. (3.18) are sizable and can be rather clearly resolved here due to the relatively large number of disorder realizations. Due to being crucial especially at the region close to the lower critical dimension, we assured convergence of the defect energies by monitoring it with increasing precision, cf. Fig. 3.19. However, to describe the deviations, one might argue in favor of a correction resulting from a shift in the effective length scale,

$$
\begin{aligned}
\Delta E \quad \sim \quad & a(L - L_0)^\theta = aL^\theta(1 - L_0/L)^\theta \\
= \quad & aL^\theta(1 + b/L + c/L^2 + \ldots) \, .
\end{aligned}
\tag{3.27}
$$

Our data do not allow to resolve more than one correction term reliably, such that we have to restrict ourselves to including only the $1/L$ or only the $1/L^2$ term. Such fits, as monitored by the quality-of-fit parameter Q [Bra98], work reasonably well. The resulting estimates of θ are statistically compatible with those resulting from fits without correction terms, but omitting data points $L < L_{\min}$ for the smaller lattices, cf. the data collected in Tab. 3.5. Note the exception of the fit with $1/L$ correction term in $d = 6$ which leads to an estimate of θ way off the other estimates, indicating the statistical instability of the fit. For $d = 7$, the limited range of system sizes precludes the use of fits including correction terms. From the quality of the fits alone, we found it impossible to arrive at a general preference for either the $1/L$ or the $1/L^2$ form. Instead, we considered the effective form

$$
\Delta E \sim aL^\theta(1 + bL^{-\omega}) \, ,
\tag{3.28}
$$

which resulted in parameters ω consistent with $\theta - \omega \approx 2$. We interpret these results in favor of a purely additive correction of the form

$$
\Delta E \sim aL^\theta + b/L^2 \, ,
\tag{3.29}
$$

and, indeed, we find this form of fits to work well, cf. the fit results collected in Tab. 3.6. The corresponding fits are denoted by the solid lines in Fig. 3.20 and 3.21. The most relevant results are those for $d = 5$, where θ appears to be still slightly negative, and for $d = 6$, where our estimate of θ is positive. We might conclude, therefore, that the scaling character of defect energies changes in between and, consequently, $5 \leq d_l \leq 6$. The results for the spin stiffness exponent θ and P/AP boundary conditions are summarized in Fig. 3.22. If we make a guess and fit a polynomial of second order, which works quite well, we arrive at an estimate for the lower critical dimension of $d_l = 5.27(4)$.
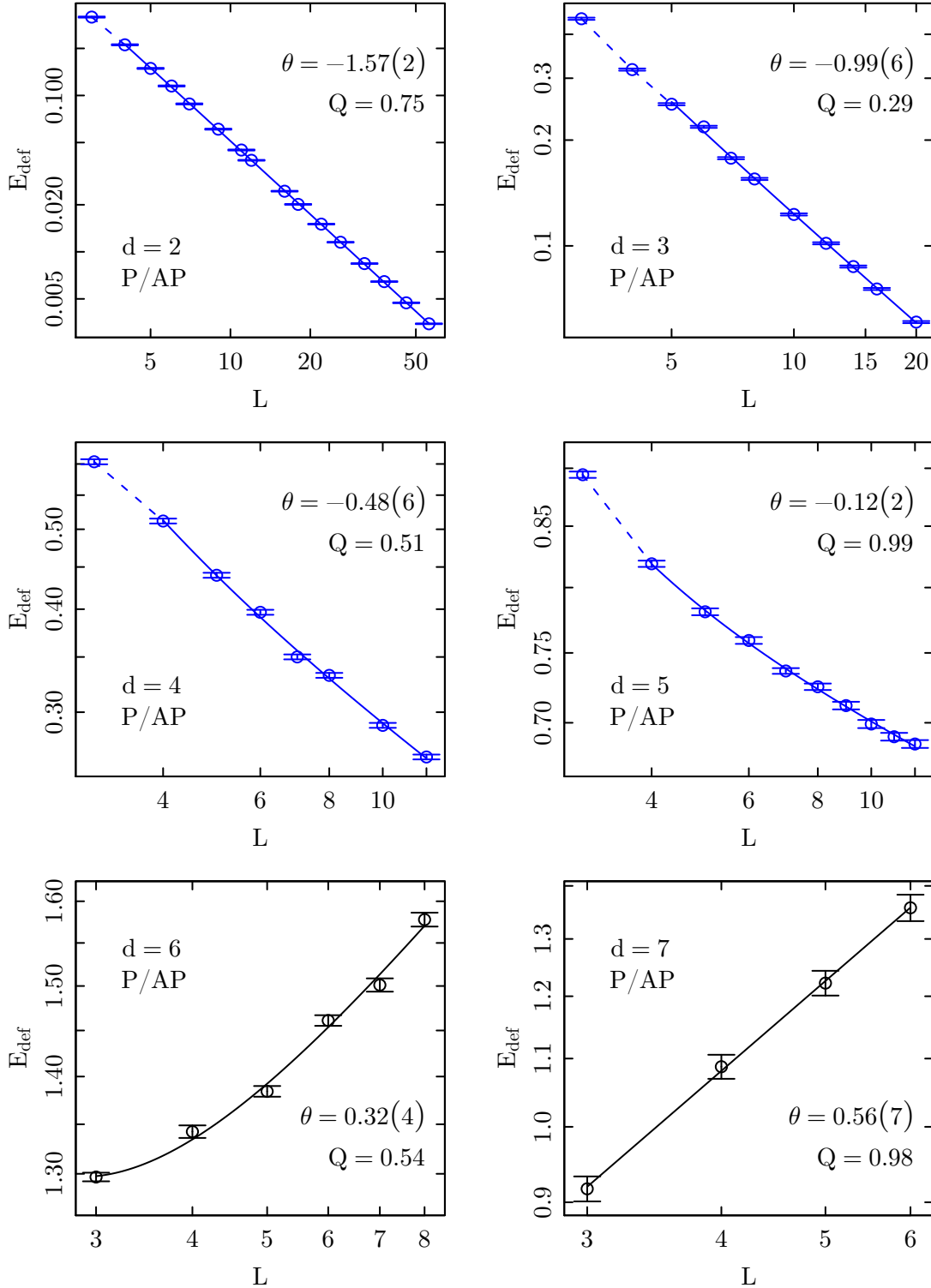
Figure 3.20.: (Color online). Defect energies for the hypercubic $m = \infty$ spin glass as a function of lattice size L for various lattice dimensions. All solid lines show fits of the functional form (3.29) to the data. The corresponding fit parameters are summarized in Tab. 3.6. The spin-stiffness exponent θ changes sign between $5 \leq d \leq 6$. An aspect ratio of $R = 2$ was used for $2 \leq d \leq 6$. Due to limited resources $R = 1$ was chosen in $d = 7$.
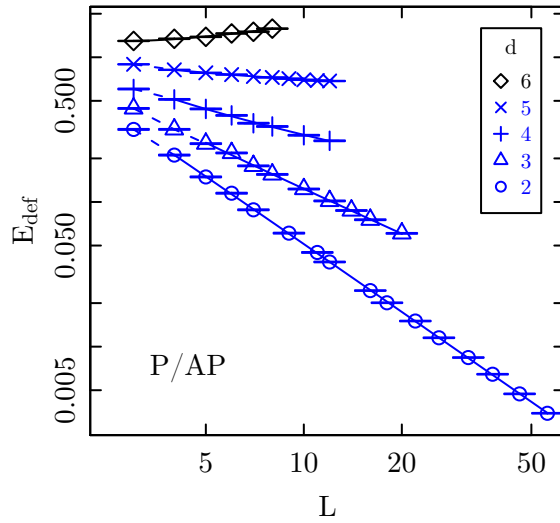
Figure 3.21.: (Color online). Defect energies for the hypercubic $m = \infty$ spin glass as a function of lattice size L for lattice dimensions $d = 2, \ldots, 6$. This is an overview of all single curves of the plots in Fig. 3.20 The spin-stiffness exponent θ changes sign between $5 \leq d \leq 6$. $d = 7$ is not shown due to the fact that a different aspect ratio was used there.
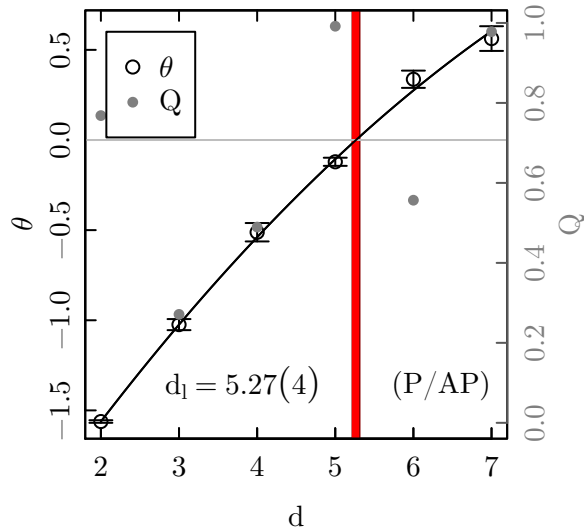
Figure 3.22.: (Color online). The evolution of the spin stiffness exponent θ with lattice dimension d for P/AP boundary conditions. The solid line stems from a guess fit with polynomial of second order. This delivers an estimate of the lower critical dimension $d_l = 5.27(4)$.

3.3.7. Defect energies with other boundary conditions

We now turn to boundary conditions different from the periodic/anti-periodic setup. First we will discuss the O/DW setup. Our corresponding results, averaged over the data for between 3000 and 5000 disorder realizations, are collected in Fig. 3.24. We find scaling corrections to be somewhat more pronounced here as compared to the P/AP setup, and they cannot fully be accounted for in all three lattice dimensions considered by either a $1/L$ correction or a $1/L^2$ correction term alone. We therefore used the effective description (3.28), which results in reasonable fits displayed in Fig. 3.24. The corresponding fit parameters are collected in Tab. 3.7. The rather low values of the quality-of-fit parameter Q in dimensions $d = 3$ and $d = 4$ are not a sign of general poor fit of the chosen functional form but, as closer inspection reveals, result from one or two outliers with relatively large deviations from the fit as compared to the (very small) statistical errors. Surprisingly, for the O/DW setup the spin-stiffness exponent θ changes sign already around $d = 3$, and it is clearly positive for the lattice dimensions $5 \leq d \leq 6$ where the crossover occurred for the P/AP boundaries. A linear fit of the three data points for θ in Fig. 3.25 results in a lower critical dimension of $d_l = 3.03(7)$.

Besides, the axis of rotation used during the change of boundary condition was chosen to be perpendicular to the space spanned by the boundary spins to be rotated, as mentioned in the beginning, cf. Sec. 3.3.5. A test run in $d = 2$ using a different axis, namely $\vec{e}_1 \in \mathbb{R}^m$, being the unit vector in one direction, did not alter the value of θ.

The last set of boundaries to be discussed here for the hypercubic model is the O/SP setup. Qualitatively they behave similar compared to the O/DW boundary conditions. It just remains to say a few words about how to do the quench update if the relative orientations of two spins at opposing boundaries are to be kept constant. Imagine that we want to align the pair of spins $\{\mathbf{S}_k, \mathbf{S}_l\}$ optimally in their collective local field, so that formally

$$(-\mathbf{S}_k) \cdot \sum_{\substack{i \in \mathcal{N}(k) \\ i \neq k}} J_{ki}\mathbf{S}_i \;\; + \;\; (-\mathbf{S}_l) \cdot \sum_{\substack{j \in \mathcal{N}(l) \\ j \neq l}} J_{lj}\mathbf{S}_j \;\; = \;\; \min! \, , \tag{3.30}$$

obeying

$$\mathbf{S}_k \cdot \mathbf{S}_l \;\; = \;\; \text{const} \tag{3.31a}$$
$$|\mathbf{S}_k| \;\; = \;\; 1 \tag{3.31b}$$
$$|\mathbf{S}_l| \;\; = \;\; 1 \, . \tag{3.31c}$$

For convenience we introduce abbreviations for the (partial) local fields,

$$\tilde{\mathbf{H}}_x = \sum_{\substack{i \in \mathcal{N}(x) \\ i \neq x}} J_{xi}\mathbf{S}_i,$$
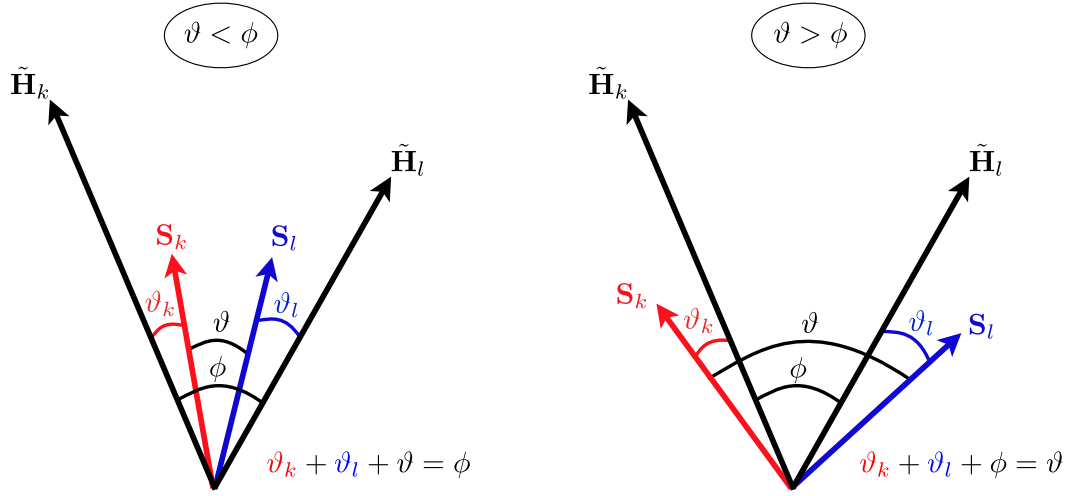
Figure 3.23.: (Color online). For spin-pair boundary conditions the relative orientations of two spins at opposing boundaries are kept constant. A minimal energy configuration is obtained if the spin-pair lies in the plane spanned by the (partial) local field vectors $\tilde{\mathbf{H}}_k$ and $\tilde{\mathbf{H}}_l$. For details see the text.

and according to Fig. 3.23 we denote

$$
\begin{align}
\phi &= \angle(\tilde{\mathbf{H}}_k, \tilde{\mathbf{H}}_l) \,, \tag{3.32a} \\
\vartheta &= \angle(\mathbf{S}_k, \mathbf{S}_l) \,, \tag{3.32b} \\
\vartheta_k &= \angle(\tilde{\mathbf{H}}_k, \mathbf{S}_k) \,, \tag{3.32c} \\
\vartheta_l &= \angle(\tilde{\mathbf{H}}_l, \mathbf{S}_l) \,. \tag{3.32d}
\end{align}
$$

We define a function f for Eq. (3.30) reading

$$
\begin{align}
f(\vartheta_k) &= -|\mathbf{S}_k||\tilde{\mathbf{H}}_k| \cos \vartheta_k - |\mathbf{S}_l||\tilde{\mathbf{H}}_l| \cos \vartheta_l \\
&= -|\tilde{\mathbf{H}}_k| \cos \vartheta_k - |\tilde{\mathbf{H}}_l| \cos \vartheta_l \,, \tag{3.33}
\end{align}
$$

with

$$
\vartheta_l = \begin{cases} \phi - \vartheta - \vartheta_k & \text{, if } \vartheta < \phi \,, \\ -\phi + \vartheta - \vartheta_k & \text{, otherwise} \,. \end{cases} \tag{3.34}
$$

We already included the reasonable assumption that a minimal energy configuration is obtained when the (partial) local fields and the spin pair lie in one plane, as indicated in Fig. 3.23.

To determine the absolute minimum in energy, we need to solve $f'(\vartheta_k) \stackrel{!}{=} 0$. There are four

solutions to this equation, namely

$$
\vartheta_k = \begin{cases} -\arccos(-X) \\ \arccos(-X) \\ -\arccos(X) \\ \arccos(X) \end{cases} , \tag{3.35}
$$

with

$$
X = \frac{|\tilde{\mathbf{H}}_k| + |\tilde{\mathbf{H}}_l|\cos(\pm\phi \mp \vartheta)}{\sqrt{|\tilde{\mathbf{H}}_k|^2 + |\tilde{\mathbf{H}}_l|^2 + 2|\tilde{\mathbf{H}}_k||\tilde{\mathbf{H}}_l|\cos(\pm\phi \mp \vartheta)}} , \tag{3.36}
$$

where the upper signs correspond to $\vartheta < \phi$ and the lower ones to $\vartheta > \phi$. Only the second derivative of f can decide about the correct value. All possible versions read

$$
f''(\vartheta_k) = \begin{cases} -|\tilde{\mathbf{H}}_k|X - |\tilde{\mathbf{H}}_l|\sin(\pm\phi \mp \vartheta + \arcsin X) \\ -|\tilde{\mathbf{H}}_k|X - |\tilde{\mathbf{H}}_l|\cos(\pm\phi \mp \vartheta + \arccos X) \\ |\tilde{\mathbf{H}}_k|X + |\tilde{\mathbf{H}}_l|\cos(\pm\phi \mp \vartheta + \arccos X) \\ |\tilde{\mathbf{H}}_k|X + |\tilde{\mathbf{H}}_l|\sin(\pm\phi \mp \vartheta + \arcsin X) \end{cases} . \tag{3.37}
$$

It should be noted that ϑ_k and ϑ_l do not exceed $\pi/2$ in their minimum configuration. If a value greater than this is obtained it can be adjusted by subtracting it from π.

Case $\vartheta < \phi$

If $\vartheta < \phi$, then we can assume that the (unnormalized) spin $\mathbf{S}_k$ can be constructed as

$$
\mathbf{S}_k = x\tilde{\mathbf{H}}_k + \tilde{\mathbf{H}}_l \tag{3.38}
$$

with a non-negative number $x \in \mathbb{R} \cap [0, \infty)$ and with

$$
\cos\vartheta_k = \frac{\tilde{\mathbf{H}}_k \cdot (x\tilde{\mathbf{H}}_k + \tilde{\mathbf{H}}_l)}{|\tilde{\mathbf{H}}_k||(x\tilde{\mathbf{H}}_k + \tilde{\mathbf{H}}_l)|} \tag{3.39}
$$

we can resolve for x. The solution reads

$$
x_{1,2} = -\frac{|\tilde{\mathbf{H}}_l|}{|\tilde{\mathbf{H}}_k|}\left(\cos\phi \pm \frac{\sin\phi}{\tan\vartheta_k}\right) . \tag{3.40}
$$

Since x was chosen to be positive

$$
x = \max(x_1, x_2) . \tag{3.41}
$$

Then, the (unnormalized) spin $\mathbf{S}_l$ could be calculated accordingly by

$$
\mathbf{S}_l = x\tilde{\mathbf{H}}_l + \tilde{\mathbf{H}}_k \tag{3.42}
$$

again with $x \in \mathbb{R} \cap [0, \infty)$ and

$$
x = \max\left(-\frac{|\tilde{\mathbf{H}}_k|}{|\tilde{\mathbf{H}}_l|}\left(\cos\phi \pm \frac{\sin\phi}{\tan\vartheta_l}\right)\right) . \tag{3.43}
$$

Case $\vartheta > \phi$

If, on the other hand $\vartheta > \phi$, then we analogously construct

$$\mathbf{S}_k = x\tilde{\mathbf{H}}_k - \tilde{\mathbf{H}}_l \tag{3.44}$$

with

$$x = \max\left(\frac{|\tilde{\mathbf{H}}_l|}{|\tilde{\mathbf{H}}_k|}\left(\cos\phi \mp \frac{\sin\phi}{\tan\vartheta_k}\right)\right) . \tag{3.45}$$

and

$$\mathbf{S}_l = x\tilde{\mathbf{H}}_l - \tilde{\mathbf{H}}_k \tag{3.46}$$

with

$$x = \max\left(\frac{|\tilde{\mathbf{H}}_k|}{|\tilde{\mathbf{H}}_l|}\left(\cos\phi \mp \frac{\sin\phi}{\tan\vartheta_l}\right)\right) . \tag{3.47}$$

d	$L_{\min}$	$aL^\theta + b/L^2$		
		θ	b	Q
2	4	$-1.57(2)$	$-0.21(36)$	0.75
3	5	$-0.99(6)$	0.57(64)	0.29
4	4	$-0.48(6)$	1.31(61)	0.51
5	4	$-0.12(2)$	0.73(36)	0.99
6	3	0.32(4)	1.46(40)	0.54

Table 3.6.: Parameters of fits of the functional form (3.29) to the data for P/AP boundaries.

d	$L_{\min}$	$aL^\theta(1 + bL^{-\omega})$			
		θ	ω	b	Q
2	6	$-0.96(1)$	1.4(10)	4.7(16)	0.27
3	4	$-0.031(6)$	1.44(24)	1.94(27)	2.6×10^{-5}
4	3	0.91(2)	0.94(13)	1.803(35)	1.5×10^{-5}

Table 3.7.: Parameters of fits of the functional form (3.28) to the data for O/DW boundaries.

d	$L_{\min}$	$aL^\theta(1 + bL^{-\omega})$			
		θ	ω	b	Q
2	5	$-1.04(5)$	1.21(2)	6.7(12)	0.21
3	3	$-0.17(1)$	1.52(29)	3.93(29)	0.54
4	3	0.70(2)	1.51(37)	3.57(26)	0.04

Table 3.8.: Parameters of fits of the functional form (3.28) to the data for O/SP boundaries.
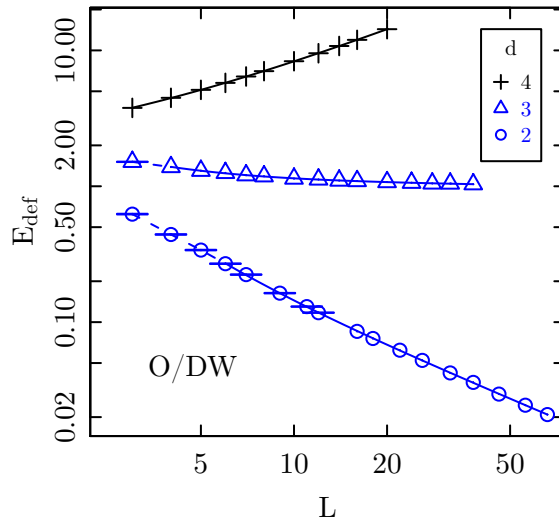
Figure 3.24.: (Color online). Defect energies for the hypercubic $m = \infty$ spin glass as a function of lattice size L for lattice dimensions $d = 2, 3, 4$ and O/DW boundary conditions. The solid lines show fits of the functional form (3.28) to the data. The corresponding fit parameters are summarized in Tab. 3.7. The spin-stiffness exponent θ changes sign in the vicinity of $d = 3$.
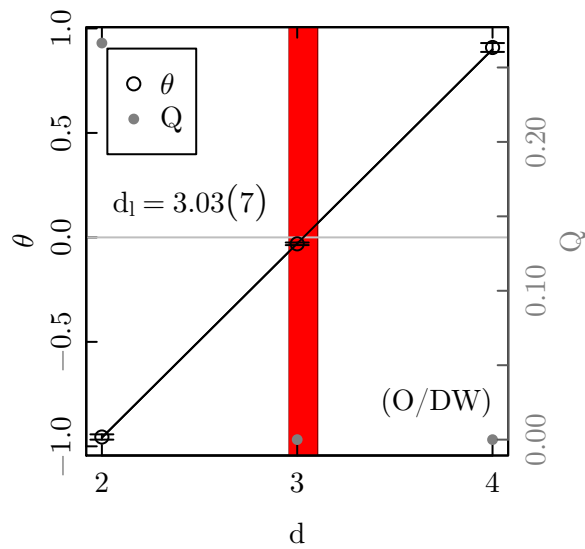
Figure 3.25.: (Color online). The evolution of the spin stiffness exponent θ with lattice dimension d for O/DW boundary conditions. The solid line stems from a linear guess fit. This delivers an estimate of the lower critical dimension $d_l = 3.03(7)$.
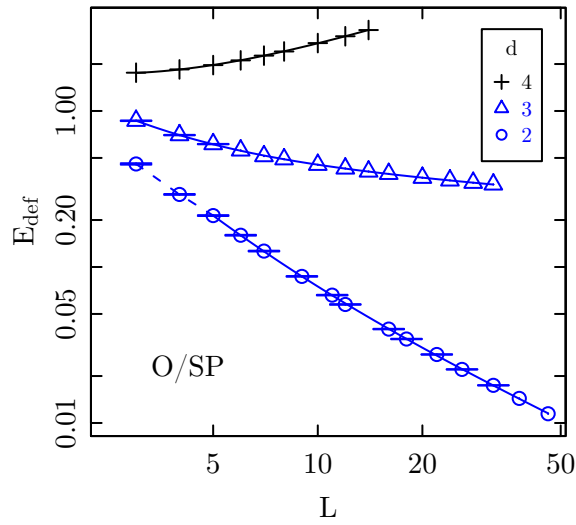
Figure 3.26.: (Color online). Defect energies for the hypercubic $m = \infty$ spin glass as a function of lattice size L for lattice dimensions $d = 2, 3, 4$ and O/SP boundary conditions. The solid lines show fits of the functional form (3.28) to the data. The corresponding fit parameters are summarized in Tab. 3.8. The spin-stiffness exponent θ changes sign in the vicinity of $d = 3$.
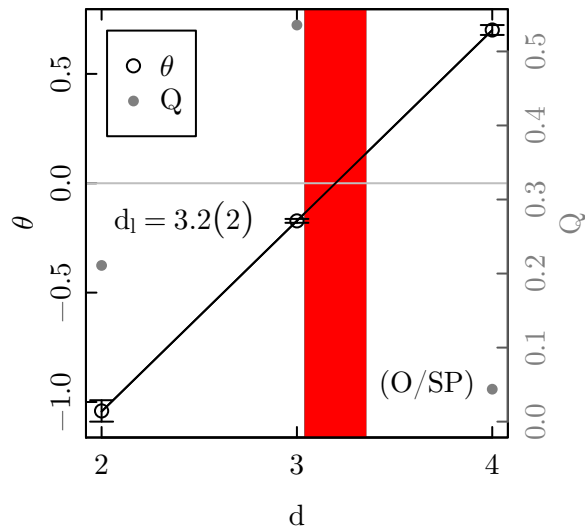
Figure 3.27.: (Color online). The evolution of the spin stiffness exponent θ with lattice dimension d for O/SP boundary conditions. The solid line stems from a linear guess fit. This delivers an estimate of the lower critical dimension $d_l = 3.2(2)$.
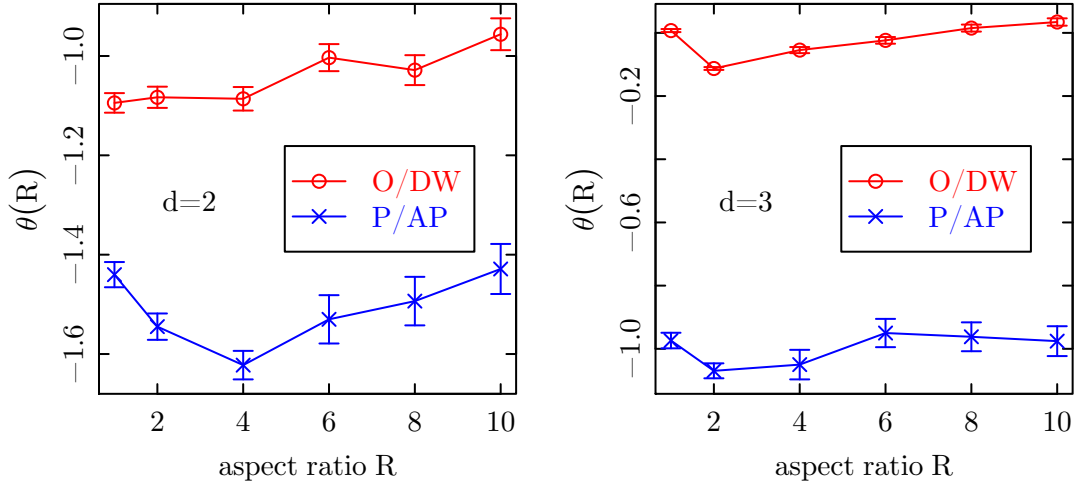
Figure 3.28.: (Color online). The aspect-ratio approach does not seem to effect the corrections to scaling in the $m \to \infty$ spin-glass model. This observation leads us to keep the aspect ratio fixed and to not analyze the scaling for $R \to \infty$.

3.3.8. Aspect ratio scaling

As anticipated at the end of section 3.3.5 we do not observe considerable improvement concerning the corrections to scaling when using the aspect-ratio technique. Measuring the defect energies and extracting the stiffness exponents for different aspect ratios $R = 1, \ldots, 10$ we see no clear effect such that we would be tempted to extrapolate the values of θ to $R \to \infty$ in $d = 2$ and 3, cf. Fig. 3.28. We used lattice sizes $L = 8, \ldots, 24$ in $d = 2$ and $L = 6, \ldots, 16$ in $d = 3$ both averaged over 500 independent disorder realizations each R and L. As the influence of R even seems to become less for an increase in the dimensionality we checked only P/AP boundary conditions in $d = 4$ and $d = 5$ (not shown) and found an almost constant $\theta(R)$. Therefore, one may conclude that it is reasonable to resort to a fixed aspect ratio R to analyze the defect energies as done in the preceding sections.

3.3.9. Comparison of boundary conditions

One might wonder whether the apparently rather different estimates of stiffness exponents from the three boundary setups could be due to them exciting different types of defects, for instance of the spin and chiral character, respectively. While the O/DW and O/SP construction certainly forms the cleaner setup in that one directly probes the energy of a single domain-wall defect, distinctions between spin and chiral excitations are subtle for this model: in general, we would associate the sign of the determinant of the considered $O(m)$ rotation matrix with the chiral degrees of freedom [Kaw10]. For the chosen setup of boundaries, however, the determinant of the rotation matrix depends on whether the number of spin dimensions occupied by the boundary spins is even or odd. Since the required number of spin components fluctuates between disorder realizations, however, the chirality
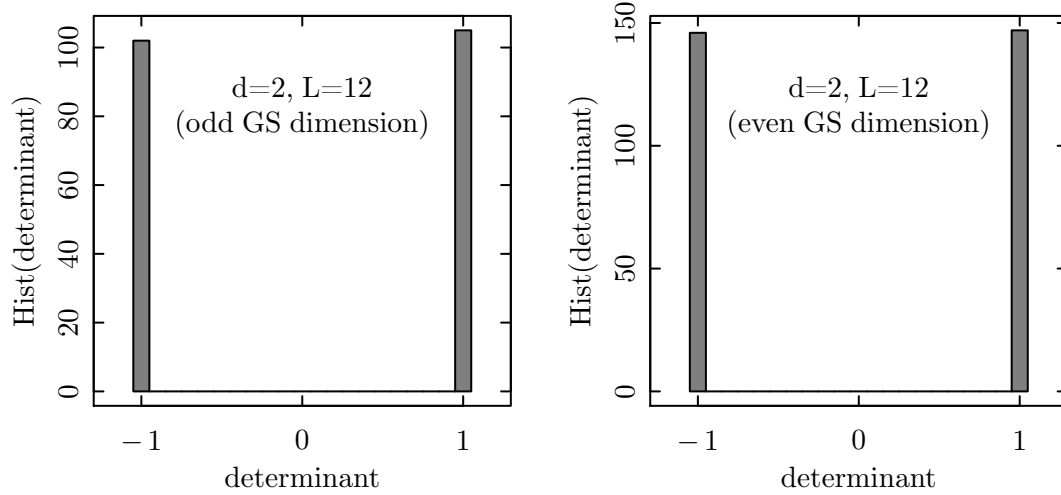
Figure 3.29.: (Color online). The sign of the determinant of the rotation matrix for the O/DW setup does obviously not depend on the number of spin-space dimensions m^* the ground state occupies being even or odd. This was tested for lattice dimensions $d = 2$ and 3 and several linear lattice sizes L. The upper showcase histogram shows results for $d = 2$, $L = 12$ and throughout $m > m^*$.

is formally maldefined after taking the disorder average. For O/DW boundary conditions we tested the dependence of the determinant on the number of necessary spin dimensions m^* being even or odd, respectively. We found positive and negative determinants equally often, cf. Fig. 3.29, so that the sign of the determinant does obviously not depend on the spin-space the ground-state occupies. Also, we find no difference in scaling behavior between disorder realizations having an even or odd spin dimension m. Therefore, it appears more plausible that the setup with O/DW and O/SP boundaries implicitly probes the physically more realistic case of taking the $N \to \infty$ limit before the $m \to \infty$ limit where, from the experience with finite m, we expect a lower critical dimension $d \approx 3$.

3.4. Summary

In this chapter the zero-temperature properties have been investigated thoroughly for the spin-glass model in the limit of infinitely many spin components. Quasi-exact ground-state calculations have been done with some ease due to the model having no metastability.

Ground-state energies have been found to be in accord with our scaling assumptions. Among many similarities we found important differences between the fully connected and the diluted version of the 1d power-law model. The ground-state energies found are consistent with calculations on a Bethe lattice of Ref. [BA06]. The sample to sample fluctuations are constant (with a scaling exponent of $\Theta_f = 1/2$) over all universality classes in the diluted version, whereas they cross over to a value $\Theta_f = 1/5$ in the infinite-range region as predicted in Ref. [Asp10] for the fully connected one. For all accessible lattice dimensions of the hypercubic model considered ($d = 2, \ldots, 7$) we found the short-range value $\Theta_f = 1/2$. A full analysis of the ground-state energy distributions revealed the Gaussian nature for all universality classes, i.e. for the whole range of σ. We found also Gaussian behavior for the hypercubic model up to the highest considered lattice dimension $d = 7$.
Lacking a theoretical quantitative description, the scaling of the spin-space dimension showed its qualitatively correct behavior with even a quantitative correct exponent $\mu = 2/5$ in the infinite-range region (1d power-law). The exponent μ decreases, as expected, for lower values of σ. The expected qualitative behavior was also seen for the hypercubic model where μ grows for increasing lattice dimension and $\mu < 2/5$ is fulfilled.

In terms of the 1d model we confirmed $\sigma_u = 3/4$ to be the 'upper critical' value corresponding to the lower critical dimension d_l. The critical value σ_u is lowered compared to $\sigma_u = 1$ for the $m < \infty$ model [KAS83]. The prediction $\theta = 3/4 - \sigma$ seems correct, although numerical values were slightly larger systematically. In the infinite-range region, however, $\theta = 1/4$ is taken on perfectly. The diluted version of the model does show an asymptotically exponential decay of the defect energies for $\sigma > 1$. Crossover effects were seen for $3/4 < \sigma < 1$, but increasing the connectivity showed a convergence towards the values resulting from simulations of the fully connected version. For $\sigma > 1$ the diluted and the fully connected 1d power-law spin glass are definitely not universal anymore. The former becomes equivalent to a real 1d short-range system. Right at $\sigma = 1$ critical exponents depend continuously on the average coordination number z. Anyway, the defect energy distributions turned out to follow a Gaussian.
In essence, we suggest to use the fully connected version of the model, since we found finite-size corrections to be more pronounced in the diluted one. Larger lattice sizes in the latter can merely impress at first sight but do not improve the quality of results.

Concerning the lower critical dimension of the $m = \infty$ spin glass on a hypercubic lattice determined with different boundary conditions we did not find any sign of these boundary conditions exciting different types of defects, for instance with spin or chiral character. It might be that P/AP boundary conditions probe the numerically implicit taking of limits $m \to \infty$ and afterwards $N \to \infty$. O/DW and O/SP boundaries might therefore probe

the physically more realistic case of taking the limits the other way around. This could be subject of extensions of the present work.

As for now, the lower critical dimension of the model with $m \to \infty$ first appears to be $5 \leq d_l \leq 6$, consistent with the results of Ref. [GBM82], but in contrast to the conjecture $d_l = 8$ of [Via88], based on a perturbation expansion. The upper critical dimension, on the other hand, is predicted to be 8 [GBM82]. The alternative sets of boundary conditions studied here might provide a means of studying the $m \to \infty$ limit of the finite-m models, for which one expects a lower critical dimension $d = 3$. We found a critical dimension $d_l = 3.03(7)$ for the open/domain-wall setup of boundary conditions and $d_l = 3.2(2)$ for the open/spin-pair one.

It is, however, striking that both the 1d power-law and the hypercubic model do show a critical value for the upper critical σ_u and the lower critical d_l, which are shifted slightly to the short-range regions as compared to theoretical predictions.

Chapter 4.

Correlation matrix calculations at finite temperature

The $T = 0$ ground-state calculations were simplified by the fact that metastability has disappeared in the infinite component limit $m \to \infty$. However, the critical behavior above the lower critical dimension d_l (or below the upper critical $\sigma_u = 3/4$ for the 1d power-law model) can only be studied with techniques operating at finite temperature. This section discusses a $T > 0$ approach using saddle-point equations, leading to an iterative set of matrix equations being well amenable to numerical investigation and permitting an exact solution of the $m \to \infty$ model [BM82]. They allow to determine the thermally averaged spin-spin correlation matrix and give access to the Edwards-Anderson order parameter q_{EA}, the spin-glass susceptibility χ_{SG}, the correlation function $G(r)$ and the correlation length ξ_L.

After shedding light on the partition function and using saddle-point techniques in order to find an expression for the correlation matrix we will deduce the saddle-point condition constituting the core of the numerical calculations. The connection to the zero-temperature calculations will be outlined. Next, the order parameter q_{EA} and the susceptibility χ_{SG} will be derived from the correlation matrix.

Furthermore, the required numerical toolkit will be described so that results can be reproduced by the reader. Theoretical insights will be tested in the successive section on the plain SK model, the one-dimensional power-law model and hyper-cubic models. The nature of the matrix equations suggests to use the fully connected version in terms of the one-dimensional power-law model, since the diluted version does not have any computational advantages.

4.1. The partition function

First of all we want to write down the partition function which includes all information about our system at equilibrium. It will be reformulated until a saddle-point approximation can help us further.

Generalizing the considered spin-glass Hamiltonian we include an external-field term such that

$$\mathcal{H} = -\frac{1}{2} \sum_{\substack{i,j=1 \\ i \neq j}}^{N} J_{ij}\, \mathbf{S}_i \cdot \mathbf{S}_j - \sum_{i=1}^{N} \mathbf{h}_i \cdot \mathbf{S}_i \,, \tag{4.1}$$

where the vectors $\mathbf{h}_i \in \mathbb{R}^m$ are Gaussian random fields with correlator

$$\overline{h_k^a h_j^b} = h^2 \delta_{kj} \delta_{ab} \, . \tag{4.2}$$

For finite as well as for infinite dimensional systems the partition function can be written as

$$
\begin{aligned}
Z &= \int_{-\infty}^{\infty} \prod_{i=1}^{N} \prod_{\alpha=1}^{m} \mathrm{d}S_i^{\alpha} \left[\prod_{j=1}^{N} \delta \left(\mathbf{S}_j^2 - m \right) \right] e^{-\beta \mathcal{H}} \\
&= \int_{-\infty}^{\infty} \prod_{i=1}^{N} \prod_{\alpha=1}^{m} \mathrm{d}S_i^{\alpha} \left[\prod_{j=1}^{N} \int_{-\infty}^{\infty} \frac{\beta \mathrm{d}k_j}{4\pi} \exp \left(i \frac{\beta k_j}{2} \left(m - \mathbf{S}_j^2 \right) \right) \right] e^{-\beta \mathcal{H}} \, ,
\end{aligned}
\tag{4.3}
$$

where the integral representation of the delta-distribution was used. Substituting variables yields

$$
\begin{aligned}
Z &\propto \int_{-\infty}^{\infty} \prod_{i=1}^{N} \prod_{\alpha=1}^{m} \mathrm{d}S_i^{\alpha} \left[\prod_{j=1}^{N} \int_{-i\infty}^{i\infty} \frac{\beta \mathrm{d}H_j}{4\pi} \exp \left(\frac{\beta H_j}{2} \left(m - \mathbf{S}_j^2 \right) \right) \right] e^{-\beta \mathcal{H}} \\
&= \int_{-\infty}^{\infty} \prod_{i=1}^{N} \prod_{\alpha=1}^{m} \mathrm{d}S_i^{\alpha} \int_{-i\infty}^{i\infty} \prod_{j=1}^{N} \frac{\beta \mathrm{d}H_j}{4\pi} \exp \left(\sum_{k=1}^{N} \frac{\beta H_k}{2} \left(m - \mathbf{S}_k^2 \right) \right) e^{-\beta \mathcal{H}} \\
&= \int_{-i\infty}^{i\infty} \prod_{j=1}^{N} \frac{\beta \mathrm{d}H_j}{4\pi} \underbrace{\left[\int_{-\infty}^{\infty} \prod_{i=1}^{N} \prod_{\alpha=1}^{m} \mathrm{d}S_i^{\alpha} \exp \left(- \sum_{k=1}^{N} \frac{\beta H_k}{2} \mathbf{S}_k^2 \right) e^{-\beta \mathcal{H}} \right]}_{I_1} \exp \left(\sum_{k=1}^{N} \frac{\beta H_k}{2} m \right) \, ,
\end{aligned}
$$
$$\tag{4.4}$$

where I_1 is the part depending on S_i^{α}, which can be evaluated as shown below. The variables H_i will turn out to have a profound physical meaning, at least as $T \to 0$. With the given Hamiltonian the exponent of I_1 reads

$$
\begin{aligned}
-\frac{\beta}{2} \sum_{i=1}^{N} H_i \mathbf{S}_i^2 &+ \frac{\beta}{2} \sum_{i,j} J_{ij} \mathbf{S}_i \cdot \mathbf{S}_j + \beta \sum_{i=1}^{N} \mathbf{h}_i \cdot \mathbf{S}_i \\
&= -\sum_{\gamma=1}^{m} \sum_{i,j} \frac{\beta}{2} \left(H_i \delta_{ij} - J_{ij} \right) S_i^{\gamma} S_j^{\gamma} + \beta \sum_{\gamma=1}^{m} \sum_i h_i^{\gamma} S_i^{\gamma} \\
&= \sum_{\gamma=1}^{m} \left[-\frac{\beta}{2} \sum_{i,j} S_i^{\gamma} A_{ij} S_j^{\gamma} + \beta \sum_i h_i^{\gamma} S_i^{\gamma} \right] \\
&= \sum_{\gamma=1}^{m} \left[-\frac{\beta}{2} \overrightarrow{S^{\gamma}} \cdot (A \overrightarrow{S^{\gamma}}) + \beta \overrightarrow{h^{\gamma}} \cdot \overrightarrow{S^{\gamma}} \right] \, .
\end{aligned}
\tag{4.5}
$$

Notice that we changed the vector notation in the last line in order to emphasize that now $\overrightarrow{X^{\alpha}} \in \mathbb{R}^N$. Above we made the definition

$$A_{ij} = H_i \delta_{ij} - J_{ij} \, . \tag{4.6}$$

The matrix A will play a central role in what will follow. It is obviously symmetric since $J_{ij} = J_{ji}$ and thus diagonalizable. We denote its eigenvalues by λ_x, and if $\lambda_x > 0$ define its inverse χ with the elements

$$\chi_{ij} = (A^{-1})_{ij} \tag{4.7}$$

and remark that also χ is symmetric.

With Eq. (4.5) we can write

$$I_1 = \prod_{\alpha=1}^{m} \left[\int_{-\infty}^{\infty} \prod_{i=1}^{N} dS_i \exp\left(-\frac{\beta}{2} \vec{S} \cdot (A\vec{S}) + \beta \overrightarrow{h^{\alpha}} \cdot \vec{S} \right) \right] = \prod_{\alpha=1}^{m} I_2(\alpha) \,, \tag{4.8}$$

where we dropped the index α for the $\overrightarrow{S^{\alpha}}$ since the integrals factorize. Integrals for different α differ only by $\overrightarrow{h^{\alpha}}$.

Due to the mentioned properties of the matrix A there exists an orthogonal transformation O with $|\det O| = 1$ and $OO^{\mathsf{T}} = \mathbf{1}$ such that $OAO^{\mathsf{T}} = A^D$ is the diagonalized matrix. By substituting $\vec{S'} = O\vec{S}$

$$\begin{aligned} \vec{S} \cdot (A\vec{S}) &= \vec{S} \cdot (\mathbf{1}A\mathbf{1}\vec{S}) = \vec{S} \cdot (O^{\mathsf{T}}OAO^{\mathsf{T}}O\vec{S}) \\ &= (O\vec{S}) \cdot ((OAO^{\mathsf{T}})(O\vec{S})) \\ &= \vec{S'} \cdot (A^D \vec{S'}) \end{aligned} \tag{4.9}$$

and

$$\begin{aligned} \overrightarrow{h^{\alpha}} \cdot \vec{S} &= \overrightarrow{h^{\alpha}}(\mathbf{1} \cdot \vec{S}) = \overrightarrow{h^{\alpha}} \cdot (O^{\mathsf{T}}O)\vec{S} = (O\overrightarrow{h^{\alpha}}) \cdot (O\vec{S}) \\ &= (O\overrightarrow{h^{\alpha}}) \cdot \vec{S'} \,. \end{aligned} \tag{4.10}$$

Having the eigenvalues λ_i at the main diagonal of A^D

$$\begin{aligned} I_2(\alpha) &= \int_{-\infty}^{\infty} \prod_{i=1}^{N} dS_i' \exp\left(-\frac{\beta}{2} \vec{S'} \cdot (A^D \vec{S'}) + \beta (O\overrightarrow{h^{\alpha}}) \cdot \vec{S'} \right) \\ &= \int_{-\infty}^{\infty} \prod_{i=1}^{N} dS_i' \exp\left(-\frac{\beta}{2} \sum_{i=1}^{N} S_i'^2 \lambda_i + \beta \sum_{i} (O\overrightarrow{h^{\alpha}})_i S_i' \right) \\ &= \prod_{i=1}^{N} \left[\int_{-\infty}^{\infty} dS_i' \exp\left(-\frac{\beta \lambda_i}{2} S_i'^2 + \beta (O\overrightarrow{h^{\alpha}})_i S_i' \right) \right] \end{aligned} \tag{4.11}$$

and we end up with N one-dimensional Gaussian integrals. Thus, we find for $\lambda_i > 0$

$$I_1 = \prod_{\alpha=1}^{m} I_2(\alpha) = \prod_{\alpha=1}^{m} \prod_{i=1}^{N} \sqrt{\frac{2\pi}{\beta \lambda_i}} \exp\left(\frac{1}{2\beta \lambda_i} \left[\beta (O\overrightarrow{h^{\alpha}})_i \right]^2 \right) \,. \tag{4.12}$$

It remains to analyze the factors in the above products.

$$p_1 := \prod_{\alpha=1}^{m} \prod_{i=1}^{N} (2\pi)^{\frac{1}{2}} = (2\pi)^{\frac{Nm}{2}} \,. \tag{4.13}$$

Since λ_i are the eigenvalues of A, $1/\lambda_i$ are the ones of $\chi = A^{-1}$. Recall that the product of all eigenvalues of a matrix is its determinant. Then,

$$
\begin{aligned}
p_2 \;&:=\; \prod_{\alpha=1}^{m}\prod_{i=1}^{N}\left(\frac{1}{\beta\lambda_i}\right)^{\frac{1}{2}} = \left(\prod_{i=1}^{N}\frac{1}{\beta\lambda_i}\right)^{\frac{m}{2}} \\
&=\; \exp\left(\frac{m}{2}\ln\det\left(\frac{1}{\beta}A^{-1}\right)\right) \\
&=\; \exp\left(\frac{m}{2}\ln\det\frac{\chi}{\beta}\right) .
\end{aligned}
\tag{4.14}
$$

and

$$
\begin{aligned}
p_3 \;&:=\; \prod_{\alpha=1}^{m}\prod_{i=1}^{N}\exp\left(\frac{\beta}{2\lambda_i}\left[(O\vec{h^\alpha})_i\right]^2\right) \\
&=\; \prod_{\alpha=1}^{m}\prod_{i=1}^{N}\exp\left(\frac{\beta}{2\lambda_i}\sum_j O_{ij}\vec{h^\alpha}_j \sum_k O_{ik}\vec{h^\alpha}_k\right) \\
&=\; \exp\left(\sum_i \frac{\beta}{2\lambda_i}\sum_{jk}O_{ij}O_{ik}\sum_{\alpha=1}^{m}h_k^\alpha h_j^\alpha\right) .
\end{aligned}
\tag{4.15}
$$

For p_3 we use Eq. (4.2) yielding

$$
\sum_{\alpha=1}^{m}h_k^\alpha h_j^\alpha = mh^2\delta_{kj}
\tag{4.16}
$$

and since O is orthogonal

$$
\sum_j O_{ij}O_{ij} = \sum_j O_{ij}O_{ji}^{\mathsf{T}} = (OO^{\mathsf{T}})_{ii} = \mathbf{1}_{ii} = 1 .
\tag{4.17}
$$

Lastly, because of the invariance of the trace operation

$$
\sum_i \frac{1}{\lambda_i} = \mathrm{Tr}\left((A^{-1})^D\right) = \mathrm{Tr}(A^{-1}) = \mathrm{Tr}(\chi) = \sum_i \chi_{ii} .
\tag{4.18}
$$

With that

$$
\begin{aligned}
p_3 \;&=\; \exp\left(\sum_i \frac{\beta}{2\lambda_i}\sum_{jk}O_{ij}O_{ik}mh^2\delta_{kj}\right) \\
&=\; \exp\left(\sum_i \frac{\beta}{2\lambda_i}\sum_j O_{ij}O_{ij}mh^2\right) \\
&=\; \exp\left(\frac{\beta}{2}\sum_i \frac{1}{\lambda_i}mh^2\right) \\
&=\; \exp\left(\frac{\beta}{2}\sum_i \chi_{ii}mh^2\right)
\end{aligned}
\tag{4.19}
$$

and finally

$$I_1 = p_1 p_2 p_3 = p_1 \exp\left(\frac{\beta m}{2}\left[h^2 \sum_i \chi_{ii} + \frac{1}{\beta}\ln\det\frac{\chi}{\beta}\right]\right) . \tag{4.20}$$

The factor p_1 is irrelevant to us, since we are actually only interested in determining the saddle point. Neglecting this factor the partition function reads then

$$Z \propto \int_{-i\infty}^{i\infty} \prod_i \frac{\beta\,\mathrm{d}H_i}{4\pi} \exp\left(-\frac{m\beta}{2}f_{\text{trial}}(\{H_i\})\right) , \tag{4.21}$$

with the trial free energy

$$f_{\text{trial}}(\{H_i\}) = \sum_j (H_j + h^2\chi_{jj}) + \frac{1}{\beta}\ln\det\frac{\chi}{\beta} . \tag{4.22}$$

4.2. Correlation matrix and the saddle-point conditions

The correlation matrix C defined as

$$C_{ij} = \frac{1}{m}\langle\mathbf{S}_i \cdot \mathbf{S}_j\rangle \tag{4.23}$$

can be calculated directly but this is a bit lengthy. The calculation, using a saddle-point approximation, is given in Appendix A and yields

$$C_{ij} = T\chi_{ij} + h^2(\chi^2)_{ij} , \tag{4.24}$$

where χ is evaluated at the saddle-point values H_i^0. The factor $1/m$ is necessary due to taking the limit $m \to \infty$ before $N \to \infty$. Taking the normalization of the spins $|\mathbf{S}_i| = \sqrt{m}$ into account and using Eq. (4.23), the main diagonal of C needs to fulfill

$$C_{ii} = 1 , \tag{4.25}$$

such that the N values of the variables H_i^0 in those N equations can be determined self-consistently via Eqs. (4.6,4.7). By using this physical approach we find by combining Eqs. (4.24) and (4.25) the condition

$$1 = T\chi_{ii} + h^2(\chi^2)_{ii} \tag{4.26}$$

fixing the saddle-point variables H_i^0. Also without using the definition (4.23) we can arrive at this condition by taking a somewhat more formal route and using the saddle-point equation

$$\text{grad}\, f_{\text{trial}} = 0 \tag{4.27}$$

for

$$-f_{\text{trial}}(\{H_k\}) := \sum_j \left(H_j + h^2 \chi_{jj}\right) + \frac{1}{\beta} \ln \det \frac{\chi}{\beta} \;, \tag{4.28}$$

and thus

$$0 = -\frac{\partial f_{\text{trial}}}{\partial H_i} = 1 + h^2 \sum_j \frac{\partial \chi_{jj}}{\partial H_i} + \frac{1}{\beta} \frac{\partial}{\partial H_i} \ln \det \frac{\chi}{\beta} \;. \tag{4.29}$$

However, the physical interpretation, namely the relation to the correlation function Eq. (4.24) and the imposed length constraint in disguise Eq. (4.25) will be missing at the end. But on the other hand we will have demonstrated that Eq. (4.26) actually constitutes the saddle-point condition.

We will start with the field-independent part of the equation. We notice

$$\ln \det \frac{\chi}{\beta} = \ln \left(\frac{1}{\beta^N} \det \chi\right) = \ln \det \chi - N \ln \beta \;, \tag{4.30}$$

where the second term is irrelevant for us since β does not depend on H_i and we are interested only in its derivative. Using the eigenvalues λ_j of the matrix A we have

$$\begin{aligned}
\ln \det \chi &= \ln \det(A^{-1}) = \ln \frac{1}{\det A} = -\ln \det A \\
&= -\ln \prod_j \lambda_j = -\sum_j \ln \lambda_j \;.
\end{aligned} \tag{4.31}$$

Differentiating with respect to H_i leads to

$$\begin{aligned}
\frac{\partial}{\partial H_i} \ln \det \chi &= -\sum_j \frac{\partial}{\partial H_i} \ln \lambda_j = -\sum_j \frac{1}{\lambda_j} \frac{\partial \lambda_j}{\partial H_i} \\
&= -\mathrm{Tr}\left(\chi^D \frac{\partial}{\partial H_i} A^D\right) \;.
\end{aligned} \tag{4.32}$$

where χ^D and A^D are the diagonalized versions of χ and A, respectively. Since according to Eq. (4.6)

$$\frac{\partial A}{\partial H_i} = \mathbf{e^{ii}} \;, \tag{4.33}$$

the elementary matrix consisting of zeroes apart from the single element $(\mathbf{e^{ii}})_{ii} = 1$ for a single $i \in \{1, \ldots, N\}$, one obtains due to the invariance of the trace operation

$$\frac{\partial}{\partial H_i} \ln \det \chi = -\mathrm{Tr}\left(\chi \frac{\partial}{\partial H_i} A\right) = -\chi_{ii} \;. \tag{4.34}$$

This is needed for the field-independent part of Eq. (4.29).

Let us now derive the field-dependent part. The general derivative $\partial \chi / \partial H_i$ can be obtained by using $A A^{-1} = A \chi = \mathbf{1}$, such that

$$\frac{\partial \mathbf{1}}{\partial H_i} = \frac{\partial A}{\partial H_i} \chi + A \frac{\partial \chi}{\partial H_i} = \mathbf{0} \;. \tag{4.35}$$

Multiplication with χ from the left and solving for the desired derivative yields

$$\frac{\partial \chi}{\partial H_i} = -\chi \frac{\partial A}{\partial H_i} \chi = -\chi \mathbf{e^{ii}} \chi \; , \tag{4.36}$$

and so

$$
\begin{aligned}
\sum_j \frac{\partial \chi_{jj}}{\partial H_i} &= -\sum_j \left(\chi \mathbf{e^{ii}} \chi \right)_{jj} = -\sum_{jkl} \chi_{jk} (\mathbf{e^{ii}})_{kl} \chi_{lj} \\
&= -\sum_{kl} (\mathbf{e^{ii}})_{kl} \sum_j \chi_{lj} \chi_{jk} = -\sum_{kl} (\mathbf{e^{ii}})_{kl} (\chi^2)_{lk} = -\sum_{kl} \delta_{ik} \delta_{kl} (\chi^2)_{lk} \\
&= -(\chi^2)_{ii} \; .
\end{aligned}
\tag{4.37}
$$

With inserting Eq. (4.34) and Eq. (4.37) into Eq. (4.29) we finally arrive at the saddle-point condition

$$1 = T\chi_{ii} + h^2 (\chi^2)_{ii} \; , \tag{4.38}$$

which is nothing else than the combination of Eq. (4.24) and (4.25) without having the physical interpretation, the relation to the correlation function. The equation is valid as $m \to \infty$ at fixed N.

4.3. The connection to T=0

As we will see below, at $T = 0$ some of the eigenvalues of the matrix A will be zero. In that case equations (4.7,4.24) are no longer well-defined. But there is a surprising connection between zero and finite temperature calculations [Has00].

As described earlier a necessary condition for a spin-configuration to be a ground-state is to have all spins being aligned to their respective local molecular fields

$$\mathbf{H}_i = \sum_{j \in \mathcal{N}(i)} J_{ij} \mathbf{S}_j \; , \tag{4.39}$$

such that

$$|\mathbf{H}_i| \mathbf{S}_i = \sum_{j \in \mathcal{N}(i)} J_{ij} \mathbf{S}_j \; . \tag{4.40}$$

Due to the lack of metastability for $m \to \infty$ this condition is even sufficient in order to ensure that the system is in the global energy minimum and thus in the ground-state. We can motivate a connection between the local fields $\mathbf{H}_i$ and the saddle-point variables H_i^0. As a result, the ambiguous name-convention of variables will be justified.

Generally, the internal energy is given by

$$U = \frac{1}{Z} \text{Tr}_{S_i^\alpha} \left[\mathcal{H} e^{-\beta \mathcal{H}} \right] = \frac{1}{Z} \text{Tr}_{S_i^\alpha} \left[-\frac{\mathrm{d}}{\mathrm{d}\beta} e^{-\beta \mathcal{H}} \right] = \frac{1}{Z} \left[-\frac{\mathrm{d}}{\mathrm{d}\beta} Z \right] = -\frac{\mathrm{d}}{\mathrm{d}\beta} \ln Z \; . \tag{4.41}$$

Using the saddle-point equation for the partition function we simplify

$$
\begin{aligned}
\ln Z \approx \ln Z^0 &= -\frac{\beta m}{2} f_{\text{trial}}(\{H_i^0\}) = \frac{\beta m}{2} \sum_j H_j^0 + \frac{m}{2} \ln \det \left(\frac{\chi^0}{\beta} \right) \\
&= \frac{\beta m}{2} \sum_j H_j^0 + \frac{m}{2} \ln \det \left(\chi^0 \right) - \frac{mN}{2} \ln \beta \; ,
\end{aligned}
\tag{4.42}
$$

where χ^0 denotes the susceptibility evaluated at the saddle-point. The variables H_i^0 depend on temperature. However, at the saddle point the gradient vanishes, cf. (4.27), and thus

$$
\begin{aligned}
\frac{\mathrm{d}}{\mathrm{d}\beta} \ln Z^0 &= \frac{\partial}{\partial \beta} \ln Z^0 + \sum_i \left(\frac{\partial}{\partial H_i^0} \ln Z^0 \right) \left(\frac{\mathrm{d} H_i^0}{\mathrm{d}\beta} \right) \\
&= \frac{\partial}{\partial \beta} \ln Z^0 - \frac{\beta m}{2} \left(\mathrm{grad}\, f_{\mathrm{trial}}(\{H_i^0\}) \right) \cdot \left(\frac{\mathrm{d}\vec{H}^0}{\mathrm{d}\beta} \right) \\
&= \frac{\partial}{\partial \beta} \ln Z^0 \,,
\end{aligned}
\tag{4.43}
$$

replacing the full derivative with a convenient partial derivative.

The ground-state energy, i.e. U in the limit $\beta \to \infty$, is then (recall the normalization $\mathbf{S}_i = \sqrt{m}$)

$$
\begin{aligned}
E_{gs} &= -\frac{m}{2} \sum_j H_j^0 = -\frac{1}{2m} \sum_j H_j^0 (\mathbf{S}_j \cdot \mathbf{S}_j) \\
&= -\frac{1}{2m} \sum_j (H_j^0 \mathbf{S}_j) \cdot \mathbf{S}_j
\end{aligned}
\tag{4.44}
$$

Obviously, the vectors $H_j^0 \mathbf{S}_j$ are parallel to the spins in the ground state.

On the other hand

$$
U = -\frac{1}{2} \sum_{\langle ij \rangle} J_{ij} \mathbf{S}_i \cdot \mathbf{S}_j = -\frac{1}{2} \sum_j \left(\sum_{i \in \mathcal{N}(j)} J_{ij} \mathbf{S}_i \right) \cdot \mathbf{S}_j \,,
\tag{4.45}
$$

such that we identify

$$
H_j^0 \mathbf{S}_j = m \sum_{i \in \mathcal{N}(j)} J_{ij} \mathbf{S}_i = m \mathbf{H}_j
\tag{4.46}
$$

and $\mathbf{H}_j$ is the local field at location j.

Remarkably, the variables H_i of Eq. (4.6) at the saddle-point are *equivalent* to the zero-temperature limit of the rescaled amplitudes $\sqrt{m}|\mathbf{H}_i|$ of the local fields Eq. (3.2). This crucial observation was first made in Ref. [Has00].

4.4. Exploiting the correlation matrix

It has been suggested first in Ref. [BM82] to use the density $\rho(\lambda)$ of eigenvalues of χ^{-1} or A to discuss the physics of random spin systems. It was shown there that the smallest eigenvalue vanishes at the critical point. For the case of the $m = \infty$ SK model in the thermodynamic limit, $\rho(\lambda)$ follows a Wigner semicircle [AM04]. Decreasing the temperature from T_{SG}, where the first eigenvalue vanishes, a fraction $m_0 \sim N^{2/5}$ of eigenvalues becomes zero as $T \to 0$ [AM04]. This corresponds to the contraction of the spin orientations into an m_0 dimensional sub-space in the limit of zero temperature, an effect reminiscent of the Bose-Einstein condensation in atomic systems. The behavior of the eigenvalue density on

cooling the system from high temperatures is illustrated for some 1d systems in Fig. 4.1. The eigenvalues can be used for calculating the order parameter q_{EA} and the spin-glass susceptibility χ_{SG}, discussed in the next section.

4.4.1. Order parameter and spin-glass susceptibility

Lee, Dhar and Young (LDY) [LDY05] as well as AM [AM04] examined the quoted saddle-point equations previously. A crucial difference between those two publications is the starting point, namely finite dimensional ($d = 2, 3$) short-range models *without* a finite temperature phase transition ($T_{SG} = 0$) in LDY as opposed to the long-range SK-model *with* a finite temperature phase transition ($T_{SG} = 1$) in AM, as presumably the lower critical dimension $d_l > 3$.

LDY considered the correlation function C_{ij} of Eq. (4.24) (with $h = 0$) and determined the Edwards-Anderson order parameter as

$$q_{EA}^2 = \lim_{r_{ij} \to \infty} [C_{ij}^2]_{av} \tag{4.47}$$

or as $q_{EA}^2 = [C_{ij}^2]_{av}$, $i \neq j$ for the SK model. Taking into account the scaling $m_0 \sim N^\mu$ of the number of non-zero spin components, they concluded that $q_{EA}^2 \sim N^{-\mu}$ in the ground state, i.e., a vanishing order parameter. Similarly, defining

$$\chi_{SG}^0 = \frac{1}{N} \sum_{i,j} [C_{ij}^2]_{av} \tag{4.48}$$

they inferred algebraically decaying correlations $[C_{ij}^2]_{av} \sim r_{ij}^{-d\mu}$ in the $m = \infty$ model, i.e., merely quasi long-range order. This is in contrast to the findings of Ref. [AJKT78] for the case of the $N \to \infty$ limit being taken *before* the $m \to \infty$ limit.

We believe that q_{EA} cannot be obtained from the long-distance limit of the correlation function squared, due to the fact that the limit $m \to \infty$ has been taken first. Rather one needs to consider the *connected* correlation function and *on-site* correlations to determine χ_{SG} and q_{EA}, and we will see that this leads to different conclusions. The basic idea is to separate contributions from the zero and non-zero modes. This discussion follows the ideas initiated in Ref. [AM04].

Consider Eq. (4.23) and factor out the cumulant part $\tilde{C}_{ij}$ of the correlation function by inserting a zero,

$$C_{ij} = \frac{1}{m} \langle \mathbf{S}_i \rangle \cdot \langle \mathbf{S}_j \rangle + \underbrace{\frac{1}{m} (\langle \mathbf{S}_i \cdot \mathbf{S}_j \rangle - \langle \mathbf{S}_i \rangle \cdot \langle \mathbf{S}_j \rangle)}_{\tilde{C}_{ij}} . \tag{4.49}$$

Due to the mentioned properties of A also the matrix C is real and symmetric according to Eq. (4.24). For their respective eigenvalues λ and ω it holds

$$\omega = \frac{T}{\lambda} + \frac{h^2}{\lambda^2} . \tag{4.50}$$

Using the spectral theorem, C has an orthonormal basis of independent eigenvectors $\{\vec{v}^n | \vec{v}^n \in \mathbb{R}^N, n = 1, \ldots, N\}$ for the set of eigenvalues $\{\omega_n \in \mathbb{R}\}$ [1], which do not need to be distinct. The spectral decomposition reads

$$C = \sum_{n=1}^{N} \omega_n \vec{v}^n \cdot (\vec{v}^n)^{\mathsf{T}} , \qquad (4.51)$$

where we use the outer product and the conjugate transpose denoted by $(\cdot)^{\mathsf{T}}$. Then

$$C \cdot \vec{v}^m = \sum_{n=1}^{N} \omega_n \vec{v}^n \cdot (\vec{v}^n)^{\mathsf{T}} \cdot \vec{v}^m = \omega_m \vec{v}^m \qquad (4.52)$$

with $(\vec{v}^n)^{\mathsf{T}} \cdot \vec{v}^m = \delta_{mn}$. Thus, for $T < T_{\mathrm{SG}}$, the elements of the correlation matrix C are given by the eigenvalue decomposition

$$C_{ij} = \vec{e}_i^{\mathsf{T}} \cdot (C \cdot \vec{e}_j) \quad = \quad \sum_{n=1}^{N} \omega_n v_i^n v_j^n \qquad (4.53)$$

$$= \quad \sum_a \left(\frac{T}{\lambda_a} + \frac{h^2}{\lambda_a^2} \right) v_i^a v_j^a + \sum_b \left(\frac{T}{\lambda_b} + \frac{h^2}{\lambda_b^2} \right) v_i^b v_j^b , \qquad (4.54)$$

where $a = 1, \ldots, m_0$ labels the m_0 eigenvalues λ_a that vanish as $T \to 0$, and λ_b, $b = N - m_0 + 1, \ldots, N$ refers to the remaining $N - m_0$ eigenvalues staying finite. Generally, λ_x denotes the xth eigenvalue and v_k^x is the kth component of the corresponding normalized eigenvector $\vec{v}^x$ of A. The separation of zero and non-zero eigenvalues is a crucial step as we will see next. An illustration of the separated eigenvalues is shown in Fig. (4.2) for a temperature close to zero. The evolution of eigenvalues with temperature can be inspected in Fig. 4.1. Very close to zero ($T = 0.01$) the eigenvalue histogram exhibits a clear-cut separation of zero and non-zero eigenvalues, at least for all σ smaller than or equal to the upper critical σ.

Until the end of this section we will set $h = 0$ since as we will see later, a finite field will destroy the ordered phase. Working at $m = m_0$ and using the reasonable assumption that the ath component of the spin $\mathbf{S}_i \in \mathbb{R}^{m_0}$ has the form

$$\langle S_i^a \rangle = \pm \sqrt{\frac{m_0 T}{\lambda_a}} v_i^a , \qquad (4.55)$$

the cumulant part of the correlation function can be identified with

$$\tilde{C}_{ij} = \sum_b \left(\frac{T}{\lambda_b} \right) v_i^b v_j^b , \qquad (4.56)$$

---

[1] The eigenvalues μ of a real, symmetric matrix M are real. This can be seen for $Mx = \mu x$ and its conjugate version $\overline{M}\overline{x} = \overline{\mu}\overline{x}$. Since M is real $\overline{M} = M$, and left-multiplication of the first with $\overline{x}^{\mathsf{T}}$ and the second with x^{T} subtraction yields $\overline{x}^{\mathsf{T}} M x - x^{\mathsf{T}} M \overline{x} = (\mu - \overline{\mu})\overline{x}^{\mathsf{T}} x$. Using the definition of symmetry $\overline{x}^{\mathsf{T}} M x = (M\overline{x})^{\mathsf{T}} x = (Mx)^{\mathsf{T}} \overline{x}$ and $x^{\mathsf{T}} M \overline{x} = (Mx)^{\mathsf{T}} \overline{x}$ the left-hand side is zero. $\overline{x}^{\mathsf{T}} x$ can only be zero if all elements of x are zero. Thus, $\mu \in \mathbb{R}$.

The according eigenvectors x can be chosen real-valued as well. Adding the eigenvalue equation and its conjugate version yields $M(x + \overline{x}) = \lambda(x + \overline{x})$. Since $x + \overline{x} = 2\mathrm{Re}(x)$ it is possible to construct a real-valued orthonormal set of basis vectors.
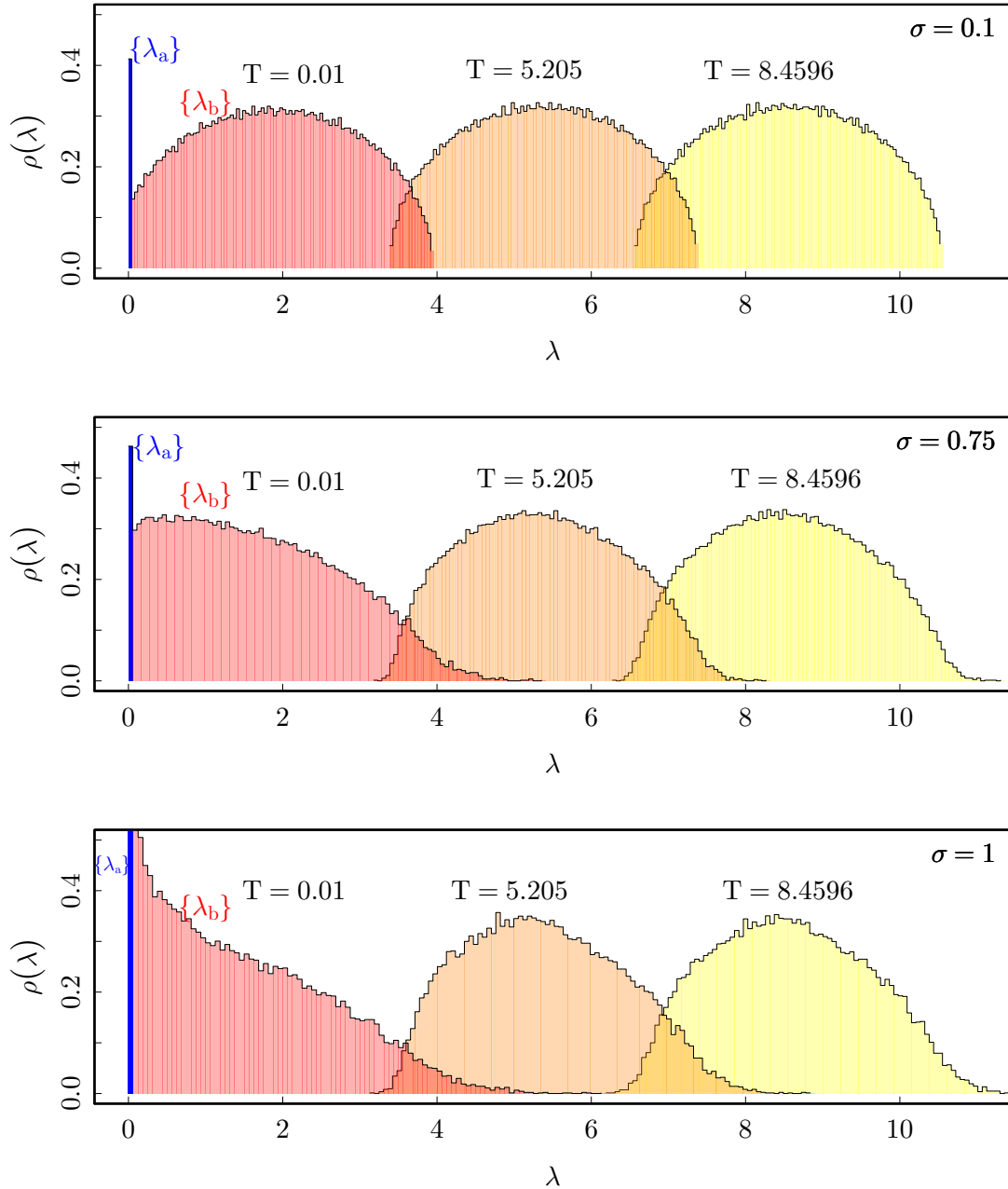
Figure 4.1.: (Color online). The eigenvalue density $\rho(\lambda)$ of the matrix A, see Eq. (4.6) for the 1d $m = \infty$ model at different values of σ. For $\sigma = 0.1$ (top) the distribution follows Wigner's semicircle law at high temperatures [AM04], or Eq. (4.76). Lowering the temperature shifts the whole distribution to lower values, until for $T \to 0$ m_0 eigenvalues $\{\lambda_a\}$ vanish, while the majority $(N - m_0)$ of eigenvalues $\{\lambda_b\}$ stay finite. In the thermodynamic limit the Wigner semicircle law is restored again also there, since $m_0/N \to 0$. For higher values of σ the Wigner semicircle law does not hold exactly anymore. At $\sigma = 0.75$ (middle) the maximum of the histogram gets lost for $T \to 0$ and has completely disappeared for $\sigma = 1$ (bottom).

being a function of the non-vanishing eigenvalues in the limit $T \to 0$.

It is natural to define the spin-glass susceptibility in terms of this connected correlation function,

$$\chi_{\mathrm{SG}} = \frac{1}{Nm^2} \sum_{i,j} [\langle \mathbf{S}_i \cdot \mathbf{S}_j \rangle - \langle \mathbf{S}_i \rangle \cdot \langle \mathbf{S}_j \rangle]^2 = \frac{1}{N} \sum_{ij} \tilde{C}_{ij}^2 \qquad (4.57)$$

$$\boxed{\chi_{\mathrm{SG}} = \frac{T^2}{N} \sum_b \frac{1}{\lambda_b^2} \, ,} \qquad (4.58)$$

where the λ_b are the non-vanishing eigenvalues. Furthermore, the Edwards-Anderson order parameter is then given by

$$q_{\mathrm{EA}} = \frac{1}{N} \sum_i \frac{\langle \mathbf{S}_i \rangle \cdot \langle \mathbf{S}_i \rangle}{m_0} = \frac{T}{N} \sum_i \sum_a \frac{v_i^a v_i^a}{\lambda_a} \qquad (4.59)$$

$$\boxed{q_{\mathrm{EA}} = \frac{T}{N} \sum_a \frac{1}{\lambda_a} \, ,} \qquad (4.60)$$

where the λ_a are the vanishing eigenvalues.

The chosen formalism leads to a non-vanishing order parameter at $T = 0$. To see this, consider

$$\frac{1}{N} \sum_{i=1}^{N} C_{ii} = \frac{T}{N} \sum_a \frac{1}{\lambda_a} + \frac{T}{N} \sum_b \frac{1}{\lambda_b} = 1 \qquad (4.61)$$

resulting from the normalization condition $C_{ii} = 1$, Eq. (4.25). The finite eigenvalues λ_b scale to a constant as $N \to \infty$ and $T \to 0$, hence the second sum in Eq. (4.61) is roughly proportional to $N^{-1} N^{1-\mu} = N^{-\mu}$ and thus vanishes in the thermodynamic limit. Hence, $q_{\mathrm{EA}} = 1$ in this limit. This in contrast to the conclusion reached from the long-distance limit of the squared correlation function in Ref. [LDY05]. The "zero" eigenvalues λ_a vanish as $T \to 0$ and as $N \to \infty$. Assuming them to be proportional to T/N^p, we conclude from Eq. (4.61) that $p = 1 - \mu$.

4.5. Numerical approach

Equations (4.6, 4.7 and 4.26) will be solved iteratively in order to find a set of values $\{H_i^0\}$ fulfilling the saddle-point condition (4.26). Essentially, this is nothing else than finding the root of a system of N independent functions of N independent variables, which, in our case of the $m \to \infty$ model, is even unique. The exact description of the procedure will be given in the following sections. First we will introduce methods to find a root. Second, in order to find the direction towards the zero we need to have a way to calculate the Jacobian. In many problems this is a limiting factor since its numerical determination is often costly. To speed up numerics considerably we calculate an expression for the exact Jacobian. Third, in order to find the one and only physically correct, i.e. real, solution and again speed up calculations, we are in need of sound initial conditions $H_i(T)$. We will deduce an expression
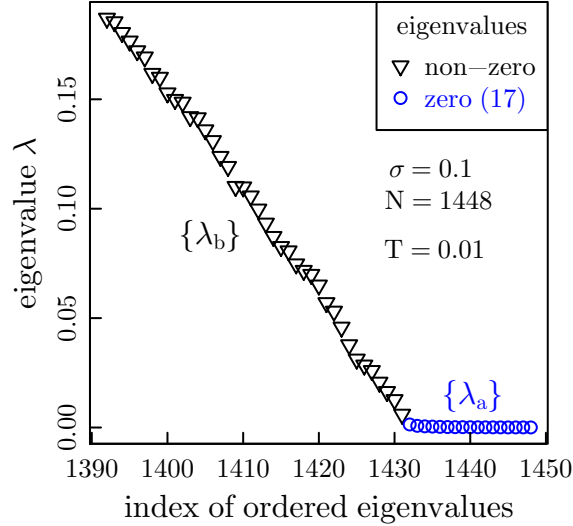
Figure 4.2.: The eigenvalues of the matrix A in Eq. (4.6) at a temperature $T = 0.01$. For this showcase example one realization of a one-dimensional power law model with $\sigma = 0.1$ and $N = 1448$ spins is considered. Shown are only the smallest eigenvalues of the whole spectrum with $N = 1448$ eigenvalues including a few of the non-zero ones $\{\lambda_b\}$ but all of the m_0 zero ones $\{\lambda_a\}$ (blue). In this example $m_0 = 17$.

for the starting values H_i in the thermodynamic limit being quite valuable also for our finite systems at large temperature. And we will determine a differential equation for the change of the H_i with (inverse) temperature to calculate reasonable initial values if temperature is lowered.

We are interested in physical observables over a wide range of temperature points. The mentioned initial conditions will hold true only for high temperatures but will not be applicable for low ones. Thus, as a fourth point we will determine a set of differential equations giving the rate of change of each H_i with temperature. With this we will be able to decrease the temperature step by step and construct good initial conditions successively also close to $T = 0$.

4.5.1. Root finding

Finding a root of a function numerically is one of the most common tasks in computer science. It is used to find a solution for any equation which can be cast into the form

$$g(x) = 0 \, , \tag{4.62}$$

where g is an arbitrary (real) function and $x \in \mathbb{R}$ a variable. To find a solution to this equation Newton as well as Raphson suggested a method known as the Newton, or also Newton-Raphson method of root finding. It requires both the evaluation of the function $g(x)$ itself as well as its derivative $g'(x)$ and approaches its solution successively by wandering along the tangent line of the function from any starting point x_0. Although not being

guaranteed to converge, it is a very convenient root solver. Using Taylor expansion we construct a sequence $(x_n)_{n \in \mathbb{N}}$ with

$$x_{n+1} = x_n - \frac{g(x_n)}{g'(x_n)} \ . \tag{4.63}$$

The derivative can be approximated by

$$g'(x_n) \approx \frac{g(x_n) - g(x_{n-1})}{x_n - x_{n-1}} \tag{4.64}$$

and by doing so the Newton-Raphson method changes name immediately to 'secant method'. It is easy to generalize this method to higher dimensions. In this case we have N independent equations g_i and N independent variables x_i and the Newton-Raphson method reads then

$$\mathbf{x}_{n+1} = \mathbf{x}_n - (J_g)^{-1} \mathbf{g}(\mathbf{x}_n) \ , \tag{4.65}$$

where J_g is the matrix of derivatives – known as the Jacobian – of the functions g_i, the elements of which are given as

$$(J_g)_{ij}(\mathbf{x}) = \frac{\partial g_i(\mathbf{x})}{\partial x_j} \ . \tag{4.66}$$

A real implementation uses a LU decomposition of the matrix J_g in order to determine the differences $\mathbf{x}_{n+1} - \mathbf{x}_n$, which are then added to the vector $\mathbf{x}_n$ to find $\mathbf{x}_{n+1}$. This is an operation of order N^2.

Also here it is possible to approximate the the derivatives by

$$(J_g)_{ij}(\mathbf{x}) \approx \frac{g_i(\mathbf{x} + h_j \mathbf{e}_j) + g_i(\mathbf{x})}{h_j}, \quad h_j = x_j \sqrt{\varepsilon} \ , \tag{4.67}$$

where ε is the machine precision. In using the approximate Jacobian also the high-dimensional Newton-Raphson method changes its name immediately to Broyden's method (or generally secant method, because it reduces to the one-dimensional secant method). Here, a real implementation uses a QR decomposition of the approximate matrix J_g in order to determine the differences $\mathbf{x}_{n+1} - \mathbf{x}_n$. As in the LU case this is a method of order N^2.

Much more detail about root finding algorithms which would distract us at this point can be found in [FTVP07].

We now want to apply the mentioned methods to our problem. According to Eqs. (4.6,4.7,4.26) we introduce N independent functions

$$\boxed{g_i(\{H_k\}) = T\chi_{ii} + h^2(\chi^2)_{ii} - 1} \tag{4.68}$$

and find their zeroes, i.e. setting $g_i(\{H_k\}) = 0$ simultaneously.

4.5.2. The exact Jacobian to the saddle-point iteration

In order to speed up numerics we want to calculate the Jacobian $\partial g_i / \partial H_j$ for the function given in Eq. (4.68) as a next step. Recalling Eq. (4.36) and

$$\left(\frac{\partial A}{\partial H_j} \right)_{mn} = \left(\mathbf{e}^{\mathbf{ij}} \right)_{mn} = \delta_{jm} \delta_{mn} \ , \tag{4.69}$$

we have for the first term

$$\left(\frac{\partial \chi}{\partial H_j}\right)_{ab} = -\sum_m \sum_n \chi_{am} \delta_{jm} \delta_{mn} \chi_{nb} \tag{4.70}$$

and can extract the diagonal elements

$$\left(\frac{\partial \chi}{\partial H_j}\right)_{ii} = -\chi_{ij}\chi_{ji} = -(\chi_{ij})^2 \ , \tag{4.71}$$

where the last step is due to χ's symmetry. Also due to symmetry we can use for the second term that

$$\frac{\partial \chi^2}{\partial H_j} = \frac{\partial \chi}{\partial H_j}\chi + \chi\frac{\partial \chi}{\partial H_j} = 2\chi\frac{\partial \chi}{\partial H_j} \ . \tag{4.72}$$

According to this

$$\left(\chi\frac{\partial \chi}{\partial H_j}\right)_{cd} = -\sum_l \sum_m \sum_n \chi_{cl}\chi_{lm}\delta_{jm}\delta_{mn}\chi_{nd} \tag{4.73}$$

so that the diagonal elements are

$$\left(\chi\frac{\partial \chi}{\partial H_j}\right)_{ii} = -\sum_l \chi_{il}\chi_{lj}\chi_{ji} = -(\chi^2)_{ij}\chi_{ij} \ , \tag{4.74}$$

Then the desired Jacobian reads

$$\boxed{(J_g)_{ij} = \frac{\partial g_i}{\partial H_j} = -T(\chi_{ij})^2 - 2h^2(\chi^2)_{ij}\chi_{ij} \ .} \tag{4.75}$$

4.5.3. Initial conditions

In order to start the iteration procedure we need to have a set of reasonably chosen initial conditions, i.e. initial values H_i. We will call them 'starting values' to discriminate them from the reoccuring determination of initial values in the course of the numerical calculation, cf. Sec. 4.5.4. So far no assumptions about the structure or the values of the interaction matrix J_{ij} have been made. For the $(m \to \infty)$ SK model, however, the elements of the symmetric and real $N \times N$-interaction matrix consist only of Gaussian random numbers with fixed mean ($\mu = 0$) and standard deviation ($\sigma = 1/\sqrt{N}$). Such matrices occur in random matrix theory. The distribution of eigenvalues is known and follows the Wigner semicircle law [Wig58, Wig67]. It assumes that for a real, symmetric $N \times N$-matrix D

(i)   the distributions $p_{ij}(D_{ij})$ for $i \leq j$ are independent,
(ii)   the distribution law for each matrix element D_{ij} is symmetric,
(iii)   all moments of the D_{ij} exist and have an upper bound independent of i and j
        (together with (ii) all odd moments vanish) and
(iv)   the second moment μ_2 is the same for all p_{ij}.

If these conditions are met, the eigenvalue density is given by

$$P_\lambda(\lambda) = \begin{cases} \frac{2}{\pi} \frac{\sqrt{4N\mu_2 - \lambda^2}}{4N\mu_2} \, , & \text{if } \lambda^2 \le 4N\mu_2 \, , \\ 0 \, , & \text{otherwise} \, , \end{cases} \qquad (4.76)$$

which reveals the inaccuracy of the name 'semicircle law'. It is rather a 'semiellipse law'. In the SK case $N\mu_2 = N\sigma^2 = 1$, due to the vanishing mean. A showcase example close to the SK case ($\sigma = 0.1$) can be found in the top panel of Fig. 4.1. This knowledge will be used in the following in order to determine the starting values H_i.

Taking Eq. (4.26) and considering the eigenvector decomposition of χ for vanishing field $h = 0$ we have

$$1 = T \sum_n \frac{(v_i^n)^2}{\lambda_n} \, . \qquad (4.77)$$

Using the orthonormal basis

$$\frac{N}{T} = \sum_{i=1}^N \frac{1}{T} = \sum_n \frac{\sum_i (v_i^n)^2}{\lambda_n} = \frac{1}{N} \sum_n \frac{1}{\lambda_n} = \int \varrho_\lambda(\lambda) \frac{1}{\lambda} d\lambda \, , \qquad (4.78)$$

where we substituted the heuristic mean value with the statistic mean of the distribution function ϱ_λ, being good for large N. ϱ_λ describes the distribution of eigenvalues λ of the matrix A which is essentially the interaction matrix, see Eq. (4.6). Thus, the main diagonal of both matrices J and A differ from the requirements the Wigner semicircle law imposes. However, being only a subset of elements of size N we can assume that the semicircle law holds for large N so that we will use it in order to solve the upper integral.

We make the ansatz that all H_i be equal to a constant H and consider the characteristic polynomial

$$\chi_A(\lambda) = \det(\mathbf{1}\lambda - A) = \det(\mathbf{1}(\lambda - H) + J) = \chi_J(\lambda - H) \, , \qquad (4.79)$$

i.e. if λ is an eigenvalue of A, then $\mu = \lambda - H$ is one of the interaction matrix J. Relating the eigenvalue distribution functions of matrix J and A via $\varrho_\mu(\mu)d\mu = \varrho_\lambda(\lambda)d\lambda$ it holds

$$\varrho_\lambda(\lambda) = \varrho_\mu(\lambda - H) \, . \qquad (4.80)$$

Using the semicircle law (4.76) for the distribution of eigenvalues μ of the interaction matrix J and recalling Eq. (4.78) we substitute $x = \lambda - H$ and arrive at

$$\begin{aligned} \frac{1}{T} &= \int \varrho_\mu(\lambda - H) \frac{1}{\lambda} d\lambda \\ &= \int_{-2}^{2} \frac{1}{2\pi} \sqrt{4 - x^2} \frac{1}{x + H} dx \\ &= \frac{1}{2}(H - \sqrt{H^2 - 4}) \, . \end{aligned} \qquad (4.81)$$

Solving for H finally amounts to

$$\boxed{H_i^0 = H = T + \frac{1}{T} \, .} \qquad (4.82)$$
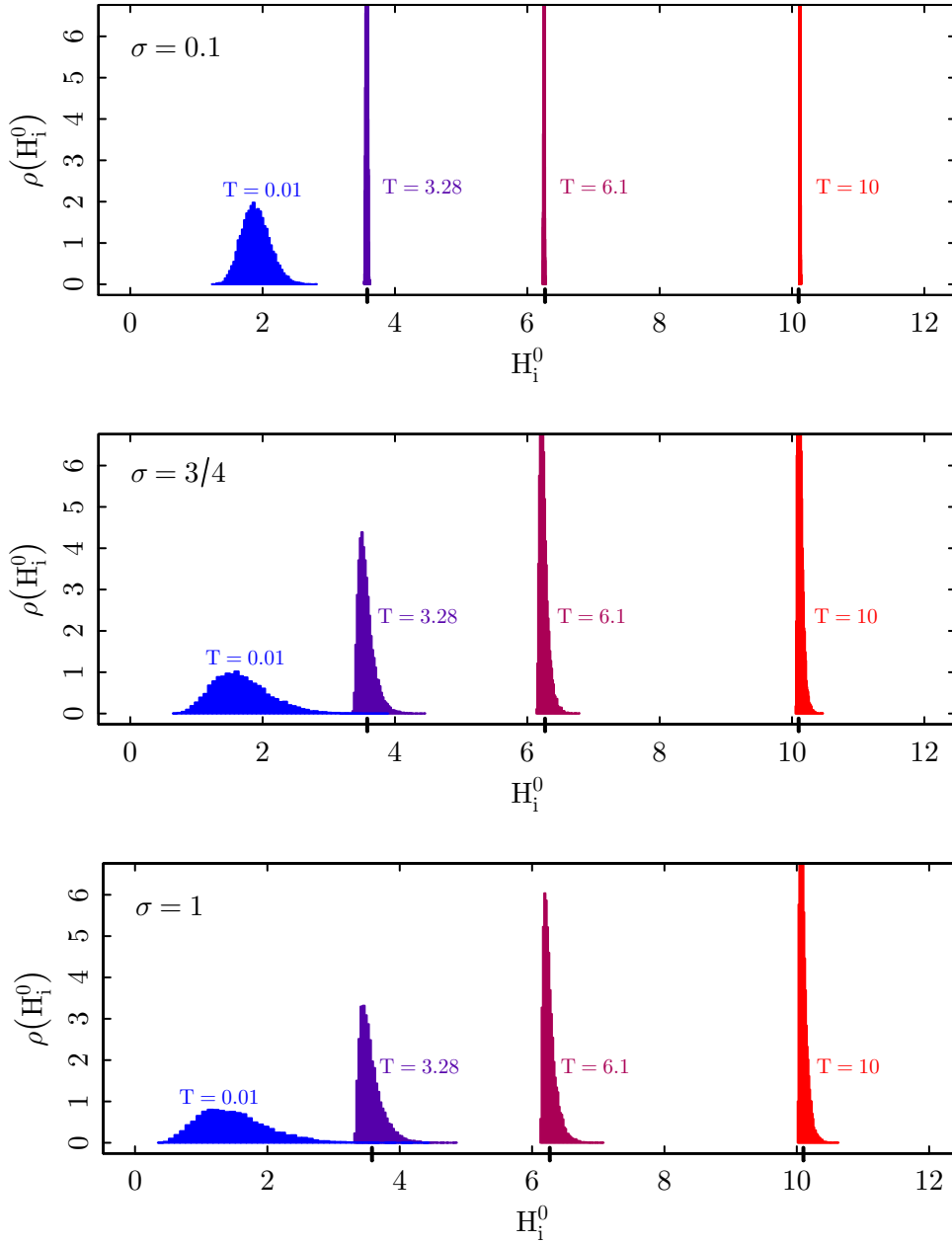
Figure 4.3.: (Color online). Density plots for the parameters H_i in Eq. (4.6) at their saddle-point values H_i^0 for $\sigma = 0.1$ (top), $\sigma = 0.75$ (middle) and $\sigma = 1.0$ (bottom). In the limit $T \to 0$ they correspond to the (rescaled) local fields $|\mathbf{H}_i|/\sqrt{m}$. As is seen here, Eq. (4.82) yields suitable starting values for the iteration at high temperatures, cf. the bold ticks on the H_i^0 axis. For increasing values of σ the distribution broadens. The normalization of the histograms is arbitrary. The system size used for this plot was $N = 1448$.

These are the correct starting values for the $(m \to \infty)$ SK model in the thermodynamic limit for $T > 1$. In our numerical analysis they will be taken as a first guess in our finite size systems starting at a sufficiently high temperature. In Fig. 4.3 it can be seen that those starting values are indeed extremely good for an initial temperature of $T_1 = 10$. Apart from the SK model we found this choice and Eq. (4.82) suitable and sufficient also for our systems in the one-dimensional power-law model even for higher values of σ.

4.5.4. Lowering the temperature

Starting at a temperature T_1 the matrix equations are solved at successively lower temperatures. The set of temperature points may be chosen in a geometrical fashion, such that the inverse temperature $\beta = 1/T$ is distributed equidistantly. In all our simulations the final temperature was chosen to be $T_f = 0.01$. Decreasing the temperature from T_k to T_{k+1} ($k > 0$, $T_{k+1} < T_k$), a new guess for the values of the H_i contributes to the stability of the algorithm. To achieve this we want to find a relation of the variables H_i varying with the inverse temperature β, i.e. a set of ordinary differential equations $\partial H_i / \partial \beta$. To this end we will use the saddle-point arguments again. Recalling the partition function Eq. (4.21)

$$
\begin{aligned}
Z \quad &\propto \quad \int_{-i\infty}^{i\infty} \prod_i \frac{\beta \mathrm{d}H_i}{4\pi} \exp\left(-\frac{m\beta}{2} f_{\mathrm{trial}}(\{H_k\})\right) \\
&\approx \quad \int_{-i\infty}^{i\infty} \prod_i \frac{\beta \mathrm{d}H_i}{4\pi} \exp\left(-\frac{m\beta}{2}\left[f_{\mathrm{trial}}(\{H_k^0\}) + \frac{1}{2}\sum_{ij} \frac{\partial^2 f_{\mathrm{trial}}(\{H_k^0\})}{\partial H_i \partial H_j} H_i H_j + \dots\right]\right) ,
\end{aligned}
$$
(4.83)

where f_{trial} is given by Eq. (4.28). For simplicity we introduce a matrix B as

$$
-\frac{1}{2}\frac{\partial^2 f_{\mathrm{trial}}(\{H_k^0\})}{\partial H_i \partial H_j} = \frac{1}{2}\left(h^2 \sum_l \frac{\partial^2 \chi_{ll}}{\partial H_i \partial H_j} + \frac{1}{\beta}\frac{\partial^2}{\partial H_i \partial H_j} \ln \det \frac{\chi}{\beta}\right) = \frac{1}{\beta} B_{ij}
$$
(4.84)

and shortly remark that this matrix is usually used for solving Eq. (4.83) in a Gaussian approximation not being carried out here. At the saddle point H_k^0 the function f_{trial} takes on its minimum such that Eq. (4.29) holds, which is equivalent to

$$
-\beta = \beta h^2 \sum_l \frac{\partial \chi_{ll}}{\partial H_i} + \frac{\partial}{\partial H_i} \ln \det \frac{\chi}{\beta}.
$$
(4.85)

The total derivative with respect to β reads

$$
\begin{aligned}
-1 \quad &= \quad h^2 \sum_l \frac{\partial \chi_{ll}}{\partial H_i} + \beta h^2 \sum_l \frac{\mathrm{d}}{\mathrm{d}\beta}\frac{\partial \chi_{ll}}{\partial H_i} + \frac{\mathrm{d}}{\mathrm{d}\beta}\frac{\partial}{\partial H_i} \ln \det \frac{\chi}{\beta} \\
&= \quad -h^2(\chi^2)_{ii} + \sum_j \left(\beta h^2 \sum_l \frac{\partial^2 \chi_{ll}}{\partial H_i \partial H_j} + \frac{\partial^2}{\partial H_i \partial H_j} \ln \det \frac{\chi}{\beta}\right)\frac{\partial H_j}{\partial \beta} \\
&= \quad -h^2(\chi^2)_{ii} + \sum_j 2 B_{ij}\frac{\partial H_j}{\partial \beta} ,
\end{aligned}
$$
(4.86)

where we used Eq. (4.37) in the second and Eq. (4.84) in the third line. With the vectors $\vec{H} = (H_1, \ldots, H_N)^\mathsf{T} \in \mathbb{R}^N$ and $\vec{w} = (w_1, \ldots, w_N)^\mathsf{T} \in \mathbb{R}^N$ with elements

$$w_j = 1 + h^2 (\chi^2)_{jj} \tag{4.87}$$

we can use the matrix notation

$$-\vec{w} = 2B \frac{\partial \vec{H}}{\partial \beta} \quad \Leftrightarrow \quad -\frac{1}{2} B^{-1} \vec{w} = \frac{\partial \vec{H}}{\partial \beta} \, , \tag{4.88}$$

such that the i-th component tells us how the variables H_i change with β

$$\frac{\partial H_i}{\partial \beta} = -\frac{1}{2} \left(B^{-1} \vec{w} \right)_i = -\frac{1}{2} \sum_j (B^{-1})_{ij} \left(1 + h^2 (\chi^2)_{jj} \right) \, . \tag{4.89}$$

The exact form of B is still unknown, though. We will employ the defining Eq. (4.84) in order to determine it. The first required derivatives have already been calculated in Eq. (4.37) and Eq. (4.34). Along with them

$$B_{ij} = -\frac{\beta h^2}{2} \frac{\partial}{\partial H_j} (\chi^2)_{ii} - \frac{1}{2} \frac{\partial}{\partial H_j} \chi_{ii} \tag{4.90}$$

and $\partial \chi / \partial H_i$ was already given in Eq. (4.71). Furthermore, Eq. (4.72) in connection with Eq. (4.74) yields

$$\frac{\partial}{\partial H_j} (\chi^2)_{ii} = -2 (\chi^2)_{ij} \chi_{ij} \, , \tag{4.91}$$

such that the exact form of B reads

$$B_{ij} = \beta h^2 (\chi^2)_{ij} \chi_{ij} + \frac{1}{2} (\chi_{ij})^2 \, , \tag{4.92}$$

which can be used along with Eq. (4.89) in the numerical treatment in order to find a new approximate set of variables $H_i(T_{k+1})$ based on the determined saddle-point values $H_i^0(T_k)$.

4.6. Short summary

In a nutshell, we are endowed now with all theoretical and numerical preliminaries in order to tackle the vector spin-glass in the limit $m \to \infty$ at finite temperature. We are dealing with the Hamiltonian

$$\mathcal{H} = -\frac{1}{2} \sum_{\substack{i,j=1 \\ i \neq j}}^{N} J_{ij} \, \mathbf{S}_i \cdot \mathbf{S}_j - \sum_{i=1}^{N} \mathbf{h}_i \cdot \mathbf{S}_i \tag{4.93}$$

with real-valued vector spins of length $|\mathbf{S}_i| = \sqrt{m}$, and Gaussian random fields $\mathbf{h}_i$. We defined a matrix A the elements of which amount to

$$A_{ij} = H_i \delta_{ij} - J_{ij} \, , \tag{4.94}$$

where J_{ij} are the elements of the interaction matrix and $H_i \in \mathbb{R}$ some variables which at the saddle point equal the rescaled amplitudes of the local molecular fields $\mathbf{H}_i/\sqrt{m}$ in the limit $T \to 0$. The matrix A occurred in the course of a partial evaluation of the partition function. Its eigenvalues λ_i played a crucial role, and for our finite system-size calculations at $T > 0$ ($\lambda_i > 0$ in this case), the elements of its inverse have been defined as

$$\chi_{ij} = (A^{-1})_{ij} \ . \tag{4.95}$$

For the correlation matrix elements

$$C_{ij} = \frac{1}{m}\langle \mathbf{S}_i \cdot \mathbf{S}_j \rangle \tag{4.96}$$

we found the expression

$$C_{ij} = T\chi_{ij} + h^2(\chi^2)_{ij} \quad , \quad C_{ii} = 1 \ , \tag{4.97}$$

where the second equation is the length constraint of the spins in disguise. Furthermore, we saw that the combination of those two equations is the saddle-point condition which can be iterated until a set of variables $\{H_i^0\}$ for Eq. (4.94) is determined giving the values of the variables H_i at the saddle-point. We formulated the problem such that merely the roots need to be found for the N equations

$$g_i(\{H_k\}) = T\chi_{ii} + h^2(\chi^2)_{ii} - 1 \overset{!}{=} 0 \tag{4.98}$$

and indicated that sound starting values at high temperature $T > 1$ are given by

$$H_i = H = T + \frac{1}{T} \ . \tag{4.99}$$

In order to iterate Eq. (4.98) until convergence with either the Newton-Raphson method, using LU decomposition of a matrix, or a similar method using a QR decomposition, we pointed out that calculations can be sped up considerably by using the exact Jacobian

$$(J_g)_{ij} = \frac{\partial g_i}{\partial H_j} = -T(\chi_{ij})^2 - 2h^2(\chi^2)_{ij}\chi_{ij} \ . \tag{4.100}$$

If the converged set of H_i^0 has been found, the eigenvalues λ_i of A can be determined. Since calculations ought to be done at a whole set of temperature points it was necessary to determine a set of differential equations giving rise to new initial conditions when switching from one temperature to another and by this ensuring the stability of the root-finding algorithm. In other words these differential equations are used to yield new initial values for the variables H_i at temperature T_{k+1} if the temperature is lowered from $T_k > T_{k+1}$ where the saddle-point values H_i^0 are already determined. They read

$$\frac{\partial H_i}{\partial \beta} = -\frac{1}{2}\sum_j (B^{-1})_{ij}\left(1 + h^2(\chi^2)_{jj}\right) \ , \tag{4.101}$$

with

$$B_{ij} = \beta h^2(\chi^2)_{ij}\chi_{ij} + \frac{1}{2}(\chi_{ij})^2 \ . \tag{4.102}$$

For each temperature point visited, the saddle-point values H_i^0 give access to the eigenvalues λ_i of the matrix A via Eq. (4.94). These are related to the eigenvalues of the correlation matrix and so we finally motivated the spin-glass susceptibility to read

$$\chi_{\mathrm{SG}} = \frac{T^2}{N} \sum_b \frac{1}{\lambda_b^2} \tag{4.103}$$

and the Edwards-Anderson order parameter

$$q_{\mathrm{EA}} = \frac{T}{N} \sum_a \frac{1}{\lambda_a} \xrightarrow{T \to 0} 1 \ , \tag{4.104}$$

where q_{EA} depends only on the zero eigenvalues λ_a, $a = 1, \dots, m_0$ and on the contrary χ_{SG} on the non-vanishing eigenvalues λ_b, $b = N - m_0 + 1, \dots, N$. We justified $\lambda_a \sim T/N^{1-\mu}$ for T close to zero.

Figure 4.4.: (Color online). The evolution of eigenvalues λ of the matrix A of Eq. (4.6) with temperature for a $L = 1448$ system with $\sigma = 0.1$. Left panel: The non-zero eigenvalues (black, dot-dashed) stay finite in the limit $T \to 0$ (biggest are left away). The others (blue, solid) scale to zero as $\sim T^x$ with $x = 1$. Note that the axes are both logarithmic. Right panel: The slopes from the plot in the left panel for a set of temperatures $0.01 \leq T \leq 1.5$. Light colors are for high temperatures, dark colors are for low ones. We discriminate finite (gray...black) and zero eigenvalues (light-blue...blue) by sorting them at $T = T_{\min} = 0.01$ into groups with $x \leq 0.5$ and $x > 0.5$.

4.7. Numerical results

To perform the analysis outlined above in Sec. 4.4, we need to separate zero from non-zero eigenvalues. For finite temperatures and finite systems, however, no eigenvalues are exactly zero. Instead, there is a difference in scaling behavior between the "zero" eigenvalues that vanish proportional to $T/N^{1-\mu}$ and the other eigenvalues that scale to a constant. This is illustrated in Fig. 4.4. To automatically distinguish between the two types of eigenvalues, one might count all those as zero that fall below a chosen threshold at the lowest considered temperature. It turned out to be more reliable, however, to base the distinction criterion directly on the temperature scaling $\propto T$ of the "zero" eigenvalues. Determining the slope of $\log \lambda(T)$ at the lowest considered temperatures, we counted those eigenvalues as scaling to zero whose slope was above 0.5. Even with this rather reliable criterion, however, there will always be a certain ambiguity as the slopes change quite continuously over the different eigenvalues, and a number of borderline cases always exists, cf. the example in Fig. 4.4. We do not find any signs of the number of zero eigenvalues changing with temperature. Instead, our results are compatible with all relevant eigenvalues starting to scale to zero as soon as $T < T_{\text{SG}}$.

At this point we can immediately clear out the impertinence of Sec. 4.4.1, where we set $h = 0$ and did not care about finite fields anymore. The case of $h \neq 0$ was dispatched swiftly in Ref. [AM04], where it was shown that the eigenvector decomposition of Eq. (4.26) has a
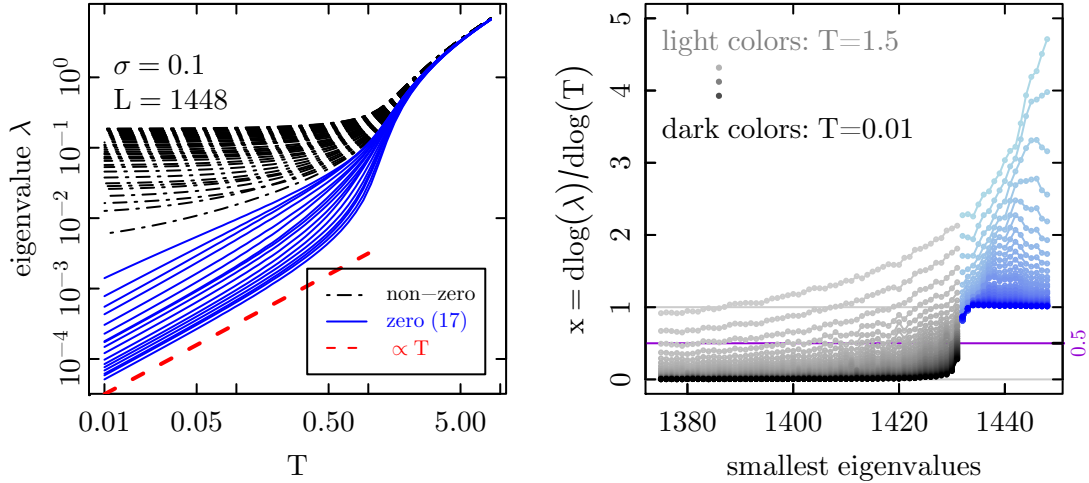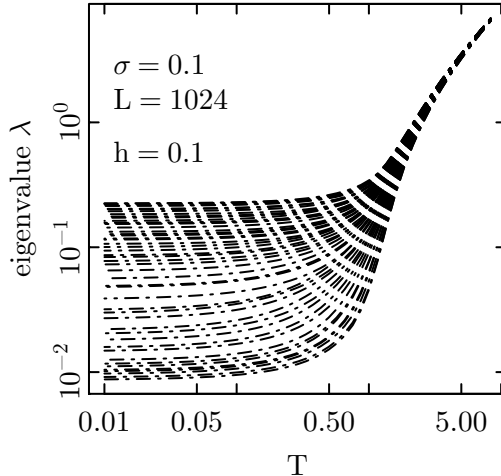
Figure 4.5.: (Color online). The evolution of eigenvalues λ of the matrix A of Eq. (4.6) with temperature for a $L = 1448$ system with $\sigma = 0.1$ in a finite external field h. All eigenvalues stay finite in the limit $T \to 0$ (biggest are left away). This is in contrast to the model with vanishing field $h = 0$, cf. Fig. 4.4.

solution for all temperatures, excluding the possibility of a phase transition. Numerical evidence is given in Fig. 4.5, where not a single eigenvalue scales to zero for a field strength of $h = 0.1$. We solve Eq. (4.98) iteratively using the Newton-Raphson method for systems with $\sigma < 0.85$, see the discussion in Ref. [LY05]. For larger σ, this approach has some numerical instabilities leading to singular matrices in the course of the LU decomposition. We switched to a method using a QR decomposition similarly to the way Broyden's method is usually implemented, see section 4.5.1.

The analysis of the eigenvalue density allows for an alternative method of calculating the spin dimension scaling exponent μ already discussed in Sec. 3.2.1. There, we determined the rank of the matrix M composed of the ground-state spin vectors. Instead, we could have extracted the local field values $|\mathbf{H}_i|$, fed them into Eq. (4.6) and determined the number of zero eigenvalues. These approaches are equivalent since the rows of M correspond to the null eigenvectors of A and the row and column ranks of a matrix are identical [AM04]. This would not have allowed us to consider sufficiently large systems, however, since there an $N \times N$ matrix must be inverted, which is in contrast to the $T = 0$ ground-state calculations where it was sufficient to determine the rank of the auxiliary, but smaller, $m \times N$ ground-state spin matrix M. The results for m_0 extracted from the finite-temperature calculation are summarized in Fig. 4.6. The outcomes are mostly compatible with those of the zero-temperature approach for the case of the fully connected model. In contrast, the $T = 0$ results for the diluted model systematically deviate from those of the fully connected model for $\sigma > 1$ as discussed above in Sec. 3.2.5, and some signs of this non-universality are already seen for $\sigma \gtrsim 0.8$.
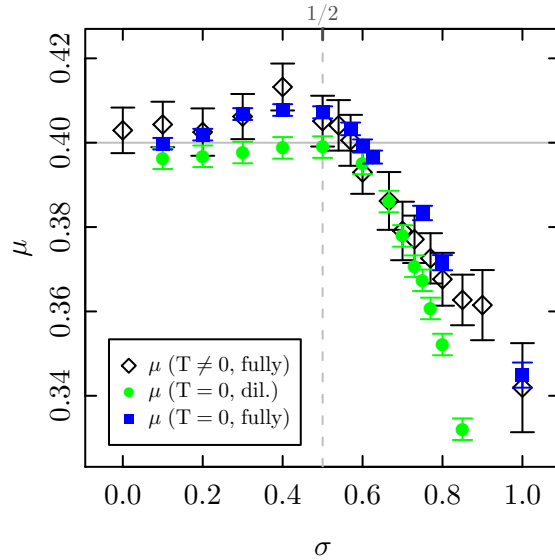
Figure 4.6.: (Color online). Spin-dimension exponent μ calculated from the eigenvalue density at finite temperatures ($T > 0$) as compared to the result reported in Sec. 3.2.1 from the ground-state computations ($T = 0$). For $\sigma = 0$ the SK model was considered directly. For the fully connected model, the results of the calculations at $T = 0$ and for $T > 0$ are well compatible.

4.7.1. Distribution of eigenvalues

Braun and Aspelmeier [BA06] suggested to use the eigenvalue spectrum for a more general understanding of scaling corrections for the case of the two competing limits $N \to \infty$ and $m \to \infty$. Their analysis is valid for the system on a Bethe lattice, but some results might generalize to the model considered here. They discuss the ground-state energy $e(m, N) = E/Nm$ per spin and spin component, which is argued to have two contributions: the ground-state energy in the limit $N \to \infty$ with $m = m_0$ large and fixed, $e_\infty + \frac{1}{4}m_0^{-y} + O(m_0^2)$, and the additional energy required for forcing the N spins into an m_0 dimensional subspace. This second contribution is proportional to the required shift of the eigenvalue spectrum $\rho(\lambda)$ to push m_0 eigenvalues to zero. Assuming the density at small λ to scale as $\rho(\lambda) \sim \lambda^x$ [BM82], the first m_0 eigenvalues occupy the interval $[0, (m_0/N)^{1/(1+x)}]$, such that the total energy is

$$e(m, N) = e_\infty + c_1 m_0^{-y} + c_2 \left(\frac{m_0}{N}\right)^{1/(1+x)} . \qquad (4.105)$$

Minimizing with respect to the number m_0 of spin components yields the scaling relation

$$\mu = \frac{1}{y(x+1)+1} . \qquad (4.106)$$

For the SK model with $x = 1/2$ (the Wigner semicircle law) and $y = 1$ [BM81], we therefore arrive at the observed $\mu = 2/5$ as desired. This scaling should hold independent of the lattice structure.
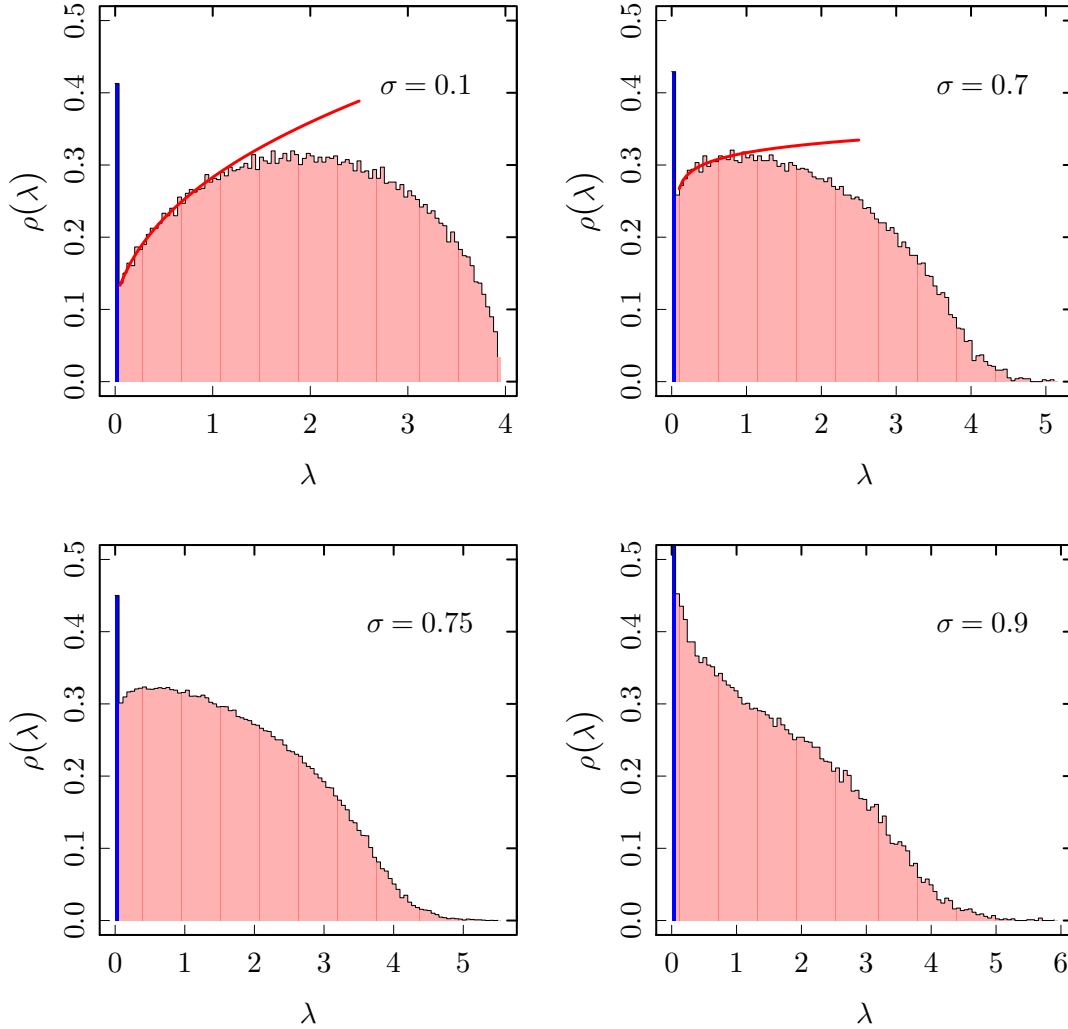
Figure 4.7.: (Color online). The eigenvalue distribution of the matrix A, cf. Eq. (4.6), at temperature $T = 0.01$ for different values of the power-law exponent σ ($N = 1448$). Wigner's semicircle form holds for the infinite-range region $0 < \sigma \leq 1/2$ in the thermodynamic limit. The red, bold line shows fits of the functional form (4.107) to the data. A positive exponent x results for $\sigma < 0.75$.
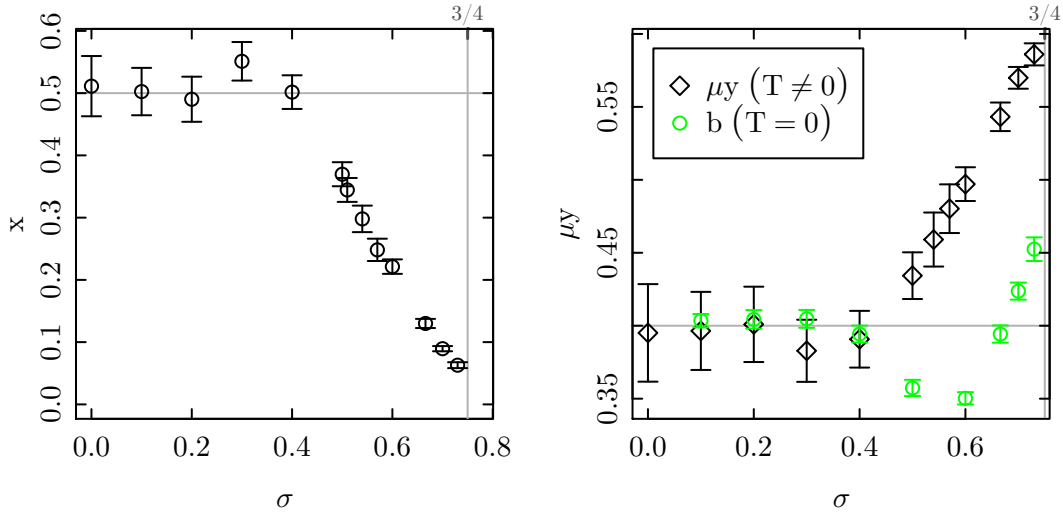
Figure 4.8.: (Color online). Left panel: The density exponent x as determined by fitting a power-law, Eq. (4.107), to the eigenvalue densities shown in Fig. 4.7. Right panel: A comparison of the exponent $z = (1 + \mu)/(1 + x)$ determined from the $T > 0$ calculations (black diamonds) with the ground-state energy correction exponent b as determined in Sec. 3.2.1 (green circles) as a function of the interaction range σ.

We determined the exponent x of the density of eigenvalues as $\lambda \to 0$ from fits of the functional form

$$\rho(\lambda) = a(\lambda + \Delta\lambda)^x \tag{4.107}$$

to the data. Here, the shift $\Delta\lambda$ is required to take the zero eigenvalues into account. To perform the fits, eigenvalues from a large number of disorder samples were accumulated, and the limit $\lambda \to 0$ was modeled by successively omitting more of the larger eigenvalues while monitoring the resulting estimate of x as well as the goodness of fit. Statistical errors on the fit results were determined using a sophisticated jackknifing analysis [Efr79]. Some example results are collected in Fig. 4.7. Fits of this functional form are possible for $\sigma < 0.75$, where the vanishing of the phase transition is signaled by $x = 0$. This is expected since at the upper critical value $\sigma = 3/4$ the vanishing of eigenvalues at any finite temperature ceases to exist [BM82]. Collecting the results for all values of σ considered, we arrive at the data shown in the left panel Fig. 4.8 which confirms our expectations of $x = 1/2$ for $\sigma \le 1/2$ and $x = 0$ for $\sigma = 3/4$. In view of the above expectations which are in-line with our numerical results, it is tempting to speculate that $x(\sigma) = 3/2 - 2\sigma$, but we have not been able to substantiate this claim with a theoretical argument.

Additionally, the authors of Ref. [BA06] suggest the scaling ansatz

$$e(m, N) - e_\infty = m^{-y} F(mN^{-\mu}) \tag{4.108}$$

where $F(x)$ is a scaling function. In the relevant limit of $m \to \infty$ before $N \to \infty$, this implies a scaling of the ground-state energy according to

$$e(m = \infty, N) - e_\infty \sim N^{-z} \tag{4.109}$$

with[1] $z = \mu y = (1 - \mu)/(1 + x)$, where we used Eq. (4.106). In the right panel of Fig. 4.8 we show the correction-to-scaling exponent b for the ground-state energies as determined in Sec. 3.2.1 in comparison to $z = (1 - \mu)/(1 + x)$ as determined from the results of μ and x for our system. Both exponents agree for $\sigma \leq 0.5$ where $b = z = 2/5$. For larger values of σ, however, b is consistently smaller than z. Therefore, if the corrections predicted here are present, they are sub-leading and can not be resolved by our numerical analysis.

4.7.2. Critical behavior

We now turn to studying the behavior of the physical observables extracted from the solution to the saddle-point equations in the vicinity of the critical point. The analysis of the spin-glass correlation length, the Edwards-Anderson order parameter and the spin-glass susceptibility allows us to compare our simulations to the theoretical predictions outlined in Sec. 2.4.4.

Correlation length

The spin-glass correlation function can be calculated from the spin-spin correlation function (4.24) via

$$G_{\text{SG}}(r) = \frac{1}{L} \sum_{r^!_{ij}=r} \left[C_{ij}^2 \right]_{\text{av}} = \frac{T^2}{L} \sum_{r^!_{ij}=r} \left[(A^{-1})_{ij}^2 \right]_{\text{av}} . \tag{4.110}$$

Note that here we use the algebraic graph distance $r^!_{ij} = \min(|i - j|, L - |i - j|)$ irrespective of whether the ring or chain geometry is considered. To arrive at the usual second-moment definition of the correlation length, we use the Fourier decomposition,

$$
\begin{aligned}
\chi_{\text{SG}}^0(k) &= \frac{T^2}{L} \sum_{i,j} \left[(A^{-1})_{ij}^2 \right]_{\text{av}} e^{ik[(i-j) \mod L]} \\
&= \frac{T^2}{L} \sum_{i,j} \left[(A^{-1})_{ij}^2 \right]_{\text{av}} \cos \left(k[(i - j) \mod L] \right) \\
&= 2 \sum_{r=0}^{\lfloor L/2 \rfloor} G_{\text{SG}}(r) \cos(kr) ,
\end{aligned}
\tag{4.111}
$$

where $\lfloor x \rfloor$ denotes the largest integer smaller than or equal to x and plug it into Eq. (2.36),

$$\xi_L = \frac{1}{2 \sin(k_{\min}/2)} \left[\frac{\chi_{\text{SG}}^0(0)}{\chi_{\text{SG}}^0(k_{\min})} - 1 \right]^{1/(2\sigma - 1)} . \tag{4.112}$$

Here, $k_{\min} = 2\pi/L$. In practice, we determine $G_{\text{SG}}(r)$ per disorder realization from the saddle-point equations. For space efficiency, storing $G_{\text{SG}}(r)$ is then preferable over storing C_{ij} directly. Note that since we are using the disconnected correlation function here, the

---

[1] Do not confuse the newly defined exponent $z = \mu y$ with the average coordination number z from earlier chapters. There is no connection.
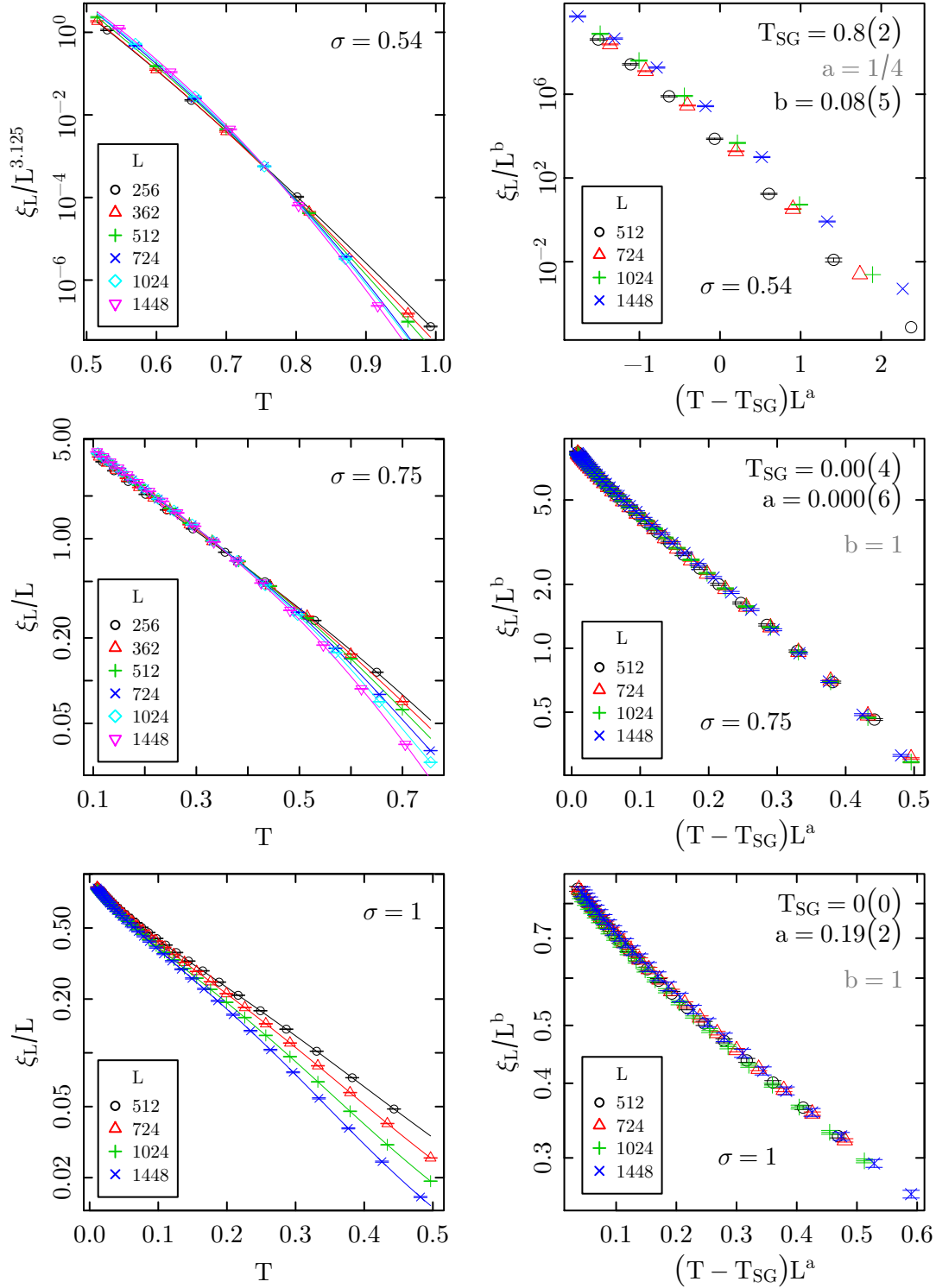
Figure 4.9.: (Color online). The spin-glass correlation length ξ_L for different lattice sizes L. Left panels: Unscaled data for three different values of σ. For $\sigma < 3/4$ lines show a clear crossing point. The crossing vanishes at $\sigma = 3/4$, where the lines for lattice sizes $L = N > 362$ lie approximately on top of each other below a certain temperature. Right panels: Data collapses of the data shown on the left. The resulting parameters are summarized in Fig. 4.10.

σ	samples/10^3
0.1	0.9-2.4
0.2	0.7-1.5
0.3	0.9-2.0
0.4	0.9-2.0
0.5	0.9-1.4
0.51	0.8-1.3
0.54	0.7-2.3
0.57	0.7-2.4
0.6	1.0-3.2
2/3	0.9-1.3
0.7	0.8-1.4
0.73	1.0-2.9
0.75	1.0-1.9
0.77	1.0-2.8
0.8	0.9-2.8
0.85	0.9-2.8
0.9	0.7-2.0
1.0	0.2-2.0

Table 4.1.: Realizations used for the $T > 0$ calculations.

estimators (2.36) only represent the correlation length above T_{SG}. Close to criticality, we expect the scaling form

$$\xi_L \sim \begin{cases} L^{\nu/4} \mathcal{X}(tL^{1/4}), & 1/2 < \sigma \leq 5/8 , \\ L\, \mathcal{X}(tL^{1/\nu}), & \sigma > 5/8 . \end{cases} \tag{4.113}$$

In the ordered phase, on the other hand, ξ_L diverges even more strongly with the system size [BCF$^+$00]. As a consequence, the curves for ξ_L/L ($\sigma > 5/8$) and $\xi_L/L^{\nu/4}$ ($1/2 \leq \sigma \leq 5/8$), respectively, will cross in the vicinity of the critical temperature.

Plots of ξ_L/L and $\xi_L/L^{\nu/4}$ resulting from the finite-temperature calculations with parameters summarized in Tab. 4.1 for three examples of σ are shown in the left panels of Fig. 4.9. Below $\sigma_u = 3/4$, we find a crossing of the curves as shown for $\sigma = 0.54$. For $\sigma > 3/4$, on the other hand, the curves only merge in the limit $T \to 0$. At the critical σ, we see a merging of the curves with an onset temperature scaling to 0 as $L \to \infty$. We note that the scaling of $\xi_L/L^{\nu/4}$ is hard to observe numerically for σ close to 1/2, where $\nu = 1/(2\sigma - 1) \to \infty$, such that a crossing point of $\xi_L/L^{\nu/4}$ is not visible for the system sizes considered here for $\sigma = 0.51$. It is possible to extract estimates for the spin-glass temperature T_{SG} and the correlation length exponent ν by re-scaling the data for different system sizes such that they collapse on the scaling function $\mathcal{X}(x)$. We used two complementary approaches for performing this collapse: method (a) consists of a joint fit of all data sets to a third-order polynomial approximating the scaling function in the chosen regime;
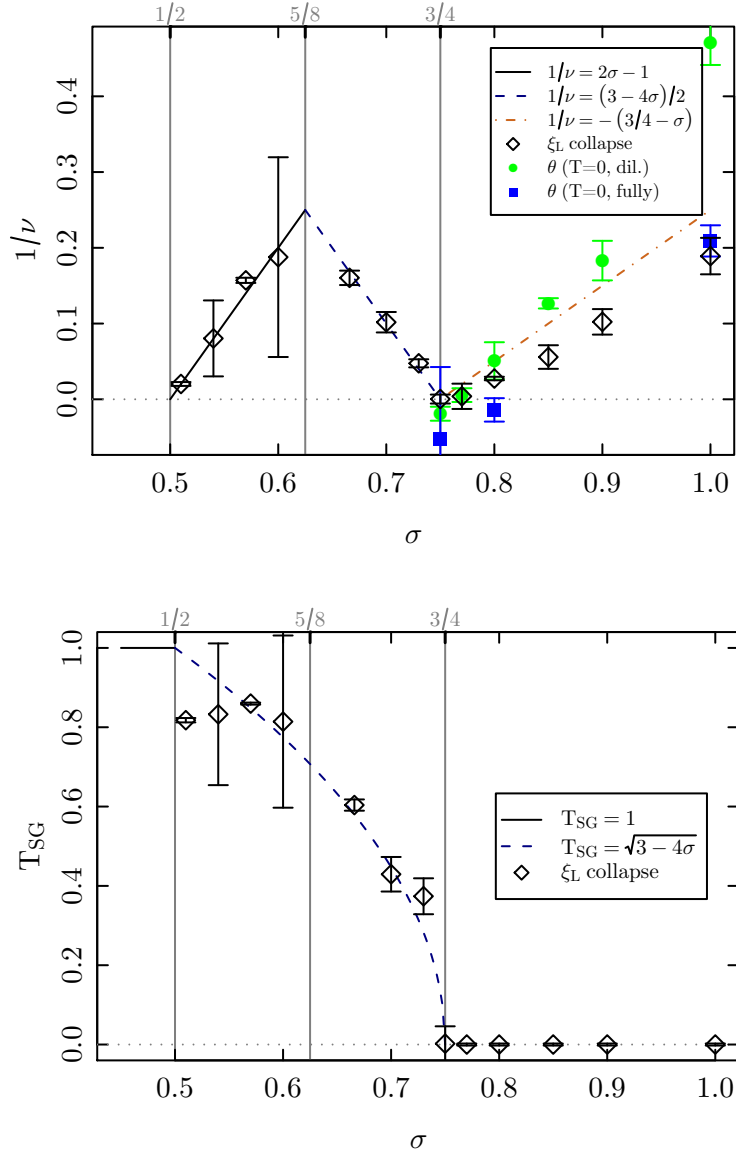
Figure 4.10.: (Color online). Spin-glass transition temperature T_{SG} and correlation length exponent ν as estimated from data collapses of the correlation length data according to the functional form Eq. (4.113). Top panel: transition temperature T_{SG} as compared to the prediction $T_{SG} = \sqrt{3 - 4\sigma}$ of Eq. (2.53). Bottom panel: $1/\nu$ and the relations $1/\nu = 2\sigma - 1$ valid in the mean-field region $1/2 < \sigma \leq 5/8$, cf. Eq. (2.38), and $1/\nu \approx (3 - 4\sigma)/2$, cf. Eq. (2.54). For $\sigma > 3/4$, where $T_{SG} = 0$, we additionally show $\nu = -1/\theta$ with our estimates of θ resulting from the defect-energy calculations. Finite and zero temperature results gained for the fully connected model coincide, whereas strong deviations are visible for the diluted model.

method (b) is the collapsing procedure suggested in Ref. [HH04] which, in turn, is based on Ref. [BS01]. In both cases, we performed the collapse on the *logarithm* of the actual data. This turns out to be necessary since, in particular for small σ, ξ_L/L spans many orders of magnitude in the range of temperatures considered here. In some cases, we also employed weights of the data points involved that decay exponentially away from the adaptively chosen value of the critical temperature. Statistical errors on the collapse parameters have been determined by a bootstrap sampling [Efr79] over the whole collapsing procedure. In the region $\sigma > 5/8$, ν was determined from the scale $tL^{1/\nu}$ of the abscissa. On the contrary, for the mean-field region $1/2 < \sigma \leq 5/8$, it was determined from the scaling $\xi_L/L^{\nu/4}$ of the ordinate. For the latter collapses, we find that the expected scaling of $tL^{1/4}$ of the argument of the scaling function is not very well reproduced, and we allow for this exponent to fluctuate to accommodate scaling corrections.

As illustrated in the right panels of Fig. 4.9, these collapses work rather well over the whole range of σ. The resulting estimates of the correlation length exponent ν and the critical temperature are summarized in Fig. 4.10. The transition temperature is consistent with $T_{\mathrm{SG}} = 0$ for $\sigma \geq 3/4$ and approaches $T_{\mathrm{SG}} = 1$ as $\sigma \to 1/2$. In between, it is compatible with the estimate $T_{\mathrm{SG}} \approx \sqrt{3 - 4\sigma}$ obtained in Sec. 2.4.4. As mentioned above, in the mean-field regime with $\sigma \to 1/2+$, finite-size corrections become very pronounced due to the divergent exponent ν. This leads to rather strong fluctuations of ν and T_{SG} as estimated from the collapsing procedures, cf. Fig. 4.10. In the bottom panel of this figure we also compare our result for $1/\nu$ extracted from collapses for $\sigma > 3/4$ with $-\theta$ from the defect-energy calculations. In general, we find acceptable agreement between zero- and finite-temperature calculations. The observed systematic deviations give an indication of the level of unresolved finite-size corrections. As $\sigma \to 1-$, results for the diluted system start to systematically deviate from those for the fully connected system due to the observed non-universality discussed in Sec. 3.2.5.

Edwards-Anderson order parameter

According to the discussion of FSS in our model, we expect

$$q_{\mathrm{EA}} \sim \begin{cases} L^{-1/4}\mathcal{Q}(tL^{1/4}), & \sigma \leq 5/8, \\ L^{-\beta/\nu}\mathcal{Q}(tL^{1/\nu}), & \sigma > 5/8. \end{cases} \tag{4.114}$$

for temperatures in the scaling window. In the thermodynamic limit, for $\sigma < 1/2$, $\beta = 1$, [AJKT78, AM04] while for $\sigma > 5/8$, β is expected to remain close to unity, so that

$$q_{\mathrm{EA}} \approx \begin{cases} 1 - T/T_{\mathrm{SG}}, & T < T_{\mathrm{SG}}, \\ 0, & T \geq T_{\mathrm{SG}}. \end{cases} \tag{4.115}$$

As is illustrated with the unscaled data in the left panel of Fig. 4.11, these expectations are borne out well by our results. In particular, the thus defined order parameter becomes unity as $T \to 0$, in contrast to the differently defined q_{EA}^0 of Eq. (4.47) and Ref. [LY05].

Right at T_{SG}, q_{EA} scales to zero. To extract T_{SG} and determine β/ν, we again employed scaling collapses. Due to the observed instability of the collapsing procedure, we also
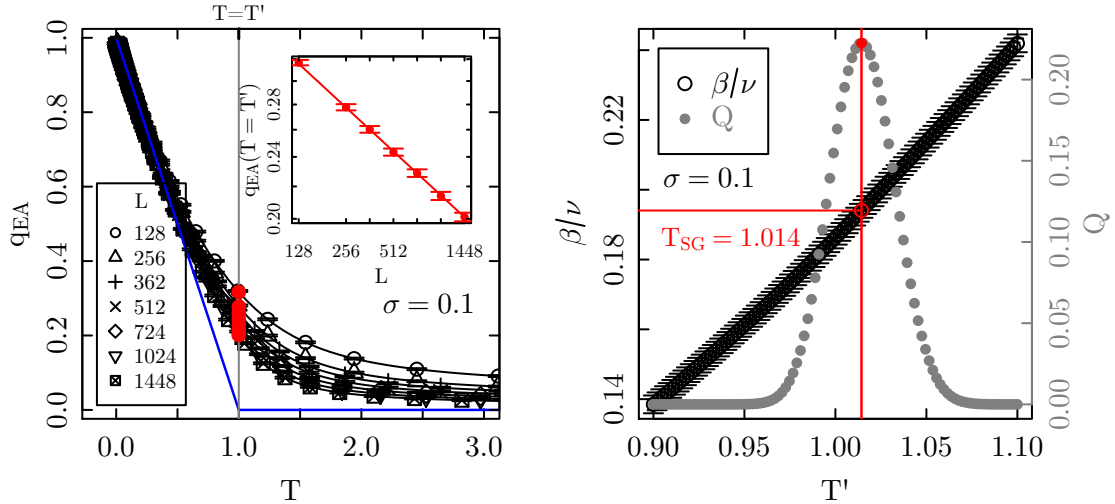
Figure 4.11.: (Color online). Scaling of the Edwards-Anderson order parameter q_{EA}. The left panel shows the dependence of q_{EA} on temperature for $\sigma = 0.1$. For $N \to \infty$, we expect the form (4.115) which is indicated by the solid blue line. Employing fits of the functional form (4.116) for a temperature interval $T_i \leq T' \leq T_f$ around the expected critical temperature (see inset of left panel), we determine T_{SG} and β/ν from the point where such fits work best, which is monitored by the quality-of-fit parameter Q, shown in the right panel. For a summary of results for all σ see Fig. 4.12.

developed an independent approach based on the quality of power-law scaling. Since scaling proportional to $L^{\beta/\nu}$ is only expected at criticality, the critical point might be determined under the assumption that it coincides with the temperature where power-law scaling is best observed. We hence performed fits according to the form

$$q_{EA}(T = T') = cL^{\beta/\nu}, \tag{4.116}$$

for an interval of temperatures $T_i \leq T' \leq T_f$ around the expected value of T_{SG}. If power-law scaling only occurs at $T = T_{SG}$ asymptotically, the quality-of-fit parameter Q should be maximized at this point, such that the information of both the critical temperature and the exponent β/ν can be extracted by this procedure. An example for this approach for $\sigma = 0.1$ is shown in the right panel of Fig. 4.11.

The overall results for the transition temperature T_{SG} and the critical exponent β/ν resulting from this analysis are summarized in Fig. 4.12, together with the corresponding results of a collapsing procedure. The estimates of the spin-glass temperature are consistent with $T_{SG} = \sqrt{3 - 4\sigma}$ in the relevant regime and become constant at $T_{SG} = 1$ for $\sigma \leq 1/2$, while they vanish for $\sigma > 3/4$, as expected. From the present analysis, T_{SG} can be resolved with more precision than from the correlation length particularly in the mean-field regime $\sigma < 5/8$. The exponent β/ν is consistent with the expectations summarized in Sec. 2.4.4, i.e., $\beta/\nu = 1/4$ for $\sigma < 5/8$ and $\beta/\nu = (3-4\sigma)/2$ for $5/8 < \sigma \leq 3/4$. The statistical precision of our determination, however, is not sufficient to rule out possible different scenarios and, in particular, to decide whether $\beta/\nu = (3 - 4\sigma)/2$ might be exact in the non-mean-field regime. Again, statistical errors are calculated by an elaborate jackknifing procedure.
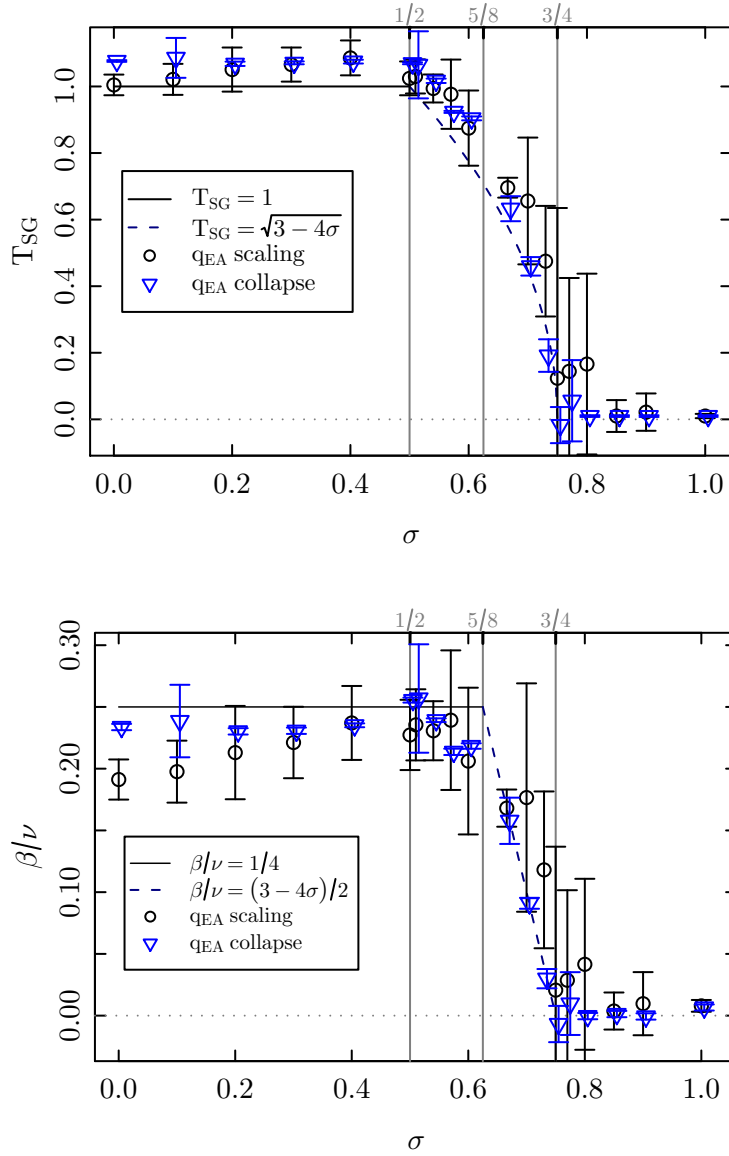
Figure 4.12.: (Color online). Transition temperature T_{SG} and critical exponent β/ν as extracted from the Q maximization procedure described in the main text and in Fig. 4.11. As a comparison we extracted these quantities from a data collapse as well. For both procedures error bars result from a jackknifing analysis.

quantity	ring	line	summed line
μ	0.372(6)	0.374(8)	0.371(7)
ξ_L			
$1/\nu$	0.000(5)	$-0.01(1)$	$-0.03(5)$
T_{SG}	0.00(4)	0.04(6)	0.01(16)
q_{EA}			
β/ν	0.01(4)	$-0.02(5)$	0.00(2)
T_{SG}	0.06(19)	$-0.09(27)$	0.00(13)

Table 4.2.: Results for different choices of the geometry of the model, which were introduced in Sec.(2.3.3). There is no significant difference for the explicitly checked value $\sigma = 3/4$.

Influence of the geometry in the 1d power-law setup

As shown in Tab. 4.2, no significant deviations between the results for the different models of a 1d geometry are observed. In this respect we are not able to recommend usage of one them. Merely the visual aids shown in Fig. 2.1 lead us to decide in favor of the ring geometry.

Spin-glass susceptibility

We finally analyzed the scaling behavior of the spin-glass susceptibility as defined from the connected correlation function in Eq. (4.58). From the discussion in Sec. 2.4.4 we expect scaling according to

$$\chi_{\mathrm{SG}} \sim \begin{cases} L^{1/4}\mathcal{C}(tL^{1/4}) & \sigma \leq 5/8, \\ L^{\gamma/\nu}\mathcal{C}(tL^{1/\nu}) & \sigma > 5/8. \end{cases} \tag{4.117}$$

In contrast to the scaling of q_{EA} it is possible here without reference to numerical derivatives to define a series of pseudo-critical temperatures from the locations of the maxima of the susceptibility,

$$T_{\mathrm{SG}}^{(\mathrm{max})} = T_{\mathrm{SG}} + cL^{-1/\nu}, \tag{4.118}$$

while the values of χ_{SG} at the maxima should then follow

$$\chi_{\mathrm{SG}}^{(\mathrm{max})} = cL^{\gamma/\nu}. \tag{4.119}$$

Fits of the corresponding forms to the data for $\sigma = 0.1$ are shown in Fig. 4.13. We find, however, that the resulting parameter estimates are afflicted by very strong finite-size corrections. In particular, the resulting estimates of $1/\nu$ are far off from our theoretical predictions as well as the results from the analysis of the correlation length.

The presence of strong corrections in the scaling of χ_{SG} is well-known from studies, e.g., of the Ising spin glass. It has been suggested [CHT06] that modified scaling forms incorporating scaling corrections might contribute towards resolving such corrections and the proposed extended scaling forms have been successfully applied to the Ising spin glass [KKY06]. In particular, one problem of the scaling form (4.117) is that it cannot reproduce
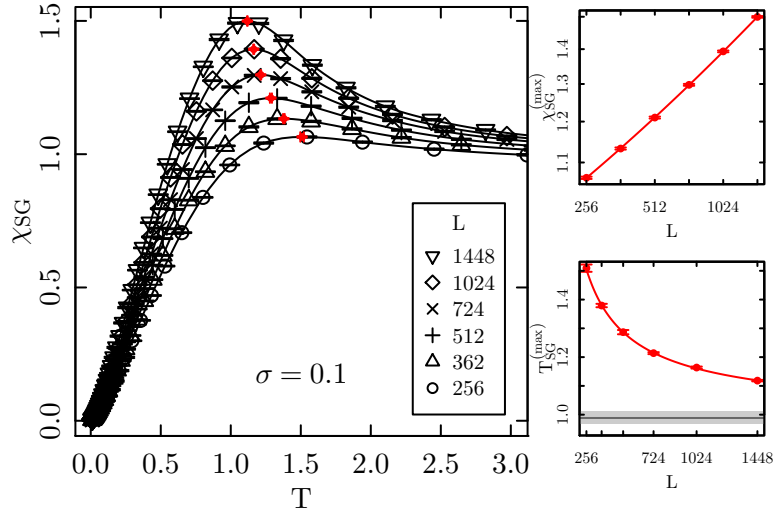
Figure 4.13.: (Color online). Scaling of maxima of the spin-glass susceptibility χ_{SG} in a showcase example with $\sigma = 0.1$.

the observed behavior $\chi_{SG} \to 1$ as $T \to \infty$, cf. Fig. 4.13: assuming that $\mathcal{C}(x) \sim x^{\alpha}$ for $x \gg 1$, asymptotic size independence of the data at large T requires that $\alpha = -\gamma$ and hence $L^{\gamma/\nu}\mathcal{C}(tL^{1/\nu}) \to 0$ as $T \to \infty$. While this is not in contradiction to scaling theory as the assumed scaling form should only apply in the critical region, having a scaling form consistent with the behavior as $T \to 0$ or $T \to \infty$ might allow to extend the scaling regime or, equivalently, reduce the observed finite-size corrections. A modified scaling form that serves this purpose is given by [CHT06]

$$\chi_{SG} = (LT)^{\gamma/\nu}\tilde{\mathcal{C}}[(LT)^{1/\nu}t], \tag{4.120}$$

which is compatible with $\chi_{SG} \to 1$ as $T \to \infty$. We used this extended scaling form to perform collapses of the finite-size data for the spin-glass susceptibility. Even though some scaling corrections are implicitly included in Eq. (4.120), these collapses are found to be rather unstable and, hence, sensitive to the choice of initial values for the parameters and the range of data points to be included for each lattice size. In view of these uncertainties, we found it impossible to extract all three parameters, T_{SG}, γ/ν and $1/\nu$ reliably from a single collapsing procedure. We hence decided to keep T_{SG} fixed at the theoretical prediction $T_{SG} = \sqrt{3 - 4\sigma}$ which, as is shown in the results of Fig. 4.11 for the order parameter, is well compatible with our numerical results. An example collapse is shown in the left panel of Fig. 4.15. The right panel shows our resulting estimates of γ/ν for $\sigma \leq 0.8$. These are roughly compatible with our expectations of $\gamma/\nu = 0.25$ for $\sigma \leq 5/8$ and $\sigma/\nu = 2\sigma - 1$ for $\sigma > 5/8$. For $\sigma \gtrsim 3/4$, we do not find stable collapses with reasonable parameters which we attribute to the fact that, there, $T_{SG} = 0$, but our data only reach down to $T_{\min} = 0.01$. The resulting values of $1/\nu$ are strongly fluctuating and hence not useful as reliable estimates of this quantity. An alternative collapsing exercise using a plot of χ_{SG} as a function of ξ/L, which should have the theoretical advantage of involving only a single adjustable parameter γ/ν did, unfortunately, not lead to more reliable results.
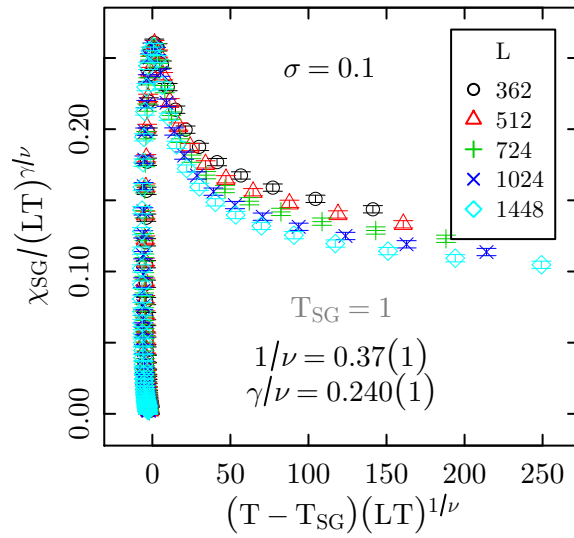
Figure 4.14.: (Color online). A collapse of χ_{SG} according to the extended scaling form (4.120) for $\sigma = 0.1$ with adaptively determined parameters $\gamma/\nu = 0.24$ and $\nu = 0.37$ ($T_{\mathrm{SG}} = 1$).
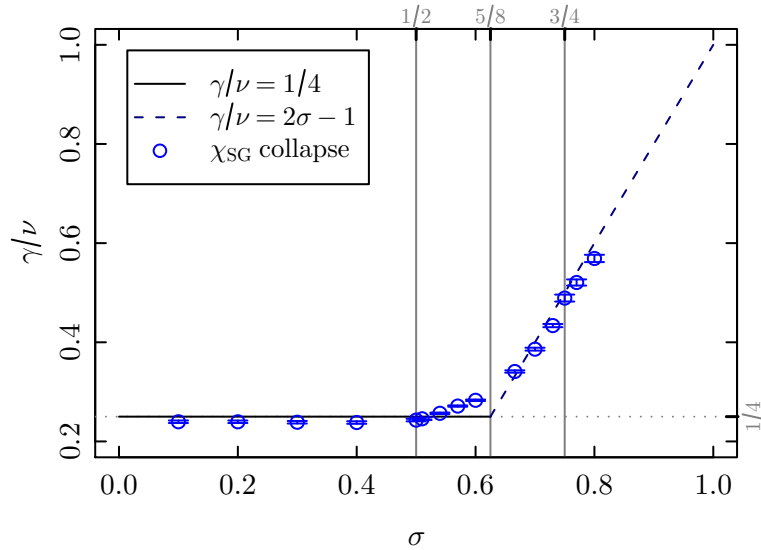
Figure 4.15.: (Color online). Estimates of γ/ν resulting from an adaptive collapsing routine, cf. Fig. 4.15, together with the theoretical expectations $\gamma/\nu = 0.25$ for $\sigma \leq 5/8$ and $\sigma/\nu = 2\sigma - 1$ for $\sigma > 5/8$, respectively.

4.7.3. Hypercubic lattices

The $T = 0$ calculations for hypercubic lattices of section 3.3 turned out to be rather fruitful. Now we want to consider those lattices in order to repeat the $T > 0$ correlation matrix calculations done for the 1d power-law model in the preceding sections. However, one finds quickly that solving the N functions (4.98) simultaneously for a hypercubic system is not as convenient as it was for the 1d power-law model. As we were able to go to system sizes $N = 1448$ for the latter (where $N = L$) without much trouble, we would have a linear lattice size of only $L = N^{1/d}$ in a hypercubic system (e.g. $L \approx 3$ for $N = 1448$ in $d = 6$).

At least the starting values of Eq. (4.82) seem still appropriate, although the probability distributions of the parameters H_i^0 are rather broad, cf. Fig. 4.16. In principle we find that the numerics still works perfectly. However, in the relevant lattice dimensions $d \geq 5$, where we suspect the lower critical dimension d_l to be, small lattice sizes prevent us from making predictions within the framework of finite temperature correlation matrix calculations. Similar to Sec. 4.7.1 we only want to mention that the exponent x might be slightly positive for $d = 6$, cf. Fig. 4.17.

In terms of the hypercubic model, we were not able to calculate our quantities for large enough lattice sizes. Even the number of lattice sizes accessible is not sufficient to do a reasonable finite-size analysis. This is partially due to the $N \times N$ matrix χ being occupied very sparsely in d dimensions, cf. Tab. 2.2. It might be a starting point to take advantage of the sparsity and implement an efficient algorithm using this fact. It seems, however, that for each lattice dimension the algorithm had to be adjusted since the structure of the matrix changes.

The only data we want to present for a consistency check is the correlation length in Fig. 4.18. As expected there is no crossing point at finite temperature for lattice dimensions $d = 2, \ldots, 5$ we have access to in terms of ξ_L. This observation, however, has to be taken with a grain of salt since at lattice dimension $d = 5$, for instance, only $L = 3$ and 4 could be used.
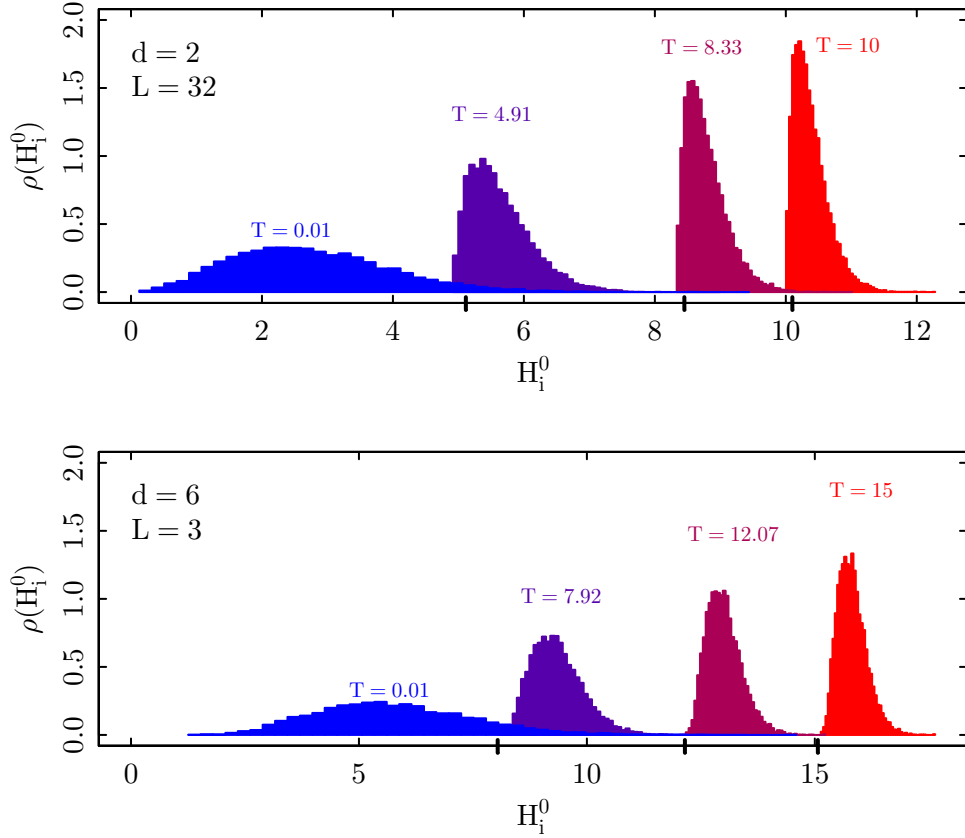
Figure 4.16.: (Color online). Density plots for the parameters H_i in Eq. (4.6) at their saddle-point values H_i^0 for hypercubic lattices of dimension $d = 2$ (top) and $d = 6$ (bottom). In the limit $T \to 0$ they correspond to the (rescaled) local fields $|\mathbf{H}_i|/\sqrt{m}$. Eq. (4.82) yields starting values for the iteration at high temperatures which are still acceptable even for very small L in the sense that the algorithm remains stable. The starting values are sketched in by bold ticks on the H_i^0 axis. Compared to Fig. 4.3 the histograms are much broader due to considerably smaller linear lattice sizes L.
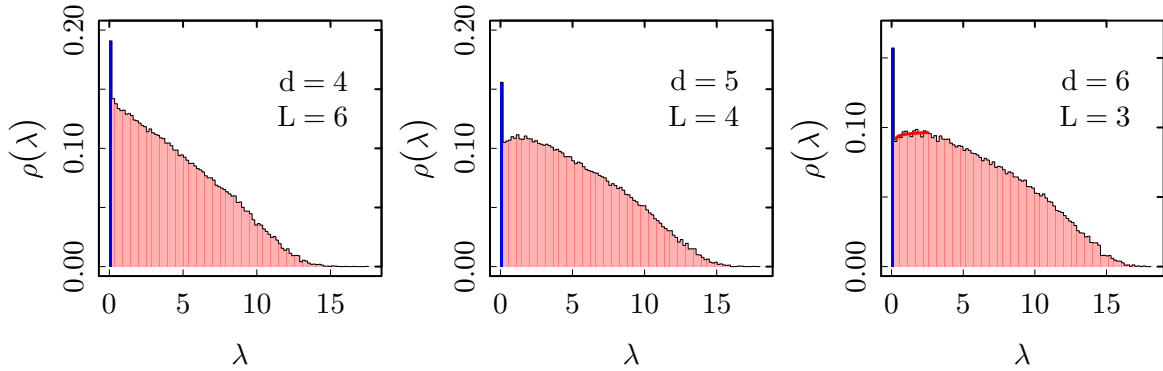
Figure 4.17.: (Color online). The eigenvalue distribution of the matrix A, cf. Eq. (4.6), at temperature $T = 0.01$ for different lattice dimensions $d = 4, 5, 6$. Wigner's semicircle form does not hold for short-range models. The red, bold line shows fits of the functional form (4.107) to the data. A positive exponent x might occur for $d = 6$. Finite-size corrections, however, prevent a more reliable statement.
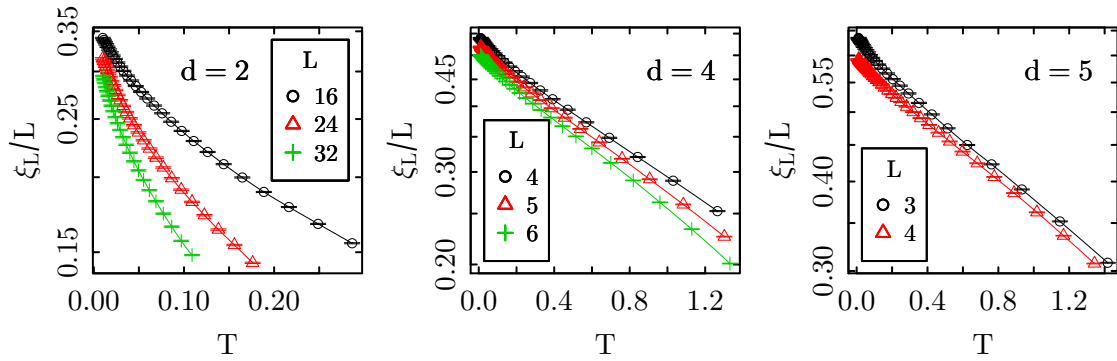
Figure 4.18.: (Color online). The spin-glass correlation length divided by system size ξ_L/L for different lattice sizes L and lattice dimensions $d = 2, 4$ and 5 (left to right). There is no crossing point as expected for those dimensions. High lattice dimensions, however, do not permit to consider reasonably large linear lattice sizes.

4.8. Summary

In this chapter we elucidated the finite temperature properties of the $m \to \infty$ spin-glass model. The numerical calculations were carried out using a set of intriguingly simple matrix equations [BM82] derived by doing a saddle-point approximation for the partition function in the beginning with which it was possible to determine the correlation matrix C. The matrix equations are the saddle-point condition and could be calculated iteratively. We also saw that the key parameters H_i occurring in the equations do correspond to the (scaled) local fields in the zero-temperature calculations in Chap. 3. Furthermore, it was suggested to calculate the order parameter q_{EA} and the spin-glass susceptibility χ_{SG} from the eigenvalues of C, which follows the ideas initiated in [AM04]. In contrast to Ref. [LY05] we argue that true long-range order exists in the low-temperature phase of the $m \to \infty$ model if appropriate definitions of the quantities are introduced. This holds true even for our numerical analysis where the limits $N \to \infty$ and $m \to \infty$ are interchanged as compared to a theoretical treatment, where the thermodynamic limit $N \to \infty$ is taken before the spin-component limit $m \to \infty$.

The whole toolkit for the numerical approach and analysis was given. For a better understanding also the according derivations were written up. Main attention has been paid to the 1d power-law model since the nature of the equations requires systems in which the number N of spins does not exceed the linear extension L too much. In the 1d model $N = L$. Taking no algorithmic advantage of the sparseness of the interaction matrix employing the fully connected version is natural. Anyway, in the light of the larger finite-size corrections of the diluted model seen in Sec. 3.2 (the $T = 0$ calculations) our expectations concerning an improvement of the quality of the results at $T > 0$ are quite low for this model. We have little hope that using algorithms for sparse matrices for the diluted version might overcompensate its shortcomings. On the other hand, the sparsity of the matrices in the case of hypercubic lattices dramatically hindered to use the full computational power and obtain striking results.

However, we were able to do a careful analysis of the numerical results for the 1d model. We extracted the critical exponents ν, γ and β from analyzes of data collapse procedures of the correlation length and the spin-glass susceptibility and scaling optimization approaches of the order parameter. The exponents obtained are consistent with the theoretical arguments given in Chap. 2.4. The critical exponents in the non-mean-field regime have been hard to determine with precision. However, one of the surprises is the utility of the simple approximate RG scheme first suggested by McMillan [McM84a] which seems to work quite well over the entire non-mean field region, $5/8 < \sigma \le 3/4$.

Trying to stand up for a certain choice of the geometry in the 1d power-law system reducing scaling corrections, apart from the ring we also looked at the chain geometry and its improvement – the chain with Ewald summation of interactions. None of the three discussed variants showed significant advantages.

Chapter 5.

Back to finite spin dimensions – a model with anisotropy

In earlier sections, we concentrated on the extreme case that the spin-space dimension is taken to infinity, i.e. $m \to \infty$. We stressed that, starting out from $m = 1$ (the Ising model) and keeping the system size fixed, metastability vanishes as m is increased. It vanishes completely, when a number $m^* \propto N^\mu$, $\mu \leq 2/5$, is reached upon which further adding spin-space dimensions does not change the ground-state energy anymore, cf. Sec. 1.4. While this limit is interesting in itself, a possible application of this observation to more realistic models such as XY ($m = 2$) or Heisenberg ($m = 3$) will be discussed now.

Being interested in the low temperature properties of, say, the ($m = 3$) Heisenberg model one will have to struggle with metastability, cf. Fig. 1.6. Finding ground states using spin quenches as done in the $m = \infty$ model will yield energy minima which do not in general correspond to the absolute minimum. Due to that we want to try to combine the $m = \infty$ with the $m = 3$ model and take advantage of the simple properties of the former to elucidate the latter. The spin-dimension $m = 3$ is chosen arbitrarily and can be chosen at will obeying $m < \infty$. One might think of splitting spin space up into the 'real' spin space one is actually interested in with m_{real} dimensions and an auxiliary space which might extend the space up to the mentioned m^*-dimensional space in which all metastability has vanished by adding $m_{\mathrm{aux}} = m^* - m_{\mathrm{real}}$ dimensions. This means that we are effectively using an $\mathrm{O}(m_{\mathrm{real}} + m_{\mathrm{aux}})$ model. Extending the hypercubic model we add an anisotropy term to the Hamiltonian, e.g. Eq. (2.2), and have then

$$\mathcal{H} = -\frac{1}{2} \sum_{\langle i,j \rangle} J_{ij} \, \mathbf{S}_i \cdot \mathbf{S}_j + \kappa \sum_i \left(\mathbf{S}_i^\perp \right)^2, \tag{5.1}$$

where the spins are ($m_{\mathrm{real}} + m_{\mathrm{aux}}$)-dimensional. It contains the 'real' and the 'auxiliary' components, so that one might decompose spins according to $\mathbf{S}_i = \mathbf{S}_i^\| + \mathbf{S}_i^\perp$. Then, $\mathbf{S}_i^\| \in \mathbb{R}^{m_{\mathrm{real}} + m_{\mathrm{aux}}}$, where the first m_{real} components can be different from zero and the others vanish. And secondly, the 'auxiliary' components are contained in $\mathbf{S}_i^\perp \in \mathbb{R}^{m_{\mathrm{real}} + m_{\mathrm{aux}}}$, with the first m_{real} components vanishing and the others in general being different from zero. By construction $\mathbf{S}_i^\| \perp \mathbf{S}_i^\perp$ and we normalize $|\mathbf{S}_i| = 1$. For instance, if $m_{\mathrm{real}} = 3$ (the Heisenberg

model) and $m_{\mathrm{aux}} = 2$ we had

$$\mathbf{S}_i = \begin{pmatrix} S_1 \\ S_2 \\ S_3 \\ S_4 \\ S_5 \end{pmatrix} = \mathbf{S}_i^{\|} + \mathbf{S}_i^{\perp} = \begin{pmatrix} S_1 \\ S_2 \\ S_3 \\ 0 \\ 0 \end{pmatrix} + \begin{pmatrix} 0 \\ 0 \\ 0 \\ S_4 \\ S_5 \end{pmatrix} . \tag{5.2}$$

The parameter κ in Eq. (5.1) controls the energy penalty for using the extra spin dimensions. For $\kappa = 0$ the (free) energy landscape is most simple, whereas increasing κ renders the system closer to the model of interest having m_{real} spin dimensions. In the limit $\kappa \to \infty$ the system corresponds to the model with m_{real} spin components exactly.

In the following sections we will introduce a small toolkit for using the upper model in future research. Spin update rules in Monte Carlo methods and the spin-quench procedure in zero-temperature calculations are altered in comparison to the spin glass model without any anisotropy. They will be derived. The algorithm for measuring the equality or distinctness of two spin configurations with continuous symmetry will be discussed. At last we will use the spin-quench procedure and determine ground states to have a direct look at the energy levels disappearing with increasing number of spin dimensions. As will be discussed briefly at the end, this can be considered as a sound starting point for future research.

5.1. Spin updates

It is not topic of this work to discuss numeric integration techniques such as the Monte Carlo method. However, if the reader is familiar with it and wants to use it in order to tackle the spin glass with the introduced anisotropy term, we give some indication now as how to adjust the Metropolis update rule in terms of the Monte Carlo importance sampling. A comprehensive introduction to Monte Carlo methods is given in, e.g. Ref. [LB09]. A short introduction biased towards spin glasses can be found in Ref. [Kat09]. Be it mentioned that we shall not use this in this chapter any further.

5.1.1. Metropolis

In order to do a spin update according to the usual Metropolis rule we need to take the anisotropy term into account. The energy difference for a spin update is then

$$\begin{aligned} \Delta E &= E_2 - E_1 \\ &= -\mathbf{S}_i' \cdot \sum_j J_{ij} \mathbf{S}_j - (-\mathbf{S}_i \cdot \sum_j J_{ij} \mathbf{S}_j) + \kappa \left[(\mathbf{S}_i'^{\perp})^2 - (\mathbf{S}_i^{\perp})^2 \right] \\ &= (\mathbf{S}_i - \mathbf{S}_i') \cdot \sum_j J_{ij} \mathbf{S}_j + \kappa \left[(\mathbf{S}_i'^{\perp})^2 - (\mathbf{S}_i^{\perp})^2 \right] . \end{aligned} \tag{5.3}$$

To choose a new spin direction or, generally speaking, to generate a random vector on a high-dimensional unit sphere, one might wonder how to do that. The next section deals
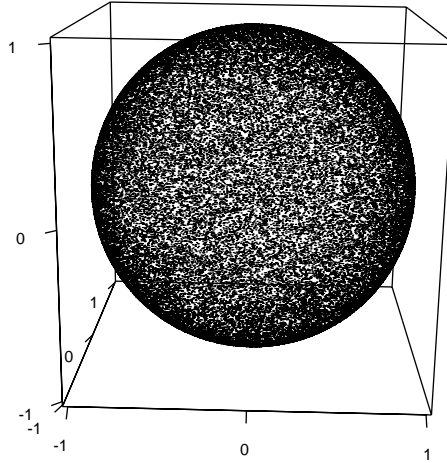
Figure 5.1.: A visual check of the uniformity of random numbers on a $\mathcal{S}_2$-sphere. 50000 random $3d$-vectors pointing onto the unit-sphere were generated using the simple *normal projection method*. There is no objection against a proper distribution of random points on the sphere.

with this topic.

However, we want to finish this section about the side step to Monte Carlo simulations with pointing to an algorithm which can also be adjusted to be κ-dependent in a similar way. Based on the heatbath algorithm, the fast linear algorithm [LQSJ04] speeds up a Monte Carlo simulation considerably for continuous spins and outperforms the Metropolis algorithm especially at low temperature. This comes about due to discretization effects.

5.1.2. Random spin vectors

It is easy to choose a new spin direction in the O($m = 1$)-Ising case. Being in one state (e.g. '*up*') there is only exactly one other state the spin can be in ('*down*', respectively). For O(m) vector spins, though, we need to sample a uniform distribution on an $\mathcal{S}_{m-1}$-sphere, or $\mathcal{S}_{m-1}$-sphere, (embedded in $\mathbb{R}^m$). For $m = 3, 4$ there are a number of efficient algorithms [Mar72, Slo83], usually being rejection methods which are quite fast. A disadvantage arises for increasing dimension m since the ratio of accepted and rejected volumes vanishes exponentially. Although the rejection method can be improved by interpolation methods, cf. [WJ00], the complexity of the algorithm is unappealing. Apart from this there is also a method introduced in Ref. [HW59] inductively transforming points on a $\mathcal{S}_{m-1}$-sphere onto an $\mathcal{S}_m$-sphere.

Furthermore, there is a fast (if only m is large enough), very simple and convenient way to generate uniformly distributed random numbers on an $\mathcal{S}_{m-1}$-sphere due to Muller, cf. Ref. [Mul59] (sometimes called *normal projection method*). In this approach one generates m independent standard normal variates X_i, $i = 1, \ldots, m$, creates a vector $\tilde{\mathbf{X}} =$

$(X_1, \ldots, X_m)$ and normalizes according to $\mathbf{X} = \tilde{\mathbf{X}}/\|\tilde{\mathbf{X}}\|$, where $\|\cdot\|$ denotes the usual Euclidean norm. Then, $\mathbf{X}$ is a vector pointing onto a random point on an $\mathcal{S}_{m-1}$-unit-sphere. For the generation of the X_i one can resort to, e.g., the well-known Box-Muller method [BM58]. A test on a $\mathcal{S}_2$-sphere, i.e. for O(3)-Heisenberg spins is shown in Fig. 5.1. There is no visual objection against the uniformity of the random numbers on the sphere.

For run-time critical applications Muller's *normal projection method* should be compared to its modifications in Refs. [Sib62] and [Tas77].

5.1.3. Spin quench

Earlier in Sec. 3.1 we saw that it is a necessary condition for the spins to be aligned to their local molecular fields for being in a minimal-energy state. Thus, the aim of the spin-quench is to minimize the energy of the spin configuration. For the $m \to \infty$ spin-glass model it was sufficient to use this fact and find the unique ground state by repeatedly quenching the spins to their respective local field until convergence. Regarding systems of finite size, it was possible to be in the limit of infinitely many spin dimensions m, if $m \geq m^*$. The ground-state energy does not change upon further adding spin dimensions. Whenever $m < m^*$, however, there is no guarantee that a ground state is unique. Nevertheless, there is no objection to using the quench technique.

Unfortunately, with the κ-term, the quench move does not look as simple as in Eq. (3.2). In order to calculate the proper quench update for the κ-dependent Hamiltonian it is useful to take a look at the κ-independent one first.

κ-independent Hamiltonian

Starting with

$$E_0(i) = - \sum_{j \in \mathcal{N}(i)} J_{ij} \mathbf{S}_i \cdot \mathbf{S}_j \, , \tag{5.4}$$

with $\mathcal{N}(i)$ being the set of all nearest neighbors of the spin at site i and the constraint

$$|\mathbf{S}_i| = 1 \, , \tag{5.5}$$

one can use the method of Lagrangian multipliers with a function

$$L(i) = E_0(i) - \lambda(1 - |\mathbf{S}_i|) \, . \tag{5.6}$$

Differentiation with respect to all spin components yields

$$
\begin{aligned}
\frac{\mathrm{d}L(i)}{\mathrm{d}\mathbf{S}_i} &= \frac{\mathrm{d}E_0(i)}{\mathrm{d}\mathbf{S}_i} + \lambda \frac{\mathrm{d}|\mathbf{S}_i|}{\mathrm{d}\mathbf{S}_i} \\
&= - \sum_{j \in \mathcal{N}(i)} J_{ij} \mathbf{S}_j + \lambda \frac{\mathbf{S}_i}{|\mathbf{S}_i|} \\
&=: -\mathbf{H}_i + \lambda \frac{\mathbf{S}_i}{|\mathbf{S}_i|} \, ,
\end{aligned}
\tag{5.7}
$$

where we used the known definition for the local field from Eq. (3.2). We are interested in the extremum of L. And so, with $\mathrm{d}L/\mathrm{d}\mathbf{S}_i \overset{!}{=} \mathbf{0}$, we update the spin at site i according to

$$\mathbf{S}'_i = \frac{|\mathbf{S}_i|}{\lambda}\mathbf{H}_i \ . \tag{5.8}$$

Using the constraint (5.5) the norm yields

$$|\mathbf{S}'_i| = \frac{|\mathbf{S}_i|}{|\lambda|}|\mathbf{H}_i|$$
$$|\lambda| = |\mathbf{H}_i| \ , \tag{5.9}$$

such that the spin quench for finding a local minimum is done via

$$\boxed{\mathbf{S}'_i = \frac{1}{|\mathbf{H}_i|}\mathbf{H}_i \ .} \tag{5.10}$$

The correct choice for the sign of λ is obvious but could also be determined with the second derivative of L.

κ-dependent Hamiltonian

We will now turn to the Hamiltonian including the anisotropy term. Here the energy function of a single spin at site i reads

$$E(i) = \underbrace{- \sum_{j\in\mathcal{N}(i)} J_{ij}\mathbf{S}_i \cdot \mathbf{S}_j}_{E_0(i)} + \kappa(\mathbf{S}_i^{\perp})^2 \ , \tag{5.11}$$

with the constraint (5.5) now reading

$$\mathbf{S}_i^2 = (\mathbf{S}_i^{\parallel})^2 + (\mathbf{S}_i^{\perp})^2 = 1 \ . \tag{5.12}$$

We use the method of Lagrangian multipliers again and define

$$L(i) = E(i) - \lambda(1 - |\mathbf{S}_i|) \ . \tag{5.13}$$

Differentiation with respect to all spin components yields

$$\begin{aligned}
\frac{\mathrm{d}L(i)}{\mathrm{d}\mathbf{S}_i} &= \frac{\mathrm{d}E_0(i)}{\mathrm{d}\mathbf{S}_i} + 2\kappa\mathbf{S}_i^{\perp} \\
&= -\mathbf{H}_i + \lambda\frac{\mathrm{d}|\mathbf{S}_i|}{\mathrm{d}\mathbf{S}_i} + 2\kappa\mathbf{S}_i^{\perp} \ .
\end{aligned} \tag{5.14}$$

Searching the extremum we can split up the equation into the real and auxiliary part according to $\mathbf{H}_i = \mathbf{H}_i^{\parallel} + \mathbf{H}_i^{\perp}$ and have

$$\begin{aligned}
-\mathbf{H}_i^{\perp} + \lambda\mathbf{S}_i^{\perp} + 2\kappa\mathbf{S}_i^{\perp} &= 0 \tag{5.15a} \\
-\mathbf{H}_i^{\parallel} + \lambda\mathbf{S}_i^{\parallel} &= 0 \ . \tag{5.15b}
\end{aligned}$$

From these equations we arrive immediately at

$$\mathbf{S}_i^{\perp} = \frac{\mathbf{H}_i^{\perp}}{\lambda + 2\kappa} \tag{5.16a}$$

$$\mathbf{S}_i^{\shortparallel} = \frac{\mathbf{H}_i^{\shortparallel}}{\lambda} . \tag{5.16b}$$

With the constraint (5.12) these equations lead to

$$1 = \frac{(\mathbf{H}_i^{\shortparallel})^2}{\lambda^2} + \frac{(\mathbf{H}_i^{\perp})^2}{(\lambda + 2\kappa)^2} , \tag{5.17}$$

being a polynomial of fourth order in λ.

This equation has, of course, four solutions. The appropriate one which minimizes the energy will give the required λ being needed to carry out the spin quench according to Eqs. (5.16). It is, however, quite nasty and is thus only given as computer code (C++) in appendix B.

5.1.4. Comparing two spin configurations

A key feature of spin glass models with finite spin dimension m is their metastability. This means that there are many different local minima. If we have two spin configurations, e.g. found after a minimum search, it might come to comparing them. We will now define useful measures to determine the relationship between two spin configurations first for $m = 1$ and then for $m > 1$.

For the Ising model, with $m = 1$ it is sufficient to calculate the overlap parameter q in order to have a measure of the similarity. It is defined by

$$q := \frac{1}{N} \sum_i S_i^{(2)} \cdot S_i^{(1)} , \tag{5.18}$$

where $S_i^{(1)}$ are the spins of configuration (1) and $S_i^{(2)}$ the ones of configuration (2), respectively. The spins are scalars from the set $\{-1, 1\}$ and have thus only an up/down, or $\mathcal{Z}(2)$ symmetry. q is bounded by $-1 \leq q \leq 1$ and the interpretation is simple – the overlap parameter takes on the value 1 if both spin configurations are identical. It takes on -1 if they are completely inverse to each other. The overlap of two spin configurations is distinct. A global flip of one of the configurations does not change anything but the sign of q.

In an O($m > 1$) model, however, we need to take into account the rotational symmetry. Comparing two spin configurations and testing their similarity is often wanted to be done only after they have been rotated into a maximally identical state.

Thus, we want to find a matrix R^* which rotates spin configuration (2) in such a manner that the overlap with configuration (1) is maximal. The recipe for finding R^* is given in

Ref. [Hen84]. Due to its brevity we will write it down here in slightly more detail. The next couple of lines introduce a special matrix, make a singular value decomposition of it and use the resulting matrices to calculate the wanted matrix R^*.

We refine definition (5.18) as

$$P := \frac{1}{N} \sum_i \mathbf{S}_i^{(2)} \cdot R \mathbf{S}_i^{(1)} , \qquad (5.19)$$

where the $\mathbf{S}_i$ are general O(m) spins again, R is a rotation matrix and want to find a rotation matrix R^* which maximizes P.

We define a matrix $Q^{(2,1)}$ with elements

$$Q_{\alpha\beta}^{(2,1)} := \frac{1}{N} \sum_i \mathbf{S}_{i\alpha}^{(2)} R \mathbf{S}_{i\beta}^{(1)} \qquad (5.20)$$

to factor out R as a first step. With it

$$\begin{aligned}
P &:= \frac{1}{N} \sum_i \sum_\alpha \mathbf{S}_{i\alpha}^{(2)} \left(\sum_\beta R_{\beta\alpha} \mathbf{S}_{i\beta}^{(1)} \right) = \frac{1}{N} \sum_{\alpha\beta} \sum_i \mathbf{S}_{i\alpha}^{(2)} \mathbf{S}_{i\beta}^{(1)} R_{\beta\alpha} \\
&= \sum_{\alpha\beta} Q_{\beta\alpha}^{(2,1)} R_{\beta\alpha} = \sum_{\alpha\beta} (Q^{(2,1)\,\mathsf{T}})_{\alpha\beta} R_{\beta\alpha} = \sum_\alpha (Q^{(2,1)\,\mathsf{T}} R)_{\alpha\alpha} \\
&= \mathrm{Tr}(Q^{(2,1)\,\mathsf{T}} R) .
\end{aligned} \qquad (5.21)$$

Next, we will use a singular value decomposition of $Q^{(2,1)}$ reading

$$\boxed{Q^{(2,1)} := R_L D R_R^{\mathsf{T}} ,} \qquad (5.22)$$

where R_L and R_R are two orthogonal matrices and D a positive definite diagonal matrix with elements d_i on its main diagonal. Then,

$$P = \mathrm{Tr}((R_L D R_R^{\mathsf{T}})^{\mathsf{T}} R) = \mathrm{Tr}(R_L^{\mathsf{T}} R R_R D^{\mathsf{T}}) = \mathrm{Tr}((R_L^{\mathsf{T}} R R_R) D) =: \mathrm{Tr}(\tilde{R} D) , \qquad (5.23)$$

where we used $(AB)^{\mathsf{T}} = B^{\mathsf{T}} A^{\mathsf{T}}$ and that the trace operation is cyclic. Furthermore, $D^{\mathsf{T}} = D$, since it is diagonal and we defined $\tilde{R} = R_L^{\mathsf{T}} R R_R$ as a new rotation matrix.

Denoting the columns of D as $\vec{d}_i = d_i \vec{e}_i$, with $d_i > 0$ and $\vec{e}_i$ being the Cartesian unit vectors, we find $\|\tilde{R}\vec{d}_i\| = \|\vec{d}_i\|$, since $\tilde{R}$ is a rotation matrix. Then $\vec{\tilde{d}} = \tilde{R}\vec{d}_i$ is a vector with components being smaller than or equal to d_i, since

$$d_i^2 = \|\vec{d}_i\|^2 = \|\tilde{R}\vec{d}_i\|^2 = \|\vec{\tilde{d}}_i\|^2 = \sum_{j=1}^m (\vec{\tilde{d}}_i)_j^2 , \qquad (5.24)$$

so that $(\vec{\tilde{d}}_i)_j^2 \leq d_i^2$. In particular $(\vec{\tilde{d}}_i)_i \leq d_i$ for all i. If the rotation diminishes these components also the trace is diminished, such that

$$P = \mathrm{Tr}(\tilde{R} D) = \mathrm{Tr}(\tilde{D}) \leq \mathrm{Tr}(D) . \qquad (5.25)$$

A maximal overlap is reached if the equality holds. This is the case if $\tilde{R} = \mathbf{1} = R_L^\mathsf{T} R^* R_R$ and thus $\overline{R}_L \mathbf{1} \overline{R}_R^\mathsf{T} = \overline{R}_L R_L^\mathsf{T} R^* R_R \overline{R}_R^\mathsf{T} = \mathbf{1} R^* \mathbf{1}$. Over all we have then

$$R^* = \overline{R}_L \overline{R}_R^\mathsf{T} , \tag{5.26}$$

being the matrix rotating the second spin configuration in a state with maximal overlap with respect to reference configuration one. The rotation matrix does not change the relative orientations of the spins in the rotated configuration.

In short, in order to find the matrix rotating a spin configuration (2) closest to a reference configuration (1) one needs to take three steps. First, matrix $Q^{(2,1)}$ in Eq. (5.20) needs to be calculated from the two spin configurations while setting $R = \mathbf{1}$. Second, a singular value decomposition of this very matrix according to Eq. (5.22) is required. And as a third step the rotation matrix R^* is generated by using Eq. (5.26) with the matrices produced in the singular value decomposition.

5.1.5. Finding local and global energy minima

We are endowed now with some necessary prerequisites like Monte Carlo moves, spin quenches and the comparison of two spin configurations to tackle the model with anisotropy. With this knowledge it is possible to make a test with, e.g., the Heisenberg model with $m = m_{\text{real}} = 3$ spin-space dimensions. For it we expect a number of metastable minimal-energy states which is growing exponentially with system size [ABM04b]. Doing a usual zero-temperature spin-quench will result in one of them. Repeating the spin-quench procedure from another high-temperature configuration, will result in another, so that one will end up with plenty of metastable states with different energies (assuming Gaussian couplings).

Recalling the upper bound m_{max} of spin-space dimensions in Eq. (1.21), adding $m_{\text{aux}} = m_{\text{max}} - m_{\text{real}}$ auxiliary spin-space dimensions we end up with a model having a trivial (free) energy landscape, cf. Sec. 1.4.

Starting at $\kappa = 0$ and making a spin-quench will result in the unique energy minimum (if the condition $m_{\text{real}} + m_{\text{aux}} \geq m_{\text{max}}$ is met). Tuning κ upwards will yield an κ-dependent energy line. The parameter κ needs to be increased in small steps (e.g. 10^{-4} in the showcase example in Fig. 5.2) after which a spin-quench is necessary to minimize the energy again. At a certain finite value of κ it is possible to find also other local minima – indicating the fact that the available spin-space is really restricted. That can be done by copying the system, and do a spin-quench minimum search a number of times always starting in a (random) high temperature spin configuration. In deed more and more local minima will appear as κ is tuned up successively. Due to using finite system sizes, $\kappa \to \infty$ is effectively reached very soon. In Fig. 5.2 there are two showcase examples of an $N = 6 \times 6 \times 6$ Heisenberg model (with $m_{\text{real}} = 3$ spin components) with additional $m_{\text{aux}} = 3$ spin-space dimensions. They are sufficient to let the model become trivial in terms of metastability. Each of the black heavy lines in Fig. 5.2 constitutes the ground-state of the infinite-component spin-glass model ($m \to \infty$, reached for $\kappa \to 0$). In the top sample shown it corresponds to the
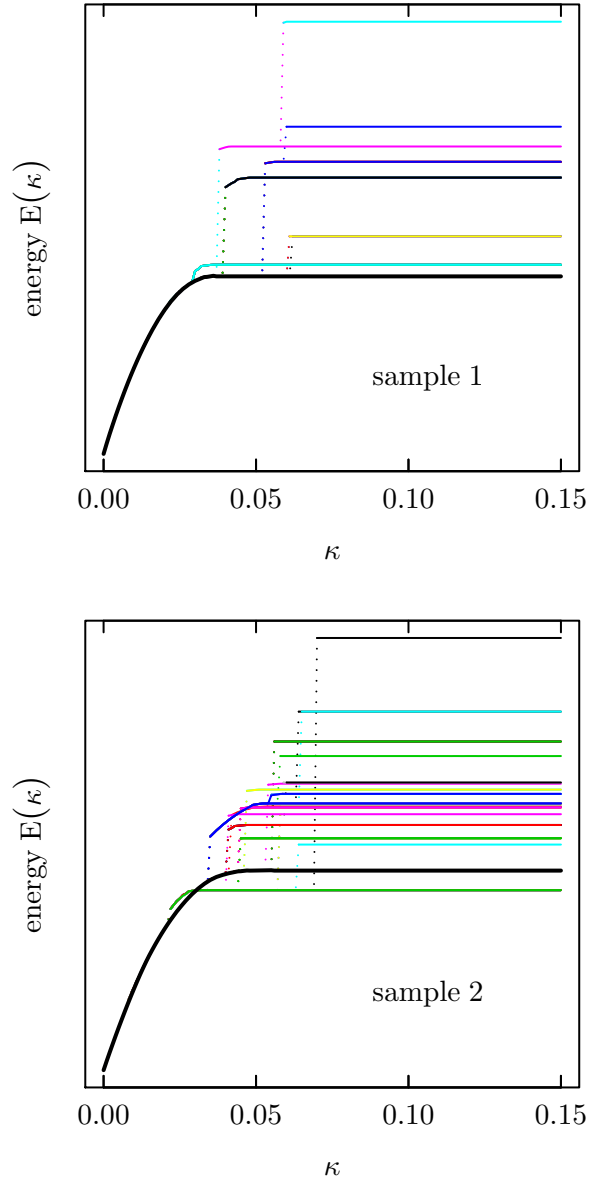
Figure 5.2.: By tuning the anisotropy parameter κ in the Hamiltonian (5.1) it is possible to change the energy landscape. Every line corresponds to the κ-dependent energy of a metastable state. If the auxiliary spin-space dimension m_{aux} is chosen large enough metastability vanishes completely in the limit $\kappa \to 0$ (effectively $m \to \infty$). This corresponds to the plots above each having only one single heavy black line in the vicinity of $\kappa = 0$. New metastable states emerge as κ is increased. Letting $\kappa \to \infty$ the original model with m_{real} spin-space dimensions is recovered having many energy levels. In practice (finite lattice sizes) already finite values of κ suffice to reach it. The above showcase examples are both samples of a $3d$ Heisenberg model ($m_{\mathrm{real}} = 3$) of low linear lattice size $L = 6$ with $m_{\mathrm{aux}} = 3$ auxiliary dimensions. Sample 1 in the top panel has a $\kappa = 0$ ground-state which evolves to the actual Heisenberg ground-state. For sample 2 in the bottom plot the Heisenberg ground-state could not be found by simply "following" the $\kappa = 0$ minimum.

true ground-state of the Heisenberg model, whereas it does not in the bottom sample. Nevertheless, a trial analysis of 100 samples resulted in 65 disorder configurations for which the $\kappa = 0$ ground-state was also the true ground state of the $\kappa \to \infty$ system, i.e. the Heisenberg model. The correctness of the ground-state was guaranteed with a probability of 99.9% by cross-checking with a quasi-exact algorithm of Weigel analogous to the one in [WG06].

One might also turn around the calculation and start at large κ, so that a spin-quench will result in one arbitrary metastable state. Decreasing κ will also yield a κ-dependent energy line – and since there are many metastable states one can produce lots of those lines by repeating the ground-state search several times, cf. Fig. 5.2. At certain values of κ a metastable state will stop to exist and the spin-quench brings the configuration into another metastable state or immediately into the state which survives in the limit $\kappa \to 0$. This is visualized by the dotted lines in Fig. 5.2. At the point of break-down of a metastable state one can check the 'distance' of the configuration to the one which the spin system evolves to after a new spin quench by calculating the overlap (5.20) with $R = R^*$ from (5.26). It can be seen then, that no matter how close the energy-level lines come, the spin configurations are obviously different. It is therefore impossible to start out from $\kappa = 0$ with one unique ground state, tune κ upwards, nudge the configuration slightly and hope to eventually 'drop' into the true Heisenberg ground-state which might have split away from the unique state in the beginning. More elaborate methods are needed. If it were as simple as that, then probably the Heisenberg model wouldn't be classified $\mathcal{NP}$-hard.
Due to that further research using this model is very appealing for the application in an algorithm analogous to the parallel tempering algorithm [SW86, HN96]. This well-known technique to investigate models with rough (free) energy landscape is used to escape local minima with using a number of identical systems (replicas) which are kept at various temperatures T_i. Each of the replicas can move in temperature space according to certain rules by changing its place with a neighboring replica. These excursions in temperature space (from low to high T and back again) guarantee a faster decorrelation and enable to simulate larger system sizes with much less effort than without this technique, e.g. [BCF$^+$00].

Rather than leaving the minima as they are and escaping them by a journey in temperature space in the parallel tempering algorithm, we can imagine an analogous technique for a number of replicas occupying different numbers of spin dimensions. One alters the free-energy landscape by changing the spin-space dimension, cf. Fig. 1.6, and thus makes an excursion in spin-space. But instead of arranging for a set of different spin-space dimensions it is more appropriate to control the number of spin dimensions the system occupies by only one parameter (in parallel tempering we also only change one parameter – the temperature), namely κ.

5.2. Summary

In this chapter a spin-glass model with anisotropy was suggested which intrinsically uses the benefits of the infinite-component spin-glass model ($m \to \infty$). A Metropolis Monte Carlo

move and the spin-quench procedure to find energy minima was derived to be able to use the model immediately. It was additionally described how to compare spin configurations of vector models with continuous symmetry to be able to find relationships of two spin configurations of spin models with continuous symmetry.

A test of the spin-quench procedure on a Heisenberg model with auxiliary spin-space dimensions was carried out and gave insight into the existence of certain energy-levels depending on the choice of the anisotropy parameter κ. The ground-state of the fully isotropic model in the limit $m \to \infty$ (reached with $\kappa = 0$ and an appropriately chosen number of auxiliary spin-space dimensions m_{aux}) does not necessarily end up in the true ground state of the Heisenberg model but does it at times.

Lastly, we pictured an appealing approach for future research using this model analogous to the well-known parallel tempering algorithm.

Chapter 6.

Real-space renormalization-group calculations for vector spin glasses

In this chapter we want to make use of the real-space renormalization-group (RSRG) approach in order to revisit vector spin glasses with more than one but a finite number of spin components, i.e. $1 < m < \infty$. For those kind of spin glasses the issue about the lower critical dimension (LCD) d_l has been hotly debated for decades. Only in the last years agreement on the LCD to be (at least close to) 3 seems to have been reached [KR05]. Nevertheless, this took a long time and various methods were used. For the replica treatment of spin glasses as e.g. in Ref. [Kre77], there appear difficulties when the number of replicas is taken to zero. Also in the droplet picture there are methods, e.g. expansions of the free energy [HLC76] in $d = 6 - \varepsilon$ with a small parameter ε, which becomes problematic, of course, if one wants to extend results to $d = 3$. RSRG calculations never gave the correct prediction of the LCD, but rather suggested, e.g., $d_l \sim 3.87$ [BB88]. As will be shown here, these calculations relied on a recursion relation for the couplings that is at variance with the states expected in the spin-glass phase. However, RSRG methods have the advantage of working directly with the physically relevant dimension. The replica trick is not needed. The core message of this chapter is to use a new recursion relation which will be derived below and yields the correct value for the LCD. Besides, the calculation confirms the outcome for the stiffness exponent θ from a very simple argument given in Ref. [AP78].

The chapter is structured as follows. First, we will have a look at the theoretical foundations of the real-space renormalization-group calculations. Second, to get a feeling for the renormalization process, we will work out the well-known recursion relations for the ferromagnet. A partial evaluation of the trace appearing in the partition function, cf. Eq. (1.3), will be done next and using a low-temperature expansion, the Migdal-Kadanoff transformation results for arbitrary spin dimension m. Third, we will attempt an analogous treatment for vector spin-glasses leading to a new Migdal-Kadanoff expression for the renormalization of the couplings. Fourth, having found this new expression, we will numerically determine the stiffness exponent θ (and deduce the LCD from it), the Lyapunov exponent and a characteristic exponent similar to the fractal dimension. Fifth, we will calculate all mentioned quantities by making an analytical approximation and confirm the numerical results. Afterwards, this chapter will be summarized and concluded.

6.1. Theoretical foundations

Basis of investigation is, as before, the Hamiltonian

$$\mathcal{H} = -\sum_{\langle i,j \rangle} J_{ij}\, \mathbf{S}_i \cdot \mathbf{S}_j \;, \tag{6.1}$$

where the sum is over all nearest neighbors indicated by the symbol $\langle i, j \rangle$. The spins $\mathbf{S}_i$ are real vector spins of arbitrary dimension $1 < m < \infty$ and the interaction variables J_{ij} are Gaussian random variables with zero mean and unit variance.

The concept of the defect energy, introduced with Eq. (1.20), was investigated thoroughly in Chap. 3. We inserted a defect of (linear) system size L into the system and analyzed its cost E_{def}. The concept of the defect energy, however, is some kind of practical realization of what is done by a renormalization procedure. There, the width σ_J of the coupling distribution changes, as we will see below. If σ_J^0 denotes the initial width of the coupling distribution, then we have a scaling argument of Ref. [BM84] stating

$$E_{\mathrm{def}} \sim \sigma_J \sim \sigma_J^0 L^{\theta} \;, \tag{6.2}$$

where θ is the stiffness exponent. It is noteworthy, that thus θ describes both the scaling behavior of the width of the coupling distribution at zero temperature and the scaling of the defect energy E_{def}. A sign change in θ signals the change of character of the phase transition, see Sec. 3.2.5.

Furthermore, for Ising spin glasses the low-temperature phase has been shown to be chaotic [FH86, BM87a] meaning that very slight noise on the couplings (which could be interpreted as the effect of a minimal temperature) triggers a drastic change in the spin order on long length scales. The noise imposes an additional energy contribution of [BB88]

$$E_+ \sim \pm \varepsilon \sigma_J^0 L^{d_s/2} \;, \tag{6.3}$$

where $\varepsilon \sigma_J^0$ measures the slight noise on the couplings and $d_s/2$ is a characteristic exponent. The latter is called fractal dimension in the ($m = 1$) Ising spin glass, since clear-cut domain walls traverse the system. For vector spin glasses, however, those domain walls are smeared out over the whole system, so that there is no obvious geometric representation of it. However, L^{d_s} specifies the typical area of a droplet surface.

There is an Imry-Ma argument [IM75] for Ising spin glasses suggesting the instability of a ground state on length scales

$$L > L^* \sim 1/\varepsilon^{1/\zeta} \;, \tag{6.4}$$

if

$$\zeta = d_s/2 - \theta > 0 \;, \tag{6.5}$$

where ζ is the Lyapunov exponent. These considerations have been done for the Ising spin glass and found to be useful also for vector spin glasses, the low-temperature phase of which has been shown to be chaotic as well [BB88]. Therefore, we consider Eqs. (6.2,6.3,6.4,6.5) suitable for the treatment of vector spin glasses with a finite number of spin dimensions $m > 1$ and use them below.

142

We want to give some inequalities derived in Ref. [FH86], which give some kind of a guideline in our calculations to follow. The fractal dimension is bounded (in Ising systems) by

$$d - 1 \leq d_s \leq d \tag{6.6}$$

and the stiffness exponent obeys

$$\theta \leq (d-1)/2 \ . \tag{6.7}$$

The quantities ζ, d_s and θ provide useful information about phase transitions. E.g., for the analogous quantities defined for the Ising ferromagnet, we have the equalities $d_s = d - 1 = \theta$ yielding $\zeta = -(d-1)/2$ [BM87a] stating that the ground state is stable at least for $d > 1$.

6.1.1. Real-space renormalization-group and hierarchical lattices

In general it is impossible to evaluate the partition function Z, cf. (1.3), since the trace operation is just too difficult to be carried out. Central idea of the RSRG is to remove degrees of freedom progressively [NV74], i.e. perform the trace operation in small steps. Thus, we need to perform the trace over a fraction of spins to obtain an effective coupling between the remaining spins. One might also consider the partial trace as a procedure renormalizing the Hamiltonian. Important to note, though, is that the partition function itself is preserved. For one-dimensional spin-models this approach yields the exact solution to the problem given. For higher dimensional models the renormalization group is in general a rather uncontrolled approximation. Anyway, according to a block-spin transformation suggested by Kadanoff [Kad76] the number of degrees of freedom is decimated from N to N/b^d, where d is the dimensionality of the lattice space and $b > 1$ a spatial rescaling factor, cf. [Fis74, Fis98]. The mentioned transformation can also be thought of as "moving" bonds – a procedure known as the Migdal-Kadanoff approximation. With it we move two or more bonds on top of each other and transform them according to a certain prescription usually named Migdal-Kadanoff recursion relation. This constitutes the core of the renormalization group: removing degrees of freedom and change or redefine the coupling constants. For a visual impression we might already have a glance at Fig. 6.5, where a hierarchical lattice with various fractal dimensions is shown. These kind of lattices allow for an exact solution for different classical spin models [GK82, KG84], which render them appealing in sight of the otherwise approximate character of the renormalization group in general dimensions $d > 1$. The decimation procedure becomes especially simple here. For a moment we will turn around the direction shown in Fig. 6.5 and iteratively enlarge the system. Then, choosing the unit cell to have n parallel paths of b segments between the 'surface'-spins ($\mathbf{S}_a$ and $\mathbf{S}_b$) we observe the following behavior. The linear lattice size L increases by a factor of b every time one bond is substituted by a unit cell (done for all bonds in the system). Thus, after $\mathfrak{q}$ iterations $L = b^{\mathfrak{q}}$. The number of edges grows as $N \sim (nb)^{\mathfrak{q}}$, where N is the number of spins. Using $N = L^d$ the fractal dimension is given by

$$d = \frac{\ln n}{\ln b} + 1 \ . \tag{6.8}$$

Thus, we can use hierarchical lattices with certain combinations of n and b to mimic hypercubic systems with a natural number of lattice dimensions. Usual choices are $b = 2$ and $n = 2$ for $d = 2$, $n = 4$ for $d = 3$, $n = 8$ for $d = 4$ and so on.

6.2. The ferromagnet

Being interested in the partition function $Z = \text{Tr}\, e^{-\beta \mathcal{H}}$ but facing too hard a challenge, the starting point of the discussion for $O(m)$ vector spins is the approximate relation

$$
e^{\tilde{K}\mathbf{S}_1 \cdot \mathbf{S}_3} \propto \text{Tr}_{\mathbf{S}_2}\, e^{K(\mathbf{S}_1 \cdot \mathbf{S}_2 + \mathbf{S}_2 \cdot \mathbf{S}_3)} \,,
\tag{6.9}
$$

where we use $K = \beta J$ and $\tilde{K} = \beta \tilde{J}$. Eq. (6.9) gives the strategy for the renormalization of 3 spins. One spin ($\mathbf{S}_2$) is traced out and the variable $\tilde{J}$ describes an effective coupling between the remaining spins $\mathbf{S}_1$ and $\mathbf{S}_3$, which were not connected directly before. Only for the spin-1/2 Ising model this is exact and yields the Migdal-Kadanoff recursion relation [BB83]

$$
\begin{aligned}
\tanh \tilde{K} &= (\tanh K)^2 \\
\tilde{K} &= \tanh^{-1}(\tanh K)^2 = \frac{1}{2}\ln(\cosh 2K) \,.
\end{aligned}
\tag{6.10}
$$

Furthermore, for m-vector systems in [BB83], with choosing $\|\mathbf{S}_i\| = \sqrt{m}$, we can calculate the approximation

$$
\tilde{K} = \frac{K}{4} \cdot \frac{I_{\frac{m-4}{2}}(2Km) + I_{\frac{m}{2}}(2Km)}{I_{\frac{m-2}{2}}(2Km)} - \frac{m-2}{8m} \,,
\tag{6.11}
$$

where $I_\nu(z)$ denotes the modified Bessel function [AS65]. We will spell out this calculation now in order to have a basis for introducing disorder and make an analogous analysis for spin glasses. The calculation consists essentially of the evaluation of the *rhs* of Eq. (6.9) in spherical coordinates and expanding both sides of the equation into a power-series in terms of the small angle $\varphi = \angle(\mathbf{S}_1, \mathbf{S}_3)$. Afterwards, according coefficients will be compared to find an expression for $\tilde{K} = \beta \tilde{J}$ as a function of the old coupling $K = \beta J$. This is valid as long as a low-temperature regime is being considered, in which the spins tend strongly to align, i.e. φ is small.

The trace over spin $\mathbf{S}_2$ corresponds to an integral over a $\mathcal{S}_{m-1}$ sphere [1]. Then,

---

[1] The infinitesimal volume element in spherical coordinates in n dimensions reads $\mathrm{d}_{\mathbb{R}^n} V = R^{n-1}\sin^{n-2}\phi_{n-1}\sin^{n-3}\phi_{n-2}\cdots\sin^1\phi_2 \mathrm{d}\phi_2 \cdots \mathrm{d}\phi_{n-1}\mathrm{d}\phi_1$

Figure 6.1: Tracing out spin $\mathbf{S}_2$ for the ferromagnet. Eventually, the according integral becomes feasible in the low temperature limit, when the spins tend to align, i.e. if φ becomes small.
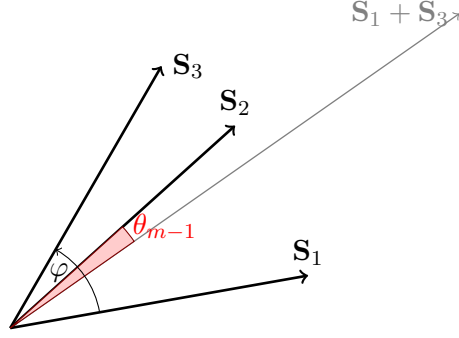
$$
\begin{aligned}
\mathrm{Tr}_{\mathbf{S}_2}\, \mathrm{e}^{K(\mathbf{S}_1 \cdot \mathbf{S}_2 + \mathbf{S}_2 \cdot \mathbf{S}_3)} &= \int_{\mathcal{S}_{m-1}} \mathrm{d}\mathbf{S}_2 \mathrm{e}^{K(\mathbf{S}_1 \cdot \mathbf{S}_2 + \mathbf{S}_2 \cdot \mathbf{S}_3)} \\
&= \int_0^{2\pi} \mathrm{d}\theta_1 \int_0^\pi \mathrm{d}\theta_2 \cdots \int_0^\pi \mathrm{d}\theta_{m-2} \int_0^\pi \mathrm{d}\theta_{m-1} m^{\frac{m-1}{2}} \\
&\quad \sin^{m-2}\theta_{m-1} \sin^{m-3}\theta_{m-2} \cdots \sin^1 \theta_2 \mathrm{e}^{K\|\mathbf{S}_1 + \mathbf{S}_3\| m^{1/2} \cos\theta_{m-1}} \\
&= m^{\frac{m-1}{2}} \overbrace{\int_0^{2\pi} \mathrm{d}\theta_1 \int_0^\pi \mathrm{d}\theta_2 \cdots \int_0^\pi \mathrm{d}\theta_{m-2} \sin^{m-3}\theta_{m-2} \cdots \sin^1 \theta_2}^{=\mathcal{S}_{m-1}} \cdot \\
&\quad \cdot \underbrace{\int_0^\pi \mathrm{d}\theta_{m-1} \sin^{m-2}\theta_{m-1} \mathrm{e}^{K\|\mathbf{S}_1 + \mathbf{S}_3\| m^{1/2} \cos\theta_{m-1}}}_{=: \hat{I}} \,, \quad (6.12)
\end{aligned}
$$

where $\mathcal{S}_{m-1}$ is the surface of a $(m-1)$-dimensional unit sphere [2] given by

$$
\mathcal{S}_{m-1} = \frac{2\pi^{\frac{m-1}{2}}}{\Gamma\left(\frac{m-1}{2}\right)} \,. \quad (6.13)
$$

It is useful to choose the direction of $\mathbf{S}_1 + \mathbf{S}_3$ as the axis the angle θ_{m-1} is associated with (the "z-axis for the spherical coordinates"). With this and $\varphi = \angle(\mathbf{S}_1, \mathbf{S}_3)$ one finds $\cos\frac{\varphi}{2} = \frac{\frac{1}{2}\|\mathbf{S}_1 + \mathbf{S}_3\|}{\|\mathbf{S}_3\|}$, so that $\|\mathbf{S}_1 + \mathbf{S}_3\| = 2m^{1/2}\cos\frac{\varphi}{2}$. The remaining integral $\hat{I}$ has the form of a modified Bessel function

$$
I_\nu(z) = \frac{\left(\frac{z}{2}\right)^\nu}{\Gamma(\nu + \frac{1}{2})\Gamma(\frac{1}{2})} \int_0^\pi \mathrm{e}^{\pm z \cos\theta} \sin^{2\nu}\theta \mathrm{d}\theta \,,
$$

where Γ is the Gamma function (recall $\Gamma(1/2) = \sqrt{\pi}$) and $\mathrm{Re}(\nu + \frac{1}{2}) > 0$, see [GR80], such that

$$
\int_0^\pi \sin^{2\nu}\theta \mathrm{e}^{z\cos\theta} \mathrm{d}\theta = I_\nu(z) \frac{\Gamma(\nu + \frac{1}{2})\sqrt{\pi}}{\left(\frac{z}{2}\right)^\nu} \,. \quad (6.14)
$$

---

[2] The volume of a n-sphere with radius R is $V_n(R) = \frac{2\pi^{n/2}}{n\Gamma(\frac{n}{2})} R^n$. Accordingly, $V_{n-1}(R) = \frac{2\pi^{\frac{n-1}{2}}}{(n-1)\Gamma(\frac{n-1}{2})} R^{n-1}$ and $\mathcal{S}_{n-1}(R) = \frac{\partial V_n(R)}{\partial R} = \frac{2\pi^{\frac{n-1}{2}}}{\Gamma(\frac{n-1}{2})} R^{n-2}$

And hence, if we identify $\nu = \frac{m-2}{2}$ and $z = K\|\mathbf{S}_1 + \mathbf{S}_3\|m^{1/2} = 2Km\cos\frac{\varphi}{2}$ it follows

$$\hat{I} = \int_0^\pi \sin^{2\frac{m-2}{2}}\theta_{m-1}\mathrm{e}^{2Km\cos\frac{\varphi}{2}\cos\theta_{m-1}}\mathrm{d}\theta_{m-1} = I_{\frac{m-2}{2}}\left(2Km\cos\frac{\varphi}{2}\right)\frac{\Gamma(\frac{m-1}{2})\sqrt{\pi}}{(Km\cos\frac{\varphi}{2})^{\frac{m-2}{2}}} \ . \tag{6.15}$$

Inserting Eq. (6.15) into Eq. (6.12) yields

$$
\begin{aligned}
\mathrm{Tr}_{\mathbf{S}_2}\,\mathrm{e}^{K(\mathbf{S}_1\cdot\mathbf{S}_2+\mathbf{S}_2\cdot\mathbf{S}_3)} &= m^{\frac{m-1}{2}}\frac{2\pi^{\frac{m-1}{2}}}{\Gamma(\frac{m-1}{2})}I_{\frac{m-2}{2}}(2Km\cos\frac{\varphi}{2})\frac{\Gamma(\frac{m-1}{2})\sqrt{\pi}}{(Km\cos\frac{\varphi}{2})^{\frac{m-2}{2}}} \\
&= m^{\frac{m-1}{2}}(2\pi)^{\frac{m}{2}}\frac{I_{\frac{m-2}{2}}(2Km\cos\frac{\varphi}{2})}{(2Km\cos\frac{\varphi}{2})^{\frac{m-2}{2}}} \\
&= \hat{A}(m)\frac{I_{\frac{m-2}{2}}(2Km\cos\frac{\varphi}{2})}{(2Km\cos\frac{\varphi}{2})^{\frac{m-2}{2}}} \ .
\end{aligned}
\tag{6.16}
$$

For reasons of convenience $\hat{A}(m) = m^{\frac{m-1}{2}}(2\pi)^{\frac{m}{2}}$ has been chosen such that the denominator is $z^{\frac{m-2}{2}}$.

6.2.1. Low-temperature expansion

The *lhs* of Eq. (6.9) is just

$$\mathrm{e}^{\tilde{K}\mathbf{S}_1\cdot\mathbf{S}_3} \overset{(*)}{=} \mathrm{e}^{\tilde{K}m\cos\varphi} \tag{6.17}$$

$$\overset{(**)}{=} \mathrm{e}^{\tilde{K}m} - \frac{\tilde{K}m}{2}\mathrm{e}^{\tilde{K}m}\varphi^2 + O(\varphi^4) \ , \tag{6.18}$$

where for $(*)$ the mentioned normalization of the spins $\|\mathbf{S}_i\| = \sqrt{m}$ has been used and for $(**)$ an expansion with respect to φ has been made. This approximation is good for $T \to 0$, when the spins tend to align in the ferromagnet. A showcase example can be seen in Fig. 6.2.

The same low-temperature approximation can be carried out, of course, for the *rhs* of Eq. (6.9), given in (6.16). Then,

$$
\begin{aligned}
\mathrm{Tr}_{\mathbf{S}_2}\,\mathrm{e}^{K(\mathbf{S}_1\cdot\mathbf{S}_2+\mathbf{S}_2\cdot\mathbf{S}_3)} &= \hat{A}(m)\frac{I_{\frac{m-2}{2}}(2Km)}{(2Km)^{\frac{m-2}{2}}} \\
&\quad -\hat{A}(m)\frac{1}{16(2Km)^{\frac{m-2}{2}}}\left[2KmI_{\frac{m-4}{2}}(2Km) + 2KmI_{\frac{m}{2}}(2Km)\right. \\
&\qquad \left. + (2-m)I_{\frac{m-2}{2}}(2Km)\right]\varphi^2 \\
&\quad +O(\varphi^4) \ .
\end{aligned}
\tag{6.19}
$$

Comparing coefficients of Eq. (6.18) and Eq. (6.19) yields for the zeroth order (note the proportionality constant $c(m)$ used to make an equation out of (6.9) – then $A(m) = c(m)\hat{A}(m)$)

$$\mathrm{e}^{\tilde{K}m} = A(m)\frac{I_{\frac{m-2}{2}}(2Km)}{(2Km)^{\frac{m-2}{2}}} \ , \tag{6.20}$$
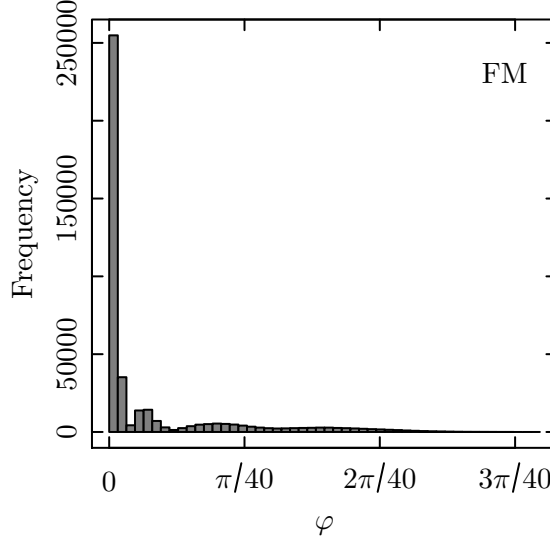
Figure 6.2.: RG showcase example for a ferromagnet for the distribution of the angle between two spins, say $\varphi = \angle(\mathbf{S}_1, \mathbf{S}_3)$ separated by two linear lattice spacings. Small angles $\varphi \ll \pi$ for $T \to 0$ justify the power law expansion done in the text. The tested system has the following properties: $d = 3$, $L = 24$, $m = 10$. The $T = 0$ ground-state search stopped at a certain accuracy so that not all φ are precisely zero.

which will be used immediately in the expression for the second order

$$
\tilde{K} = \frac{2}{m\mathrm{e}^{\tilde{K}m}} \frac{A(m)}{16(2Km)^{\frac{m-2}{2}}} \cdot
$$
$$
\left[2KmI_{\frac{m-4}{2}}(2Km) + 2KmI_{\frac{m}{2}}(2Km) - (m-2)I_{\frac{m-2}{2}}(2Km) \right] \quad (6.21\text{a})
$$

$$
\overset{Eq. \; (6.20)}{=} \frac{K}{4} \cdot \frac{I_{\frac{m-4}{2}}(2Km) + I_{\frac{m}{2}}(2Km)}{I_{\frac{m-2}{2}}(2Km)} - \frac{m-2}{8m} \quad (6.21\text{b})
$$

$$
= \frac{KI_{\frac{m}{2}}(2Km)}{2I_{\frac{m-2}{2}}(2Km)} , \quad (6.21\text{c})
$$

producing the recursion relation we wanted to find in the first place, viz. Eq. (6.11). The last equality uses the identity [AS65]

$$
zI_{\nu-1}(z) - zI_{\nu+1}(z) = 2\nu I_\nu(z) . \quad (6.22)
$$

For checking the behavior when $T \to 0$ ($\beta = \frac{1}{k_B T} \to \infty$), it is useful to switch back to $\beta J = K$. Independent of m, we infer $\tilde{J} = J/2$ from (6.21c) for $\beta \to \infty$.

For the special case $m = 3$ Eq. (6.21b) yields at finite temperature

$$
\tilde{K} = \frac{K}{4}\left(2\coth(6K) - \frac{1}{6K} \right) - \frac{1}{24}
$$
$$
= \frac{K}{2}\coth(6K) - \frac{1}{12} , \quad (6.23)
$$

Figure 6.3: Tracing out spin $\mathbf{S_2}$ for the SG. The connection between the angles $\tilde{\varphi} = \angle(K_{12}\mathbf{S}_1, K_{23}\mathbf{S}_3)$ and $\varphi = \angle(\mathbf{S}_1, \mathbf{S}_3)$ is such that either $\tilde{\varphi} = \varphi$ or $\pi - \varphi$ is small implying that either $\cos\tilde{\varphi} = \cos\varphi$ or $(-\cos\varphi)$ is close to unity. In a concise way $\cos\tilde{\varphi} = \mathrm{sgn}(K_{12}K_{23})\cos\varphi$.

and so the coupling needs to be transformed as

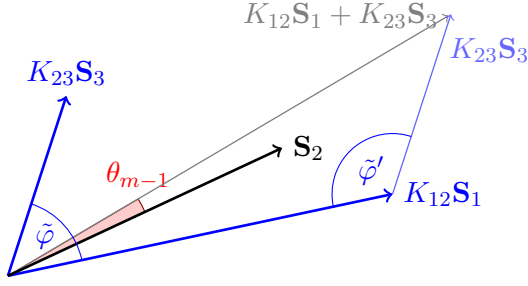$$\tilde{J} = \frac{J}{2}\coth(6\beta J) - \frac{1}{24\beta} \xrightarrow{\beta\to\infty} \frac{J}{2} \,, \tag{6.24}$$

at zero temperature, since $\coth(x) \xrightarrow{x\to\infty} 1$. In a quantum mechanical treatment it is found [Sti79]

$$\tilde{K} = \frac{1}{4}\ln\frac{1}{3}(2\mathrm{e}^{2K} + \mathrm{e}^{-4K}) \,, \tag{6.25}$$

for $T > 0$, which differs from (6.23). Nevertheless, the limit $\beta \to \infty$, which we are interested in, is the same.

6.3. Introducing disorder – the spin glass

For a spin glass the interactions are random in magnitude and sign and therefore we change Eq. (6.9) so that $K_{ij} = \beta J_{ij} \neq K = \mathrm{const.}$ by writing

$$\boxed{\mathrm{e}^{\tilde{K}_{13}\mathbf{S}_1\cdot\mathbf{S}_3} \propto \mathrm{Tr}_{\mathbf{S}_2}\,\mathrm{e}^{K_{12}\mathbf{S}_1\cdot\mathbf{S}_2 + K_{23}\mathbf{S}_2\cdot\mathbf{S}_3}} \,. \tag{6.26}$$

Then, in order to evaluate the trace we need to adapt the arguments presented above accordingly. The exponent of the *rhs* reads

$$\begin{aligned} K_{12}\mathbf{S}_1\cdot\mathbf{S}_2 + K_{23}\mathbf{S}_2\cdot\mathbf{S}_3 &= (K_{12}\mathbf{S}_1 + K_{23}\mathbf{S}_3)\cdot\mathbf{S}_2 \\ &= \|K_{12}\mathbf{S}_1 + K_{23}\mathbf{S}_3\|\|\mathbf{S}_2\|\cos\theta_{m-1} \,. \end{aligned} \tag{6.27}$$

For finding an expression for $l_{123} = \|K_{12}\mathbf{S}_1 + K_{23}\mathbf{S}_3\|$ it is useful to have a look at Fig. 6.3. There it can be read off that $\tilde{\varphi} + \tilde{\varphi}' = \pi$ such that $\cos\tilde{\varphi}' = \cos(\pi - \tilde{\varphi}) = -\cos\tilde{\varphi} = -\mathrm{sgn}(K_{12}K_{23})\cos\varphi$. Using basic trigonometry

$$-\cos\tilde{\varphi} = \frac{m|K_{12}|^2 + m|K_{23}|^2 - l_{123}^2}{2m|K_{12}||K_{23}|} \tag{6.28}$$

$$\begin{aligned} l_{123}^2 = \|K_{12}\mathbf{S}_1 + K_{23}\mathbf{S}_3\|^2 &= m(|K_{12}|^2 + |K_{23}|^2 + 2\,\mathrm{sgn}(K_{12}K_{23})|K_{12}K_{23}|\cos\varphi) \\ &= m(|K_{12}|^2 + |K_{23}|^2 + 2K_{12}K_{23}\cos\varphi) \,. \end{aligned} \tag{6.29}$$

According to the integration in Eq. (6.12) this time the trace reads (recall $\|\mathbf{S}_i\| = m^{1/2}$)

$$\text{Tr}_{\mathbf{S}_2}\, e^{K_{12}\mathbf{S}_1\cdot\mathbf{S}_2 + K_{23}\mathbf{S}_2\cdot\mathbf{S}_3} \;=\; m^{\frac{m-1}{2}}\frac{2\pi^{\frac{m-1}{2}}}{\Gamma\left(\frac{m-1}{2}\right)}\cdot$$

$$\int_0^\pi \mathrm{d}\theta_{m-1}\sin^{m-2}\theta_{m-1}\,e^{\pm m\sqrt{|K_{12}|^2+|K_{23}|^2+2K_{12}K_{23}\cos\varphi}\,\cos\theta_{m-1}}$$

$$=\; m^{\frac{m-1}{2}}\frac{2\pi^{\frac{m-1}{2}}}{\Gamma\left(\frac{m-1}{2}\right)}\cdot I_{\frac{m-2}{2}}\left(mh(K_{12},K_{23},\varphi)\right)\frac{\Gamma(\frac{m-1}{2})\Gamma(\frac{1}{2})}{\left(\frac{m}{2}h(K_{12},K_{23},\varphi)\right)^{\frac{m-2}{2}}}$$

$$=\; \hat{B}(m)\frac{I_{\frac{m-2}{2}}\left(mh(K_{12},K_{23},\varphi)\right)}{\left(mh(K_{12},K_{23},\varphi)\right)^{\frac{m-2}{2}}}\;, \tag{6.30}$$

with $\hat{B}(m) = (2m)^{\frac{m-1}{2}}\pi^{\frac{m}{2}}$ and $h(K_{12},K_{23},\varphi) := \sqrt{|K_{12}|^2+|K_{23}|^2+2K_{12}K_{23}\cos\varphi}$, which reduces to $2K|\cos(\varphi/2)|$, if $K_{12} = K_{23}$, i.e. the ferromagnetic result.

Now Eq. (6.26) reads

$$e^{\tilde{K}_{13}m\cos\varphi} \propto \hat{B}(m)\frac{I_{\frac{m-2}{2}}\left(mh(K_{12},K_{23},\varphi)\right)}{\left(mh(K_{12},K_{23},\varphi)\right)^{\frac{m-2}{2}}}\;, \tag{6.31}$$

since the *lhs* stays the same as in the ferromagnetic case (6.17). The power-law expansion done for the ferromagnet cannot be adopted here, since φ will not tend to zero as $T \to 0$. Conflicting interactions prevent the spins from aligning into a parallel/anti-parallel configuration. A showcase example for the distribution of the angles φ in a $d = 3$, $L = 24$, $m = 10$ system is given in Fig.(6.4). Those angles are calculated for spins being separated by two linear lattice spacings (in each case along one space direction). Obviously, an expansion around $\varphi = 0$ is not justified.

6.3.1. Expansion about $\varphi = \pi/2$

In the ferromagnetic case we arrived at Eq. (6.21c) by an expansion around $\varphi = 0$. As Fig. (6.4) shows, there is no angle φ about which it is completely justified to expand. However, if at all, symmetry considerations suggest to expand Eq. (6.31) around $\varphi = \pi/2$. This is next on the agenda to obtain a recursion relation and compare to the version found in literature.

The *lhs* reads then

$$e^{\tilde{K}\mathbf{S}_1\cdot\mathbf{S}_3} \;=\; e^{m\beta\tilde{J}\cos\varphi}$$

$$=\; 1\left(\varphi-\frac{\pi}{2}\right)^0 - m\beta\tilde{J}\left(\varphi-\frac{\pi}{2}\right)^1 + O\left(\left(\varphi-\frac{\pi}{2}\right)^2\right)\;. \tag{6.32}$$
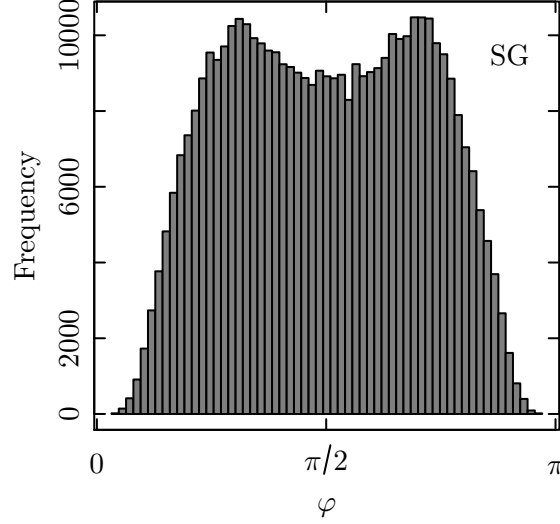
Figure 6.4.: RG showcase example at $T = 0$ for the distribution of the angles between two spins, say $\varphi = \angle(\mathbf{S}_1, \mathbf{S}_3)$ separated by two linear lattice spacings and intermediate spin $\mathbf{S}_2$ which we want to trace out in the renormalization step. This distribution is in strong contrast to the distribution for the FM in fig.(6.2). The tested system has the following properties: $d = 3$, $L = 24$, $m = 10$. The angles φ where obtained after a ground-state search.

With $x_{\pi/2} = \beta m \sqrt{J_{12}^2 + J_{23}^2}$ the *rhs* yields the equation

$$
\mathrm{Tr}_{\mathbf{S}_2}\, \mathrm{e}^{K_{12}\mathbf{S}_1 \cdot \mathbf{S}_2 + K_{23}\mathbf{S}_2 \cdot \mathbf{S}_3} =
$$

$$
\frac{c_{\pi/2}\hat{B}(m)}{x_{\pi/2}^{\frac{m}{2}-1}} I_{\frac{m-2}{2}}(x_{\pi/2}) \left(\varphi - \frac{\pi}{2}\right)^0
$$

$$
-\frac{c_{\pi/2}\hat{B}(m)}{x_{\pi/2}^{\frac{m}{2}-1}} \frac{m\beta}{2} \frac{J_{12}J_{23}}{\sqrt{J_{12}^2 + J_{23}^2}} \left[I_{\frac{m-4}{2}}(x_{\pi/2}) - \frac{m-2}{x_{\pi/2}} I_{\frac{m}{2}}(x_{\pi/2}) + I_{\frac{m}{2}}(x_{\pi/2}) \right] \left(\varphi - \frac{\pi}{2}\right)^1
$$

$$
+ O\left(\left(\varphi - \frac{\pi}{2}\right)^2\right) . \tag{6.33}
$$

Comparing coefficients to zeroth and first order yields

$$
\tilde{J}_{13} = \frac{1}{2}\frac{J_{12}J_{23}}{\sqrt{J_{12}^2 + J_{23}^2}} \left[\frac{I_{\frac{m-4}{2}}(x_{\pi/2})}{I_{\frac{m-2}{2}}(x_{\pi/2})} - \frac{m-2}{m\beta\sqrt{J_{12}^2 + J_{23}^2}} + \frac{I_{\frac{m}{2}}(x_{\pi/2})}{I_{\frac{m-2}{2}}(x_{\pi/2})} \right] \tag{6.34a}
$$

$$
\xrightarrow{\beta\to\infty} \frac{J_{12}J_{23}}{\sqrt{J_{12}^2 + J_{23}^2}} . \tag{6.34b}
$$

It differs from the relation found in literature ([AP78] and [MCM+86]), reading
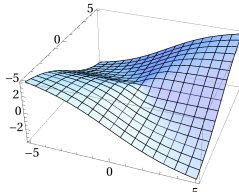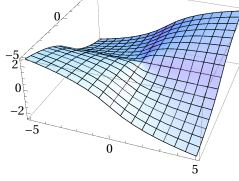
	recursion relation	$J_{12} = J_{23} = J$	(thumbnail)
(A) $\varphi = \pi/2$	$\tilde{J}_{13} = \frac{J_{12}J_{23}}{\sqrt{J_{12}^2 + J_{23}^2}}$	$\frac{J}{\sqrt{2}}$	(a)
(B) literature	$\tilde{J}_{13} = \frac{J_{12}J_{23}}{|J_{12}| + |J_{23}|}$	$\frac{J}{2}$	(b)

Table 6.1.: The summary of the new and old Migdal-Kadanoff relation to renormalize couplings at $T = 0$. The plots show the resulting couplings $\tilde{J}_{13}$ for initial combinations of couplings $J_{12}, J_{23} \in [-5, 5]$.

$$\frac{1}{\tilde{J}_{13}^{(\text{elast})}} \xrightarrow{\beta \to \infty} \operatorname{sgn}(J_{12}J_{23}) \left(\frac{1}{|J_{12}|} + \frac{1}{|J_{23}|} \right)$$

$$= \frac{J_{12}J_{23}}{|J_{12}| + |J_{23}|} . \tag{6.35}$$

This relation is said to hold true in the strong coupling limit for random(-sign) couplings and to be equivalent to adding elastic compliances where the intermediate spin can adjust itself at will [AP78]. By chance or not, also here $\tilde{J}_{13} = J/2$, if $J_{12} = J_{23} = J$, i.e. the ferromagnet.

Tab. 6.1 compares the Migdal-Kadanoff relation from literature to the one calculated here. In the following two sections we will use the new recursion relation to calculate θ, ζ and d_s both numerically and analytically.

6.4. Numerical approach

Now that there is a new Migdal-Kadanoff transformation for the exchange couplings it is an easy numerical task to determine the stiffness exponent θ, the Lyapunov exponent ζ and the characteristic exponent d_s. This will be done along the lines of Ref. [BB88] and boils down to follow the width and the distance of the probability functions of two coupling variable pools under the calculated Migdal-Kadanoff transformation.

For the time being we want to determine the stiffness exponent θ. For that it suffices to consider only one pool of N_c couplings $\{J_i\}$, the elements of which are drawn independently and identical from a Gaussian distribution with zero mean and unit variance. One full
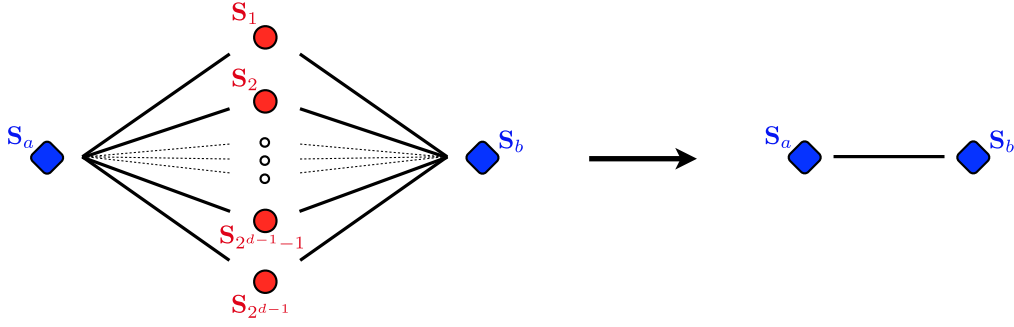
Figure 6.5.: A hierarchical lattice is well suited for a 3-spin renormalization. For a d-dimensional system on a hierarchical lattice with length scale $b = 2$ we trace out 2^{d-1} single spins $\mathbf{S}_1, \ldots, \mathbf{S}_{2^{d-1}}$ successively by using the recursion relation (6.36) for each one of them and sum up according to (6.37) to form a new single coupling between spins $\mathbf{S}_a$ and $\mathbf{S}_b$.

renormalization iteration will take this pool and generate a new one of the same size. To see how this works we need to agree on a lattice type. As discussed above in Sec. 6.1.1, hierarchical lattices, instead of hypercubic ones, are very well suited for a single renormalization step since their structure can be transformed straightforwardly, cf. Fig. 6.5. We employ a lattice with n parallel paths of a length scale specified by $b = 2$ segments. To obtain results in $d = 2, 3$ and 4 dimensions we choose $n = 2, 4$ and 8, since the connection to a space dimension d is given by, cf. (6.8),

$$d = \frac{\ln n}{\ln b} + 1 \ .$$

Choosing $b = 2$, see Fig. (6.5), the representative form of three spins in a row is gained where one spin in the middle is traced out. I.e. the two couplings between spins $\mathbf{S}_a$, $\mathbf{S}_k$ and $\mathbf{S}_b$ will be renormalized according to

$$\tilde{J}_{ab}(k) = \frac{J_{ak}J_{kb}}{\sqrt{J_{ak}^2 + J_{kb}^2}} \ , \tag{6.36}$$

such that spin $\mathbf{S}_k$ is traced out (J_{ij} stands for the interaction between spin $\mathbf{S}_i$ and $\mathbf{S}_j$). The full new coupling is then gained by summing over all 2^{d-1} intermediate paths each containing one spin via

$$\tilde{J}_{ab} = \sum_{k=1}^{2^{d-1}} \tilde{J}_{ab}(k) \ . \tag{6.37}$$

Note, that the variables $J_{a'b'}$ are randomly chosen from the entire pool $\{J_i\}$. In contrast to coupling variables from the (old) pool at iteration step $\mathfrak{q}$ the ones from the (new) pool at iteration step $\mathfrak{q} + 1$ are marked with a tilde on top.

Thus, for generating one new coupling for the new pool 2^{d-1} couplings of the old one are required, which are chosen at random. Obviously, in a full iteration step of N_c transformations, each of the old couplings will have been used $2^{d-1} + 1$ times on average. At the end

one can calculate the width (standard deviation) σ_J of the new distribution. As mentioned above, this width is expected to scale as in Eq. (6.2). The iteration will be done $\mathfrak{q}$ times and the length scale is then given by $L = 2^{\mathfrak{q}}$. According to Eq. (6.2) the width will change by the factor 2^{θ} after one iteration ($\mathfrak{q} = 1$).

The result of this procedure is shown in Fig. 6.6. Using Eq. (6.2) we can extract θ numerically. According to our calculations, averaged over 1000 different coupling pools of size $N_c = 10^5$, we were able to determine the stiffness exponent to very high precision. Fits to the data had throughout a quality-of-fit parameter Q [Bra98] of almost unity. Tab. 6.2 summarizes all values for $d = 2, 3, 4$. For our setup on a hierarchical lattice this means $n = 2, 4, 8$ (recall $b \equiv 2$). Our requirement in Eq. (6.7) is fulfilled and thus we find the lower critical dimension to be exactly $d_l = 3$.

The procedure needs to be extended [BB87] in order to find the Lyapunov exponent ζ which decides about the stability of the spin-glass phase. We replicate the initial pool of couplings $\{J_i\}$ and impose a Gaussian noise to have a second pool of couplings $\{J_i^*\}$ with

$$J_i^* = J_i + x_i \,, \tag{6.38}$$

where the x_i are independent Gaussian random variables with zero mean and a variance of $\sigma_x^2 = \varepsilon^2 = 10^{-12}$. Manipulations made on that pool need to be done in exact accordance with the first. Then we can measure the distance of the two pools with the bounded quantity

$$D^2 = \frac{\sum_i \left(J_i - J_i^*\right)^2}{\sum_i J_i^2 + J_i^{*\,2}} \,. \tag{6.39}$$

It will be calculated at each iteration step as well. Taking into account Eq. (6.2) and (6.3), the nominator is proportional to L^{d_s} and the denominator to $L^{2\theta} + L^{d_s}$ and thus

$$D^2 \sim \frac{1}{cL^{2\theta-d_s} + 1} \approx L^{d_s-2\theta} = L^{2\zeta} = 2^{2\zeta\mathfrak{q}} \,. \tag{6.40}$$

One finds that D^2 saturates after $\mathfrak{q}^*$ iterations at the value 1, i.e. uncorrelated pools, after an initial exponential increase according to (6.40). This means that two almost identical coupling pools diverge exponentially under iteration, see Fig. 6.7. The rate of divergence is described by the Lyapunov exponent ζ. Find also this quantity summarized in Tab. 6.2. Recalling Eq. (6.4), we can therefore say that for perturbations at length scales of $L > L^* \approx 10^9$ the ground state is unstable. This might also be inferred from Fig. 6.7, where after $\mathfrak{q}^* \approx 30$ iterations the pools are completely uncorrelated, such that $L^* \sim 2^{\mathfrak{q}^*} \approx 10^9$. Lastly, d_s is determined by Eq. (6.5) and also given in Tab. 6.2. It does not meet the requirement (6.6) but is positive throughout.

6.5. Analytical approach

It is also possible to determine the scaling exponents analytically in an approximation analogous to the analysis in Ref. [BB88]. We will compute the change of the width of the coupling distribution for both the unperturbed and the perturbed coupling pool after one
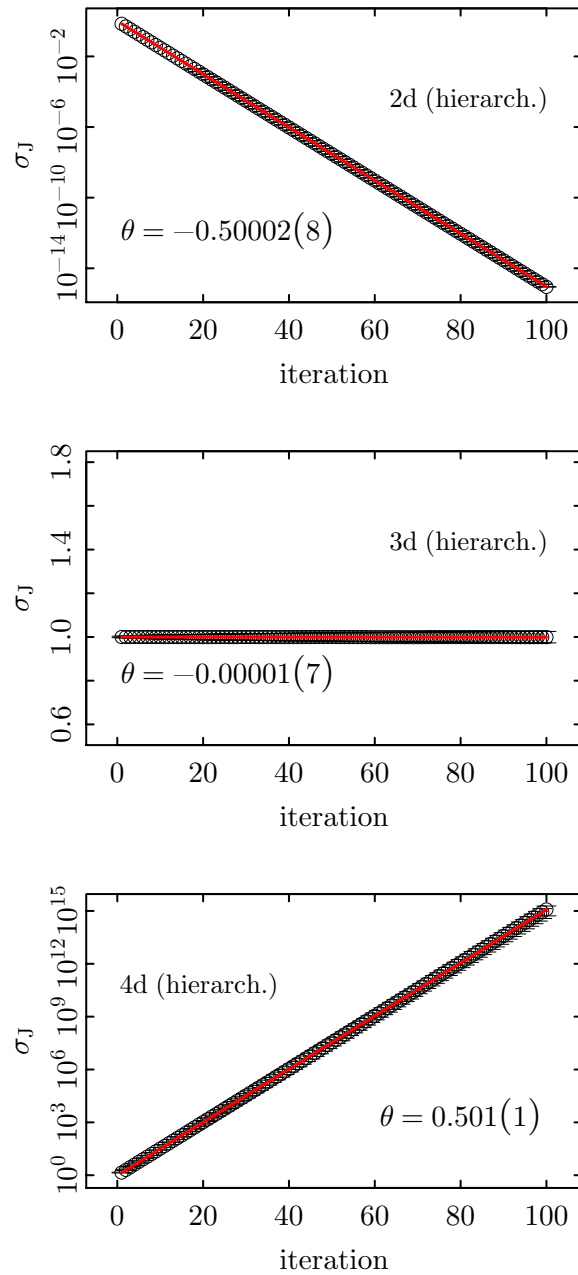
Figure 6.6.: The evolution of the width of the coupling distribution using the newly derived Migdal-Kadanoff transformation (6.34b). A hierarchical lattice was used in order to obtain results in dimensions $d = 2, 3, 4$. The stiffness exponent θ can be determined from the slope of those linear-logarithmic plots using Eq. (6.2) with the length scale $L = 2^q$. θ changes sign exactly at $d = 3$, thus constituting the lower critical dimension.
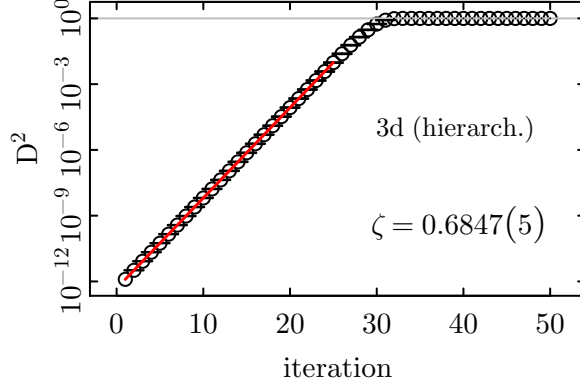
Figure 6.7.: A quantity measuring the distance of two exchange coupling pools which differ only by a Gaussian noise at the beginning ($D^2 \gtrapprox 0$). After a power-law increase according to Eq. (6.40) D^2 saturates after $\mathfrak{q}^*$ iterations at unity, corresponding to uncorrelated pools. The quality-of-fit Q is one for all $d = 2, 3, 4$.

full renormalization step $\mathfrak{q} = 1$. We will use the properties of the random variables J_i and x_i being drawn from independent identically distributed Gaussian probability distributions.

Following the numerical approach we will concentrate on the unperturbed coupling pool first. We can extract θ with it analytically as well. The key quantity, namely the width, is gained via $\sigma_{\tilde{J}} = (\langle \tilde{J}_{ab}^2 \rangle - \langle \tilde{J}_{ab} \rangle^2)^{1/2}$, where $\langle \cdot \rangle$ denote averages with a Gaussian measure. And after one iteration, i.e. $L = 2^1$, we expect $\sigma_{\tilde{J}} = 2^\theta \sigma_J$ due to (6.2). Being an odd function the first moment $\langle \tilde{J}_{ab} \rangle$ vanishes. We will therefore write down only the second moment of the coupling variable distribution

$$
\begin{aligned}
\langle \tilde{J}_{ab}^2 \rangle &= \left\langle \left(\sum_k \tilde{J}_{ab}(k) \right)^2 \right\rangle = 2^{d-1} \left\langle \tilde{J}_{ab}^2(k) \right\rangle \\
&= 2^{d-1} \left\langle \frac{J_{ak}^2 J_{kb}^2}{J_{ak}^2 + J_{kb}^2} \right\rangle \\
&= 2^{d-1} \left(\left\langle \frac{J_{ak}^2 J_{kb}^2}{J_{ak}^2 + J_{kb}^2} \right\rangle \frac{1}{\langle J_{ak}^2 \rangle} \right) \langle J_{ak}^2 \rangle \\
&=: 2^{d-1} \lambda_J \langle J_{ak}^2 \rangle \, .
\end{aligned}
\tag{6.41}
$$

The integral can be evaluated and reads

$$
\lambda_J = \int_{-\infty}^{\infty} \frac{\mathrm{d}y_1 \mathrm{d}y_2}{2\pi} \frac{y_1^2 y_2^2}{y_1^2 + y_2^2} \exp\left(-\frac{1}{2} \left(y_1^2 + y_2^2 \right) \right) = \frac{1}{4} \, .
\tag{6.42}
$$

So we read off that

$$
2^{d-1} \lambda_J = 2^{2\theta} \, ,
\tag{6.43}
$$

leading to

$$
\boxed{2\theta = d - 1 + \frac{\ln \lambda_J}{\ln 2} = d - 3 \, .}
\tag{6.44}
$$

Obviously, this coincides perfectly with the numerical results, cf. Tab. 6.2. Furthermore, the inequality $\theta \leq (d-1)/2$ given in [FH86] is satisfied and the very simple argument in [AP78] stating that $\theta = (d-3)/2$ is confirmed.

In order to shed light on the exponents related to the perturbation we incorporate the second pool of couplings in our considerations now. Recalling the recursion relation in Eq. (6.34b) and the structure of the hierarchical lattice in Eq. (6.36), we have for the perturbed coupling pool

$$\tilde{J}_{ab}^*(k) = \frac{J_{ak}^* J_{kb}^*}{\sqrt{\left(J_{ak}^*\right)^2 + \left(J_{kb}^*\right)^2}} \; . \tag{6.45}$$

The relation to the unperturbed pool can be seen with inserting Eq. (6.38) and expanding to first order to arrive at

$$\tilde{J}_{ab}^*(k) = \tilde{J}_{ab}(k) + \frac{J_{ak}^3 x_{kb} + J_{kb}^3 x_{ak}}{\left[J_{ak}^2 + J_{kb}^2\right]^{3/2}} = \tilde{J}_{ab}(k) + \delta\tilde{J}_{ab}(k) \; . \tag{6.46}$$

According to Eq. (6.37)

$$\delta\tilde{J}_{ab} = \sum_k \delta\tilde{J}_{ab}(k) \; . \tag{6.47}$$

Let us elucidate the effect of the noise on the width of the coupling distribution. Note, that averages are taken now over both the variables J and x. Both sets are completely independent from each other, such that the contribution to the width of the unperturbed pool is given by (6.41). Only the contribution of the noise term is still missing for the width $\sigma_{\tilde{J}_{ab}^*}$. As before, also here the first moment $\langle\delta\tilde{J}_{ab}\rangle$ vanishes. Then, again, it is sufficient to calculate the second moment of the noise term $\langle(\delta\tilde{J}_{ab})^2\rangle$ after one renormalization step ($\mathfrak{q} = 1$) and so

$$\begin{aligned}
\left\langle\left(\delta\tilde{J}_{ab}\right)^2\right\rangle &= \sum_{i,j}\left\langle\delta\tilde{J}_{ab}(i)\delta\tilde{J}_{ab}(j)\right\rangle = \sum_i\left\langle\left(\delta\tilde{J}_{ab}(i)\right)^2\right\rangle \overset{(*)}{=} 2^{d-1}\left\langle\left(\delta\tilde{J}_{ab}(k)\right)^2\right\rangle \\
&= 2^{d-1}\left\langle\left(\frac{J_{ak}^3 x_{kb} + J_{kb}^3 x_{ak}}{\left[J_{ak}^2 + J_{kb}^2\right]^{3/2}}\right)^2\right\rangle \\
&= 2^{d-1}\left\langle\frac{J_{ak}^6 + J_{kb}^6}{\left[J_{ak}^2 + J_{kb}^2\right]^3}\right\rangle\varepsilon^2 \\
&=: 2^{d-1}\lambda_B\varepsilon^2 \; ,
\end{aligned} \tag{6.48}$$

with $\varepsilon^2 = \langle x^2\rangle$, due to our requirements for (6.38). After $(*)$ we have used that all contributions to the sum are identical. Then we can evaluate the integral

$$\lambda_B = 2\int_{-\infty}^{\infty}\frac{dy_1 dy_2}{2\pi}\frac{y_1^6}{\left(y_1^2 + y_2^2\right)^3}\exp\left(-\frac{1}{2}\left(y_1^2 + y_2^2\right)\right) = \frac{5}{8} \; . \tag{6.49}$$

Doing the same reasoning as before and taking Eq. (6.3) we have

$$2^{d-1}\lambda_B = 2^{d_s} \tag{6.50}$$

d	θ	ζ	d_s
2	-0.50002(8)	0.7188(6)	0.437(1)
	-0.5	*0.660964*	*0.3219281*
3	-0.00001(7)	0.6847(5)	1.37(1)
	0	*0.660964*	*1.321928*
4	0.501(1)	0.68(1)	2.36(2)
	0.5	*0.660964*	*2.321928*

Table 6.2.: Summary of the results gained with the new Migdal-Kadanoff relation Eq. (6.34b) at $T = 0$. The stiffness exponent changes sign exactly at $d = 3$, such that this can be identified with the lower critical dimension for vector spin glasses. Plain numbers are calculated numerically, gray italic numbers give results of the analytic approximation.

and are able to conclude

$$d_s = d - 1 + \frac{\ln \lambda_B}{\ln 2} = d - 1 + \frac{\ln 5/8}{\ln 2} \ . \tag{6.51}$$

The last equation seems a bit unfortunate in the light of the droplet picture. In Ref. [FH88] it is argued that $d_s > d - 1$ – but this is strictly valid only for the ($m = 1$) Ising model. Recalling Eq. (6.5) the combination of (6.51) and (6.44) yields

$$\zeta = \frac{1}{2 \ln 2} \ln \frac{\lambda_B}{\lambda_J} = \frac{\ln 5/2}{2 \ln 2} \ . \tag{6.52}$$

The quantities d_s and ζ are also given in table 6.1 for lattice dimensions $d = 2, 3, 4$. They deviate from the numerical data especially pronounced for low dimensions. One might think that the approximation in Eq. (6.40) is too crude. However, tests with a slightly changed (unbounded) measure for the distance as

$$D_u^2 = \frac{1}{N_c} \sum_i (J_i - J_i^*)^2 \tag{6.53}$$

for which $D_u^2 \sim 2^{d_s \mathfrak{q}}$, as long as $\mathfrak{q} < \mathfrak{q}^*$, showed that numerical results do not change. Note also Tab. 6.3, where results of the exact same numerical and analytical analysis for the old Migdal-Kadanoff relation are summarized. This table is the equivalent of Tab. 6.2 using Eq. (6.35) instead of (6.34b).

6.6. Summary

In this chapter we derived a new Migdal-Kadanoff relation for transforming the couplings in a real-space renormalization-group calculation for vector spin systems with a finite number

of spin components $m > 1$. This approach did not yield the correct lower critical dimension before, since the barely justified relation (6.35) was employed. Only a very simple argument in Ref. [AP78] suggested $\theta = (d-3)/2$. We derived a new Migdal-Kadanoff relation, cf. (6.34b), and used hierarchical lattices to investigate stiffness exponents θ, characteristic exponents d_s and Lyapunov exponents ζ both numerically and analytically.

We were able to calculate stiffness exponents for different lattice dimensionalities to very high precision numerically. The successive analytical approximation confirmed the numerically determined values strikingly well, so that the lower critical dimension could be extracted here with $d_l = 3$, which supports last findings with different techniques [KR05]. Analogously, we reconfirmed the chaotic nature of the ground state by finding a positive Lyapunov exponent ζ and saw on which length scales $L > L^* = 10^9$ a ground state is unstable against perturbation. Furthermore, we analyzed a quantity d_s similar to the fractal dimension in Ising spin glasses ($m = 1$) and found it to be positive throughout. However, the constraint (6.6) is not met, since our results show $d_s < d - 1$. We could not come up with an argument as to why this value is not determined accurately. For both quantities d_s and ζ there are slight deviations in the values obtained from numerical and analytical analysis becoming more pronounced for low lattice dimensionalities.

Due to the discrepancies seen for d_s and ζ, we carried out the numerical part for the old Migdal-Kadanoff relation (6.35) additionally, in order to compare to the analytical analysis done in Ref. [BB88] from which we were inspired. There, d_s deviates even more from the constraint (6.6) and especially $d_s < 0$ in lattice dimension $d = 2$. Also the lower critical dimension had been determined to be $d_l \approx 3.87$. The authors of [BB88] claim that analytical and numerical results do not deviate more than 2%. It is not obvious which quantities they had a look at numerically, as also there are no values given. However, we found that analytical and numerical results agree well only for θ, whereas d_s and ζ deviate much more.

d	θ	ζ	d_s
2	-0.92312(7)	0.7325(7)	-0.3812(9)
	-0.9358809	*0.6761714*	*-0.519419*
3	-0.43093(7)	0.7026(6)	0.5433(8)
	-0.4358809	*0.6761714*	*0.480581*
4	0.067(1)	0.69(1)	1.51(2)
	0.0641191	*0.6761714*	*1.480581*

Table 6.3.: Summary of the results yielded with the old Migdal-Kadanoff relation Eq. (6.35) at $T = 0$. The stiffness exponent changes sign between $d = 3$ and 4. Plain numbers are calculated numerically, italic numbers give results of the analytic approximation. The claim of [BB88] that deviations between analytical and numerical calculations agree within 2% seems to be stated a bit generously, probably referring implicitly only to θ. Unfortunately they do not quote any numerical results. Note, that in any way $d_s < 0$ for $d = 2$.

Chapter 7.

Conclusion

This thesis covered different areas of vector spin-glass models. Due to the chapters of the thesis shedding light on partially rather distant aspects, they were tried to be kept more or less self-contained. Each of them, apart from the introduction has its own summary. Nevertheless, we want to give a coarse summary now and conclude.

The abundance of vector spin-glass models was shown in chapter 1 after key concepts of equilibrium statistical mechanics were recalled. As "natural" spin glasses are best described by low dimensional models with a low finite number of spin components, we pointed out that the field theoretic approach of starting out from mean-field theory (in a sense $d \to \infty$) is still hotly debated if the lattice dimension d goes below the upper critical dimension d_u. An alternative approach might be to consider an $1/m$ expansion of the infinite component-limit $m \to \infty$. A prerequisite to this is to have the knowledge about the $m \to \infty$ spin-glass model, which was discussed thoroughly. In chapter 2 we introduced several flavors of the spin-glass Hamiltonian each time adjusted to the considered geometry. Being well amenable to numerical simulations we emphasized the 1d power-law model, which can be tuned easily through all universality classes by changing only one single parameter σ while the geometry is fixed. Therefore, scaling arguments led us to stating numerous predictions for the critical exponents. We also motivated the phase diagram and compared it to the spin-glass model with a finite number m of spin components. The distinctive feature of the $m \to \infty$ limit is the shifting of both the lower and the upper critical dimension if hypercubic models are concerned or the upper as well as the lower critical σ if we consider 1d power-law models.

In chapter 3 we discussed on the zero-temperature properties of both the hypercubic and the 1d power-law model. The relative ease of doing so is owed to a remarkable feature of the $m \to \infty$ model – its complete lack of metastability. We were able to determine the lower critical dimension (LCD) d_l of the former and also the upper critical σ_u of the latter which was consistent with the arguments given in chapter 1. We were able to support $d_l = 6$ [GBM82] with our result $5 \leq d_l \leq 6$ using periodic/anti-periodic boundary conditions in contrast to the claim $d_l = d_u = 8$ of Ref. [Via88]. Using two other sets of boundary conditions we found d_l to be in the vicinity of 3 and consider this finding as a possible candidate for studying the $m \to \infty$ limit of the finite-m models, for which one expects a lower critical dimension $d_l = 3$. In terms of the 1d power-law model the corresponding upper critical value was argued to be $\sigma_u = 3/4$ and found to be consistent with numerics. Several other quantities were looked at and a diverse behavior was found for the fully connected and the

diluted version of the 1d power-law model for the sample to sample exponent Θ_f, which takes on the trivial value $1/2$ in the latter. For the fully connected model we found evidence that $\Theta_f = 1/5$ for $\sigma \leq 1/2$ as was predicted in [Asp10] and $\Theta_f = 1/2$, otherwise. Considering the whole distribution of ground state energies we found Gaussian behavior independent of interaction range, i.e., the power-law exponent σ. The same was found for hypercubic models in dimension $d = 2, \ldots, 7$. Remarkably, we found evidence for the non-universality of the fully connected and the diluted version for $\sigma > 1$, which is in contrast to the claim of Ref. [LPRTRL08]. Similar indications were found only recently in [Juh12].

Since only finite-temperature approaches can elucidate the physics above the lower critical dimension d_l in the hypercubic and below the upper critical σ_u in the 1d power-law model we carried out correlation-matrix calculations in chapter 4. We derived a known set of matrix equations (being the saddle-point condition) which can be solved iteratively. With them we calculated the correlation matrix and suggested a way of calculating the order parameter q_{EA} and the spin-glass susceptibility χ_{SG} from it. We followed the ideas initiated in [AM04] and found true long-range order arising in the low-temperature phase, which is in contrast to Ref. [LY05]. Critical exponents determined numerically with different types of analyzes were consistent with our predictions from chapter 1. The calculations were done mainly for the 1d power-law model since the hypercubic model turned out not to be suitable for the matrix equations due to the extreme sparseness of the according matrices.

Up to this point we gained a rather comprehensive picture of the properties and the finite-size behavior of the spin glass in the limit of infinitely many spin components ($m \to \infty$) in all universality classes. Since we consider this model a promising starting point for investigations of the more natural spin glasses with a finite number m of spin dimensions chapter 5 demonstrated a way to benefit from its simplifications in the numerical treatment. A model with anisotropy was suggested and various aspects of it were discussed. Excitingly, we saw how metastability evolves with decreasing spin dimension when leaving the limit $m \to \infty$ towards $m = 3$, the Heisenberg model. A small numerical toolkit was constructed and being promising for the analysis of the low-temperature phase of natural spin-glass models we suggested an algorithm similar to the parallel tempering approach for future research.

In chapter 6 we found ourselves finally back at finite spin dimensions. A novel Migdal-Kadanoff relation was derived for a real-space renormalization-group calculation. With it we were able to determine the correct lower critical dimension, namely $d_l = 3$, for finite-component vector spin glasses both numerically and analytically. To our knowledge, this has not been accomplished before with real-space renormalization-group approaches. A quantity similar to the fractal dimension in Ising spin glasses was determined and the Lyapunov exponent, too. With the latter it was possible to determine the length-scale at which ground states are unstable against perturbation. A comparison to earlier research was done at the end.

Appendix

Appendix A.

The correlation matrix

We will write down the tedious calculation of the correlation matrix. Starting out with the definition

$$
\begin{aligned}
C_{ij} &= \frac{1}{m}\langle \mathbf{S}_i \mathbf{S}_j \rangle \\
&= \frac{1}{mZ} \int_{-\infty}^{\infty} \prod_{k=1}^{N} \prod_{\alpha=1}^{m} \mathrm{d}S_k^{\alpha} \left[\prod_{l=1}^{N} \delta(\mathbf{S}_l^2 - m) \right] \sum_{\gamma=1}^{m} S_i^{\gamma} S_j^{\gamma} e^{-\beta \mathcal{H}},
\end{aligned}
\tag{A.1}
$$

we proceed as in Sec. 4.1 and change variables to arrive at

$$
\begin{aligned}
C_{ij} &\propto \frac{1}{mZ} \int_{-i\infty}^{i\infty} \prod_{l=1}^{N} \frac{\beta \mathrm{d}H_l}{4\pi} \exp\left(\sum_{n=1}^{N} \frac{\beta H_n}{2} m \right) \times \\
&\quad \times \underbrace{\int_{-\infty}^{\infty} \prod_{k=1}^{N} \prod_{\alpha=1}^{m} \mathrm{d}S_k^{\alpha} \sum_{\gamma} S_i^{\gamma} S_j^{\gamma} \exp \sum_{\iota=1}^{m} \left[-\frac{\beta}{2} \vec{S}^{\iota} \cdot \left(A\vec{S}^{\iota} \right) + \beta \sum_{p} h_p^{\iota} S_p^{\iota} \right]}_{I}.
\end{aligned}
\tag{A.2}
$$

The last integral amounts to

$$
\begin{aligned}
I &= \int_{-\infty}^{\infty} \prod_{k=1}^{N} \prod_{\alpha=1}^{m} \mathrm{d}S_k^{\alpha} \sum_{\gamma} \frac{\partial}{\beta \partial h_i^{\gamma}} \frac{\partial}{\beta \partial h_j^{\gamma}} \exp \sum_{\iota=1}^{m} \left[-\frac{\beta}{2} \vec{S}^{\iota} \cdot (A\vec{S}^{\iota}) + \beta \sum_{p} h_p^{\iota} S_p^{\iota} \right] \\
&= \sum_{\gamma} \frac{\partial}{\beta \partial h_i^{\gamma}} \frac{\partial}{\beta \partial h_j^{\gamma}} \int_{-\infty}^{\infty} \prod_{k=1}^{N} \prod_{\alpha=1}^{m} \mathrm{d}S_k^{\alpha} \exp \sum_{\iota=1}^{m} \left[-\frac{\beta}{2} \vec{S}^{\iota} \cdot (A\vec{S}^{\iota}) + \beta \sum_{p} h_p^{\iota} S_p^{\iota} \right] \\
&= p_1 p_2 \sum_{\gamma} \frac{\partial}{\beta \partial h_i^{\gamma}} \frac{\partial}{\beta \partial h_j^{\gamma}} \underbrace{\exp\left(\sum_{k} \frac{\beta}{2\lambda_k} \sum_{pq} O_{kp} O_{kq} \sum_{\alpha=1}^{m} h_p^{\alpha} h_q^{\alpha} \right)}_{G(\{\vec{h}^{\alpha}\})},
\end{aligned}
\tag{A.3}
$$

where p_1 and p_2 can be taken from Eq. 4.13 and 4.14. Then

$$
\begin{aligned}
I/(p_1 p_2) &= \sum_\gamma \frac{\partial}{\beta \partial h_i^\gamma} \left[\sum_k \frac{1}{2\lambda_k} \sum_{pq} O_{kp} O_{kq} \sum_{\alpha=1}^m \left(h_p^\alpha \delta_{\alpha,\gamma} \delta_{p,j} + h_q^\alpha \delta_{\alpha,\gamma} \delta_{q,j} \right) \right] G(\{\vec{h}^\alpha\}) \\
&= \sum_\gamma \frac{\partial}{\beta \partial h_i^\gamma} \left[\sum_k \frac{1}{2\lambda_k} \sum_{pq} O_{kp} O_{kq} \left(h_p^\gamma \delta_{p,j} + h_q^\gamma \delta_{q,j} \right) \right] G(\{\vec{h}^\alpha\}) \\
&= \sum_\gamma \frac{\partial}{\beta \partial h_i^\gamma} \left[\sum_k \frac{1}{2\lambda_k} \sum_p O_{kp} O_{kj} \left(2 h_p^\gamma \right) \right] G(\{\vec{h}^\alpha\}) \\
&= \sum_\gamma \left(T \left[\sum_k \frac{1}{\lambda_k} \sum_p O_{kp} O_{kj} \delta_{p,i} \right] + \right. \\
&\quad \left. + \left[\sum_k \frac{1}{\lambda_k} \sum_p O_{kp} O_{kj} h_p^\gamma \right] \left[\sum_k \frac{1}{\lambda_k} \sum_p O_{kp} O_{ki} h_p^\gamma \right] \right) G(\{\vec{h}^\alpha\}). \quad (A.4)
\end{aligned}
$$

For the field independent term of $I/(p_1 p_2)$ we find

$$
\begin{aligned}
\sum_\gamma T \sum_k \frac{1}{\lambda_k} \sum_p O_{kp} O_{kj} \delta_{p,i} &= mT \sum_k \frac{1}{\lambda_k} O_{ki} O_{kj} = mT \sum_k \frac{1}{\lambda_k} O_{ik}^\mathsf{T} O_{kj} \\
&= mT \sum_{k,r} O_{ik}^\mathsf{T} \frac{\delta_{k,r}}{\lambda_k} O_{rj} = mT (O^\mathsf{T} \chi^D O)_{ij} \\
&= mT \chi_{ij}. \quad (A.5)
\end{aligned}
$$

Note that χ depends on the variables H_i, which is important for Eq. A.2. For the field dependent term in Eq. A.4 we use

$$
\begin{aligned}
\sum_k \frac{1}{\lambda_k} \sum_p O_{kp} O_{kj} h_p^\gamma &= \sum_p \left[\sum_{kr} O_{pk}^\mathsf{T} \frac{\delta_{kr}}{\lambda_k} O_{rj} \right] h_p^\gamma = \sum_p \left[\sum_{kr} O_{pk}^\mathsf{T} \chi_{kr}^D O_{rj} \right] h_p^\gamma \\
&= \sum_p \left[O^\mathsf{T} \chi^D O \right]_{pj} h_p^\gamma = \sum_p \chi_{pj} h_p^\gamma = \sum_p \chi_{jp} h_p^\gamma \\
&= (\chi h^\gamma)_i \quad (A.6)
\end{aligned}
$$

and take the self-averaging into account to gain

$$
\begin{aligned}
\sum_\gamma (\chi h^\gamma)_i (\chi h^\gamma)_j &= \sum_\gamma \sum_p \chi_{ip} h_p^\gamma \sum_q \chi_{jq} h_q^\gamma = \sum_{qp} \chi_{jq} \chi_{ip} \sum_\gamma h_p^\gamma h_q^\gamma \\
&= \sum_{qp} \chi_{jq} \chi_{ip} \, mh^2 \delta_{pq} = mh^2 \sum_q \chi_{jq} \chi_{qi} \\
&= mh^2 (\chi^2)_{ji}. \quad (A.7)
\end{aligned}
$$

Appendix A. The correlation matrix

Finally we employ a saddle-point approximation, i.e. $m \to \infty$, so that

$$
\begin{aligned}
C_{ij} \quad &\propto \quad \frac{1}{mZ} \int_{-i\infty}^{i\infty} \prod_{l=1}^{N} \frac{\beta \mathrm{d}H_l}{4\pi} \exp\left(\sum_{n=1}^{N} \frac{\beta H_n}{2} m\right) p_1 p_2 \left[mT\chi_{ij} + mh^2(\chi^2)_{ji}\right] G(\{\vec{h}^\alpha\}) \\
&= \quad \frac{1}{Z} \int_{-i\infty}^{i\infty} \prod_{l=1}^{N} \frac{\beta \mathrm{d}H_l}{4\pi} \exp\left(-\beta m f_{\text{trial}}(\{H_k\})\right) \left[T\chi_{ij} + h^2(\chi^2)_{ji}\right] \\
&\approx \quad \frac{1}{Z} \exp\left(-\beta m f_{\text{trial}}(\{H_k^0\})\right) \left[T\chi_{ij}(\{H_k^0\}) + h^2(\chi^2)_{ji}(\{H_k^0\})\right] \\
&= \quad \frac{1}{Z} Z_0 \left[T\chi_{ij}(\{H_k^0\}) + h^2(\chi^2)_{ji}(\{H_k^0\})\right] \\
&\approx \quad T\chi_{ij}(\{H_k^0\}) + h^2(\chi^2)_{ji}(\{H_k^0\}) .
\end{aligned} \tag{A.8}
$$

The last step makes the saddle-point approximation by substituting the value of the integral with the value of its integrand at the minimum of f_{trial}. Assuming that we also calculate the partition function Z in this brute approximation, Z_0 and Z cancel.

Appendix B.

The κ-spin quench

```
#ifndef EVAL_LAMBDA_H
#define EVAL_LAMBDA_H

// This code evaluates the Lagrange-multiplier for the local
// spin-quench procedure taking into account kappa-suppressed extra-dimensions

#include <complex>
typedef std::complex<double> cdouble;

// Note that this function works for performance reasons only for
// (a2 != 0) OR (b2 != 0) OR (k != 0)
double eval_lambda( double a2, double b2, double k )
{
    // h_i := -\sum_{j\in NN(i)} J_{ij}*S_j  ... the local field at site i
    //
    // a2 = |h_i^{parallel}|^2
    // b2 = |h_i^{perpendicular}|^2
    // k = kappa

    double k2( k*k );
    double A(  pow(2.,1./3.) );
    double B(  -(a2 + b2) + 4*k*k );

    double  C( 432.*a2*a2*k2 - 1728.*a2*k*k*k*k + 432.*a2*k2*B + 2*B*B*B );
    cdouble D( pow( C - sqrt( cdouble( -4.*B*B*B*B*B*B + C*C, 0. ) ), 1./3.) );
    // if all parameters a2,b2 and k were 0 the next line produced a "nan"
    cdouble E( sqrt( a2+b2 + B/3. + (A*B*B)/(3.*D) + D/(3.*A) ) );

    cdouble res( - k + E/2. +
                0.5 * sqrt(
                        a2+b2 + 4.*k2 + (-B)/3 - (A*B*B)/(3.*D) - D/(3.*A) +
                        (32.*a2*k - 64.*k*k*k + 16.*k*(B)) / (4.*E)
                    )
            );

    return real(res);
}
#endif // EVAL_LAMBDA_H
```

Appendix B. The κ-spin quench

Bibliography

[ABM04a]   A. Andreanov, F. Barbieri, O. C. Martin. *Large deviations in spin-glass ground-state energies*. The European Physical Journal B, **41**(3) pp. 365–375 (2004). (doi)

[ABM04b]   T. Aspelmeier, A. Bray, M. Moore. *Complexity of Ising Spin Glasses*. Physical Review Letters, **92**(8) pp. 1–4 (2004). (doi)

[ABMM08]   T. Aspelmeier, A. Billoire, E. Marinari, M. a. Moore. *Finite-size corrections in the Sherrington–Kirkpatrick model*. Journal of Physics A: Mathematical and Theoretical, **41**(32) p. 324008 (2008). (doi)

[AF10]   J. J. Alonso, J. F. Fernández. *Monte Carlo study of the spin-glass phase of the site-diluted dipolar Ising model*. Physical Review B, **81**(6) pp. 1–14 (2010). (doi)

[AJKT78]   J. R. L. de Almeida, R. C. Jones, J. M. Kosterlitz, D. J. Thouless. *The infinite-ranged spin glass with m-component spins*. Journal of Physics C: Solid State Physics, **11**(21) pp. L871–L875 (1978). (doi)

[AM04]   T. Aspelmeier, M. Moore. *Generalized Bose-Einstein Phase Transition in Large-m Component Spin Glasses*. Physical Review Letters, **92**(7) pp. 1–4 (2004). (doi)

[AMY03]   T. Aspelmeier, M. Moore, A. Young. *Interface Energies in Ising Spin Glasses*. Physical Review Letters, **90**(12) pp. 1–4 (2003). (doi)

[AP78]   P. Anderson, C. Pond. *Anomalous Dimensionalities in the Spin-Glass Problem*. Physical Review Letters, **40**(13) pp. 903–906 (1978). (doi)

[AS65]   M. Abramowitz, I. A. Stegun (eds.). *Handbook of Mathematical Functions: with Formulas, Graphs, and Mathematical Tables (Dover Books on Mathematics)*. Dover Publications (1965). ISBN 0486612724

[Asp10]   T. Aspelmeier. *Sample-to-sample fluctuations and bond chaos in the m-component spin glass*. Physical Review B, **81**(9) pp. 1–9 (2010). (doi)

[BA06]   a. Braun, T. Aspelmeier. *The m-component spin glass on a Bethe lattice*. Physical Review B, **74**(14) pp. 1–9 (2006). (doi)

[Bar82]   F. Barahona. *On the computational complexity of Ising spin glass models*. Journal of Physics A: Mathematical and General, **15**(10) pp. 3241–3253 (1982). (doi)

Bibliography

[BB83]   A. Benyoussef, N. Boccara. *Existence of spin-glass phases for three- and four-dimensional Ising and Heisenberg models*. Journal of Physics C: Solid State Physics, **16**(10) pp. 1901–1918 (1983). (doi)

[BB87]   J. R. Banavar, J. Bray. *Chaos in spin glasses: A renormalization-group study*. Physical Review B, **35**(16) pp. 8888–8890 (1987). (doi)

[BB88]   J. Banavar, A. Bray. *Heisenberg and Potts spin glasses: A renormalization-group study*. Physical Review B, **38**(4) pp. 2564–2569 (1988). (doi)

[BB01]   I. Benjamini, N. Berger. *The diameter of long-range percolation clusters on finite cycles*. Random Structures and Algorithms, **19**(2) pp. 102–111 (2001). (doi)

[BC82]   J. Banavar, M. Cieplak. *Nature of Ordering in Spin-Glasses*. Physical Review Letters, **48**(12) pp. 832–835 (1982). (doi)

[BCF⁺00]   H. Ballesteros, et al. *Critical behavior of the three-dimensional Ising spin glass*. Physical Review B, **62**(21) pp. 14237–14245 (2000). (doi)

[Bey08]   F. Beyer. *Monte Carlo simulation techniques and minimal energy states in the Edwards-Anderson spin glass model*. Diploma thesis, (unpublished) (2008)

[BF11]   S. Boettcher, S. Falkner. *Finite-Size Corrections for Ground States of Edwards-Anderson Spin Glasses*. arXiv:1110.6242v1 (2011)

[Bin85]   K. Binder. *Critical properties and finite-size effects of the five-dimensional Ising model*. Zeitschrift für Physik B Condensed Matter, **61**(1) pp. 13–23 (1985). (doi)

[BK05]   K. Binder, W. Kob. *Glassy Materials and Disordered Solids: An Introduction to Their Statistical Mechanics*. World Scientific Publishing Company (2005). ISBN 978-9812565105

[BKM03]   J.-P. Bouchaud, F. Krzakala, O. Martin. *Energy exponents and corrections to scaling in Ising spin glasses*. Physical Review B, **68**(22) pp. 1–11 (2003). (doi)

[BM58]   G. E. P. Box, M. E. Muller. *A Note on the Generation of Random Normal Deviates*. Ann. Math. Statist., **29**(2) pp. 610–611 (1958)

[BM77]   A. J. Bray, M. A. Moore. *Monte Carlo evidence for the absence of a phase transition in the two-dimensional Ising spin glass*. Journal of Physics F: Metal Physics, **7**(12) pp. L333–L337 (1977). (doi)

[BM79]   A. J. Bray, M. A. Moore. *Replica symmetry and massless modes in spin glasses. II. Non-Ising spins*. Journal of Physics C: Solid State Physics, **12**(7) pp. 1349–1361 (1979). (doi)

[BM81]   A. J. Bray, M. A. Moore. *Metastable states, internal field distributions and magnetic excitations in spin glasses*. Journal of Physics C: Solid State Physics, **14**(19) pp. 2629–2664 (1981). (doi)

[BM82]   A. J. Bray, M. A. Moore. *On the eigenvalue spectrum of the susceptibility matrix for random spin systems*. Journal of Physics C: Solid State Physics, **15**(23) pp. L765–L771 (1982). (doi)

[BM84]   A. J. Bray, M. A. Moore. *Lower critical dimension of Ising spin glasses: a numerical study*. Journal of Physics C: Solid State Physics, **17**(18) pp. L463–L468 (1984). (doi)

[BM87a]   A. J. Bray, M. Moore. *Chaotic Nature of the Spin-Glass Phase*. Physical Review Letters, **58**(1) pp. 57–60 (1987). (doi)

[BM87b]   A. J. Bray, M. Moore. *Scaling theory of the ordered phase of spin glasses*. In I. van Hemmen J., Morgenstern (ed.), *Heidelberg Colloquium on glassy dynamics*, pp. 121–153. Springer Berlin / Heidelberg (1987). (doi)

[BMY86]   A. Bray, M. Moore, A. Young. *Lower Critical Dimension of Metallic Vector Spin-Glasses*. Physical Review Letters, **56**(24) pp. 2641–2644 (1986). (doi)

[BNJ08]   E. Bittner, A. Nußbaumer, W. Janke. *Make Life Simple: Unleash the Full Power of the Parallel Tempering Algorithm*. Physical Review Letters, **101**(13) pp. 1–4 (2008). (doi)

[Boe05a]   S. Boettcher. *Extremal optimization for Sherrington-Kirkpatrick spin glasses*. The European Physical Journal B, **46**(4) pp. 501–505 (2005). (doi)

[Boe05b]   S. Boettcher. *Stiffness of the Edwards-Anderson Model in all Dimensions*. Physical Review Letters, **95**(19) pp. 1–4 (2005). (doi)

[Boe10]   S. Boettcher. *Numerical results for spin glass ground states on Bethe lattices: Gaussian bonds*. The European Physical Journal B, **74**(3) pp. 363–371 (2010). (doi)

[Bra98]   S. Brandt. *Data Analysis: Statistical and Computational Methods for Scientists and Engineers*. Springer, Berlin, 3 edn. (1998). ISBN 978-0387984988

[BS01]   S. M. Bhattacharjee, F. Seno. *A measure of data collapse for scaling*. Journal of Physics A: Mathematical and General, **34**(33) p. 6375 (2001). (doi)

[BW11]   F. Beyer, M. Weigel. *Spin stiffness of vector spin glasses*. Computer Physics Communications, **182**(9) pp. 1883–1887 (2011). (doi)

[BWM12]   F. Beyer, M. Weigel, M. A. Moore. *One-dimensional infinite-component vector spin glass with long-range interactions*. Physical Review B, **86**(1) p. 014431 (2012). (doi)

Bibliography

[BY86a]   R. Bhatt, A. Young. *Long range Ising spin glasses: Critical behavior and ultrametricity*. Journal of Magnetism and Magnetic Materials, **54-57** pp. 191–193 (1986). (doi)

[BY86b]   K. Binder, A. P. Young. *Spin glasses: Experimental facts, theoretical concepts, and open questions*. Reviews of Modern Physics, **58**(4) pp. 801–976 (1986). (doi)

[CBM02]   a. Carter, A. Bray, M. Moore. *Aspect-Ratio Scaling and the Stiffness Exponent θ for Ising Spin Glasses*. Physical Review Letters, **88**(7) pp. 18–21 (2002). (doi)

[CCAMM$^+$06] I. Campos, et al. *Spin-Glass Transition of the Three-Dimensional Heisenberg Spin Glass*. Physical Review Letters, **97**(21) pp. 1–4 (2006). (doi)

[Cha08]   S. Chandra. *Dependence of ground-state energy of classical n-vector spins on n*. Physical Review E, **77**(2) p. 021125 (2008). (doi)

[CHK04]   I. Campbell, A. Hartmann, H. Katzgraber. *Energy size effects of two-dimensional Ising spin glasses*. Physical Review B, **70**(5) pp. 1–10 (2004). (doi)

[CHT06]   I. Campbell, K. Hukushima, H. Takayama. *Extended Scaling Scheme for Critically Divergent Quantities in Ferromagnets and Spin Glasses*. Physical Review Letters, **97**(11) pp. 1–4 (2006). (doi)

[CM72]   V. Cannella, J. Mydosh. *Magnetic Ordering in Gold-Iron Alloys*. Physical Review B, **6**(11) pp. 4220–4237 (1972). (doi)

[Der80]   B. Derrida. *Random-Energy Model: Limit of a Family of Disordered Models*. Physical Review Letters, **45**(2) pp. 79–82 (1980). (doi)

[Dys69]   F. J. Dyson. *Existence of a phase-transition in a one-dimensional Ising ferromagnet*. Communications in Mathematical Physics, **12**(2) pp. 91–107 (1969). (doi)

[Dys71]   F. Dyson. *An Ising ferromagnet with discontinuous long-range order*. Communications in Mathematical Physics, **21**(4) pp. 269–283 (1971). (doi)

[EA75]   S. F. Edwards, P. W. Anderson. *Theory of spin glasses*. Journal of Physics F: Metal Physics, **5**(5) pp. 965–974 (1975). (doi)

[Efr79]   B. Efron. *Bootstrap Methods: Another Look at the Jackknife*. The Annals of Statistics, **7**(1) pp. 1–26 (1979). (doi)

[EH85]   A. C. D. Enter, J. L. Hemmen. *Absence of phase transitions in certain one-dimensional long-range random systems*. Journal of Statistical Physics, **39**(1-2) pp. 1–13 (1985). (doi)

[FH77]   R. Fisch, A. Harris. *Series Study of a Spin-Glass Model in Continuous Dimensionality*. Physical Review Letters, **38**(14) pp. 785–787 (1977). (doi)

[FH86]   D. Fisher, D. Huse. *Ordered Phase of Short-Range Ising Spin-Glasses*. Physical Review Letters, **56**(15) pp. 1601–1604 (1986). (doi)

[FH88]   D. Fisher, D. Huse. *Equilibrium behavior of the spin-glass ordered phase*. Physical Review B, **38**(1) pp. 386–411 (1988). (doi)

[Fis74]   M. Fisher. *The renormalization group in the theory of critical behavior*. Reviews of Modern Physics, **46**(4) pp. 597–616 (1974)

[Fis98]   M. Fisher. *Renormalization group theory: Its basis and formulation in statistical physics*. Reviews of Modern Physics, **70**(2) pp. 653–681 (1998). (doi)

[FMMPG$^+$09] L. Fernandez, et al. *Phase transition in the three dimensional Heisenberg spin glass: Finite-size scaling analysis*. Physical Review B, **80**(2) pp. 1–5 (2009). (doi)

[FMN72]   M. Fisher, S.-k. Ma, B. Nickel. *Critical Exponents for Long-Range Interactions*. Physical Review Letters, **29**(14) pp. 917–920 (1972). (doi)

[FTVP07]   W. H. P. Flannery, S. A. Teukolsky, W. T. Vetterling, B. P. *Numerical Recipes 3rd Edition: The Art of Scientific Computing*. Cambridge University Press, New York, NY, USA, 3 edn. (2007). ISBN 0521880688

[GBM82]   J. E. Green, A. J. Bray, M. A. Moore. *Critical behaviour of an m-vector spin glass for m = ∞*. Journal of Physics A: Mathematical and General, **15**(7) pp. 2307–2314 (1982). (doi)

[GK82]   R. B. Griffiths, M. Kaufman. *Spin systems on hierarchical lattices. Introduction and thermodynamic limit*. Physical Review B, **26**(9) pp. 5022–5032 (1982). (doi)

[Gol92]   N. Goldenfeld. *Lectures on Phase Transitions and the Renormalization Group*. Addison-Wesley Publishing Company (1992). ISBN 0-201-55409-7

[GR80]   I. Gradshteyn, I. Ryzhik. *Table of Integrals, Series and Products*. Academic Press Inc., 2 edn. (1980). ISBN 978-0122947605

[Has00]   M. Hastings. *Ground State and Spin-Glass Phase of the Large-N Infinite-Range Spin Glass via Supersymmetry*. Journal of Statistical Physics, **99**(1) pp. 171–217 (2000). (doi)

[Hen84]   C. Henley. *Computer search for defects in a D= 3 Heisenberg spin glass*. Annals of Physics, **156** pp. 324–367 (1984)

[HH04]   J. Houdayer, A. Hartmann. *Low-temperature behavior of two-dimensional Gaussian Ising spin glasses*. Physical Review B, **70**(1) pp. 1–7 (2004). (doi)

Bibliography

[HLC76]   A. B. Harris, T. C. Lubensky, J.-H. Chen. *Critical Properties of Spin-Glasses*. Priest, **36**(8) pp. 415–418 (1976). (doi)

[HM00]   J. Houdayer, O. C. Martin. *A geometrical picture for finite-dimensional spin glasses*. Europhysics Letters (EPL), **49**(6) pp. 794–800 (2000). (doi)

[HN96]   K. Hukushima, K. Nemoto. *Exchange Monte Carlo Method and Application to Spin Glass Simulations*. Journal of the Physics Society Japan, **65**(6) pp. 1604–1608 (1996). (doi)

[HPV08]   M. Hasenbusch, A. Pelissetto, E. Vicari. *Critical behavior of three-dimensional Ising spin glass models*. Physical Review B, **78**(21) p. 214205 (2008). (doi)

[HR01]   A. Hartmann, H. Rieger. *Optimization Algorithms in Physics*. Wiley-VCH Verlag GmbH & Co. KGaA (2001). ISBN 978-3527403073

[HW59]   J. S. Hicks, R. F. Wheeling. *An efficient method for generating uniformly distributed points on the surface of an n-dimensional sphere*. Communications of the ACM, **2**(4) pp. 17–19 (1959). (doi)

[IM75]   Y. Imry, S.-k. Ma. *Random-Field Instability of the Ordered State of Continuous Symmetry*. Physical Review Letters, **35**(21) pp. 1399–1401 (1975). (doi)

[Juh12]   R. Juhász. *Competition between quenched disorder and long-range connections: A numerical study of diffusion*. Physical Review E, **85**(1) pp. 1–8 (2012). (doi)

[JY05]   J. Jones, A. Young. *Finite-size scaling of the correlation length above the upper critical dimension in the five-dimensional Ising model*. Physical Review B, **71**(17) pp. 3–7 (2005). (doi)

[KA99]   J. Kosterlitz, N. Akino. *Numerical Study of Spin and Chiral Order in a Two-Dimensional XY Spin Glass*. Physical Review Letters, **82**(20) pp. 4094–4097 (1999). (doi)

[Kad76]   L. P. Kadanoff. *Notes on Migdal's recursion formulas*. Annals of Physics, **100** pp. 359–394 (1976). (doi)

[KAS83]   G. Kotliar, P. Anderson, D. Stein. *One-dimensional spin-glass model with long-range random interactions*. Physical Review B, **27**(1) pp. 602–605 (1983)

[Kat09]   H. G. Katzgraber. *Introduction to Monte Carlo Methods*. arXiv:0905.1629v3 (2009)

[Kaw10]   H. Kawamura. *Two models of spin glasses — Ising versus Heisenberg*. Journal of Physics: Conference Series, **233** p. 012012 (2010). (doi)

[KG84]   M. Kaufman, R. B. Griffiths. *Spin systems on hierarchical lattices. II. Some examples of soluble models*. Physical Review B, **30**(1) p. 244 (1984)

[KKL$^+$05]   H. Katzgraber, et al. *Universality-class dependence of energy distributions in spin glasses*. Physical Review B, **72**(9) pp. 1–14 (2005). (doi)

[KKY06]   H. Katzgraber, M. Körner, A. P. Young. *Universality in three-dimensional Ising spin glasses: A Monte Carlo study*. Physical Review B, **73**(22) pp. 1–11 (2006). (doi)

[KLY09]   H. Katzgraber, D. Larson, A. Young. *Study of the de Almeida–Thouless Line Using Power-Law Diluted One-Dimensional Ising Spin Glasses*. Physical Review Letters, **102**(17) pp. 1–4 (2009). (doi)

[KM00]   F. Krzakala, O. Martin. *Spin and Link Overlaps in Three-Dimensional Spin Glasses*. Physical Review Letters, **85**(14) pp. 3013–3016 (2000). (doi)

[KR05]   N. Kawashima, H. Rieger. *Frustrated Spin Systems*. In: H. T. Diep (Ed.). World Scientific, Singapore (2005). ISBN 981-256-091-2

[Kre77]   U. Krey. *Instability of Heisenberg-spin-glass-phase transitions*. Physics Letters A, **64**(1) pp. 125–127 (1977). (doi)

[KTJ76]   J. Kosterlitz, D. Thouless, R. Jones. *Spherical Model of a Spin-Glass*. Physical Review Letters, **36**(20) pp. 1217–1220 (1976). (doi)

[KY03]   H. Katzgraber, A. P. Young. *Monte Carlo studies of the one-dimensional Ising spin glass with power-law interactions*. Physical Review B, **67**(13) pp. 1–8 (2003). (doi)

[KY05]   H. Katzgraber, A. P. Young. *Probing the Almeida-Thouless line away from the mean-field model*. Physical Review B, **72**(18) pp. 1–5 (2005). (doi)

[LB09]   D. P. Landau, K. Binder. *A Guide to Monte Carlo Simulations in Statistical Physics*. Cambridge University Press, 3 edn. (2009). ISBN 978-0521768481

[LDY05]   L. Lee, A. Dhar, A. P. Young. *Spin glasses in the limit of an infinite number of spin components*. Physical Review E, **71**(3) pp. 1–9 (2005). (doi)

[Leu99]   L. Leuzzi. *Critical behaviour and ultrametricity of Ising spin-glass with long-range interactions*. Journal of Physics A: Mathematical and General, **32**(8) pp. 1417–1426 (1999). (doi)

[LKMY10]   D. Larson, H. G. Katzgraber, M. A. Moore, A. P. Young. *Numerical studies of a one-dimensional three-spin spin-glass model with long-range interactions*. Physical Review B, **81**(6) pp. 1–8 (2010). (doi)

[LPRTRL08]   L. Leuzzi, G. Parisi, F. Ricci-Tersenghi, J. Ruiz-Lorenzo. *Dilute One-Dimensional Spin Glasses with Power Law Decaying Interactions*. Physical Review Letters, **101**(10) pp. 7–10 (2008). (doi)

Bibliography

[LQSJ04]   D. Loison, C. L. Qin, K. D. Schotte, X. F. Jin. *Canonical local algorithms for spin systems: heat bath and Hasting's methods*. The European Physical Journal B, **41**(3) pp. 395–412 (2004). (doi)

[LY05]   L. Lee, A. Young. *Defect energy of infinite-component vector spin glasses*. Physical Review E, **72**(3) p. 036124 (2005). (doi)

[Mar72]   G. Marsaglia. *Choosing a Point from the Surface of a Sphere*. The Annals of Mathematical Statistics, **43**(2) pp. 645–646 (1972)

[Mas02]   J.-i. Maskawa. *Ordered phase and non-equilibrium fluctuation in stock market*. Physica A: Statistical Mechanics and its Applications, **311**(3-4) pp. 563–570 (2002). (doi)

[McM84a]   W. McMillan. *Domain-wall renormalization-group study of the two-dimensional random Ising model*. Physical Review B, **29**(7) pp. 4026–4029 (1984). (doi)

[McM84b]   W. L. McMillan. *Scaling theory of Ising spin glasses*. Journal of Physics C: Solid State Physics, **17**(18) pp. 3179–3187 (1984). (doi)

[MCM+86]   B. Morris, et al. *Zero-temperature critical behaviour of vector spin glasses*. Journal of Physics C: Solid State Physics, **19** pp. 1157–1171 (1986). (doi)

[Moo05]   M. A. Moore. *The stability of the replica-symmetric state in finite-dimensional spin glasses*. Journal of Physics A: Mathematical and General, **38**(46) pp. L783–L789 (2005). (doi)

[Moo10]   M. Moore. *Ordered phase of the one-dimensional Ising spin glass with long-range interactions*. Physical Review B, **82**(1) pp. 1–8 (2010). (doi)

[Mor11]   T. Mori. *Instability of the mean-field states and generalization of phase separation in long-range interacting systems*. Physical Review E, **84**(3) p. 14 (2011). (doi)

[MP00]   E. Marinari, G. Parisi. *Effects of changing the boundary conditions on the ground state of Ising spin glasses*. Physical Review B, **62**(17) pp. 11677–11685 (2000). (doi)

[MP01]   E. Marinari, G. Parisi. *Effects of a Bulk Perturbation on the Ground State of 3D Ising Spin Glasses*. Physical Review Letters, **86**(17) pp. 3887–3890 (2001). (doi)

[MPS+84]   M. Mézard, et al. *Nature of the Spin-Glass Phase*. Physical Review Letters, **52**(13) pp. 1156–1159 (1984). (doi)

[MPV87]   M. Mezard, G. Parisi, M. Virasoro. *Spin Glass Theory and Beyond*. World Scientific, Singapore (1987). ISBN 9971501163

176

[Mul59] M. E. Muller. *A note on a method for generating points uniformly on n-dimensional spheres*. Communications of the ACM, **2**(4) pp. 19–20 (1959). (doi)

[Myd93] J. Mydosh. *Spin glasses : an experimental introduction*. CRC Press (1993). ISBN 978-0748400386

[Nis01] H. Nishimori. *Statistical Physics of Spin Glasses and Information Processing: An Introduction*. Oxford University Press (2001). ISBN 0198509405

[NS86] C. M. Newman, L. S. Schulman. *One dimensional $1/|j - i|^S$ percolation models: The existence of a transition for $S \leq 2$*. Communications in Mathematical Physics, **104**(4) pp. 547–571 (1986). (doi)

[NS03] C. M. Newman, D. L. Stein. *Finite-Dimensional Spin Glasses: States, Excitations, and Interfaces*. Annales Henri Poincaré, **4**(S1) pp. 497–503 (2003). (doi)

[NV74] T. Niemeyer, J. Van Leeuwen. *Wilson theory for 2-dimensional Ising spin systems*. Physica, **71**(1) pp. 17–40 (1974). (doi)

[Ons44] L. Onsager. *Crystal Statistics. I. A Two-Dimensional Model with an Order-Disorder Transition*. Physical Review, **65**(3-4) pp. 117–149 (1944). (doi)

[Par79] G. Parisi. *Infinite Number of Order Parameters for Spin-Glasses*. Physical Review Letters, **43**(23) pp. 1754–1756 (1979). (doi)

[Par80] G. Parisi. *The order parameter for spin glasses: a function on the interval 0-1*. Journal of Physics A: Mathematical and General, **13**(3) pp. 1101–1112 (1980). (doi)

[PR10] G. Parisi, T. Rizzo. *Large deviations of the free energy in diluted mean-field spin-glass*. Journal of Physics A: Mathematical and Theoretical, **43**(4) p. 045001 (2010). (doi)

[Pri90] V. Privman. *Finite Size Scaling and Numerical Simulation of Statistical Systems*. World Scientific, Singapore (1990). ISBN 9810237960

[PY00] M. Palassini, A. Young. *Nature of the Spin Glass State*. Physical Review Letters, **85**(14) pp. 3017–3020 (2000). (doi)

[PY08] J. Pixley, A. Young. *Large-scale Monte Carlo simulations of the three-dimensional XY spin glass*. Physical Review B, **78**(1) pp. 1–7 (2008). (doi)

[Sch83] L. S. Schulman. *Long range percolation in one dimension*. Journal of Physics A: Mathematical and General, **16**(17) pp. L639–L641 (1983). (doi)

[Set06] J. Sethna. *Statistical Mechanics: Entropy, Order Parameters and Complexity*. Oxford University Press (2006). ISBN 978-0198566779. (www)

Bibliography

[Sib62]   M. Sibuya. *A method for generating uniformly distributed points on N-dimensional spheres*. Annals of the Institute of Statistical Mathematics, **14**(1) pp. 81–85 (1962). (doi)

[SK75]   D. Sherrington, S. Kirkpatrick. *Solvable Model of a Spin-Glass*. Physical Review Letters, **35**(26) pp. 1792–1796 (1975). (doi)

[Slo83]   N. J. A. Sloane. *Encrypting by Random Rotations*. Lecture Notes in Computer Science, **149** pp. 71–128 (1983). (doi)

[Ste72]   G. Stell. *Scaling Theory of the Critical Region for Systems with Long-Range Forces*. Physical Review B, **5**(3) pp. 981–985 (1972). (doi)

[Ste92]   D. L. Stein. *Spin Glasses and Biology*. World Scientific Pub Co (1992). ISBN 978-9971505387

[Sti79]   R. B. Stinchcombe. *Critical properties of dilute Heisenberg and Ising magnets*. Journal of Physics C: Solid State Physics, **12**(21) pp. 4533–4552 (1979). (doi)

[Suz73]   M. Suzuki. *Critical Exponents for Long-Range Interactions. I*. Progress of Theoretical Physics, **49**(2) pp. 424–441 (1973). (doi)

[SW86]   R. H. Swendsen, J.-S. Wang. *Replica Monte Carlo Simulation of Spin-Glasses*. Physical Review Letters, **57**(21) pp. 2607–2609 (1986). (doi)

[SY11a]   A. Sharma, A. Young. *de Almeida–Thouless line studied using one-dimensional power-law diluted Heisenberg spin glasses*. Physical Review B, **84**(1) pp. 1–7 (2011). (doi)

[SY11b]   A. Sharma, A. Young. *Phase transitions in the one-dimensional long-range diluted Heisenberg spin glass*. Physical Review B, **83**(21) pp. 1–10 (2011). (doi)

[Tal03]   M. Talagrand. *The generalized Parisi formula*. Comptes Rendus Mathematique, **337**(2) pp. 111–114 (2003). (doi)

[Tas77]   Y. Tashiro. *On methods for generating uniform random points on the surface of a sphere*. Annals of the Institute of Statistical Mathematics, **29**(1) pp. 295–300 (1977). (doi)

[Tem06]   T. Temesvári. *Is the droplet theory for the Ising spin glass inconsistent with the replica field theory?*. Journal of Physics A: Mathematical and General, **39**(2) pp. L61–L67 (2006). (doi)

[THT04]   S. Trebst, D. Huse, M. Troyer. *Optimizing the ensemble for equilibration in broad-histogram Monte Carlo simulations*. Physical Review E, **70**(4) pp. 1–5 (2004). (doi)

[VB85]   L. Viana, A. J. Bray. *Phase diagrams for dilute spin glasses*. Journal of Physics C: Solid State Physics, **18**(15) pp. 3037–3051 (1985). (doi)

[Via88]   L. Viana. *Infinite-component spin-glass model in the low-temperature phase*. Journal of Physics A: Mathematical and General, **21**(3) pp. 803–813 (1988). (doi)

[Vil77]   J. Villain. *Two-level systems in a spin-glass model : I . General formalism and two-dimensional model*. J. Phys. C: Solid State Phys., **10**(23) pp. 4793—-4803 (1977). (doi)

[VK09]   D. X. Viet, H. Kawamura. *Monte Carlo studies of chiral and spin ordering of the three-dimensional Heisenberg spin glass*. Phys.Rev. B, **80**(6) p. 064418 (2009). (doi)

[VK10]   D. Viet, H. Kawamura. *Spin-Chirality Decoupling in the One-Dimensional Heisenberg Spin Glass with Long-Range Power-Law Interactions*. Physical Review Letters, **105**(9) p. 5 (2010). (doi)

[Wei07]   M. Weigel. *Genetic embedded matching approach to ground states in continuous-spin systems*. Physical Review E, **76**(6) pp. 1–16 (2007). (doi)

[WG06]   M. Weigel, M. Gingras. *Ground States and Defect Energies of the Two-Dimensional XY Spin Glass from a Quasiexact Algorithm*. Physical Review Letters, **96**(9) p. 097206 (2006). (doi)

[WG08]   M. Weigel, M. Gingras. *Zero-temperature phase of the XY spin glass in two dimensions: Genetic embedded matching heuristic*. Physical Review B, **77**(10) pp. 1–17 (2008). (doi)

[Wig58]   E. Wigner. *On the distribution of the roots of certain symmetric matrices*. The Annals of Mathematics, **67**(2) pp. 325–327 (1958)

[Wig67]   E. Wigner. *Random matrices in physics*. Siam Review, **9**(1) pp. 1–23 (1967)

[WJ00]   M. Weigel, W. Janke. *Monte Carlo study of the scaling of universal correlation lengths in three-dimensional O(n) spin models*. Physical Review B, **62**(10) pp. 6343–6359 (2000). (doi)

[Yeo93]   J. M. Yeomans. *Statistical Mechanics of Phase Transitions*. Oxford University Press (1993). ISBN 978-0198517306

Bibliography

180

Curriculum vitae

(removed)